

**LOCAL NETWORK HETEROGENEITIES IN PHOTOPOLYMERIZED HYDROGELS PROMOTE  
CARTILAGE TISSUE REGENERATION**

by

STANLEY CHU

B.S., Georgia Institute of Technology, 2013

M.S., University of Colorado, 2015

A thesis submitted to the  
Faculty of the Graduate School of the  
University of Colorado in partial fulfillment  
of the requirement for the degree of  
Doctor of Philosophy  
Department of Chemical Engineering  
2019

This thesis entitled:

Local Network Heterogeneities in Photopolymerized Hydrogels Promote Cartilage Tissue  
Regeneration

written by Stanley Chu

has been approved for the Department of Chemical Engineering

---

Dr. Stephanie J. Bryant

---

Dr. Franck J. Vernerey

Date: \_\_\_\_\_

The final copy of this thesis has been examined by the signatories, and we find that both the content and the form meet acceptable presentation standards of scholarly work in the above mentioned discipline.

## **Abstract**

Chu, Stanley (Ph.D., Chemical Engineering)

Local Network Heterogeneities in Photopolymerized Hydrogels Promote Cartilage Tissue Regeneration

Thesis directed by Professor Stephanie J. Bryant

Cartilage tissue engineering using biodegradable scaffolds as carriers for chondrocytes presents a promising strategy to regenerate cartilage damaged by age or injury. Photopolymerizable poly(ethylene glycol) (PEG) hydrogel scaffolds that can be modified to permit tunable degradation present an opportunity to tailor scaffolds to the patient's cells. Scaffold degradation must be matched to the rate of matrix deposition in order to prevent construct failure, which is a significant design challenge further complicated by the effects of age.

The goal of this thesis was to characterize polymer network formation of photopolymerizable hydrogels and its modes of hydrolytic and enzymatic degradation. By understanding how each mode of degradation behaves, it is possible to design hydrogels tailored to patient specific needs. Initial work focused on the characterization of newly formed cell-laden photopolymerized PEG hydrogels. Young (bovine donor of age ~3 weeks) and adult (bovine donor of age 1-3 years) chondrocytes were encapsulated in radical mediated hydrogels and were found to reduce the bulk crosslinking density resulting in lower overall compressive moduli compared to acellular hydrogels. Furthermore, confocal fluorescence microscopy of these hydrogels suggested that there exists a gradient of reduced crosslinking density around encapsulated cells. These findings were studied for their effect on polymer network degradation and tissue formation in hydrolytically and enzymatically degradable hydrogels. The heterogeneous

formation of the hydrogel caused by encapsulated cells were found to be critical in promoting localized hydrogel degradation and tissue connectivity thereby reducing the chances of construct failure. Finally, a strategy employing IGF-1 was investigated for stimulating the anabolic activity of older chondrocytes. Improving the tissue regenerative potential of older chondrocytes will help develop a tissue engineering platform for patients of varying age. Soluble IGF-1 was found to slightly increase collagen production of encapsulated adult chondrocytes; however, there was no significant increase in glycosaminoglycan production or noticeable differences in tissue spatial elaboration. A different mode of growth factor employment or growth factor choice should be investigated and may elicit a more positive response from older chondrocytes. Overall, this thesis identified new control parameters in rationally designing hydrogels for cartilage engineering applications in a wide range of patients.

To my family, who has supported me  
through every stage in life.

## **Acknowledgments**

The work detailed in this dissertation is only part of all the effort put into this thesis. Throughout my journey in graduate school, I have several people to thank for both their scientific advice and moral support.

First and foremost, I must thank my mom Vicky Yu and my siblings Heidi and Kevin Chu. Although distance may have separated us physically, I've always felt close to all of you in my heart. Through the good times and bad times, we've had each other to lean on. My PhD would not be possible without your encouragement and support. I must also thank the rest of my family. This dissertation is a culmination of not only my work but also all the sacrifices and challenges that you have faced immigrating to North America in order to create a better life for me.

Thank you to all my friends that have grown alongside me in Atlanta. You have been my role models in pursuing my dreams and academic achievements and have always been a consistent shoulder to lean on when I feel homesick. Thank you to all the friends I've made in Boulder and the graduate students of Chemical Engineering at CU Boulder. You have provided endless emotional support and friendship when I needed it.

Thank you to Dr. Julie Champion and the Champion Lab at Georgia Tech, especially Dr. Lina Herrera-Estrada. You have provided me with invaluable experience in a research lab as well as life skills. Without you, I would not be prepared for what lay ahead of me in graduate school.

Thank you to Stephanie Bryant who has been much more than advisor to me. When I first entered the graduate program, I knew I wanted an advisor who can guide my research as well as sympathize with the highs and lows of graduate school. You have been much more than that to me during my time here. You have provided invaluable advice for success in graduate school but

you've also been a confidant of my personal struggles! Thank you for putting up with me during my emotional rollercoaster ride of graduate school!

To my lab, I cannot possibly find all the words to describe how much you mean to me. To Stacey Skaalure and Elizabeth Aisenbrey, you two have been such great role models to me. I deeply admire your work ethic and your ability to balance life and work. If I could only be a fraction as successful as you are, I would consider myself lucky. To Aaron Aziz, thank you for providing me a sense of brotherhood and inclusiveness in the group when I first joined. To Margaret Schneider, you have been my sister throughout my time in the lab. I would not have achieved this without you, your company, your empathy, your strength. To Leila Saleh and Alex Anderson, your joining the group transformed our lab into a family and we are all better for it; thank you. To Michael, thank you for providing me a sense of community. To Camila, Kristen, Archish, and Sarah, thank you for renewing the morale of our lab and providing even more diverse experiences and wisdom to our group. And to Mollie, the next generation of the cartilage project, thank you for your passion and energy. It has been refreshing for an old man like me and (H.A.G.S.) don't ever change!

I am grateful to the various funding sources that have support me and my research during my time at CU Boulder. These include a Pharmaceutical Biotechnology Training Grant from the National Institute of Health, a fellowship from the Graduate Assistance in Areas of National Need from the Department of Education, and grants from the National Institute of Health (#1R01AR065441).

There are many more people that I have not named here that have helped me along my journey.

Thank you all, I truly appreciate you!



## TABLE OF CONTENTS

Content	Page
<b>Chapter 1. Introduction</b> .....	1
1.1 Hydrogels .....	1
1.2 Degradable Hydrogels.....	3
1.3 The Role of Computational Modeling in Cartilage Tissue Engineering .....	4
1.4 Patient Variability and Personalized Regenerative Medicine.....	6
1.5 Approach of This Dissertation.....	7
1.6 References .....	8
<b>Chapter 2. Objectives</b> .....	13
2.1 Characterize the cell-hydrogel microenvironment in cell-laden hydrogels .....	14
2.2 Identify the effect of heterogeneities within the hydrogel on macroscopic cartilage tissue formation by encapsulated cells .....	14
2.3 Develop a hydrogel platform for donors of varying regenerative capabilities .....	14
<b>Chapter 3: Chondrocyte-mediated reductions in local crosslinking density in radical polymerized hydrogels</b> .....	15
Abstract.....	15
3.1 Introduction .....	15
3.2 Materials and Methods.....	18
3.2.1 Chondrocyte Isolation.....	18
3.2.2 PEG Macromer Synthesis.....	19
3.2.3 Hydrogel Formation .....	23
3.2.4 Hydrogel Characterization .....	25
3.2.5 Fluorescence Microscopy .....	26
3.2.6 Statistics .....	26
3.3 Results.....	28
3.3.1 Encapsulated chondrocytes in photopolymerized hydrogels reduce the bulk	

compressive modulus. ....	28
3.3.2 Cellular Interference of Polymer Network Formation is Affected by Donor. .....	31
3.3.3 Polymer Chemistry Affects Cell-Polymer Interactions. ....	32
3.3.4 Encapsulated Cells Reduce Local Network Crosslinking in Fluorescently Labeled Hydrogels.....	37
3.3.5 Hydrolytically Degradable Hydrogels Undergo Heterogeneous Degradation. ....	40
3.4 Discussion.....	41
3.5 Conclusions .....	48
3.6 Acknowledgments.....	48
3.7 References .....	49
<b>Chapter 4: Establishment of Cell Mimetic Particles and Hydrogel Degradation Model .....</b>	<b>52</b>
Abstract.....	52
4.1 Introduction .....	53
4.2 Materials and Methods.....	54
4.2.1 Microparticle Formation .....	54
4.2.2 Microparticle Characterization .....	55
4.2.3 Macromer Synthesis .....	55
4.2.4 Microparticle Encapsulation in Fluorescent Hydrogels .....	56
4.2.5 Semi-quantitative and Statistical Analysis of Hydrogel Degradation .....	57
4.3 Results.....	57
4.3.1 Microparticle Characterization .....	59
4.3.2 Hydrogel Degradation.....	60
4.4 Discussion.....	65
4.5 Conclusions .....	69
4.6 Acknowledgments.....	69

4.7 References .....	70
<b>Chapter 5: Understanding the Spatiotemporal Degradation Behavior of Aggrecanase-Sensitive Poly(ethylene glycol) Hydrogels for use in Cartilage Tissue Engineering .....</b>	<b>71</b>
Abstract.....	71
5.1 Introduction .....	72
5.2 Materials and Methods.....	75
5.2.1 Chondrocyte Isolation.....	75
5.2.2 Enzyme Kinetics Assay .....	75
5.2.3 Macromer Synthesis .....	76
5.2.4 Hydrogel Formation and Cell Encapsulation .....	77
5.2.5 Characterization of Acellular and Cell-Laden Hydrogels .....	78
5.2.6 Viability and Biochemical Analysis.....	79
5.2.7 Histology and Immunohistochemistry.....	80
5.2.8 Aggrecanase Activity.....	81
5.2.9 Statistical Analysis.....	82
5.2.10 Mathematical and Numerical Modeling.....	82
5.3 Results and Discussion .....	90
5.3.1 Model Inputs.....	91
5.3.2 Assessing Spatial Heterogeneities in Crosslink Density: Combined Modeling and Experimental Results .....	93
5.3.3 Estimating ECM modulus: Combined Modeling and Experimental Results.....	96
5.3.4 1-Dimensional Single Cell Simulations: Enzyme and Hydrogel Fronts .....	100
5.3.5 3-Dimensional Multi-Cell Simulations: Macroscopic Hydrogel and ECM Evolution .....	104
5.4 Conclusions .....	112
5.5 Acknowledgments.....	113

5.6 References .....	113
<b>Chapter 6: Local heterogeneities improve matrix connectivity in degradable and photoclickable PEG hydrogels for applications in tissue engineering .....</b>	<b>119</b>
Abstract.....	119
6.1 Introduction .....	120
6.2 Materials and Methods.....	123
6.2.1 Macromer Synthesis .....	123
6.2.2 Chondrocyte Isolation.....	124
6.2.3 Chondrocyte Encapsulation and Culture .....	124
6.2.4 Hydrogel Construct Characterization .....	125
6.2.5 Biochemical Analysis.....	125
6.2.6 Immunohistochemistry.....	126
6.2.7 Modeling.....	127
6.2.8 Statistics .....	133
6.3 Results and Discussion .....	133
6.4 Conclusions .....	153
6.5 Acknowledgments.....	153
6.6 References .....	154
<b>Chapter 7: Improving the Tissue Engineering Potential of Adult Chondrocytes via Growth Factors .....</b>	<b>158</b>
Abstract.....	158
7.1 Introduction .....	158
7.2 Materials and Methods.....	160
7.2.1 Chondrocyte Isolation.....	160
7.2.2 2D Growth Factor Screen.....	161
7.2.3 Macromer Synthesis .....	162

7.2.4 Chondrocyte Expansion .....	163
7.2.5 Hydrogel Formation and 3D Cell Culture .....	164
7.2.6 Hydrogel Characterization .....	164
7.2.7 Biochemical Assays .....	165
7.2.8 Enzyme Activity Assays .....	165
7.2.9 Immunohistochemistry and Microscopy .....	166
7.2.10 Statistics .....	166
7.3 Results and Discussion .....	167
7.3.1 Effect of FGF-2 and IGF-1 on Matrix Production on Chondrocytes Cultured in 2D .....	167
7.3.2 Effect of IGF-1 on Matrix Production on Chondrocytes Cultured in 3D ....	168
7.3.3 Personalizing Matrix Assisted Autologous Chondrocyte Implantation (MACI) .....	180
7.4 Conclusions and Future Work .....	182
7.5 Acknowledgments .....	183
7.6 References .....	183
<b>Chapter 8: Conclusions and Recommendations .....</b>	<b>186</b>
8.1 Conclusions .....	186
8.2 Recommendations .....	189
8.2.1 Hydrogel Characterization and Control over Cell-Polymer Interactions...	190
8.2.2 Characterizing Hydrogel Degradation.....	191
8.2.3 Stimulation of Chondrocytes to Augment Anabolic Activity .....	192
8.3 Long Term Goals .....	192
8.4 References .....	193
Bibliography .....	195

## LIST OF TABLES

<b>Table</b>	<b>Page</b>
<b>Chapter 3</b>	
Table 1. Chemical structures of macromolecular monomers (macromers) and crosslinker used in this study.....	22
<b>Chapter 5</b>	
Table 1. Input parameters used in the model. ....	92
Table 2. Volume fraction of cells used in the modeling experiments. ....	96
<b>Chapter 6</b>	
Table 1. Model Parameters.....	137
Table 2. Cluster and Background Parameters .....	137

## LIST OF FIGURES

Figure	Page
<b>Chapter 3</b>	
Figure 1. A general schematic representation of hydrogel formation. Monomers are mixed with cells in a precursor solution. Here, a multiarmed macromer with a linear bifunctional crosslinker is shown; however, monomers with different architectures are used. A full list of polymer chemistries used in this chapter is shown in Table 1. Cells may or may not be included to create cell-laden or acellular hydrogels. The precursor solution is then polymerized via photopolymerization (in the case of PEG-NB and PEG-CAP-NB crosslinked by dithiol molecules and PEGDA macromers) or via a temperature drop (in the case of agarose). The crosslinked hydrogel physically entraps cells. In the case of photopolymerized hydrogels, several radicals are formed. Upon exposure to ultraviolet light, the photoinitiator is cleaved to produce a radical. This radical abstracts a hydrogen from the monomers to produce kinetic chains. In the case of polymerization via thiol-ene click chemistry, carbon and thiyl radicals are generated (the structures of the monomers used following this polymerization scheme can be found in Table 1 A, B, E, and F). For homopolymerization of acrylate functionalized PEG, acrylyl radicals are formed (Table 1 C). Additionally, several reactive oxygen species (ROS) are formed if ambient oxygen is present. Figures are not drawn to scale. ....	28
Figure 2. Young bovine chondrocytes were encapsulated in a variety of radical-polymerized hydrogels at increasing cell concentrations. A) PEG-NB crosslinked with PEGdSH. B) PEG-NB crosslinked with an MMP-sensitive peptide GCVPLSLYSGCG. C) PEG-NB crosslinked with an ADAMTS-sensitive peptide CRDTEGEARGSVIDRC. D) PEG-CAP-NB crosslinked with PEGdSH. E) PEGDA. F) As a negative control, chondrocytes were encapsulated in a physically crosslinked agarose (1.5 wt%) gel. The p values reported in the upper right corner of each panel denote if cell concentration was a significant factor in hydrogel modulus. ....	30
Figure 3. Comparison of hydrogel moduli encapsulated with cells from young and adult donors. Hydrogels were formed by crosslinking 8-arm PEG-NB with a nondegradable PEGdSH crosslinker. A) Moduli of hydrogels encapsulated with cells from three different young bovine donors. B) Moduli of hydrogels encapsulated with cells from three different adult bovine donors. C) Comparison of hydrogel moduli of constructs encapsulated with young and adult donors.....	32
Figure 4. To investigate if chondrocytes interacted with multifunctional monomers, chondrocytes were incubated in a solution containing 8-arm PEG-NB or PEGdSH (A). After 10 mins of incubation, the monomers were separated via centrifugation and polymerized with an increasing concentration of the other monomer. Compressive moduli of hydrogels formed from fresh and soaked 8-arm PEG-NB (B) or fresh and soaked PEGdSH (C).....	33

Figure 5. Compressive moduli of hydrogels formed by crosslinking 8-arm PEG-NB with a PEGdSH crosslinker. The initial formulation was 10% (g/g) PEG-NB crosslinked at a 1:1 [thiol]:[ene] stoichiometric ratio. The concentration of 8-arm PEG-NB was decreased while keeping the concentration of PEGdSH constant. Significant differences in modulus was observed after a 0.2% (g/g) decrease in PEG-NB ( $p < 0.0001$ ). ..... 34

Figure 6. Modulus of hydrogels formed from fresh monomers and monomers exposed to cells. Chondrocytes were suspended in a solution containing the precursor monomers (A) or soaked in a solution containing precursor monomers and then separated (B). The mixtures from (A) and (B) are then photopolymerized to form acellular and cellular hydrogels (C). Comparison of hydrogel moduli of PEG-NB (blue) and PEG-CAP-NB (yellow) formed with different monomer pretreatments and cell encapsulation concentrations. D) Compressive moduli of acellular PEG-NB and PEG-CAP hydrogels. E) Compressive moduli of PEG-NB and PEG-CAP-NB hydrogels normalized to the respective moduli in panel (D). Hydrogels were formed from monomers soaked in solutions with varying cell concentrations ('soak') and encapsulated with various cell concentrations ('cellular'). ..... 36

Figure 7. Confocal microscopy of cells encapsulated in fluorescently labeled hydrogels. Dithiolated crosslinkers were fluorescently labeled using a maleimide-conjugated fluorophore (A). These fluorescently labeled thiols were mixed with multi-armed PEG with either cells or fluorescent polystyrene beads (B) to form fluorescently labeled hydrogels (C). D) (Inset) Confocal microscopy image of fluorescent polystyrene beads (red) in a fluorescently labeled PEG hydrogel (green). Fluorescence profile of the line in the inset. The blue arrow highlights the bead and the red arrow highlights the gradient in PEG density around the bead. E) (Inset) Confocal microscopy image of Calcein-stained chondrocytes (green) encapsulated in a fluorescently labeled PEG hydrogel (red) crosslinked with a nondegradable crosslinker. Fluorescence profile of the line in the inset. F) (Inset) Confocal microscopy image of Calcein-stained chondrocytes (green) encapsulated in a fluorescently labeled PEG hydrogel (red) crosslinked with an enzymatically degradable crosslinker (MMP-degradable GCVPLS-LYSGCG). Fluorescence profile of the line in the inset. The blue arrow highlights the cell (the boundary between the cell and hydrogel network is denoted by a dashed vertical line) and the red arrow highlights the gradient in PEG density around the cell. G) Measurements of the ratio of the width of the PEG density gradient (red arrows in panel D, E, and F) to the diameter of the cell or polystyrene bead diameter (blue arrows in panel D, E, and F). For each hydrogel condition, fluorescence profiles ( $n=100$ ) were analyzed across 3-4 hydrogels..... 38

Figure 8. Top row) Confocal microscopy images of fluorescently labeled nondegradable hydrogels cultured over 10 days. The histogram represents the growth of the void areas (degradation) over 10 days. Bottom row) Confocal microscopy images of fluorescently labeled hydrolytically degradable hydrogels cultured over 10 days. The histogram represents the growth of the void areas (degradation) over 10 days ..... 41



Figure 9. Schematic of possible outcomes in cell-laden hydrolytically degradable hydrogels. A) Cells encapsulated in a hydrogel with a spatially homogeneous crosslinking density resulting in the hydrogel reaching global reverse gelation. B) Cells encapsulated in a hydrogel with a gradient of crosslinking density around the cell resulting in the area around the cell reaching reverse gelation first. C) Confocal microscopy images of cells encapsulated in a hydrolytically degradable hydrogel observed over 10 days. Red = PEG. Green = cells (calcein). Scale bar = 50  $\mu\text{m}$ ; Images are sum of z-stacks. .... 47

## Chapter 4

Figure 1. A) Microparticles formed from poly (lactic-co-glycolic acid) (PLGA) were mixed with eight-arm PEG-norbornene (PEG-NB, MW 20kDa) crosslinked with an MMP-sensitive peptide crosslinker (GCVPLS-LYSGCG, MW 1155). A fraction of the crosslinkers were tagged with a fluorophore. The mixture was photopolymerized to create a crosslinked network with physically entrapped microparticles. B) As the PLGA microparticles hydrolytically degrade, they release their collagenase payload. The released collagenase then degrades the MMP-sensitive crosslinks of the hydrogel network. .... 58

Figure 2. A) Sample SEM images of microparticles with no enzyme encapsulated, 0.20 mg collagenase/mg PLGA, and 0.13 mg collagenase/mg PLGA. B) Cumulative enzyme release kinetics of PLGA microparticles loaded with 0.20 mg collagenase/mg PLGA and 0.13 mg collagenase/mg PLGA. A (\*) at each time point denotes that cumulative enzyme release at each time point is significantly ( $p < 0.04$ ) different between the two microparticle conditions. .... 60

Figure 3. Modulus of hydrogel constructs loaded with blank particles, 0.20 mg collagenase/mg PLGA particles, and 0.13 mg collagenase/mg PLGA particles. A) Absolute modulus of hydrogels loaded with particles. B) Normalized modulus of hydrogels loaded with particles. .... 62

Figure 4. A) Laser scanning confocal microscopy (LSCM) images of fluorescently labeled hydrogels encapsulated with blank particles, 0.20 mg collagenase/mg PLGA, or 0.13 mg collagenase/mg PLGA. The dark regions can be attributed to the space occupied by microparticles and degraded areas of hydrogel. B) Histograms showing the area of void spaces over time. A p-value shows that the histogram from 90 hrs is statistically different from the histogram from 46.5 hrs for the same enzyme concentration. The number of voids counted for hydrogels with blank particles was ( $n \approx 2000$ ), with 0.20 mg collagenase/mg PLGA particles was ( $n \approx 3000-4000$ ), and 0.13 mg collagenase/mg PLGA particles was ( $n \approx 3000-5000$ ). The mean diameter of each distribution is represented in the top left corner of each histogram with the standard deviation represented in parentheses. .... 64

## Chapter 5

Figure 1. Schematic of hydrogel formation and cell encapsulation by a photoclickable thiol:norbornene reaction. A) Non-degradable hydrogels were formed by reacting monomers of eight-arm PEG-norbornene (PEG-NB) with crosslinkers of PEG-dithiol (PEGdSH) under cytocompatible photoinitiating conditions. The thiol:ene molar ratio used to form the hydrogels and the resulting compressive modulus ( $E$ ) after cell encapsulation and 24 hours of swelling are provided. B) Enzyme-sensitive hydrogels were formed by reacting monomers of eight-arm PEG-norbornene (PEG-NB) with bis-cysteine peptide crosslinkers sensitive to aggrecanase, CRDTEGE-ARGSVIDRC, under cytocompatible photoinitiating conditions. The thiol:ene molar ratio used to form the hydrogels and the resulting compressive modulus ( $E$ ) after cell encapsulation and 24 hours of swelling are provided. C) Two cell sources based on donor age and joint were investigated and are referred to as juvenile chondrocytes and adult chondrocytes. .... 78

Figure 2. A multiscale computational model is used to describe spatiotemporal behavior of cell-secreted enzymes, hydrogel degradation, ECM growth, and macroscopic properties. A) At the sub-microscale, the model describes the spatiotemporal evolution of the hydrogel crosslink density where cell-secreted enzymes cleave hydrogel crosslinks in the polymer network (red) allowing for the spatial elaboration of neo-tissue. A chondrocyte is depicted secreting enzymes (green) and ECM molecules (black). Complete degradation near the cell surface is required for ECM molecule diffusion. B) At the microscale, the model considers regions of high cell densities (i.e., clusters of cells) and regions of low cell densities (single cells, i.e., non-clusters) to describe the evolution of mechanical properties. Particularly, the spatial crosslinking density around cells is characterized. C) The macroscale considers clustered cell distributions over large regions and its effect in the temporal evolution of mechanical properties. .... 83

Figure 3. Characterization of the initial properties of cell-laden aggrecanase-sensitive hydrogels. A) The compressive modulus of aggrecanase-sensitive hydrogels with and without encapsulated chondrocytes. B) Representative confocal microscopy image of living (green) juvenile chondrocytes encapsulated in an aggrecanase-sensitive hydrogel at day 1. There is evidence of spatial heterogeneities in cell distribution, showing regions with clustering of cells and regions of single cells. Magnification is 100x. C) The term  $R_d$  is introduced, which describes the extent of a hydrogel crosslink density gradient around cells immediately after encapsulation.  $R_d$  is defined as the distance between the cell boundary (shown in orange) to the point at which the crosslinking density reaches 99% of the bulk hydrogel crosslinking ( $\rho_{x,o}$ ). D) Modeling results describing the compressive modulus of a cell-laden hydrogel (solid blue line) as a function of increasing  $R_d$ . The cells are assumed to have a modulus of 1 kPa. The ordinate axis is normalized to the modulus of the gel with no cells corresponding to a  $R_d$  value of zero. The crossover point of the experimentally determined compressive modulus of a cell-laden aggrecanase-sensitive hydrogel (solid black dot) and the simulated compressive modulus yields an average value of  $R_d$  (dotted black line). E) Representative volume elements (RVEs) of cells with increasing  $R_d$ . As  $R_d$  increases, the crosslinking density between cells decreases which causing a reduction in the (*cont'd*)

(Chapter 5 Figure 3 cont'd) overall compressive modulus and leading to failure of the hydrogel. Note that reverse gelation occurs at  $\rho_x/\rho_{x0} = 0.563$ . The experimental data shown here are for juvenile chondrocytes. .... 94

Figure 4. Characterization of the ECM modulus in non-degradable hydrogels seeded with juvenile chondrocytes. A) The compressive modulus of non-degradable hydrogel constructs encapsulated with chondrocytes with culture time. B) Production rate of ECM molecules (sGAGs and total collagen) by encapsulated chondrocytes in non-degradable hydrogels with culture time. C) Representative microscopy image of a section stained for sGAGs (red) of chondrocytes encapsulated in non-degradable hydrogels at 6 weeks. Scale bar is 25  $\mu\text{m}$ . The yellow arrows indicate the thickness of the ECM with average and (standard deviation). Modeling results for construct modulus as a function of different ECM moduli. The crossover point of the simulated construct modulus (solid blue line) and the experimental construct modulus (solid black dot) gives the estimated ECM modulus (dotted black line). D) Representative microscopy image of a section stained for sGAGs (red) of chondrocytes encapsulated in non-degradable hydrogels at 12 weeks. Scale bar is 25  $\mu\text{m}$ . The yellow arrows indicate the thickness of the ECM with average and (standard deviation). Modeling results for construct modulus as a function of different ECM moduli. The crossover point of the simulated construct modulus (solid blue line) and the experimental construct modulus (solid black dot) gives the estimated ECM modulus (dotted black line). E) The ECM modulus as a function of ECM concentration ( $C_{\text{ECM}}$ ) within the hydrogel construct as determined by the model (circle). A linear fit gives a relationship between the ECM concentration and the ECM modulus. .... 98

Figure 5. Characterization of the spatiotemporal degradation of aggrecanase-sensitive hydrogels. A and D) Rate of enzyme (aggrecanase) production per cell per day for juvenile and adult chondrocytes encapsulated in the aggrecanase-sensitive hydrogel is shown. B and E) Enzyme (aggrecanase) concentration as a function of distance from the cell ( $x$ ) normalized to a critical length,  $L_c$  (defined as the average distance between two individual cells assuming a homogenous distribution of cells, which is 50  $\mu\text{m}$ ), where  $x=0$  is the boundary of a single cell is shown. Enzyme concentration is shown for day 1, week 3, week 6, week 9 and week 12 for juvenile and adult chondrocytes. C and F) Hydrogel crosslink density (normalized to the initial crosslinking density  $\rho_{x,0}$ ) is shown as a function of distance from the cell ( $x$ ) normalized to a critical length,  $L_c$  is shown. Hydrogel crosslink density is shown for day 1, week 3, week 6, week 9 and week 12 for juvenile and adult chondrocytes. The critical length,  $L_c$ , is 50  $\mu\text{m}$ . .... 102

Figure 6. Characterization of ECM production and construct modulus for aggrecanase-sensitive hydrogels encapsulated with juvenile or adult chondrocytes over 12 weeks. A) Production rate of ECM molecules (sGAGs and total collagen) by chondrocytes in aggrecanase-sensitive hydrogels. B) The experimentally measured compressive modulus of aggrecanase-sensitive hydrogels for juvenile (black) and adult (gray) chondrocytes as a function of culture time. The overall compressive modulus of the cell-laden constructs steadily decreased with culture time ( $p < 0.001$ ) and was affected ( $p = 0.049$ ) by cell source. C and D) Representative microscopy images of a section stained for sGAGs (red) of juvenile or adult chondrocytes encapsulated in aggrecanase-sensitive hydrogels at 12 weeks. Scale bar is 1 mm. Scale bars for zoomed in sections of hydrogel are 50  $\mu\text{m}$ . ..... 105

Figure 7. Cumulative amount of ECM produced for juvenile and adult chondrocytes encapsulated in nondegradable (ND) and degradable (DEG) hydrogels after 12 weeks of culture. The amount found in media (white bar) and the amount found in the constructs (grey bar) are shown. Total amount of ECM was similar in nondegradable and degradable hydrogels for the same cell source. .... 106

Figure 8. A) The degradation of the polymer network through time in the environment of multiple juvenile cells (i). The tissue evolution through time in the environment of multiple juvenile cells (ii). Collagen II immunohistological stains of juvenile cells (iii). Aggrecan immunohistological stains of juvenile cells (iv). B) The degradation of the polymer network through time in the environment of multiple juvenile cells (i). The tissue evolution through time in the environment of multiple juvenile cells (ii). Collagen II immunohistological stains of juvenile cells (iii). Aggrecan immunohistological stains of juvenile cells (iv). C) The degradation of the polymer network through time in the environment of multiple adult cells (i). The tissue evolution through time in the environment of multiple adult cells (ii). Collagen II immunohistological stains of adult cells (iii). Aggrecan immunohistological stains of adult cells (iv). D) The degradation of the polymer network through time in the environment of multiple adult cells (i). The tissue evolution through time in the environment of multiple adult cells (ii). Collagen II immunohistological stains of adult cells (iii). Aggrecan immunohistological stains of adult cells (iv). Panels A and C represent modeling results and experimental observations in clustered regions, while panels B and D represent nonclustered regions. Scale bar is 50  $\mu\text{m}$ . ..... 109

## Chapter 6

Figure 1. A hierarchical multiscale computational approach of a cell-laden hydrogel. The submicro-scale is represented by the hydrogel. The micro-scale is represented by a finite number of cells embedded in a hydrogel whose crosslink density varies according to its distance from the cell. The macro-scale is represented by a macroscopic hydrogel construct for which cell density is located at a macroscopic point  $\mathbf{x}_i$  and is represented by a heterogeneous function  $f(\mathbf{x})$ ..... 128

Figure 2. A) Representative confocal microscopy images of cell viability one-day after encapsulation in PEG-CAP hydrogels for seeding densities of 50, 100, and 150 million chondrocytes per volume (mL) of precursor solution. Live cells fluoresce green; dead cells fluoresce red; scale bar = 50  $\mu\text{m}$ . B) Cell number measured through DNA content one-day after encapsulation for seeding densities of 50, 100, and 150 million chondrocytes per volume (mL) of precursor solution. C) The initial compressive modulus of cell-laden PEG-CAP hydrogel one-day after encapsulation for seeding densities of 0, 50, 100, and 150 million chondrocytes/mL of precursor solution..... 134

Figure 3. A) Top Row: Representative confocal microscopy images of only live cells (green) in hydrogels with encapsulated chondrocytes at low (50M cells/mL), medium (100M cells/mL) and high (150M cells/mL) cell seeding densities, which were used in the cluster analysis. The microscopy images are the same images in Figure 2A, but with only live cells depicted. Scale bar = 50  $\mu\text{m}$ . Bottom Row: 2D simulation results showing cluster mapping for each of the three different cell densities. B) Top/bottom rows: Representative volume elements for microscale background and clustered cell densities, respectively, for low, medium, and high cell seeding densities showing the crosslink density gradient. Cells are shown in green. Middle row: Macroscale constructs with a heterogeneous distribution of cell volume fraction. C) Modeling results (gray bars) of the initial macroscopic compressive modulus ( $E_0$ ) assuming the hydrogel constructs act as a composite material with the presence of cell clusters and the experimentally determined initial compressive modulus (black squares). Errors bars represent standard deviation for the model (n=5) and experiments (n=3). ..... 138

Figure 4. A) A schematic of  $R_d$ . The radius  $R_d$  is defined as the zone where the hydrogel crosslink density is reduced due to the cell's interaction with radicals. As such,  $R_d$  controls the crosslink density at a distance  $x$  from the cell surface. B) The effect of  $R_d$  on the spatial variation in hydrogel crosslink density between two cells. Two cases are shown for a low local cell volume fraction ( $f=0.05$ ) and a high local cell volume fraction ( $f=0.20$ ) for varying values of  $R_d$ . Results from 3D simulations for  $f=0.05$  (top) and  $f=0.20$  (bottom) are shown for the two cases for  $R_d/R_c = 7$  where cells (green) are embedded within a hydrogel. The spatial variation in crosslink density ( $\rho_x$ ) is shown decreasing from red (equivalent to the bulk crosslink density) to blue (equivalent to the reverse gelation point). The distance between cells ( $d_{\text{cell}}$ ) varies based on the volume fraction and was 3.43  $\mu\text{m}$  and 1.42  $\mu\text{m}$  for  $f=0.05$  and  $f=0.20$ , respectively. C) Simulation results are shown for the macroscopic compressive modulus for the two cases of cell volume fraction as a function of  $R_d/R_c$ . The modulus is normalized to the modulus at  $R_d=0$ . The black line represents  $f=0.05$  and the gray line represents  $f=0.20$ . Simulation data are presented as mean with standard deviation for  $n=3$ . D) Simulations for the initial compressive modulus of low, medium, and high cell seeding density are shown as a function of  $R_d/R_c$ . An  $R_d/R_c$  of 27 was selected based on minimizing the error between simulations and experiments (black squares). Data are presented as mean with standard deviation ( $n=3$ ). E) The initial compressive modulus for each seeding density for both the experiments (white bars) and simulations with  $R_d/R_c=27$  (gray bars). Experimental and modeling data are presented as mean with standard deviation ( $n=3$ ). ..... 141

Figure 5. Characterization of the cell-laden hydrogel constructs as a function of culture time for A) compressive modulus, B) DNA content, C) sulfated glycosaminoglycan (sGAG) content per construct, D) sGAG per DNA, E) total collagen content per construct, and F) total collagen content per DNA for low (50M cells/mL) (○), medium (100M cells/mL) (□), and high (150M cells/mL) (◇) density. Dot plots are shown for individual repeats and the horizontal line represents the mean. .... 143

Figure 6. Representative confocal microscopy images of immunohistological sections stained for collagen II and aggrecan after 1 day (i.e., week 0), week 4 or week 12 of culture for hydrogel with low (A), medium (B) and high (C) cell densities. Nuclei are stained with DAPI (blue). Scale bar = 20 μm. .... 145

Figure 7. Simulation results for low, medium, and high cell densities showing A) normalized crosslink density (○) and ECM concentration (◇), where crosslink density is normalized to the crosslink density of the acellular construct, and B) representative volume elements depicting the spatial distribution of ECM and crosslink density at 0, 15, and 30 days for low, medium, and high cell densities. C) Evolution of *E*, the compressive modulus, (○) over time (experimental data from week 0 and 4 shown as solid squares, ▴). Error bars represent standard deviation from 3 different simulations or experimental replicates (n=3). .... 147

## Chapter 7

Figure 1. A) Hydroxyproline production normalized to DNA content of young and adult chondrocytes cultured over a period of six days. B) sGAG production normalized to DNA content of young and adult chondrocytes cultured over a period of six days. By day 6, application of soluble IGF-1 at 50 ng/mL enhanced hydroxyproline and sGAG production of adult chondrocytes similar to that of young chondrocytes (highlighted by a red rectangle). .... 168

Figure 2. Representative confocal microscopy image of living (green) juvenile chondrocytes encapsulated in MMP-sensitive hydrogels. There is evidence of spatial heterogeneities in cell distribution, showing regions with clustering of cells and regions of single cells. Magnification is 100x. Viability remained high throughout the four-week culture. Scale bars are 50 μm. .... 170

Figure 3. Average DNA content (A) and bulk compressive modulus (B) of cell-laden hydrogels through four weeks. In (A), an (\*) denotes that the DNA content in both hydrogel conditions with adult chondrocytes were significantly different than hydrogels encapsulated with young chondrocytes at each time point. In (B), an (\*) denote that the average modulus of both hydrogel conditions with adult chondrocytes were significantly different than hydrogels encapsulated with young chondrocytes at each time point. .... 171

Figure 4. A) Cumulative hydroxyproline production in hydrogel constructs encapsulated with young and adult chondrocytes cultured over a period of four weeks. B) Cumulative sGAG production in hydrogel constructs encapsulated young and adult chondrocytes cultured over a period of four weeks. .... 172

Figure 5. Enzyme activity of young and adult chondrocytes cultured over a period of four weeks. Application of soluble IGF-1 at 50 ng/mL reduced enzyme activity of adult chondrocytes by week 4. .... 173

Figure 6. Representative microscopy images of hydrogel sections stained for sGAGs (red) of young or adult chondrocytes encapsulated in MMP-sensitive hydrogels. Scale bars are 50  $\mu$ m. .... 174

Figure 7. Representative microscopy images of hydrogel sections stained for collagen II (green) of young or adult chondrocytes encapsulated in MMP-sensitive hydrogels. Cell nuclei were counterstained with DAPI (blue). Scale bars are 50  $\mu$ m. .... 176

Figure 8. Representative microscopy images of hydrogel sections stained for collagen I (green) of young or adult chondrocytes encapsulated in MMP-sensitive hydrogels. Cell nuclei were counterstained with DAPI (blue). Scale bars are 50  $\mu$ m. .... 177

Figure 9. Representative microscopy images of hydrogel sections stained for the C1, 2C epitope (green), a marker of collagen degradation, of young or adult chondrocytes encapsulated in MMP-sensitive hydrogels. Cell nuclei were counterstained with DAPI (blue). Scale bars are 50  $\mu$ m. 179

Figure 10. Schematic representation of a personalized hydrogel platform. A) A cartilage explant is obtained from the patient from a non-load bearing section of cartilage. B) After liberation from the cartilage matrix, harvested chondrocytes are expanded in culture. C) During chondrocyte expansion, the chondrocytes are screened for their tissue and enzyme production capacities. In the case of cartilage tissue engineering, collagen and aggrecan (or sGAGs) are of importance. D) The patient's specific tissue and enzyme synthesis rates are input parameters to a computational model that simulates tissue deposition and enzyme-mediated hydrogel degradation based on patient specific rates. E) The computational model formulates a patient-specific hydrogel design in order to match hydrogel degradation and tissue production to avoid construct failure. F) The expanded chondrocytes from step (B) are combined with a precursor solution matching the hydrogel formulation designed in step (E). G) The chondrocyte-precursor solution is injected into the cartilage defect and polymerized in situ. .... 181

## Chapter 1. Introduction

### 1.1 Hydrogels

Hydrogels, broadly defined as highly swollen polymer networks with >80% water content, are excellent vehicles for cell encapsulation<sup>1</sup> and therefore have promising potential in regenerative tissue engineering applications. Hydrogels are made of crosslinked polymer chains, which can be composed of naturally derived biopolymer chains or synthetic polymers. Implantable hydrogel scaffolds composed of naturally occurring polymers, such as collagen<sup>2</sup>, agarose<sup>3</sup>, or hyaluronic acid<sup>4</sup>, are attractive due to their natural bioactivity<sup>5,6</sup> and degradability<sup>6</sup> in the body. However, the properties of hydrogels (e.g. mechanical properties and degradation rates) formed from naturally derived biopolymers are difficult to control<sup>1</sup>. On the other hand, hydrogels made of synthetic polymers offer far more chemical control, allowing the user to impart different biofunctionalities and properties to the hydrogel<sup>7-9</sup>. For instance, bioactive molecules such as growth factors have been incorporated into the polymer network to provide sustained and localized growth factor exposure<sup>10,11</sup> and enzyme-labile peptides have been used as crosslinks to form bioresponsive hydrogels<sup>11-13</sup>. Hydrogel material properties such as stiffness can be controlled through modulating monomer concentration<sup>14,15</sup> and polymer chemistries can be altered to create dynamic, adaptable networks to influence cell phenotype<sup>16-18</sup> and matrix producing capabilities<sup>19</sup>. Additionally, network chemistries can be altered to create stimuli-responsive 'smart' hydrogels<sup>20</sup> and also to enable spatiotemporal control over degradation to direct cell growth<sup>21,22</sup>.

Hydrogels are particularly well suited for regenerative therapies of orthopaedic tissues. Matrix producing cells (e.g. osteoblasts, tenocytes, chondrocytes, etc.) can be physically



entrapped in the hydrogel which initially acts as a substitute for the tissue of interest and as a support scaffold for the encapsulated cells. The hydrogel can further be customized to provide biochemical or mechanical cues to the cells that potentially augment cellular bioactivity. Hydrogel platforms are particularly well suited for cartilage tissue engineering therapies because the 3D environment can maintain the rounded morphology of chondrogenic cells<sup>5</sup> without further hydrogel modification.

In regenerative cartilage strategies, the choice of cell type to encapsulate in the hydrogel is of interest. Current clinical therapies that rely on the regenerative potential of cells include microfracture that recruit mesenchymal stem cells (MSCs) from the bone marrow and autologous chondrocyte implantation (ACI) that relocates healthy cartilage cells originating from the patient to the cartilage defect secured by a periosteal patch. Current research in the field utilizes both stem cells and/or chondrocytes encapsulated in 3D hydrogels (made of natural or synthetic polymers). Stem cells are attractive due to their multilineage potential and more abundant numbers (due to their ability to be harvested from a variety of sources); however, differentiation into and maintenance of the chondrogenic phenotype remains a challenge and often the cartilage produced by differentiated stem cells is a mechanically inferior, collagen I-rich fibrocartilage<sup>5</sup>. On the other hand, chondrocytes are already in the native cartilage phenotype and have been shown to produce a more hyaline-like cartilage rich in collagen II<sup>7</sup>.

Natural healthy cartilage is primarily composed of collagen II and aggrecan proteins. Small collagen precursors called tropocollagen make up the collagen II architecture which can reach up to microns in length<sup>23</sup>. Aggrecan is a high molecular weight (up to  $3 \times 10^6$  Da<sup>24</sup>) core protein that serves as an anchor to sulfated glycosaminoglycans (GAGs) such as keratan sulfate and

chondroitin sulfate and these complexes can reach up to 400 nm in length<sup>25,26</sup>. These negatively charged GAGs cause the cartilage to swell with water imparting the cartilage with compressive strength<sup>27</sup>. The aggrecan and GAGs form a bottle-brush like structure which attaches to a core hyaluronic acid polysaccharide forming an even larger structure. These cartilage macromolecules are too large to diffuse through the mesh size many hydrogel scaffolds. Indeed, research studies encapsulating primary chondrocytes in nondegradable hydrogels have shown deposited collagen II and aggrecan matrices to be restricted to the pericellular space<sup>28</sup>. Physically restricted extracellular matrices (ECMs) have even been shown to reduce the total amount of collagen and aggrecan produced by encapsulated chondrocytes<sup>28</sup>. On the other hand, hydrogels with increased degradability have been shown to increase collagen II synthesis of encapsulated chondrocytes compared to collagen I synthesis<sup>14,28</sup> and also allows for spatial elaboration of neotissue<sup>28,29</sup>. Therefore, current research efforts have been focused on utilizing degradable hydrogels for cartilage tissue engineering.

## **1.2 Degradable Hydrogels**

To create degradable synthetic hydrogels, chemical bonds that are susceptible cleavage by water or enzymes can be introduced into the network architecture. As these bonds are cleaved, the mesh size of the hydrogel also increases allowing for large tissue molecules to diffuse away from the encapsulated cell. Since water is ever present in hydrogels (and even in cartilage makes up to 80% of the wet weight of cartilage), hydrogels susceptible to hydrolytic cleavage undergo global bulk degradation whereas degradation is necessary only near the cell due to its appositional ECM production. Therefore, hydrolytic degradation often leads to a dramatic loss in hydrogel mechanical properties over time leading to a greater risk in construct failure (i.e., loss

of hydrogel prior to tissue connectivity). However, some studies utilizing hydrolytically degradable cell-laden hydrogels have supported the formation of hyaline-like cartilage<sup>30</sup>. Instead, research efforts have increasingly been more focused in incorporating enzymatically degradable peptide crosslinks in the hydrogel network. An enzymatic mode of degradation is attractive because it has the potential to be localized to the area around the cell thereby reducing the risk of construct failure during the transitional phase from polymer to neotissue. Furthermore, the amino acid sequence of peptide crosslinks can be specifically designed to be cleaved by enzymes in the chondrocyte secretome and selected based on the temporal secretion of enzymes as a function of cartilage disease progression<sup>10-13</sup>. Additionally, peptide crosslinks can potentially be the subject of protein engineering to create sequences that are more readily incorporated into the hydrogel architecture or to alter the reactivity towards enzymes<sup>9</sup>.

### **1.3 The Role of Computational Modeling in Cartilage Tissue Engineering**

While degradable cell-laden hydrogels are a promising platform for cartilage defect repair, significant challenges still exist in the design of these hydrogels for cartilage tissue engineering. A successful hydrogel platform for tissue engineering can be characterized by three phases: 1) an initial solid phase of the hydrogel construct, which is composed purely of cells encapsulated in a polymer network; 2) a transitional solid phase where the polymer network degrades and is replaced by neotissue; and 3) the chondrocytes are embedded in a matrix composed completely of a neotissue solid phase where the cells continue to maintain and remodel the ECM. In the transitional phase, the hydrogel construct has the potential for failure if the degradation of the network is too fast relative to the matrix producing potential of the encapsulated cells. On the other hand, if degradation is too slow, newly formed ECM will be

restricted to the space around cells. Therefore, a critical challenge in the design of degradable hydrogels for tissue engineering applications is to finely tune the rate of hydrogel degradation such that it approximates the rate of tissue production<sup>1,5</sup>. As both hydrogel degradation can be tuned (via changes in the polymer chemical structure and the selection of peptide sequences) and tissue production can vary (due to donor-to-donor differences and external stimuli such as growth factors), tissue engineers have looked towards developing and utilizing computational methods to analyze the tissue engineering experimental space.

Hydrogel degradation is an important feature in many tissue engineering applications and thus understanding of hydrogel degradation is a crucial component in designing hydrogels. In an effort to understand both hydrolytic and enzymatic degradation, models are being developed based on the reaction kinetics of hydrolytic degradation<sup>31,32</sup> and the kinetics of peptide degradation by enzymes based on Michaelis-Menten kinetics<sup>33</sup>. These models are built on the foundation of Flory-Rehner theory<sup>34</sup> that can be used to derive the hydrogel crosslinking density. Rubber elasticity theory<sup>15</sup> then describes how the crosslinking density contributes to the mechanical properties of the hydrogel. In tissue engineering applications, the diffusion of nutrients and biomolecules through the hydrogel are important and are described by Lustig and Peppas<sup>35</sup>. Statistical models of hydrolytic bulk degradation have been established<sup>13-15</sup> and have been instrumental in understanding the degradation of non-linear polymer systems. Enzymatic degradation, however, is often difficult to experimentally characterize and observe and thus this mode of degradation is poorly understood. Models characterizing enzymatic degradation focus on the reaction-diffusion kinetics of the enzyme and peptide crosslinker substrate.

The use of hydrogels in regenerative cartilage tissue engineering is often a dynamic process with the encapsulated cells continually depositing new matrix while the polymer network degrades. Thus, it can be quite challenging to model this composite material with ever changing volume fractions of each phase. Efforts have been made to understand the role of hydrogel degradation in the context of tissue growth<sup>29,37-40</sup>. Computational models have been developed that describe cell-laden hydrogels as a composite of three phases: solid, fluid, and unbound tissue molecules<sup>29</sup>. These models identified that hydrogel degradation is necessary for tissue transport. Lalitha-Sridhar et al. has developed fundamental principles in designing degradable hydrogels for the circumvention of hydrogel failure<sup>38</sup> and described spatiotemporal hydrogel degradation<sup>37</sup>.

#### **1.4 Patient Variability and Personalized Regenerative Medicine**

In the field of medicine, it is recognized that “one-size-fits-all” therapies will have variable therapeutic outcomes due to individual donor variations. Recently, there has been a move towards personalized medicine with the most publicized example being individual genomic sequencing for predicting an individual’s genetic risk factors for diseases. Indeed, there has been growing recognition that the next era of medicine will require therapeutic strategies to be tailored to individuals to improve patient outcomes<sup>41</sup>. In 2016, the Obama Administration invested \$215 million to launch the Precision Medicine Initiative, a collective of federal research efforts to move toward individualized care. These include the National Institute of Health’s (NIH) Precision Medicine Initiative (PMI) Cohort Program which envisions the participation of over 1 million individuals to understand long-term factors in health and disease. The Food and Drug Administration (FDA) is working towards developing standards and methods for testing the quality of personalized therapeutic strategies.

Autologous chondrocyte implantation (ACI) is a current clinical treatment used for cartilage defect repair; however, the long-term success of this strategy is variable and is dependent on the bioactivity of the patient's cells. Patient age is a significant and well-documented factor in the bioactivity of chondrocytes with older chondrocytes having less regenerative capabilities than younger chondrocytes<sup>5</sup>. In addition to age, other factors such as patient genetics, sex, ethnicity, health status, and level of activity can all play a role in the regenerative potential of the cells<sup>42</sup>. Therefore, a robust hydrogel platform must be developed to overcome donor variability to improve tissue engineering outcomes for all.

Towards the goal of individualized hydrogel therapies, computational models that can accurately describe hydrogel degradation and tissue production can become powerful predictive tools for tissue engineers and can also help identify critical parameters in hydrogel design. Collectively, scaffold design, cell bioactivity, and predictive computational resources can push regenerative medicine strategies into a new era of personalized medicine<sup>43</sup>.

### **1.5 Approach of This Dissertation**

This research has focused on identifying new design parameters and considerations when designing degradable hydrogels for cartilage tissue regeneration. Specifically, this research has employed crosslinked poly (ethylene glycol) (PEG) as the primary component to hydrogels due to its ease of use, hydrophilic properties, and promise in cartilage tissue engineering. Chondrocyte sources from bovine and porcine were used as model cells, although the major findings in this dissertation can readily be translated to other polymer chemistries as well as cell types.

The approach of this dissertation begins by elucidating some of the phenomena that occur during cellular photoencapsulation. The overarching aim is to more clearly define the initial state of the hydrogel which is critical in developing computational models to understand hydrogel degradation and tissue formation. These models are then applied to hydrolytically degradable and enzyme-sensitive hydrogel platforms to identify hydrogel design parameters that were critical in promoting tissue formation. The model is rooted in physical equations rather than empirical correlations, making it more robust in its translation to other polymer chemistries and cell bioactivities. Finally, this dissertation addresses some of the challenges associated with donor variability. Primary bovine chondrocytes of different ages are used to represent a difference in the regenerative potential of chondrocytes. Insulin-like Growth Factor 1 (IGF-1) is applied to adult chondrocytes encapsulated in hydrogels and the resulting tissue is compared to that of young chondrocytes and untreated adult chondrocytes. Additionally, the future work in developing methods for creating a computationally-driven rationally-designed hydrogel are described.

## 1.6 References

1. Nicodemus, G. D. & Bryant, S. J. Cell Encapsulation in Biodegradable Hydrogels for Tissue Engineering Applications. *Tissue Eng. Part B Rev.* **14**, 149–165 (2008).
2. Glowacki, J. & Mizuno, S. Collagen scaffolds for tissue engineering. *Biopolymers* **89**, 338–344 (2008).
3. A library of tunable agarose carbomer-based hydrogels for tissue engineering applications: The role of cross-linkers - Rossi - 2012 - Journal of Applied Polymer Science - Wiley Online Library. Available at: <https://onlinelibrary.wiley.com/doi/epdf/10.1002/app.34731>. (Accessed: 29th September 2018)
4. Jin, R. *et al.* Synthesis and characterization of hyaluronic acid–poly(ethylene glycol) hydrogels via Michael addition: An injectable biomaterial for cartilage repair. *Acta Biomater.* **6**, 1968–1977 (2010).

5. Chung, C. & Burdick, J. A. Engineering cartilage tissue. *Adv. Drug Deliv. Rev.* **60**, 243–262 (2008).
6. Lutolf, M. P. & Hubbell, J. A. Synthetic biomaterials as instructive extracellular microenvironments for morphogenesis in tissue engineering. *Nat. Biotechnol.* **23**, 47–55 (2005).
7. AO Research Institute Davos, Clavadelerstrasse 8, 7270 Davos Platz, Switzerland *et al.* Tissue engineering for articular cartilage repair – the state of the art. *Eur. Cell. Mater.* **25**, 248–267 (2013).
8. Bryant, S. J., Durand, K. L. & Anseth, K. S. Manipulations in hydrogel chemistry control photoencapsulated chondrocyte behavior and their extracellular matrix production. *J. Biomed. Mater. Res. A* **67A**, 1430–1436 (2003).
9. Lutolf, M. P. *et al.* Synthetic matrix metalloproteinase-sensitive hydrogels for the conduction of tissue regeneration: Engineering cell-invasion characteristics. *Proc. Natl. Acad. Sci.* **100**, 5413–5418 (2003).
10. Sridhar, B. V., Doyle, N. R., Randolph, M. A. & Anseth, K. S. Covalently tethered TGF- $\beta$ 1 with encapsulated chondrocytes in a PEG hydrogel system enhances extracellular matrix production. *J. Biomed. Mater. Res. A* **102**, 4464–4472 (2014).
11. Sridhar, B. V. *et al.* Development of a Cellularly Degradable PEG Hydrogel to Promote Articular Cartilage Extracellular Matrix Deposition. *Adv. Healthc. Mater.* **4**, 702–713 (2015).
12. Skaalure, S. C., Chu, S. & Bryant, S. J. An Enzyme-sensitive PEG Hydrogel Based on Aggrecan Catabolism for Cartilage Tissue Engineering. *Adv. Healthc. Mater.* **4**, 420–431 (2015).
13. Aisenbrey, E. A. & Bryant, S. J. A MMP7-sensitive photoclickable biomimetic hydrogel for MSC encapsulation towards engineering human cartilage. *J. Biomed. Mater. Res. A* **0**,
14. Bryant, S. J. & Anseth, K. S. Hydrogel properties influence ECM production by chondrocytes photoencapsulated in poly (ethylene glycol) hydrogels. *J. Biomed. Mater. Res.* **59**, 63–72 (2002).
15. Anseth, K. S., Bowman, C. N. & Brannon-Peppas, L. Mechanical properties of hydrogels and their experimental determination. *Biomaterials* **17**, 1647–1657 (1996).
16. Engler, A. J., Sen, S., Sweeney, H. L. & Discher, D. E. Matrix Elasticity Directs Stem Cell Lineage Specification. *Cell* **126**, 677–689 (2006).



17. Chaudhuri, O. *et al.* Substrate stress relaxation regulates cell spreading. *Nat. Commun.* **6**, 6365 (2015).
18. Hydrogels with tunable stress relaxation regulate stem cell fate and activity | Nature Materials. Available at: <https://www.nature.com/articles/nmat4489>. (Accessed: 14th November 2018)
19. Richardson, B. M., Wilcox, D. G., Randolph, M. A. & Anseth, K. S. Hydrazone covalent adaptable networks modulate extracellular matrix deposition for cartilage tissue engineering. *Acta Biomater.* (2018). doi:10.1016/j.actbio.2018.11.014
20. Xia, L.-W. *et al.* Nano-structured smart hydrogels with rapid response and high elasticity. *Nat. Commun.* **4**, 2226 (2013).
21. Secondary Photocrosslinking of Click Hydrogels To Probe Myoblast Mechanotransduction in Three Dimensions - Journal of the American Chemical Society (ACS Publications). Available at: <https://pubs.acs.org/doi/10.1021/jacs.8b07551>. (Accessed: 15th November 2018)
22. Brown, T. E. *et al.* Photopolymerized dynamic hydrogels with tunable viscoelastic properties through thioester exchange. *Biomaterials* **178**, 496–503 (2018).
23. Kääh, M. J., Ap Gwynn, I. & Nötzli, H. P. Collagen fibre arrangement in the tibial plateau articular cartilage of man and other mammalian species. *J. Anat.* **193**, 23–34 (1998).
24. Nap, R. J. & Szleifer, I. Structure and Interactions of Aggrecans: Statistical Thermodynamic Approach. *Biophys. J.* **95**, 4570–4583 (2008).
25. Horkay, F., Basser, P. J., Hecht, A.-M. & Geissler, E. Gel-like behavior in aggrecan assemblies. *J. Chem. Phys.* **128**, 135103 (2008).
26. Ng, L. *et al.* Individual cartilage aggrecan macromolecules and their constituent glycosaminoglycans visualized via atomic force microscopy. *J. Struct. Biol.* **143**, 242–257 (2003).
27. Kiani, C., Chen, L., Wu, Y. J., Yee, A. J. & Yang, B. B. Structure and function of aggrecan. *Cell Res.* **12**, 19–32 (2002).
28. Bryant, S. J. & Anseth, K. S. Controlling the spatial distribution of ECM components in degradable PEG hydrogels for tissue engineering cartilage. *J. Biomed. Mater. Res. A* **64A**, 70–79 (2003).

29. Dhote, V. *et al.* On the role of hydrogel structure and degradation in controlling the transport of cell-secreted matrix molecules for engineered cartilage. *J. Mech. Behav. Biomed. Mater.* **19**, 61–74 (2013).
30. Neumann, A. J., Quinn, T. & Bryant, S. J. Nondestructive evaluation of a new hydrolytically degradable and photo-clickable PEG hydrogel for cartilage tissue engineering. *Acta Biomater.* **39**, 1–11 (2016).
31. Metters, A. T., Bowman, C. N. & Anseth, K. S. A Statistical Kinetic Model for the Bulk Degradation of PLA-b-PEG-b-PLA Hydrogel Networks. *J. Phys. Chem. B* **104**, 7043–7049 (2000).
32. Martens, P., Metters, A. T., Anseth, K. S. & Bowman, C. N. A Generalized Bulk-Degradation Model for Hydrogel Networks Formed from Multivinyl Cross-linking Molecules. *J. Phys. Chem. B* **105**, 5131–5138 (2001).
33. Skaalure, S. C., Akalp, U., Vernerey, F. J. & Bryant, S. J. Tuning Reaction and Diffusion Mediated Degradation of Enzyme-Sensitive Hydrogels. *Adv. Healthc. Mater.* **5**, 432–438 (2016).
34. Flory, P. J. *Principles of Polymer Chemistry*. (Cornell University Press, 1953).
35. Lustig, S. R. & Peppas, N. A. Solute diffusion in swollen membranes. IX. Scaling laws for solute diffusion in gels. *J. Appl. Polym. Sci.* **36**, 735–747 (1988).
36. Metters, A. T., Anseth, K. S. & Bowman, C. N. Fundamental studies of a novel, biodegradable PEG-b-PLA hydrogel. *Polymer* **41**, 3993–4004 (2000).
37. Lalitha Sridhar, S. & Vernerey, F. Localized Enzymatic Degradation of Polymers: Physics and Scaling Laws. *Phys. Rev. Appl.* **9**, 031001 (2018).
38. Sridhar, S. L. *et al.* Heterogeneity is key to hydrogel-based cartilage tissue regeneration. *Soft Matter* **13**, 4841–4855 (2017).
39. Akalp, U., Bryant, S. J. & Vernerey, F. J. Tuning tissue growth with scaffold degradation in enzyme-sensitive hydrogels: a mathematical model. *Soft Matter* **12**, 7505–7520 (2016).
40. Dhote, V. & Vernerey, F. J. Mathematical model of the role of degradation on matrix development in hydrogel scaffold. *Biomech. Model. Mechanobiol.* **13**, 167–183 (2013).
41. Aguado, B. A., Grim, J. C., Rosales, A. M., Watson-Capps, J. J. & Anseth, K. S. Engineering precision biomaterials for personalized medicine. *Sci. Transl. Med.* **10**, eaam8645 (2018).

42. Behery, O., Siston, R. A., Harris, J. D. & Flanigan, D. C. Treatment of Cartilage Defects of the Knee: Expanding on the Existing Algorithm. *Clin. J. Sport Med.* **24**, 21–30 (2014).
43. Bryant, S. J. & Vernerey, F. J. Programmable Hydrogels for Cell Encapsulation and Neo-Tissue Growth to Enable Personalized Tissue Engineering. *Adv. Healthc. Mater.* **7**, (2018).

## **Chapter 2. Objectives**

The success of tissue engineering strategies using hydrogels depends on tuning the rate of hydrogel degradation relative to the rate of tissue production by encapsulated cells. This dissertation investigates critical parameters affecting polymer network formation and degradation and how these parameters influence tissue deposition. The overall hypothesis for this dissertation is that locally degrading hydrogels (through the use of enzymatically and hydrolytically sensitive polymer chemistries) support cartilage deposition by encapsulated chondrocytes while simultaneously preserving hydrogel mechanics. By tuning hydrogel degradation to reflect a blend of bulk and local degradation regimes, hydrogels for cartilage regeneration can be tailored to individual patient enzyme and matrix synthesis rates and enhance macroscopic cartilage tissue deposition and growth. The first objective was to characterize the local heterogeneities in the cell-hydrogel microenvironment in order to better understand locally degrading hydrogels. From these observations, the remainder of the dissertation was directed towards understanding how local variations in hydrogel crosslinking density contribute to macroscopic tissue deposition. These new understandings will ultimately allow us provide a more informed design of hydrogels tailored to account for patient-to-patient variations.

**2.1 Objective 1: Characterize the cell-hydrogel microenvironment in cell-laden hydrogels.**

**2.2 Objective 2: Identify the effect of heterogeneities within the hydrogel on macroscopic cartilage tissue formation by encapsulated cells.**

**2.3 Objective 3: Develop a hydrogel platform for donors of varying regenerative capabilities.**

These three objectives outline an approach to understanding hydrogel degradation and utilizing it towards designing personalized hydrogels. The first objective characterized the spatial hydrogel crosslinking density after hydrogel formation. By understanding the initial state of the polymer network, the hydrogel degradation behavior was characterized as a function of space and time. In the second objective, these spatial heterogeneities in crosslinking density are analyzed for their effect on tissue development and hydrogel degradation. Here, a computational model is applied to characterize and understand enzyme diffusion and tissue diffusion on the local cellular scale. Finally, a strategy is proposed towards augmenting the anabolic capabilities of cells with low regenerative potential and personalizing hydrogel-based regenerative medicine for donors of varying bioactivity.

## **Chapter 3. Chondrocyte-mediated reductions in local crosslinking density in radical polymerized hydrogels**

### **Abstract**

Many tissue engineering applications involve the use of encapsulated cells in order to regenerate the tissue of interest. The cell-matrix interactions are of particular interest due to previous findings that matrix stiffness directs cell morphology and phenotype and more recently, the development of cell-mediated degradable hydrogels proves a greater need to characterize the local cell-matrix environment to more accurately predict the time course of hydrogel degradation. In this work, evidence is provided that points toward the ability of suspended cells to inhibit the formation of photopolymerized polymer networks. Specifically, the bulk compressive modulus of cell-laden thiol-norbornene and acrylate hydrogels was reduced as a function of increasing cell encapsulation concentration. Encapsulation of cells in fluorescently labeled hydrogels also showed a gradient in PEG density around the cell. These data indicate that cells can reduce the concentration of monomers in the prepolymer solution and that cells interfere with the polymerization reaction, possibly by quenching free-radicals and inhibition of polymerization around cells. These interactions lead to an overall softer hydrogel as well as local reductions in crosslink density, both of which affect the local microenvironment around cells.

### **3.1 Introduction**

Synthetic hydrogel platforms formed by radical mediated chain polymerizations have been the subject of research in a variety of tissue engineering applications including (but not limited to) cartilage<sup>1,2</sup>, bone<sup>3</sup>, tendon<sup>4</sup>, and neural<sup>5</sup> regenerative tissue engineering. These hydrogels formed via free-radical polymerization are attractive due to their ability to allow for

rapid gelation times with high cell viability and facile incorporation of peptides without post-synthetic modification<sup>6</sup>.

Hydrogels made from synthetic polymers are attractive because they offer the user a high degree of control over mechanics and degradation<sup>7</sup>. Hydrogels formed from synthetic polymers are highly reproducible and tunable, allowing for researchers to study fundamental cell-matrix interactions as well as hydrogel degradation both of which are important in many tissue engineering applications involving encapsulated cells. For example, Engler *et al.*<sup>8</sup> described that stem cells seeded on preformed hydrogels differentiated into different phenotypes dependent on the stiffness of the hydrogel. Bryant *et al.* showed that hydrogel mechanics influence the quality of the neocartilage tissue developed<sup>9</sup> and hydrogel degradation is critical for promoting the spatial distribution of neocartilage<sup>10</sup>. Today, efforts are ever increasing to tightly control the microenvironment of cells encapsulated in hydrogels to promote tissue formation. However, some researchers have reported discrepancies in the mechanical properties of acellular versus cellular hydrogels. Cell-laden poly(ethylene glycol) (PEG) hydrogels have been observed to be softer than acellular hydrogels of the same monomer concentration<sup>9,11-13</sup>. While these studies ultimately showed that their hydrogels supported cartilaginous tissue deposition, the irreproducibility between acellular and cellular hydrogels suggests that encapsulated cells alter the polymer network while the hydrogel is being formed. As this directly affects hydrogel material properties and degradation, understanding this phenomenon is critical towards the rational design of hydrogels.

Photopolymerized hydrogels are attractive due to their ability to be injected to the desired site as a liquid solution and then polymerized on site. The polymerization of the

monomers occurs through a radical mediated process and has rapid gelation times. The curing process can be carried out under mild conditions (physiological temperature and pH) and is minimally cytotoxic to encapsulated cells<sup>14</sup>. However, encapsulated cells in photopolymerized hydrogels have been reported to be susceptible to oxidation by reactive oxygen species (ROS)<sup>15</sup> which could potentially lead to alterations of the crosslinked polymer network due to the cells acting as chain transfer agents.

PEG is a common synthetic polymer to create hydrogels due to its relative bioinertness; however, several studies have reported that PEG molecules can interact with lipid bilayer membranes<sup>16,17</sup>. The type of interaction, however, depends on the molecular weight of the PEG molecule. Low ( $\sim \leq 1$  kDa) to moderate ( $\sim 8$ -10kDa) PEG molecular weights have been shown to weakly adsorb to lipid bilayer membranes, while high PEG molecular weights ( $\geq 20$  kDa) adsorb strongly. The latter is attributed to the ability for multiple segments of a PEG molecule to interact with the membrane, leading to an overall stronger interaction. Weakly adsorbed PEG with molecular weights of  $\sim 8$ -10 kDa has been shown to act as a membrane sealant and protect cells from external physiochemical insults<sup>18-20</sup>. This protection effect is more pronounced with the introduction of hydrophobic segments, which has been observed with the Pluronic®-type polymers, where the hydrophobic segments help to stabilize the polymer at the membrane<sup>17</sup>. However if two membranes are in close proximity, weakly adsorbed PEG can become depleted at the surface of the membranes, creating a differential osmotic stress that drives membrane fusion; this process is referred to as the depletion effect<sup>16,21,22</sup>. Overall, these prior studies demonstrate a complex interaction between PEG molecules and lipid bilayer membranes.



This chapter seeks to answer several questions: 1) do encapsulated cells influence the formation of hydrogels that are produced via radical-mediated polymerization, 2) if so, does this affect the hydrogel properties globally or locally? And 3) does this cellular interference depend on cell donor? To address these questions, we use primary bovine chondrocytes as a model cell type to parallel the aforementioned studies and encapsulate them in a variety of radical-mediated polymer networks.

## **3.2 Materials and Methods**

### ***3.2.1 Chondrocyte Isolation***

Primary bovine chondrocytes were freshly isolated from either a young (1-3 weeks old) calf knee (Research 87, Boylston, MA) or an adult (1-2 years old) steer foot (Arapahoe Foods Inc., Lafayette, CO). Specifically, cartilage pieces were harvested from the femoral condyles and patellar groove of the calf knee and the metacarpalphalangeal joints of steer feet. Chondrocytes harvested from the calf knee are referred to as young chondrocytes and chondrocytes harvested from the steer foot are referred to as adult chondrocytes. Cartilage chunks were then rinsed in warm PBS with antibiotics (50 U/mL penicillin, 50 µg/mL streptomycin, 20 µg/mL gentamicin, and 0.5 µg fungizone). The cartilage was then digested for 15-17 h at 37°C in a 600 U/mL collagenase type II (Worthington Biochemical Corp., Lakewood, NJ) solution in Dulbecco's modified Eagle's medium (DMEM; Invitrogen, Carlsbad, CA). The digest solution was then passed through a 100 µm cell strainer (Falcon, Corning, NY) to remove any undigested cartilage pieces. The filtered cell suspension was then washed in PBS with antibiotics and 0.02% EDTA (Invitrogen, Carlsbad, CA). Cell viability was assessed using the Trypan Blue viability assay. Viability of the young chondrocytes were >89% and viability of the adult chondrocytes were >85%.

### **3.2.2 PEG Macromer Synthesis**

*PEG-Norbornene*: An 8-arm PEG-norbornene (PEG-NB) macromer (Table 1A) was synthesized by reacting 8-arm PEG-NH<sub>2</sub> (20 kDa, Jenkem Technology USA, Plano, TX) with four molar excess 5-norbornene-2-carboxylic acid (Sigma-Aldrich, St. Louis, MO), three molar excess of O-(7-azabenzotriazol-1-yl)-N,N,N',N'-tetramethyluronium hexafluorophosphate (HATU, ChemImpex International, Inc., Woodale, IL) and six molar excess of N,N-Diisopropylethylamine in dimethylformamide (Fisher Scientific, Fairlawn, NJ) overnight at room temperature under argon. The final product, PEG-NB, was recovered and purified by precipitation in ice-cold diethyl ether (Sigma-Aldrich), filtration, dialysis in de-ionized water over several days, and lyophilization. Norbornene conjugation to each arm of the 8-arm PEG-NH<sub>2</sub> was determined with <sup>1</sup>H nuclear magnetic resonance spectroscopy by comparing the olefinic hydrogen peaks in the norbornene ( $\delta = 5.9-6.25$  ppm) to the methylene hydrogen peaks in the PEG backbone ( $\delta = 3.4-3.9$  ppm). The norbornene conjugation was determined to be ~100%.

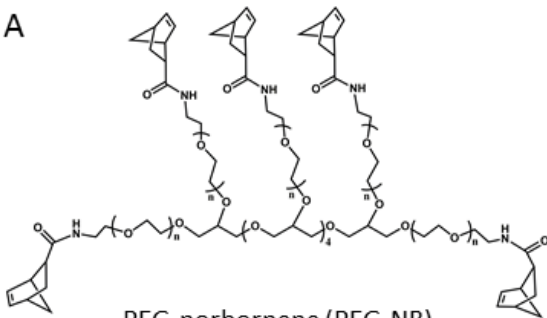
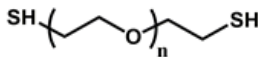
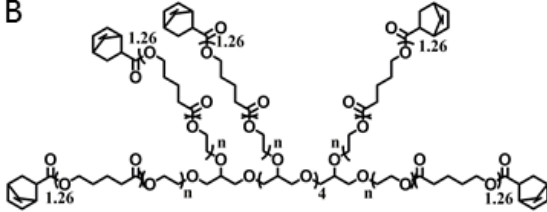
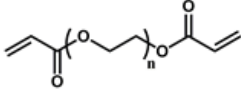
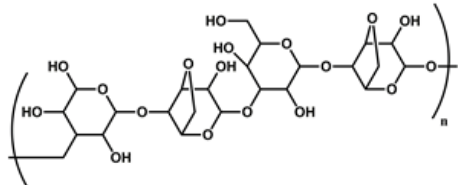
A hydrolytically degradable PEG-NB was created via conjugating norbornene groups to an 8-arm PEG terminated with a hydroxyl group (PEG-O-NB). Briefly, 8-arm PEG-OH (20 kDa, Jenkem Technology USA, Plano, TX) was reacted with 10 molar excess of 5-norbornene-2-carboxylic acid (Sigma-Aldrich), 10 molar excess of N,N'-diisopropylcarbodiimide (DIC, Sigma-Aldrich), and 10 molar excess pyridine (Sigma-Aldrich) in dichloromethane (DCM, Sigma-Aldrich) overnight at room temperature under argon. The final product, PEG-NB, was recovered and purified by precipitation in ice-cold diethyl ether (Sigma-Aldrich), filtration, dialysis in de-ionized water over several days, and lyophilization. Norbornene conjugation to each arm of the 8-arm PEG-NH<sub>2</sub> was determined with <sup>1</sup>H nuclear magnetic resonance spectroscopy by comparing the olefinic

hydrogen peaks in the norbornene ( $\delta = 5.9\text{-}6.25$  ppm) to the methylene hydrogen peaks in the PEG backbone ( $\delta = 3.4\text{-}3.9$  ppm). The norbornene conjugation was determined to be  $\sim 90\%$ .

*PEG-Caprolactone-Norbornene*: Macromers of 8-arm PEG-caprolactone functionalized with norbornene (PEG-CAP-NB) (Table 1B) were synthesized in a two-step process using protocols adapted from Bryant *et al*<sup>23</sup>. Briefly, 8-arm PEG-hexaglycerol (20 kDa) was reacted with 1.5 molar excess  $\epsilon$ -caprolactone using tin(II) ethylhexanoate as the ring opening catalyst. The reaction was carried out at 140 °C for 6 h under vacuum. The intermediate product PEG-CAP was recovered by precipitation in ice-cold diethyl ether. PEG-CAP was reacted overnight at room temperature under argon with N,N'-diisopropylcarbodiimide (10 molar excess), 4-dimethylaminopyridine (1 molar excess), pyridine (10 molar excess), and 5-norbornene-2-carboxylic acid (10 molar excess) in dichloromethane. The final product, PEG-CAP-NB, was purified through filtration over activated carbon and precipitated in diethyl ether. The precipitate was dried and dissolved in a minimal amount of chloroform. The solution was washed twice in a glycine buffer and once in a brine solution. The purified product was recovered via precipitation in diethyl ether, lyophilized, and confirmed by <sup>1</sup>H nuclear magnetic resonance spectroscopy. The number of caprolactones per PEG arm was determined to be on average 1.26 by comparing the peak area for the methylene protons in the caprolactone ( $\delta = 2.25\text{-}2.4$  ppm) to the peak area of the methylene protons in PEG ( $\delta = 3.25\text{-}3.9$  ppm). Norbornene conjugation was determined to be 65% by comparing the peak area of the vinyl protons ( $\delta = 5.9\text{-}6.25$  ppm) to the methylene protons in PEG.

*PEG Diacrylate:* PEG diacrylate (PEGDA) (Table 1C) was synthesized by reacting 0.4 M acryloyl chloride (Sigma-Aldrich) with 0.1 M PEG (3000 Da; Fluka, St. Louis, MO) in the presence of 0.4 M triethylamine (Sigma-Aldrich) in dry toluene at room temperature overnight with constant stirring and protection from light. PEGDA was filtered over alumina, purified by precipitation in cold diethyl ether three times, dried under vacuum, and stored at 4°C. The degree of acrylation was determined by <sup>1</sup>H NMR by comparing the vinyl resonances ( $\delta = 5.84, 6.16, 6.43$  ppm) to the area under the peaks for the methylene protons associated with PEG ( $\delta = 3.25-3.9$  ppm) in deuterated chloroform (Cambridge Isotope Laboratories). The percent acrylation was determined to be greater than 95%.

Table 1. Chemical structures of macromolecular monomers (macromers) and crosslinker used in this study.

Macromers	Crosslinkers
<p><b>A</b></p>  <p>PEG-norbornene (PEG-NB) MW 20,000</p>	<p><b>E</b></p>  <p>PEG dithiol (PEGdSH) MW 1,000</p>
<p><b>B</b></p>  <p>PEG-caprolactone-norbornene (PEG-CAP-NB) MW 20,000</p>	<p><b>F</b></p> <p>GCVPLS-LYSGCG</p> <p>MMP sensitive peptide crosslinker MW 1,155</p>
<p><b>C</b></p>  <p>PEG-diacrylate (PEGDA) MW 4,600</p>	<p><b>G</b></p> <p>CRDTEGE-ARGSVIDRC</p> <p>ADAMTS sensitive peptide crosslinker MW 1,765</p>
<p><b>D</b></p>  <p>Agarose</p>	

### 3.2.3 Hydrogel Formation

*Hydrogel Formation with Cells:* In order to investigate the effect of cells on polymer network formation, the hydrogel formation process was tailored to isolate certain variables. The hydrogel formation process will be detailed below per each experiment and a general schematic is shown in Figure 1.

To measure the effect of cell concentration on the hydrogel bulk compressive modulus, primary bovine chondrocytes were encapsulated in a variety of polymer networks. A precursor solution was prepared with 10% (g/g) PEG-NB mixed with either PEG dithiol (PEGdSH 1kDa; Sigma-Aldrich, St. Louis, MO) (Table 1E), an MMP degradable peptide (MMP peptide, GCVPLS-LYSGCG; GenScript, Piscataway, NJ) (Table 1F), or an ADAMTS degradable peptide (ADAMTS peptide, CRDTEGE-ARGSVIDRC; GenScript) (Table 1G) at a [thiol]:[ene] = 1, and 0.05% (g/g) photoinitiator (Irgacure 2959, Ciba Specialty Chemicals, Tarrytown, NY) in PBS. Freshly isolated chondrocytes were combined with the precursor solution at 50, 100, or 150 million cells/mL precursor solution. The PEGdSH crosslinker, the ADAMTS-sensitive peptide crosslinker, and the MMP-sensitive peptide crosslinker were used as received.

PEG-CAP-NB was solubilized in PBS one day before cell encapsulation to promote dissolution and stored at 4°C to minimize hydrolysis. A precursor solution was prepared with 10% (g/g) PEG-CAP-NB, PEG dithiol (PEGdSH 1 kDa, [thiol]:[ene] = 1), and 0.05% (g/g) I2959 photoinitiator in PBS. Freshly isolated chondrocytes were combined with the precursor solution at 50, 100, or 150 million cells/mL precursor solution.

A precursor solution of 10% (g/g) PEGDA was prepared with 0.05% I2959 photoinitiator in PBS. Freshly isolated chondrocytes were combined with the precursor solution at 50, 100, or 150 million cells/mL precursor solution.

The precursor solutions mixed with cells as described above were polymerized with UV light (352 nm, 6 mW/cm<sup>2</sup>) for 5 min (in the case of PEGDA, the precursor solution was exposed to UV light for 10 min). Hydrogels were rinsed in PBS with antibiotics and then cultured overnight in chondrocyte growth medium (DMEM supplemented with 10% FBS, 50 U/mL penicillin, 50 µg/mL streptomycin, 0.5 µg/mL fungizone, 20 µg/mL gentamicin, 10 mM HEPES buffer, 0.1 M MEM-NEAA, 0.4 mM L-proline, 4 mM GlutaGro, 110 mg/L sodium pyruvate, and 50 mg/mL L-ascorbic acid) at 37°C and 5% CO<sub>2</sub> in a humid environment. For agarose hydrogels, a solution of 1.5% (g/g) agarose (agarose type IX; Sigma-Aldrich) (Table 1D) in PBS was prepared. The solution was allowed to cool to room temperature before combining the chondrocytes at 50, 100, and 150 million cells/mL of agarose solution. The chondrocyte-agarose solution was cooled to 4°C to form the hydrogel. The hydrogels were cultured in chondrocyte growth medium overnight.

*Hydrogel Formation after Monomer Exposure to Cells:* To investigate if cells could interact with PEG monomers, precursor solutions were prepared of either 8-arm PEG-NB only or PEGdSH only. Cells were added to the precursor solution such that the final concentration of cells would be 50x10<sup>6</sup> cells/mL of precursor solution containing both 8-arm PEG-NB and PEGdSH. The cells were allowed to incubate (hereafter referred to as 'soak') in the precursor solution for 10 mins at room temperature. The cells were then separated from the precursor solution via centrifugation (10 min at 1200 rpm) and the supernatant was mixed with increasing concentrations of the complementary monomer. I2959 photoinitiator was added at a final concentration of 0.05% (v/v)

and the precursor solution was photopolymerized with UV light (352 nm, 6 mW/cm<sup>2</sup>) for 5 min. Hydrogels were rinsed in PBS with antibiotics and then cultured overnight in chondrocyte growth medium at 37°C and 5% CO<sub>2</sub> in a humid environment.

*Formation of Fluorescently Labeled Hydrogels:* Hydrogels formed for fluorescence microscopy were formed with pre-labeled fluorescent crosslinkers. Nondegradable PEGdSH and the MMP-sensitive peptide was incubated with either an A488 or A546 maleimide-conjugated fluorophore (ThermoFisher Scientific, Lafayette, CO) for at least 30 mins at 37°C prior to hydrogel formation with the thiol functional groups in ~400x molar excess of maleimide. Fluorescent polystyrene beads (10 μm diameter, Ex/Em 580/605; ThermoFisher Scientific, Lafayette, CO) were encapsulated at a concentration of 10x10<sup>6</sup> beads/mL of precursor solution composed of 10% (g/g) hydrolytically degradable PEG-O-NB and PEGdSH (1kDa, [thiol]:[ene] = 1). In another set of hydrogels, young bovine chondrocytes were encapsulated at a concentration of 20x10<sup>6</sup> cells/mL of precursor solution composed of 10% (g/g) PEG-NB, PEG dithiol (PEGdSH 1 kDa) at a [thiol]:[ene] = 0.65, and 0.05% (g/g) I2959 photoinitiator in PBS. In a third set of hydrogels, young bovine chondrocytes were encapsulated at a concentration of 20x10<sup>6</sup> cells/mL of precursor solution composed of 10% (g/g) PEG-NB, an MMP-sensitive crosslinker (1155 Da) at a [thiol]:[ene] = 0.65, and 0.05% (g/g) I2959 photoinitiator in PBS. Hydrogels encapsulated with polystyrene beads were kept in PBS and hydrogels encapsulated with chondrocytes were kept in chondrocyte growth media. PBS or chondrocyte growth media was replaced every two to three days.

### **3.2.4 Hydrogel Characterization**

All hydrogels were allowed to swell overnight in chondrocyte media at 37°C. Hydrogels were assessed for compressive modulus (n = 3-4). The diameter and height of the hydrogels were



manually measured using calipers. Hydrogels were compressed to 15% strain at a rate of 10% height/min (MTS Synergie 100, 10 N). The compressive modulus was measured by estimating the slope of the linear region of stress–strain curves from 10 to 15% strain.

### **3.2.5 Fluorescence Microscopy**

Cell-laden hydrogels were treated with calcein AM to stain for live cells prior to imaging. Images were acquired by laser scanning confocal microscopy (Axiovert 40 C, Zeiss, Thornwood, NY) at 400× magnification. Measures of the distance of the gradient in fluorescence intensity around encapsulated beads and cells was taken from 100 measurements per condition (3-4 hydrogels per condition or ~25-35 cells per hydrogel). The distance of the gradient was defined as the length from the boundary of the cell to the boundary of the bulk of the gel. The bulk gel is characterized visually by a general plateau in fluorescence intensity. A measurement window is selected in the bulk region to obtain an average fluorescence value such that the standard deviation in fluorescence is less than 6. The boundary of the bulk gel is defined to be the point where the fluorescence intensity is 95% of the bulk fluorescence value. Images were analyzed using ImageJ software. Void quantification was performed using MATLAB. Areas of no fluorescence intensity were recognized as areas of hydrogel degradation using built in MATLAB functions. The number and size of the areas were quantified.

### **3.2.6 Statistics**

Data are presented as the mean of  $n = 3$  replicates (unless otherwise stated) with standard deviation represented parenthetically in the text or as error bars in the figures. Statistical analysis was performed using MiniTab. Data were confirmed to be normally distributed using a Shapiro-Wilk test and met the requirements for ANOVA to be performed. Hydrogel moduli were analyzed

with a one-way ANOVA with cell concentration or PEG concentration % (g/g) as a factor. Hydrogel moduli for different cell donors were analyzed with a two-way ANOVA with a Tukey's post-hoc test ( $\alpha = 0.05$ ) with donor and cell encapsulation concentration as factors. Measures of hydrogel moduli formed from soaked monomers were analyzed with an ANOVA with a Tukey's post-hoc test ( $\alpha = 0.05$ ). Differences in acellular hydrogel moduli were analyzed using a t-test. Comparisons between the hydrogel moduli of cellular PEG-NB and PEG-CAP-NB were analyzed by a three-way ANOVA with polymer type, cell concentration, and soaking with cells as factors. The three-way interaction was found to be statistically significant, so a series of two-way ANOVAs were performed with Tukey's post-hoc test ( $\alpha = 0.05$ ). An ANOVA with Tukey's post-hoc test ( $\alpha = 0.05$ ) was used to determine significant differences between the ratio of gradient width: cell diameter in polystyrene and chondrocyte-laden hydrogels. A p-value of  $<0.05$  was used to determine statistical significance.

### 3.3 Results

#### 3.3.1 Encapsulated chondrocytes in photopolymerized hydrogels reduce the bulk compressive modulus.

Primary bovine chondrocytes freshly harvested from a young calf donor were encapsulated in several free-radical polymerized PEG hydrogels (Figure 1). Agarose was used as a control, where encapsulation of cells does not involve free-radicals. After swelling in chondrocyte growth media for 24 hr, the compressive moduli of the hydrogels were measured. The moduli of PEG hydrogels showed dependence on the cell encapsulation concentration, with the hydrogel compressive modulus decreasing ( $p < 0.0002$ ) with increasing cell concentration (Figure 2A-E).

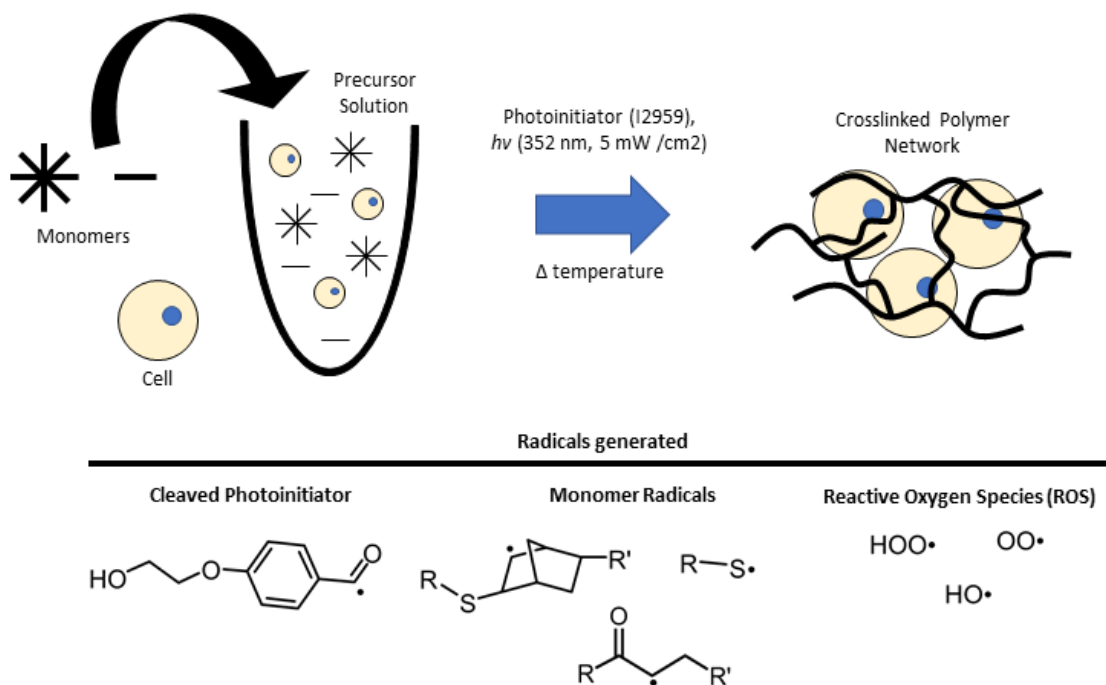


Figure 1. A general schematic representation of hydrogel formation. Monomers are mixed with cells in a precursor solution. Here, a multiarmed macromer with a linear bifunctional crosslinker is shown; however, monomers with different architectures are used. A full list of polymer chemistries used in this chapter is shown in Table 1. Cells may or may not be included to create cell-laden or acellular hydrogels. The precursor solution is then polymerized via photopolymerization (in the case of PEG-NB and PEG-CAP-NB crosslinked by dithiol molecules

and PEGDA macromers) or via a temperature drop (in the case of agarose). The crosslinked hydrogel physically entraps cells. In the case of photopolymerized hydrogels, several radicals are formed. Upon exposure to ultraviolet light, the photoinitiator is cleaved to produce a radical. This radical abstracts a hydrogen from the monomers to produce kinetic chains. In the case of polymerization via thiol-ene click chemistry, carbon and thiyl radicals are generated (the structures of the monomers used following this polymerization scheme can be found in Table 1 A, B, E, and F). For homopolymerization of acrylate functionalized PEG, acrylyl radicals are formed (Table 1 C). Additionally, several reactive oxygen species (ROS) are formed if ambient oxygen is present. Figures are not drawn to scale.

The compressive modulus of hydrogels made of 8-arm PEG-NB crosslinked with a PEGdSH linker showed a decrease ( $p < 0.0001$ ) as a function of the cell encapsulation concentration (Figure 2A). A similar trend was seen in PEG-NB hydrogels crosslinked with two different peptides, an MMP-degradable peptide (Figure 2B) and an ADAMTS-degradable peptide (Figure 2C), showing a decrease ( $p < 0.0001$ ) in modulus with increasing cell concentration. Hydrogels formed from 8-arm PEG-CAP-NB and PEGdSH (Figure 2D) were softer ( $p < 0.0001$ ) with increasing cell encapsulation concentration. Cellular PEGDA hydrogels showed a decrease ( $p < 0.0001$ ) in modulus with increasing cell concentration; however, only the  $150 \times 10^6$  cells/mL case was significantly softer ( $p < 0.0025$ ) than the acellular case (Figure 2E). The modulus of physically crosslinked agarose hydrogels was not dependent on the cell encapsulation concentration (Figure 2F).

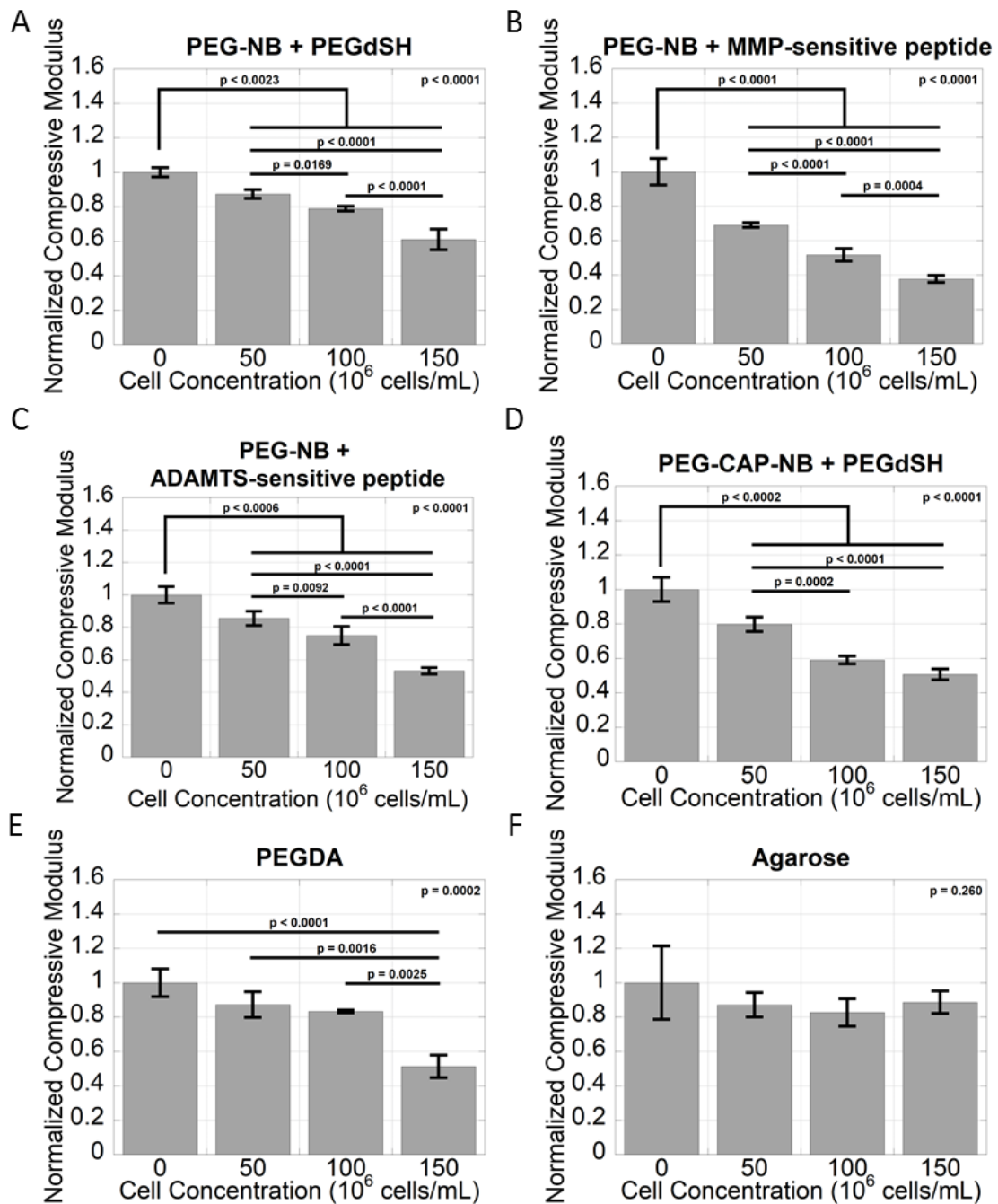


Figure 2. Young bovine chondrocytes were encapsulated in a variety of radical-polymerized hydrogels at increasing cell concentrations. A) PEG-NB crosslinked with PEGdSH. B) PEG-NB crosslinked with an MMP-sensitive peptide GCVPLSLYSGCG. C) PEG-NB crosslinked with an ADAMTS-sensitive peptide CRDTEGEARGSVDIRC. D) PEG-CAP-NB crosslinked with PEGdSH. E) PEGDA. F) As a negative control, chondrocytes were encapsulated in a physically crosslinked

agarose (1.5 wt%) gel. The p values reported in the upper right corner of each panel denote if cell concentration was a significant factor in hydrogel modulus.

### ***3.3.2 Cellular Interference of Polymer Network Formation is Affected by Donor.***

We also investigated if different donors have an impact on construct modulus as a function of cell concentration (Figure 3). Specifically, we compared PEG-NB hydrogels crosslinked with PEGdSH encapsulated with different young and adult donors. We investigated whether encapsulating cells from different donors influenced the degree of hydrogel modulus reduction, with donor age representing the wide range of donor bioactivity. For both populations of young and adult chondrocytes, cell concentration was ( $p < 0.001$ ) a factor in reducing hydrogel modulus consistent with previous results. Additionally, donor was found to be a significant factor in reducing hydrogel modulus ( $p < 0.001$ ). Within populations of young chondrocytes, a deviation in hydrogel modulus was observed beginning at an encapsulation concentration of  $100 \times 10^6$  cells/mL (Figure 3A). In adult chondrocytes, differences in hydrogel modulus were observed at lower encapsulation concentrations of  $50 \times 10^6$  cells/mL (Figure 3B). When comparing the effect of young chondrocytes versus adult chondrocytes, donor age was found to be a significant factor in reducing hydrogel modulus ( $p < 0.001$ ) with adult chondrocytes reducing the hydrogel modulus more than young chondrocytes (Figure 3C).

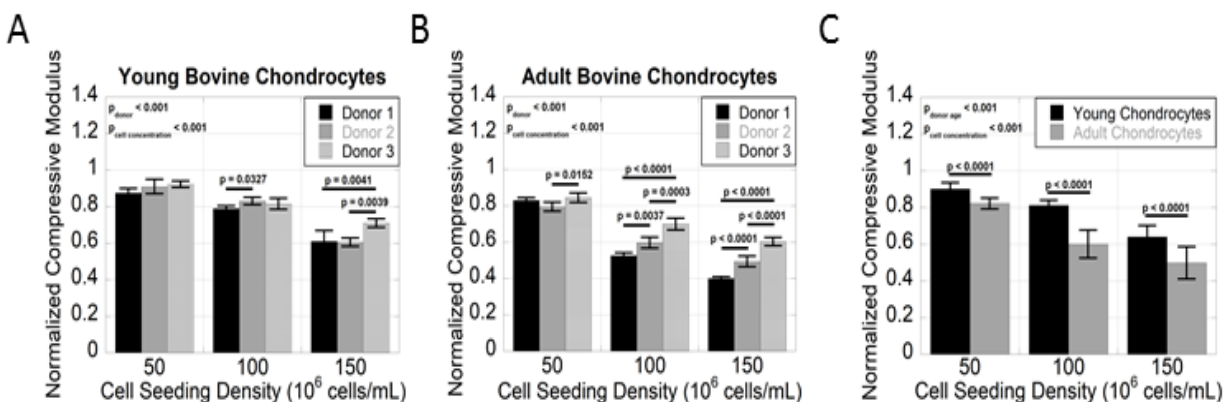


Figure 3. Comparison of hydrogel moduli encapsulated with cells from young and adult donors. Hydrogels were formed by crosslinking 8-arm PEG-NB with a nondegradable PEGdSH crosslinker. A) Moduli of hydrogels encapsulated with cells from three different young bovine donors. B) Moduli of hydrogels encapsulated with cells from three different adult bovine donors. C) Comparison of hydrogel moduli of constructs encapsulated with young and adult donors.

### 3.3.3 Polymer Chemistry Affects Cell-Polymer Interactions.

The compressive moduli of hydrogels formed from a precursor solution of only 8-arm PEG-NB exposed to cells were not significantly different than hydrogels formed from 8-arm PEG-NB that were not soaked in cells (Figure 4A), suggesting that cells do not significantly interact with the 8-arm PEG-NB macromer. However, hydrogels formed from PEGdSH that were soaked in cells were softer ( $p < 0.0001$ ) than hydrogels formed from PEGdSH that were not soaked in cells (Figure 4B), suggesting that cells are able to interact with dithiol crosslinkers. It is important to note that although the hydrogels formed from soaked PEG-NB were not significantly different from hydrogels formed from fresh PEG-NB, it does not preclude the possibility that cells can interact with PEG-NB, simply that this bulk mechanical test may not be sensitive enough to detect changes. To determine the sensitivity of bulk mechanical test, hydrogels were formed with decreasing 8-arm PEG-NB content (Figure 5). PEG-NB content was a significant factor in hydrogel modulus ( $p < 0.0001$ ), but this effect was only observed when PEG-NB concentrations were

reduced by 0.4% (g/g) (i.e., 9.6% compared to 10% (g/g)) or more. This result indicates that a loss of 0.2% or less does not affect the compressive modulus of the bulk hydrogel.

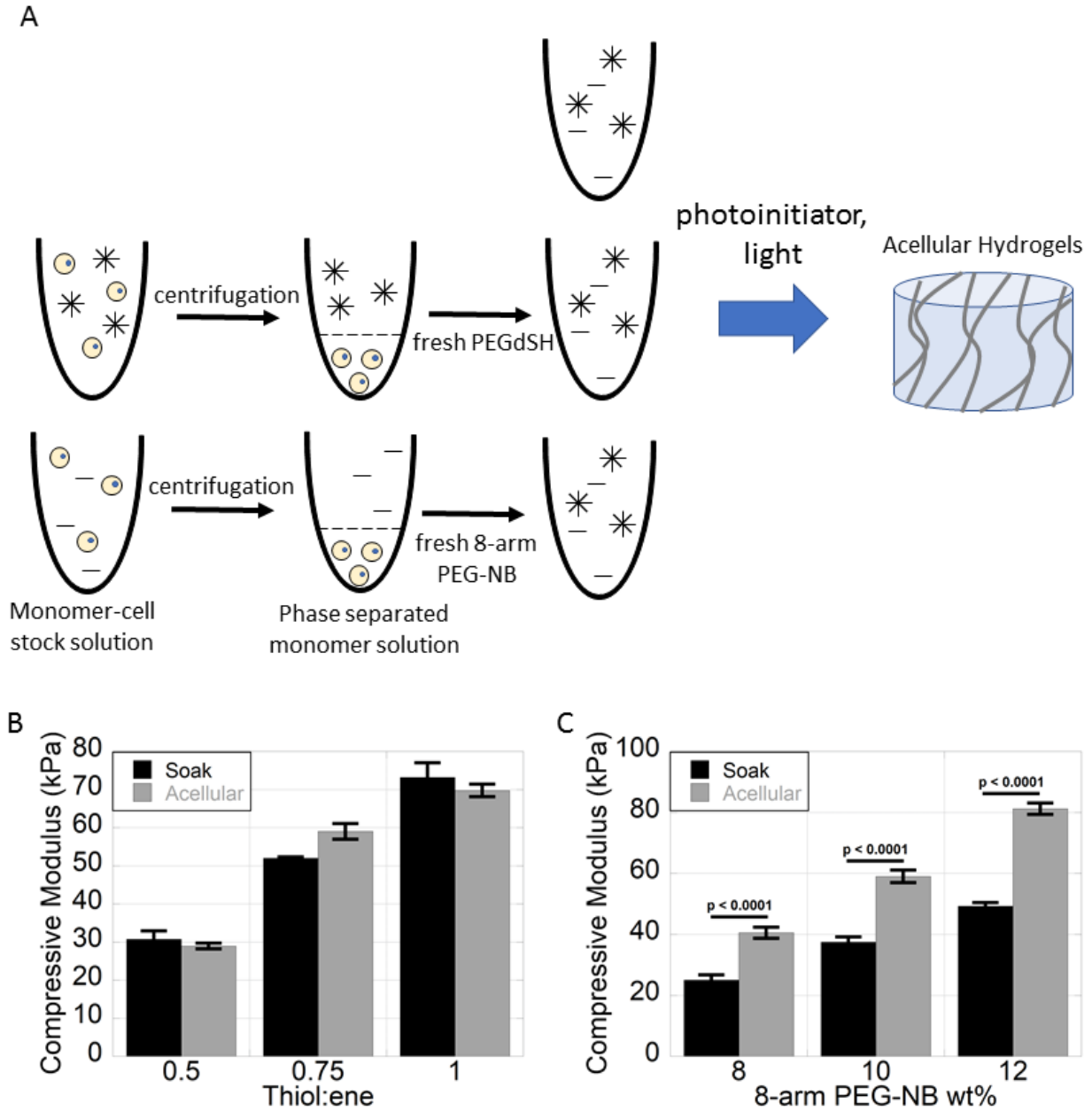


Figure 4. To investigate if chondrocytes interacted with multifunctional monomers, chondrocytes were incubated in a solution containing 8-arm PEG-NB or PEGdSH (A). After 10 mins of incubation, the monomers were separated via centrifugation and polymerized with an increasing



concentration of the other monomer. Compressive moduli of hydrogels formed from fresh and soaked 8-arm PEG-NB (B) or fresh and soaked PEGdSH (C).

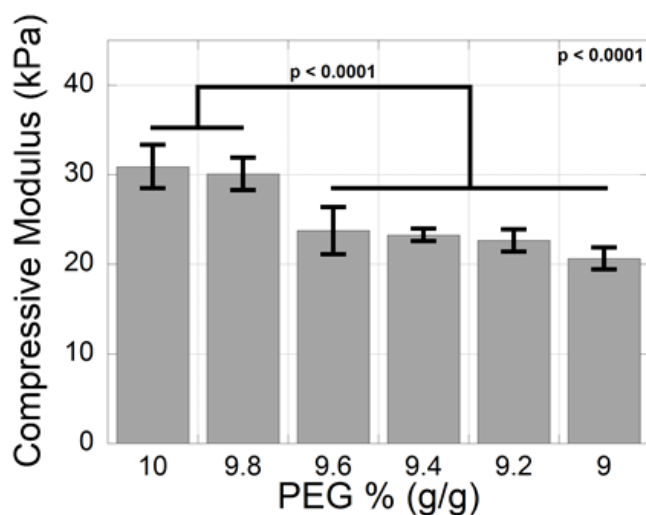


Figure 5. Compressive moduli of hydrogels formed by crosslinking 8-arm PEG-NB with a PEGdSH crosslinker. The initial formulation was 10% (g/g) PEG-NB crosslinked at a 1:1 [thiol]:[ene] stoichiometric ratio. The concentration of 8-arm PEG-NB was decreased while keeping the concentration of PEGdSH constant. Significant differences in modulus was observed after a 0.2% (g/g) decrease in PEG-NB ( $p < 0.0001$ ).

To determine if macromer hydrophobicity affected the ability for cells to deplete monomers in solution, solutions of PEG-NB or PEG-CAP-NB with the PEGdSH were soaked in various cell concentrations, separated, and polymerized. The moduli of the hydrogels were compared to cellular hydrogels of the same formulation (Figure 6). As a baseline, the hydrogel modulus of acellular PEG-NB and PEG-CAP-NB hydrogels were measured (Figure 6A). The moduli of acellular PEG-CAP-NB hydrogels were lower ( $p < 0.001$ ) than PEG-NB hydrogels. PEG-NB and PEG-CAP-NB solutions were soaked in varying cell concentrations and encapsulated at different cell concentrations (Figure 6B). The hydrogel moduli were normalized to that reported in Figure 6A to investigate relative reductions in hydrogel modulus. Cell encapsulation concentration was a significant factor in reducing hydrogel modulus for both PEG-NB ( $p = 0.007$ ) and PEG-CAP-NB

( $p < 0.0001$ ) hydrogels. In PEG-NB hydrogels, soaking the monomers before polymerization did not affect the hydrogel modulus; however, soaking was a factor ( $p < 0.001$ ) in PEG-CAP-NB hydrogel modulus. Cell concentration and soaking significantly reduced ( $p = 0.021$  and  $p < 0.001$ , respectively) the modulus of PEG-CAP-NB hydrogels more than PEG-NB hydrogels at  $100 \times 10^6$  cells/mL and  $150 \times 10^6$  cells/mL. Overall, polymer chemistry was a factor ( $p < 0.001$ ) in reductions in modulus. The hydrogel moduli of PEG-CAP-NB hydrogels were more sensitive to cell encapsulation concentration and to cell exposure pre-polymerization suggesting that polymer chemistry and hydrophobicity are crucial factors in cell-polymer interactions that reduce the hydrogel modulus on a bulk scale.

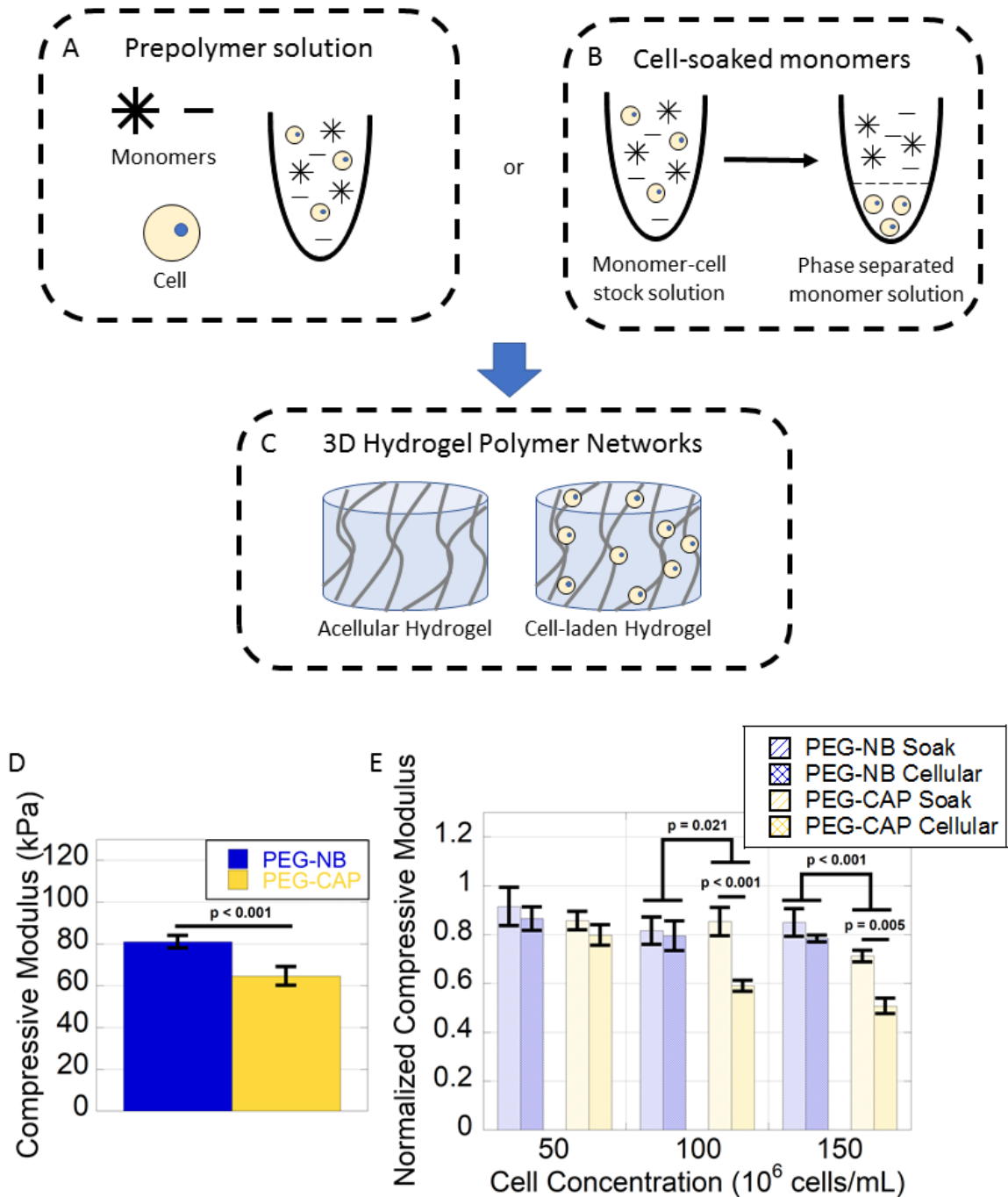


Figure 6. Modulus of hydrogels formed from fresh monomers and monomers exposed to cells. Chondrocytes were suspended in a solution containing the precursor monomers (A) or soaked in a solution containing precursor monomers and then separated (B). The mixtures from (A) and (B) are then photopolymerized to form acellular and cellular hydrogels (C). Comparison of hydrogel moduli of PEG-NB (blue) and PEG-CAP-NB (yellow) formed with different monomer pretreatments and cell encapsulation concentrations. D) Compressive moduli of acellular PEG-

NB and PEG-CAP hydrogels. E) Compressive moduli of PEG-NB and PEG-CAP-NB hydrogels normalized to the respective moduli in panel (D). Hydrogels were formed from monomers soaked in solutions with varying cell concentrations ('soak') and encapsulated with various cell concentrations ('cellular').

#### ***3.3.4 Encapsulated Cells Reduce Local Network Crosslinking in Fluorescently Labeled Hydrogels.***

We sought to investigate how chondrocytes affect the polymer network locally around them. Young bovine chondrocytes were encapsulated in a fluorescently labeled hydrogel<sup>24</sup> and the fluorescence intensity across the cell was analyzed (Figure 7). As a control, polystyrene (PS) beads of similar size (reported to be 9.9 (0.1)  $\mu\text{m}$  by the manufacturer) to the cells were encapsulated in fluorescently labeled hydrogels.

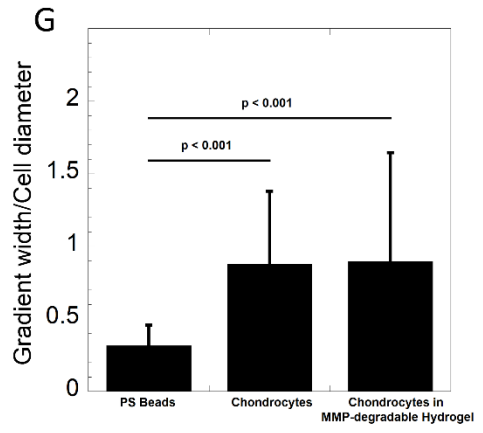
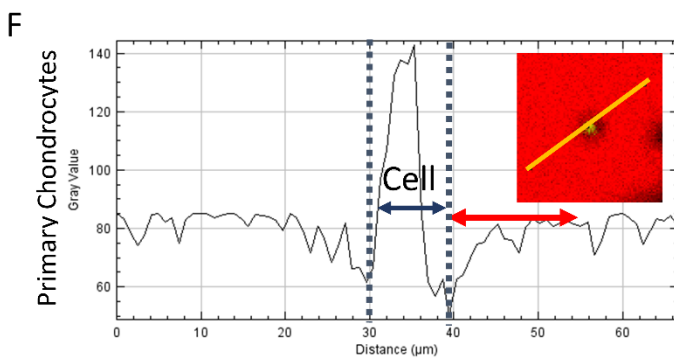
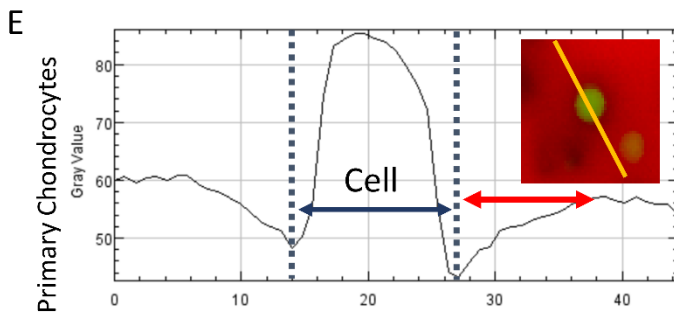
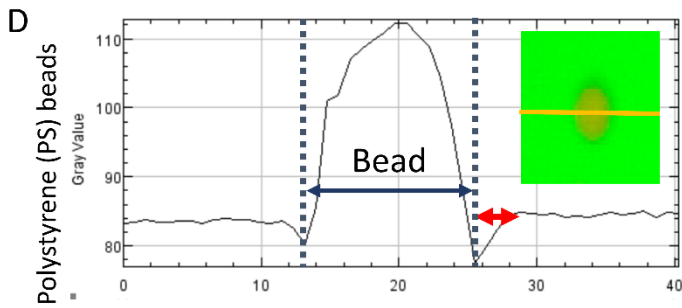
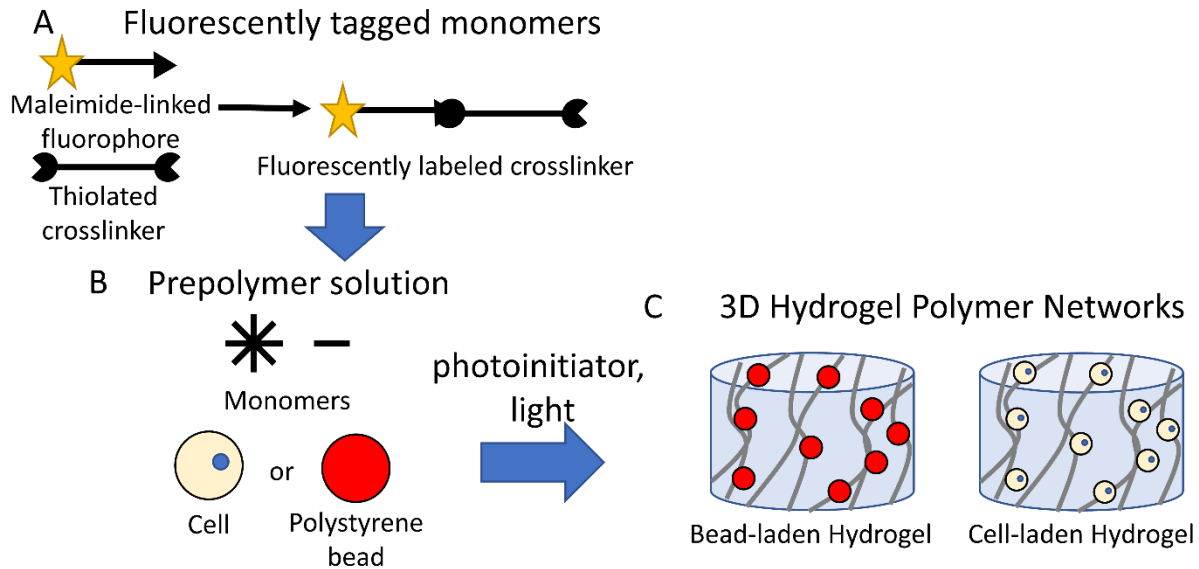


Figure 7. Confocal microscopy of cells encapsulated in fluorescently labeled hydrogels. Dithiolated crosslinkers were fluorescently labeled using a maleimide-conjugated fluorophore (A). These fluorescently labeled thiols were mixed with multi-armed PEG with either cells or fluorescent polystyrene beads (B) to form fluorescently labeled hydrogels (C). D) (Inset) Confocal microscopy image of fluorescent polystyrene beads (red) in a fluorescently labeled PEG hydrogel (green). Fluorescence profile of the line in the inset. The blue arrow highlights the bead and the red arrow highlights the gradient in PEG density around the bead. E) (Inset) Confocal microscopy image of Calcein-stained chondrocytes (green) encapsulated in a fluorescently labeled PEG hydrogel (red) crosslinked with a nondegradable crosslinker. Fluorescence profile of the line in the inset. F) (Inset) Confocal microscopy image of Calcein-stained chondrocytes (green) encapsulated in a fluorescently labeled PEG hydrogel (red) crosslinked with an enzymatically degradable crosslinker (MMP-degradable GCVPLS-LYSGCG). Fluorescence profile of the line in the inset. The blue arrow highlights the cell (the boundary between the cell and hydrogel network is denoted by a dashed vertical line) and the red arrow highlights the gradient in PEG density around the cell. G) Measurements of the ratio of the width of the PEG density gradient (red arrows in panel D, E, and F) to the diameter of the cell or polystyrene bead diameter (blue arrows in panel D, E, and F). For each hydrogel condition, fluorescence profiles ( $n=100$ ) were analyzed across 3-4 hydrogels.

Confocal microscopy was used to observe the PS beads (Figure 7D inset) and chondrocytes encapsulated in fluorescently labeled hydrogels immediately after encapsulation (Figure 7E and F inset). There was an observed gradient in PEG fluorescence (highlighted by the red arrow) around the particle (highlighted by the blue arrow). The average particle diameter was recorded by measuring 100 particles and averaged  $9.4 (1.2) \mu\text{m}$ , which is in good agreement with the manufacturer. Chondrocytes were encapsulated in the same hydrogel formulation as the PS beads (Figure 7E inset) and also encapsulated in a peptide-crosslinked hydrogel (Figure 7F inset). The average cell diameter measured from 300 cells across all hydrogel conditions was  $9.8 (2.3) \mu\text{m}$ . Similar values of chondrocyte diameter have been previously reported<sup>25,26</sup>. The fluorescence profile of a line drawn across the bead or the cell for each hydrogel is shown in Figure 7DEF. A small decrease in hydrogel fluorescence around the PS bead is observed (Figure 7D). Comparatively, we observed a spatially larger gradient in PEG fluorescence around the chondrocyte in both a PEGdSH-crosslinked hydrogel (Figure 7E) and a peptide-crosslinked

hydrogel (Figure 7F) suggesting that the chondrocyte was interfering locally with hydrogel formation.

Quantitative analysis revealed that encapsulated chondrocytes created a significantly larger gradient in PEG fluorescence around the cell compared to PS beads (Figure 7G). Chondrocytes encapsulated in a hydrogel crosslinked with PEGdSH created a larger gradient compared to PS beads ( $p < 0.001$ ). Similarly, chondrocytes in an MMP-sensitive gel had a larger gradient in PEG around the cell compared to PS beads ( $p < 0.001$ ). There were no significant differences in gradient sizes between PEGdSH and peptide crosslinked gels.

### ***3.3.5 Hydrolytically Degradable Hydrogels Undergo Heterogeneous Degradation.***

Young primary bovine chondrocytes were encapsulated in hydrolytically degradable hydrogels for 10 days to observe their patterns of degradation. As a control, young chondrocytes from the same donor were encapsulated in nondegradable hydrogels of an identical formulation (Figure 9). In both sets of hydrogels, cells labeled with Calcein can be observed in void pockets, consistent with above observations. Void pockets with no visible cells inside can be attributed to cells that did not survive the photoencapsulation process and thus were not labeled. Hydrolytically degradable hydrogels are shown to undergo heterogeneous degradation with a growing population of large void areas by day 10. The appearance of these large void areas by day 10 are statistically significant ( $p < 0.0001$ ) from the day 0 histogram. The number of these large void areas are relatively smaller due to individual void pockets merging to form larger areas of degradation.

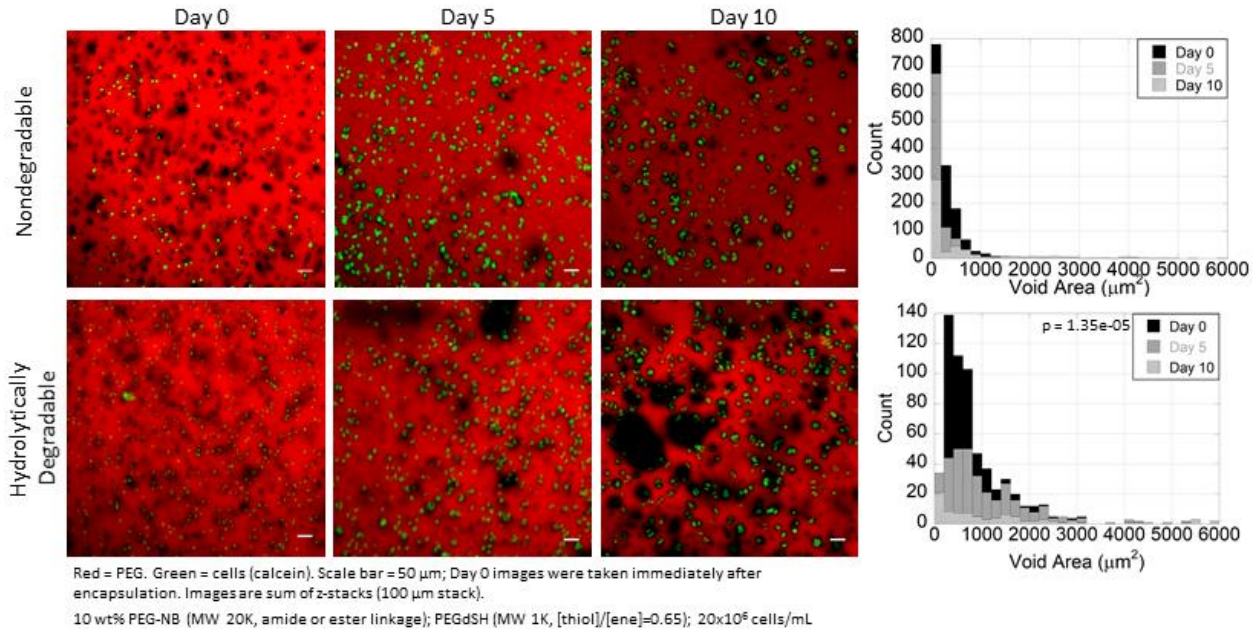


Figure 8. Top row) Confocal microscopy images of fluorescently labeled nondegradable hydrogels cultured over 10 days. The histogram represents the growth of the void areas (degradation) over 10 days. Bottom row) Confocal microscopy images of fluorescently labeled hydrolytically degradable hydrogels cultured over 10 days. The histogram represents the growth of the void areas (degradation) over 10 days.

### 3.4 Discussion

Cell encapsulation in poly(ethylene glycol) hydrogels formed by radical-mediated polymerization reactions have emerged as a promising 3D *in vitro* cell culture platform and *in vivo* cell delivery vehicle. However this work demonstrates that during the process of encapsulation, cells interact with the hydrogel precursor molecules and affect spatially the final network structure of the hydrogel. As a result, the local hydrogel properties surrounding the cells and the overall macroscopic properties of the hydrogel are altered. We demonstrate these findings for chondrocytes encapsulated in degradable PEG hydrogels.

Immediately after equilibrium swelling, the bulk compressive modulus of photopolymerized hydrogels were significantly lower when cells were encapsulated compared



to acellular hydrogels of the same monomer concentration. Moreover, the degree to which the modulus reduced directly correlated to the number of cells encapsulated, with a larger reduction in modulus as the cell encapsulation concentration increased. The hydrogel modulus also varied when encapsulating cells from different donors. Together, this suggests that cells play an active role before or during polymerization that reduces the bulk compressive hydrogel modulus.

Chondrocytes suspended in the hydrogel precursor solution sequestered macromers, reducing their concentration in solution and leading to an overall reduced bulk crosslink density. This observation was confirmed by temporarily exposing the macromers to chondrocytes prior to forming acellular hydrogels. Interestingly, our findings demonstrate that chondrocytes interact strongly with the PEG crosslinker, but minimally with the higher molecular weight 8-arm PEG-NB macromer. Comparing to acellular hydrogels not exposed to cells, the molar concentration required to achieve the observed cellular effects can be estimated for each macromer. For example, for the PEG crosslinker to reduce the compressive modulus by ~30% (i.e., for the 10% PEG-NB condition in Figure 4C), ~5-10 mM of the crosslinker has to be sequestered by the cells. On the contrary, for the 8-arm PEG-NB to have no effect on modulus, the amount sequestered by the cells must be less than 0.2 mM (i.e., Figure 5). Thus, the number molecules sequestered by the cells is ~25-50-fold higher for the PEG crosslinker than the 8-arm PEG-NB molecules. The weak interaction of a small PEG molecule to a lipid bilayer membrane is unlikely to be sufficient to explain the observed results. However, once weakly adsorbed the presence of thiols on the crosslinker may subsequently form disulfide bonds with cell-surface thiols<sup>27</sup>.

On the contrary, the 8-arm PEG macromer despite having a 20 kDa molecular weight did not lead to significant interactions with the chondrocytes and did not affect the overall hydrogel

properties. It has been reported that star polymers have a greater propensity to contribute to the depletion effect over linear polymers of similar size and this propensity increases with the number of arms<sup>28</sup>. Thus, it is possible that the 8-arm PEG-NB of 20kDa may interact weakly to the cell membrane while linear PEG molecules of similar molecular weight can adsorb strongly to the membrane<sup>16</sup>. Interestingly, the introduction of hydrophobic units based on caprolactone had a greater effect on the bulk hydrogel properties suggesting that hydrophobicity may enhance cellular interaction with the 8arm PEG macromer. This result is consistent with the observations comparing PEG and the amphiphilic Pluronic® P188 polymer<sup>17</sup>.

Reductions in hydrogel modulus was found to be variable between donors of the same age range with more variability found in older donors. Furthermore, adult chondrocytes reduced the modulus of hydrogels significantly more than younger chondrocytes. The chondrocytes used in this chapter were harvested from full thickness cartilage which contains chondrocytes of varying metabolic behaviors. The variability in reductions of cell-laden hydrogel modulus can be explained in part due to the usage of a heterogeneous chondrocyte population which can presumably alter from donor to donor. Chondrocytes in native cartilage have been shown to have low proliferative potential and therefore are thought to survive throughout the majority of the organism's lifespan<sup>29</sup>. Thus, extrinsic damage such as mechanical stimulation or exposure to reactive oxygen species can cause accumulated cell aging, further causing chondrocyte heterogeneity. This extrinsic damage is thought to cause changes in older chondrocytes such as increased catabolic activity and cytokine expression, hallmarks of osteoarthritis<sup>30</sup>. Oxidative stress has been shown to induce stress to the endoplasmic reticulum<sup>31,32</sup> which plays a critical role in the proper expression, folding, and transport of many proteins. Thus, aging can potentially

change the protein ligand profile of the chondrocyte plasma membrane. For example, aging has been shown to increase the expression of the Receptor for Advanced Glycation End (RAGE) products<sup>33</sup>. Together, this suggests that adult chondrocyte donors have accumulated varied levels of stress to the cells. This leads to altered surface protein profiles and thus variable interactions with the thiolated monomers used in this study.

Taken together, our data suggest that chondrocytes interact weakly with the PEG-based macromers in the hydrogel precursor solution via the PEG chemistry. Other chemical functionalities on the monomers may also play a critical role in interfering with polymer network formation. The presence of thiols on the PEG and peptide crosslinkers can enhance the cell-polymer interaction resulting in sequestration of the monomers leading to the consistent observations of reduced moduli of PEG hydrogels crosslinked with PEGdSH and two different peptide crosslinkers compared to acellular hydrogels. We estimate that the dithiolated crosslinkers can diffuse up to several hundred microns through an aqueous solvent based on size and handling time (i.e., 10 min) before polymerization. Additionally, hydrophobic segments (i.e., caprolactone) can enhance the cell-polymer interaction resulting in sequestration of the monomers. This effect leads to a significant reduction in the macromers in solution and contributes to a measurable reduction in the resulting hydrogel crosslinking.

Free-radical initiated polymerizations are advantageous due to their rapid curing times; however, the polymerization mechanism creates free-radicals that can potentially be quenched by the cells. The photoinitiator generates an initiator radical upon cleavage which abstracts a hydrogen from the monomers to create living polymer chains. These monomer radicals include thiyl and carbon radicals. If ambient oxygen is present, reactive oxygen species, such as peroxy

radicals, are also generated<sup>34,35</sup>. Cells have mechanisms to protect them from free-radicals and thus have the capability to quench all of these radicals generated during encapsulation. This is one explanation for the observed drop in modulus of cellular hydrogels formed from PEG diacrylate compared to acellular constructs. Polymerization of acrylate systems have previously been shown to be more inhibited by the formation of ROS compared to thiol-ene systems<sup>15</sup>. This enables the cells to act as chain transfer agents effectively terminating the propagating polymer. Furthermore, cells in a photopolymerized acrylate system have been shown to experience lipid peroxidation after encapsulation<sup>36</sup>.

Radicals are a highly reactive species and have a short lifespan. Therefore, termination of propagating chains due to chain transfer to the cells is presumably limited to the immediate vicinity around the cell. Post-encapsulation, a gradient in the polymer density from the cell surface to the bulk hydrogel was observed. Comparatively, this distance over which the gradient was observed was significantly greater than that which was measured for polystyrene beads, suggesting a cell-mediated effect. This observation suggests that the cells locally affect the formation of the hydrogel. One potential explanation is that cells act as radical scavengers that locally inhibit the polymerization, resulting in a decrease in the hydrogel crosslink density in the immediate vicinity of the cell. Radical species formed during the polymerization have the potential to react with cells through several mechanisms such as lipid peroxidation<sup>37</sup>, which we have reported to be elevated in radical-mediated encapsulation of chondrocytes compared to agarose<sup>38</sup>, modification of transmembrane proteins<sup>39</sup>, and cell-surface thiols<sup>40</sup>.

Encapsulated cells were observed to create a gradient in crosslinking density in both hydrolytically and enzymatically degradable hydrogels. This gradient has implications in altering

hydrogel degradation patterns especially in hydrolytically degradable hydrogels. Hydrolytically degradable hydrogels undergo a global bulk degradation due to the ubiquitous presence of water in the hydrogel. The gradient in crosslinking density around the cell reaches reverse gelation before the rest of the hydrogel causing pockets of void space while the bulk of the gel remains intact. Without this gradient, the hydrogel would globally reach reverse gelation at one time. By day 10 of culture of cellular hydrolytically degradable hydrogels, a population of large void areas appeared in hydrolytically degradable hydrogels which were not observed in nondegradable hydrogels, suggesting that a gradient in crosslinking density around cells must exist.

Cells interfere with polymer network formation before and during photopolymerization. In the prepolymer solution, they can interact with monomers such that they reduce the concentration of monomers on a bulk scale, thereby reducing the bulk compressive modulus as a function of cell encapsulation concentration. During polymerization, propagating radicals generated may terminate on the cell membrane. Due to the short-lived nature of radicals, they are expected to be quenched much faster than they can diffuse resulting in a gradient in crosslinking density around cells. This gradient alters the way in which hydrogels degrade, most notably in hydrolytically degradable gels. Hydrolytically degradable gels undergo bulk uniform degradation. In homogeneously formed networks (Figure 10A), hydrogel degradation should result in global reverse gelation. However, in heterogeneously formed networks with cell-induced gradients (Figure 10B), the region around a cell reaches reverse gelation before the bulk of the gel. Experimentally, we see regions of void spaces (corresponding to degradation) growing heterogeneously (Figure 10C), suggesting that a gradient in crosslinking density around cells must exist.

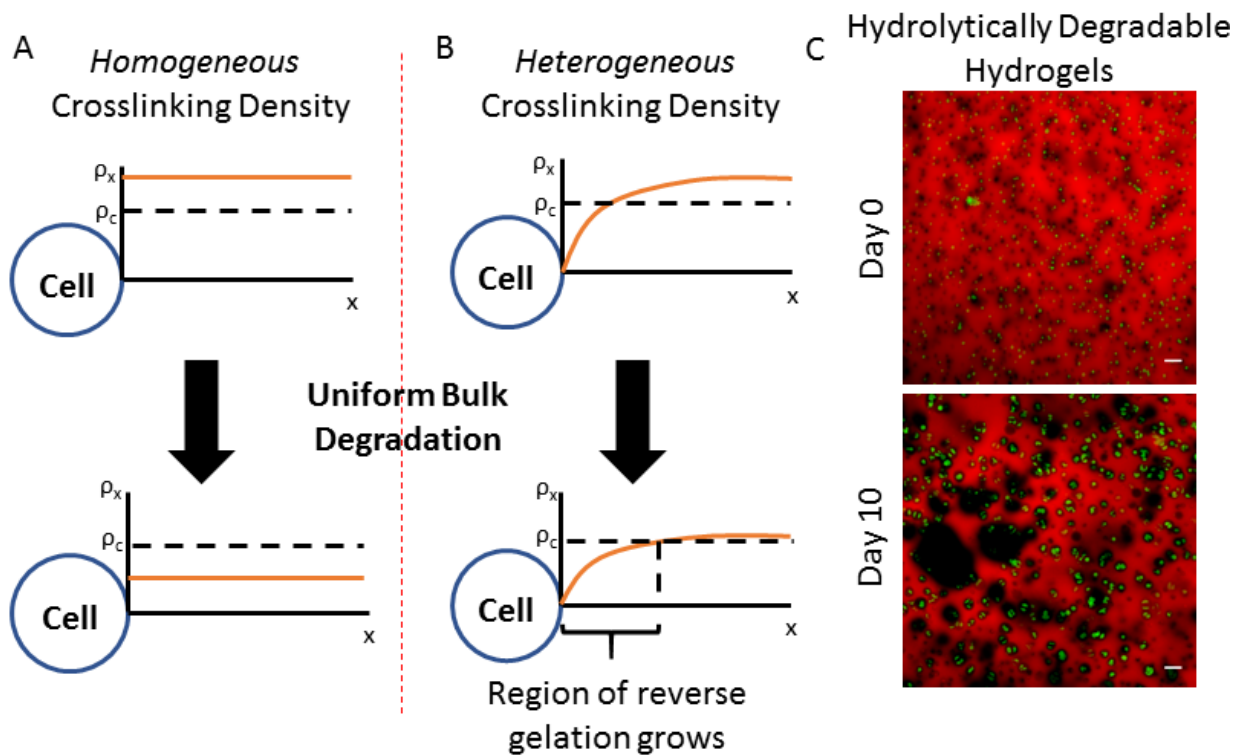


Figure 9. Schematic of possible outcomes in cell-laden hydrolytically degradable hydrogels. A) Cells encapsulated in a hydrogel with a spatially homogeneous crosslinking density resulting in the hydrogel reaching global reverse gelation. B) Cells encapsulated in a hydrogel with a gradient of crosslinking density around the cell resulting in the area around the cell reaching reverse gelation first. C) Confocal microscopy images of cells encapsulated in a hydrolytically degradable hydrogel observed over 10 days. Red = PEG. Green = cells (calcein). Scale bar = 50  $\mu\text{m}$ ; Images are sum of z-stacks.

The results of this study have been limited by the sensitivity of the techniques used. More refined and precise techniques capable of characterizing the cellular microenvironment in real-time would provide more insight on cell-polymer interactions. Additionally, only a few polymer properties are investigated in influencing cell-polymer interactions, namely thiolation, acrylation, and hydrophobicity. Other polymer properties, such as architecture and molecular weight, may also prove to be important but are not explored here. Finally, chondrocytes are used as a model cell type so that these results are most directly translatable to cartilage tissue engineering applications. However, the possible mechanisms explored here (such as cell-surface thiol

disulfide formation and radical chain transfer to the cell) would presumably be present in other cell types.

### **3.5 Conclusions**

This study demonstrates that chondrocytes have the ability to interact with both PEG based and thiolated monomers to such an extent as to cause a bulk decrease in hydrogel modulus. This bulk decrease in modulus is also observed in other PEG systems utilizing thiolated peptide crosslinkers, suggesting that disulfide bridges forming between the cell and crosslinker is one possible mechanism of interaction. A PEG concentration gradient around the cell leading to a gradient in crosslinking density that is also formed through radical termination on the cell and limited by radical diffusion. These results are critical in controlling the reproducibility of hydrogel constructs as well as controlling the microenvironment around the cell. Furthermore, cells were found to create a gradient in crosslinking density in the area around them which has implications in hydrogel degradation patterns.

### **3.6 Acknowledgments**

Research reported in this publication was supported by the National Institute of Arthritis and Musculoskeletal and Skin Diseases of the National Institutes of Health under Award Number 1R01AR065441. The authors acknowledge the National Institute of Health (NIH) Institutional Pharmaceutical Training fellowship and the Graduate Assistance in Areas of National Need (GAANN) Biomaterials from the Department of Education to SC. The technical assistance of Mollie Maples is also greatly appreciated.

### 3.7 References

1. Skaalure, S. C., Chu, S. & Bryant, S. J. An Enzyme-sensitive PEG Hydrogel Based on Aggrecan Catabolism for Cartilage Tissue Engineering. *Adv. Healthc. Mater.* **4**, 420–431 (2015).
2. Aisenbrey, E. A. & Bryant, S. J. A MMP7-sensitive photoclickable biomimetic hydrogel for MSC encapsulation towards engineering human cartilage. *J. Biomed. Mater. Res. A* **0**,
3. Liu, M. *et al.* Injectable hydrogels for cartilage and bone tissue engineering. *Bone Res.* **5**, 17014 (2017).
4. Patel, D., Sharma, S., Screen, H. R. C. & Bryant, S. J. Effects of cell adhesion motif, fiber stiffness, and cyclic strain on tenocyte gene expression in a tendon mimetic fiber composite hydrogel. *Biochem. Biophys. Res. Commun.* **499**, 642–647 (2018).
5. Aurand, E. R., Lampe, K. J. & Bjugstad, K. B. Defining and designing polymers and hydrogels for neural tissue engineering. *Neurosci. Res.* **72**, 199–213 (2012).
6. Fairbanks, B. D. *et al.* A Versatile Synthetic Extracellular Matrix Mimic via Thiol-Norbornene Photopolymerization. *Adv. Mater.* **21**, 5005–5010 (2009).
7. Nicodemus, G. D. & Bryant, S. J. Cell Encapsulation in Biodegradable Hydrogels for Tissue Engineering Applications. *Tissue Eng. Part B Rev.* **14**, 149–165 (2008).
8. Engler, A. J., Sen, S., Sweeney, H. L. & Discher, D. E. Matrix Elasticity Directs Stem Cell Lineage Specification. *Cell* **126**, 677–689 (2006).
9. Bryant, S. J. & Anseth, K. S. Hydrogel properties influence ECM production by chondrocytes photoencapsulated in poly(ethylene glycol) hydrogels. *J. Biomed. Mater. Res.* **59**, 63–72 (2002).
10. Bryant, S. J. & Anseth, K. S. Controlling the spatial distribution of ECM components in degradable PEG hydrogels for tissue engineering cartilage. *J. Biomed. Mater. Res. A* **64A**, 70–79 (2003).
11. Appelman, T. P., Mizrahi, J., Elisseeff, J. H. & Seliktar, D. The differential effect of scaffold composition and architecture on chondrocyte response to mechanical stimulation. *Biomaterials* **30**, 518–525 (2009).
12. Neumann, A. J., Quinn, T. & Bryant, S. J. Nondestructive evaluation of a new hydrolytically degradable and photo-clickable PEG hydrogel for cartilage tissue engineering. *Acta Biomater.* **39**, 1–11 (2016).
13. Rice, M. A., Waters, K. R. & Anseth, K. S. Ultrasound monitoring of cartilaginous matrix evolution in degradable PEG hydrogels. *Acta Biomater.* **5**, 152–161 (2009).
14. Nguyen, K. T. & West, J. L. Photopolymerizable hydrogels for tissue engineering applications. *Biomaterials* **23**, 4307–4314 (2002).



15. Roberts, J. J. & Bryant, S. J. Comparison of Photopolymerizable Thiol-ene PEG and Acrylate-Based PEG Hydrogels for Cartilage Development. *Biomaterials* **34**, 9969–9979 (2013).
16. Kuhl, T. *et al.* Direct Measurement of Polyethylene Glycol Induced Depletion Attraction between Lipid Bilayers. *Langmuir* **12**, 3003–3014 (1996).
17. Kim, M. *et al.* Surface Plasmon Resonance Study of the Binding of PEO–PPO–PEO Triblock Copolymer and PEO Homopolymer to Supported Lipid Bilayers. *Langmuir* **34**, 6703–6712 (2018).
18. Yasuda, S. *et al.* Dystrophic heart failure blocked by membrane sealant poloxamer. *Nature* **436**, 1025–1029 (2005).
19. Liu-Snyder, P., Logan, M. P., Shi, R., Smith, D. T. & Borgens, R. B. Neuroprotection from secondary injury by polyethylene glycol requires its internalization. *J. Exp. Biol.* **210**, 1455–1462 (2007).
20. Mina, E. W., Lasagna-Reeves, C., Glabe, C. G. & Kaye, R. Poloxamer 188 Copolymer Membrane Sealant Rescues Toxicity of Amyloid Oligomers In Vitro. *J. Mol. Biol.* **391**, 577–585 (2009).
21. Chapter 18 Induction of Mammalian Somatic Cell Hybridization by Polyethylene Glycol. *Methods Cell Biol.* **15**, 325–338 (1977).
22. Ross, P. C. & Hui, S. W. Polyethylene glycol enhances lipoplex-cell association and lipofection. *Biochim. Biophys. Acta BBA - Biomembr.* **1421**, 273–283 (1999).
23. Bryant, S. J., Cuy, J. L., Hauch, K. D. & Ratner, B. D. Photo-patterning of porous hydrogels for tissue engineering. *Biomaterials* **28**, 2978–2986 (2007).
24. Skaalure, S. C., Akalp, U., Vernerey, F. J. & Bryant, S. J. Tuning Reaction and Diffusion Mediated Degradation of Enzyme-Sensitive Hydrogels. *Adv. Healthc. Mater.* **5**, 432–438 (2016).
25. Sanchez-Adams, J. & Athanasiou, K. A. Biomechanical Characterization of Single Chondrocytes. in *Cellular and Biomolecular Mechanics and Mechanobiology* (ed. Gefen, A.) **4**, 247–266 (Springer Berlin Heidelberg, 2010).
26. Sasazaki, Y., Seedhom, B. B. & Shore, R. Morphology of the bovine chondrocyte and of its cytoskeleton in isolation and in situ: are chondrocytes ubiquitously paired through the entire layer of articular cartilage? *Rheumatology* **47**, 1641–1646 (2008).
27. Aubry, S. *et al.* Cell-surface thiols affect cell entry of disulfide-conjugated peptides. *FASEB J.* **23**, 2956–2967 (2009).
28. Woodward, C. E. & Forsman, J. Density Functional Study of Surface Forces in Solutions Containing Star-Shaped Polymers. *Macromolecules* **37**, 7034–7041 (2004).

29. Li, Y., Wei, X., Zhou, J. & Wei, L. The Age-Related Changes in Cartilage and Osteoarthritis. *BioMed Res. Int.* **2013**, e916530 (2013).
30. Loeser, R. F. Aging and Osteoarthritis: The Role of Chondrocyte Senescence and Aging Changes in the Cartilage Matrix. *Osteoarthr. Cartil. OARS Osteoarthr. Res. Soc.* **17**, 971–979 (2009).
31. Yang, L., Carlson, S. G., McBurney, D. & Horton, W. E. Multiple Signals Induce Endoplasmic Reticulum Stress in Both Primary and Immortalized Chondrocytes Resulting in Loss of Differentiation, Impaired Cell Growth, and Apoptosis. *J. Biol. Chem.* **280**, 31156–31165 (2005).
32. Yang, L., McBurney, D., Tang, S.-C., Carlson, S. G. & Horton, W. E. A novel role for Bcl-2 associated-athanogene-1 (Bag-1) in regulation of the endoplasmic reticulum stress response in mammalian chondrocytes. *J. Cell. Biochem.* **102**, 786–800 (2007).
33. Loeser, R. F. *et al.* Articular Chondrocytes Express the Receptor for Advanced Glycation End Products. *Arthritis Rheum.* **52**, 2376–2385 (2005).
34. O’Brien, A. K. & Bowman, C. N. Impact of Oxygen on Photopolymerization Kinetics and Polymer Structure. *Macromolecules* **39**, 2501–2506 (2006).
35. Bentivoglio Ruiz, C., Machado, L., Volponi, J. & Segura Pino, E. Oxygen Inhibition and Coating Thickness Effects on Uv Radiation Curing of Weatherfast Clearcoats Studied by Photo-DSC. *J. Therm. Anal. Calorim.* **75**, 507–512 (2004).
36. Farnsworth, N., Bensard, C. & Bryant, S. J. The role of the PCM in reducing oxidative stress induced by radical initiated photoencapsulation of chondrocytes in poly(ethylene glycol) hydrogels. *Osteoarthritis Cartilage* **20**, 1326–1335 (2012).
37. Lobo, V., Patil, A., Phatak, A. & Chandra, N. Free radicals, antioxidants and functional foods: Impact on human health. *Pharmacogn. Rev.* **4**, 118–126 (2010).
38. Farnsworth, N., Bensard, C. & Bryant, S. J. The role of the PCM in reducing oxidative stress induced by radical initiated photoencapsulation of chondrocytes in poly(ethylene glycol) hydrogels. *Osteoarthritis Cartilage* **20**, 1326–1335 (2012).
39. Richards, D. M. C., Dean, R. T. & Jessup, W. Membrane proteins are critical targets in free radical mediated cytolysis. *Biochim. Biophys. Acta BBA - Biomembr.* **946**, 281–288 (1988).
40. Donoghue, N., Yam, P. T., Jiang, X. M. & Hogg, P. J. Presence of closely spaced protein thiols on the surface of mammalian cells. *Protein Sci. Publ. Protein Soc.* **9**, 2436–2445 (2000).

## Chapter 4. Establishment of Cell Mimetic Particles as a Hydrogel Degradation Model

### Abstract

Hydrogels used in tissue engineering applications are typically much softer than their respective native tissue, necessitated by the need to maintain nutrient transport to support cells after encapsulation. An indirect measurement of tissue production by encapsulated cells is an observed increase in the bulk modulus of the hydrogel. Conversely, hydrogel degradation leads to softening of the hydrogels. Thus, the hydrogel modulus at any point in time will be a result of the complex interactions between hydrogel degradation and tissue deposition. Here, we describe experimental methods to decouple hydrogel degradation from tissue production to study their respective contributions to the overall hydrogel modulus. The overarching goal is to identify critical factors that influence whether hydrogel degradation follows either local or bulk degradation regimes. To achieve this, we use cell-mimetic poly (lactic-co-glycolic acid) (PLGA) microparticles that are loaded with enzyme and then are encapsulated in fluorescently labeled hydrogels crosslinked with peptide sequences susceptible to the specific enzyme in the particle. The use of cell-mimetic enzyme-releasing microparticles allows one to characterize hydrogel degradation without the contributing effects of tissue production on hydrogel construct modulus. In this chapter, preliminary work is presented to study the effects of enzyme concentration on degradation behavior and a discussion is offered to further expand on how these techniques can be used to explore different degradation regimes. The microparticles are initially loaded with 0.13 and 0.2 mg collagenase/mg PLGA encapsulated in the matrix metalloproteinase-sensitive hydrogels of the same crosslinking density. The bulk compressive moduli of the hydrogels were measured to monitor hydrogel degradation. Further, hydrogel

degradation was tracked through compression testing and laser scanning confocal microscopy (LSCM). The bulk compressive modulus of hydrogels loaded with particles with 0.13 mg collagenase/mg PLGA decreased at a rate faster than the decrease in modulus of hydrogels loaded with particles with 0.2 mg collagenase/mg PLGA, suggesting that high concentrations of enzyme may cause hydrogels to locally degrade. A higher enzyme concentration shifts the degradation front to be sharper causing a hydrogel degradation to be more localized around the microparticle, while the lower enzyme concentration allows the enzyme to readily diffuse throughout the hydrogel resulting in a wide degradation front.

#### **4.1 Introduction**

Successful tissue engineering strategies consisting of encapsulated matrix-producing cells in a hydrogel require complete degradation of the hydrogel and its replacement by newly synthesized tissue. To achieve a seamless transfer from hydrogel to tissue, hydrogel degradation should be closely tuned to match the rate of tissue production<sup>1</sup>. One promising strategy is cell-mediated degradable hydrogels where peptide crosslinkers are incorporated into the hydrogel and are susceptible to cleavage by enzymes secreted by the encapsulated cells. Enzyme-sensitive hydrogels offer the potential of localized degradation of the hydrogel around the cell while providing space for neotissue to deposit. Hydrogel degradation will vary in space and time based on enzyme diffusion and reaction kinetics<sup>2</sup>. At the same time, tissue is deposited, but only in regions where hydrogel has completely degraded<sup>3,4</sup>. This closely coupled behavior makes it particularly difficult to study the mechanisms of degradation. In this chapter, experimental methods to decouple hydrogel degradation from tissue production are examined. This work expands upon on previous studies by the group<sup>2</sup> which developed enzyme-releasing cell mimetics

to characterize hydrogel degradation. Specifically, microparticles were encapsulated in hydrogels of varying crosslinking density to study the factors that influence hydrogel degradation towards local versus bulk degradation regimes. The cell-mimetics are poly (lactic-co-glycolic acid) (PLGA) particles with entrapped enzymes and when encapsulated in an enzyme-sensitive hydrogel allow for degradation of the hydrogel to be investigated without tissue deposition. In this chapter, we created microparticles loaded with different amounts of enzyme and encapsulated them in enzyme-sensitive hydrogels of the same initial crosslinking density. This cell-mimetic platform can be further expanded to investigate critical factors that influence the mechanisms of hydrogel degradation that lead to bulk or localized degradation.

## **4.2 Materials and Methods**

### ***4.2.1 Microparticle Formation***

Microspheres made of hydrolytically degradable poly (lactic-co-glycolic acid) (50:50 poly(DL-lactide-co-glycolide) (PLGA), 1.13 inherent viscosity; (Durect, Birmingham, AL)) were formed using a water-oil-water double emulsion technique<sup>2,5,6</sup> and loaded with an enzyme blend Collagenase Type II (hereafter referred to as collagenase; Worthington Biochemical Corporation, Lakewood, NJ). Briefly, PLGA was dissolved in methylene chloride (ThermoFisher, Fair Lawn, NJ) at a concentration of 150 mg PLGA/mL and then mixed with the encapsulant (Collagenase Type II at a concentration of 20 or 30 mg protein/100  $\mu$ L of PBS (Corning, Corning, NY)). The mixture was emulsified using a probe sonicator (Microson 2000 Ultrasonic Cell disruptor; Misonix, Farmingdale, NY) for 15 s. The emulsion was transferred to an emulsifying agent made of poly (vinyl alcohol) (PVA MW 30,000-70,000; Sigma-Aldrich, St. Louis, MO) and sucrose (Sigma-Aldrich, St. Louis, MO). The mixture was allowed to evaporate in an open beaker overnight while

stirring. The mixture was centrifuged at 4000 rpm for 10 minutes and washed three times in diH<sub>2</sub>O. The final mixture was resuspended in diH<sub>2</sub>O, flash frozen in liquid nitrogen, and lyophilized for at least 48 h.

#### **4.2.2 Microparticle Characterization**

The double emulsion technique for PLGA microparticle formation led to a distribution of particle sizes. Particle morphology and size were visualized using Scanning Electron Microscopy (SEM, JEOL JSM-6480LV).

The release kinetics of protein in the microparticles were characterized. 10 mg of each particle condition (n = 3) were suspended in PBS supplemented with 0.6 mM CaCl<sub>2</sub> and 0.9 mM MgCl<sub>2</sub> (Invitrogen, Carlsbad, CA). The particle suspension was incubated at 37°C on a figure-eight shaker plate (70 rpm). At each time point, the suspension was vortexed and centrifuged (4 min, 13000 rpm). The PBS was collected, flash frozen, and stored at -80°C until analysis. Fresh PBS was provided to the particles at each collection time point. The protein content was quantified using the NanoOrange Protein Quantification Kit.

#### **4.2.3 Macromer Synthesis**

An 8-arm PEG-norbornene (PEG-NB) macromer was synthesized by reacting 8-arm PEG-NH<sub>2</sub> (20 kDa; Jenkem Technology USA, Plano, TX) with four molar excess 5-norbornene-2-carboxylic acid (Sigma-Aldrich, St. Louis, MO), three molar excess of O-(7-azabenzotriazol-1-yl)-N,N,N',N'-tetramethyluronium hexafluorophosphate (HATU; ChemImpex International, Inc., Woodale, IL) and six molar excess of N,N-Diisopropylethylamine in dimethylformamide (ThermoFisher, Fairlawn, NJ) overnight at room temperature under argon. The final product,

PEG-NB, was recovered and purified by precipitation in diethyl ether (Sigma-Aldrich, St. Louis, MO), filtration, dialysis (regenerated cellulose 1000 MWCO dialysis tubing; Spectrum Labs, Rancho Dominguez, CA) in de-ionized water over several days, and lyophilization. Norbornene conjugation to each arm of the 8-arm PEG-NH<sub>2</sub> was determined with <sup>1</sup>H nuclear magnetic resonance spectroscopy by comparing the olefinic hydrogen peaks in the norbornene ( $\delta = 5.9-6.25$  ppm) to the methylene hydrogen peaks in the PEG backbone ( $\delta = 3.4-3.9$  ppm). The norbornene conjugation was determined to be ~100%. The matrix metalloproteinase (MMP)-sensitive peptide crosslinker, GCVPLS-LYSGCG (GenScript, Piscataway, NJ) was used as received.

#### ***4.2.4 Microparticle Encapsulation in Fluorescent Hydrogels***

Fluorescent hydrogels were prepared by introducing  $0.01 \times 10^{-3}$  M AlexaFluor-546 C5 maleimide (ThermoFisher, Fairlawn, NJ) in the precursor solution and allowed to conjugate for at 37°C for 30 mins prior to polymerization. The fluorophore is a maleimide-conjugated fluorophore that readily attaches to free thiols. The fluorophore was reacted at an excess of thiols (approximately [thiol]:[fluorophore] = 400) such that a small percentage of the dithiolated crosslinkers become monothiol tethers. Thus, the fluorophore is essentially attached to the dangling ends of non-crosslinked PEG arms and the fluorescence of the hydrogel can be related to polymer density. The precursor solution was mixed with protein-loaded microparticles at a final concentration of 12 mg microparticles/mL. Fluorescent PEG hydrogels were formed by a photoclickable reaction between 8-arm PEG-NB and an MMP sensitive peptide GCVPLS-LYSGCG (5% (g/g) 8-arm PEG-NB, [thiol]:[ene] = 0.9) in the presence of a photoinitiator Irgacure 2959 (0.05 wt% I2959; Ciba Specialty Chemicals, Tarrytown, NY) and 352 nm light at 6 mW/cm<sup>-2</sup> for 7 min (Figure 1A).

Hydrogels were characterized by their compressive modulus which was measured from the linear region of the stress–strain curve by compressing hydrogels at a rate of 10% per min to 15% strain (n = 3–4) using a mechanical tester (MTS Synergie 100, 10N, Eden Prairie, MN). Hydrogel degradation was observed starting immediately (day 0) after polymerization using a laser-scanning confocal microscope (LSCM, Zeiss LSM 510, Thornwood, NY) at 100x magnification.

#### ***4.2.5 Semi-quantitative and Statistical Analysis of Hydrogel Degradation***

ImageJ software and MATLAB were used to semi-quantitatively assess changes in void growth (i.e. hydrogel degradation). Void space diameters were measured (n ≈ 3000 measurements per time point or otherwise specified) and the nonparametric Kolmogorov–Smirnov test was used to determine changes in the void size distributions after 3 d ( $\alpha = 0.05$ ). For the enzyme release kinetics, a two-way ANOVA ( $\alpha=0.05$ ) was performed for with time and enzyme concentration as factors. For the modulus of hydrogels, a two-way ANOVA ( $\alpha=0.05$ ) was performed with time and enzyme concentration as factors. A follow-up one-way analysis of variance was performed to determine the significance of enzyme concentration at each time point as well as the overall significance of time for each enzyme concentration.

### **4.3 Results**

Synthetic hydrolytically degradable microparticles loaded with an enzyme encapsulant can be used as cell substitutes, mimicking their enzyme-releasing properties without their tissue-producing capabilities. These particles were photoencapsulated into an enzyme-sensitive fluorescently-labeled polymer network (Figure 1A) to study hydrogel degradation in the absence of tissue deposition, two competing factors contributing to hydrogel modulus. As the



microparticles degrade, they release their enzyme payload to degrade the enzyme-labile crosslinks of the polymer network (Figure 1B). Below, the enzyme-release characteristics of these microparticles are described and how they mediate hydrogel degradation when encapsulated into MMP-sensitive hydrogels.

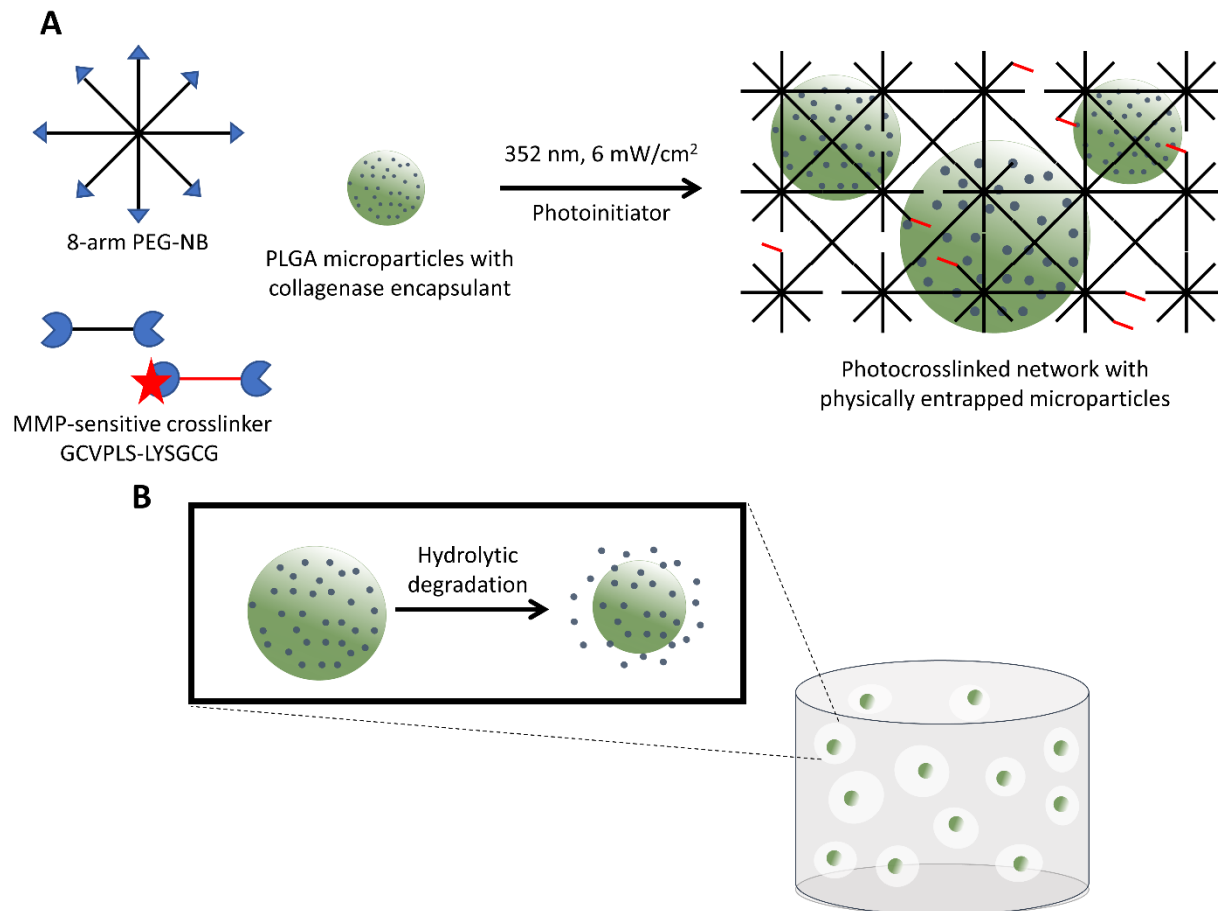


Figure 1. A) Microparticles formed from poly (lactic-co-glycolic acid) (PLGA) were mixed with eight-arm PEG-norbornene (PEG-NB, MW 20kDa) crosslinked with an MMP-sensitive peptide crosslinker (GCVPLS-LYSGCG, MW 1155). A fraction of the crosslinkers were tagged with a fluorophore. The mixture was photopolymerized to create a crosslinked network with physically entrapped microparticles. B) As the PLGA microparticles hydrolytically degrade, they release their collagenase payload. The released collagenase then degrades the MMP-sensitive crosslinks of the hydrogel network.

#### **4.3.1 Microparticle Characterization**

Microparticles were fabricated by initially mixing either 0.20 mg collagenase/mg PLGA or 0.13 mg collagenase/mg PLGA in a water-oil-water double emulsion technique as described previously<sup>2,6</sup>. Blank particles were created as a negative control. Sample SEM images showing size and morphology of the blank particles and enzyme-loaded particles are shown in Figure 2A. The cumulative release profile of protein from the hydrolytically degradable PLGA microparticles was characterized under physiological pH conditions (Figure 2B). Particles loaded with either concentration showed a rapid release of their encapsulant initially followed by a sustained release. Particles initially loaded with 0.20 mg collagenase/mg PLGA released more enzyme at each time point compared to particles initially loaded with 0.13 mg collagenase/mg PLGA ( $p < 0.04$ ). For each particle condition, time was a significant factor in the amount of collagenase released ( $p < 0.001$ ).

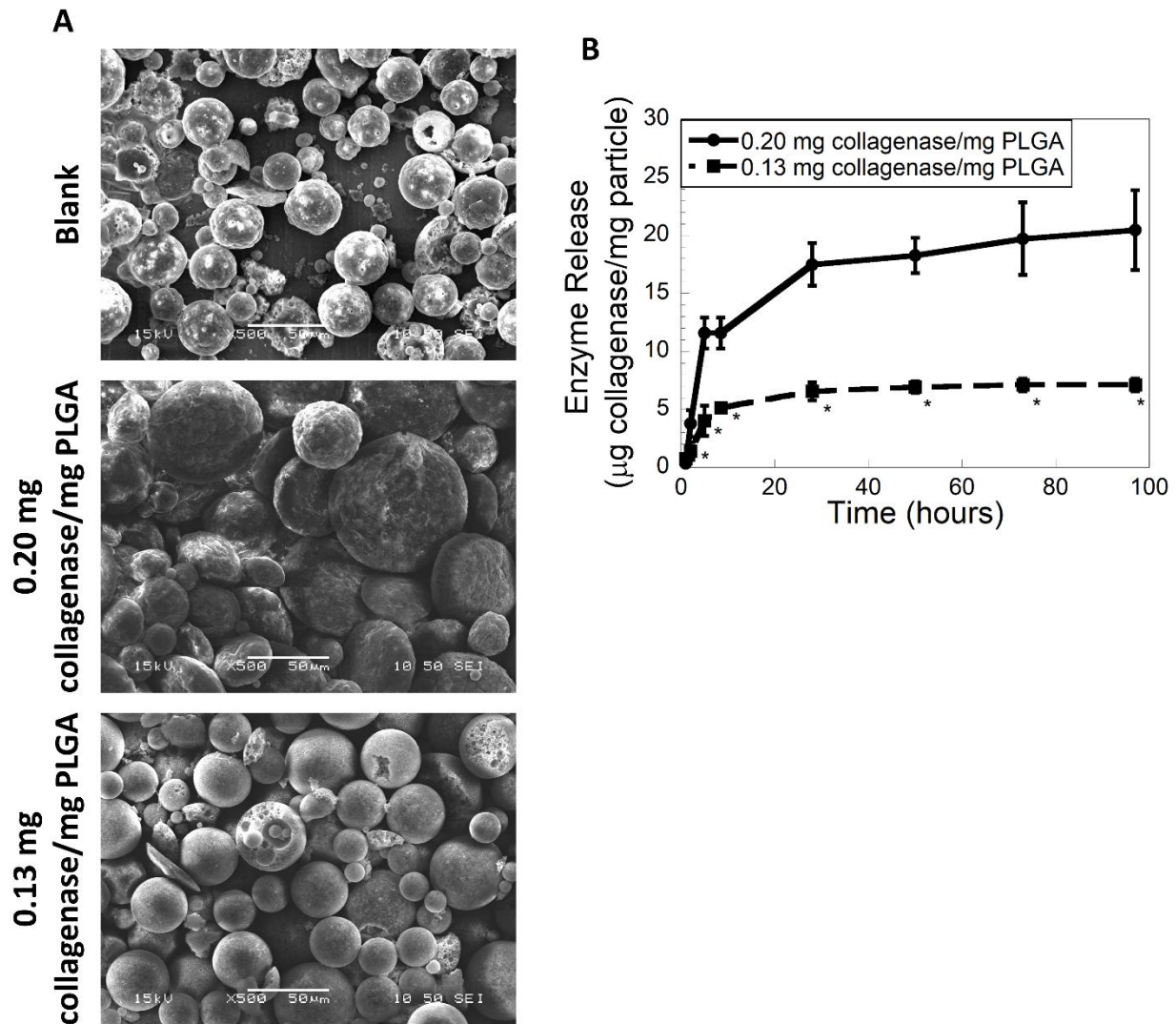


Figure 4. A) Sample SEM images of microparticles with no enzyme encapsulated, 0.20 mg collagenase/mg PLGA, and 0.13 mg collagenase/mg PLGA. B) Cumulative enzyme release kinetics of PLGA microparticles loaded with 0.20 mg collagenase/mg PLGA and 0.13 mg collagenase/mg PLGA. A (\*) at each time point denotes that cumulative enzyme release at each time point is significantly ( $p < 0.04$ ) different between the two microparticle conditions.

#### 4.3.2 Hydrogel Degradation

Blank microparticles and microparticles loaded with 0.20 mg collagenase/mg PLGA and 0.13 mg collagenase/mg PLGA were encapsulated in fluorescently labeled MMP-sensitive hydrogels of similar crosslinking densities (as controlled by keeping the same concentration of monomers in the precursor solution). The hydrogel modulus was recorded as a function of time

(Figure 3A). The modulus of constructs encapsulated with enzyme-loaded microparticles decreased over the course of ~150 hours ( $p < 0.01$ ); however, the modulus of constructs encapsulated with blank particles did not change with time. Interestingly, the average modulus of constructs loaded with 0.13 mg collagenase/mg PLGA (4.5 (1.7)) was lower than the average modulus of hydrogels loaded with 0.20 mg collagenase/mg PLGA (14.6 (4.7)) ( $p = 0.012$ ) after ~150 hours. Hydrogels loaded with 0.20 mg collagenase/mg PLGA particles experienced a ~40% decrease in modulus after ~150 hours, whereas hydrogels loaded with 0.13 mg collagenase/mg PLGA particles experienced an ~80% decrease in modulus (Figure 3B). At all time points, the modulus of hydrogels loaded with 0.20 mg collagenase/mg PLGA were not significantly different from the modulus of hydrogels loaded with blank particles; however, time was a significant factor ( $p = 0.01$ ) in reducing the modulus of hydrogels loaded with 0.20 mg collagenase/mg PLGA whereas time was not a significant factor in changing the moduli of hydrogels encapsulated with blank particles.

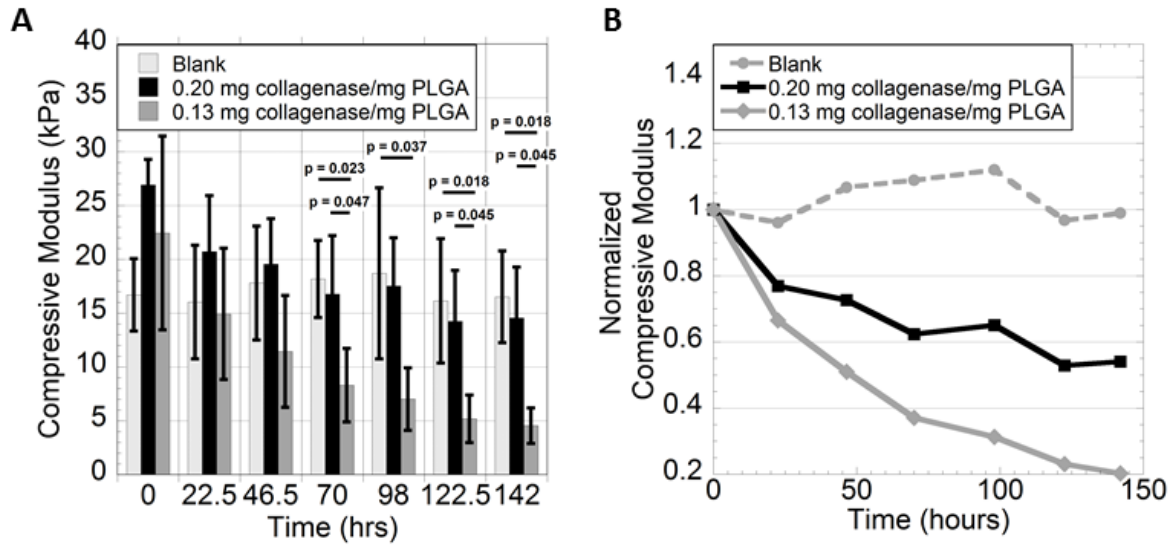


Figure 5. Modulus of hydrogel constructs loaded with blank particles, 0.20 mg collagenase/mg PLGA particles, and 0.13 mg collagenase/mg PLGA particles. A) Absolute modulus of hydrogels loaded with particles. B) Normalized modulus of hydrogels loaded with particles.

Microparticle-laden hydrogels were observed using LCSM starting immediately after encapsulation (0 hr) and over several days (Figure 4A). The degradation of these hydrogels as a result of enzyme release from microparticles can be seen via the decrease in hydrogel fluorescence and the growth of the void spaces (corresponding to the space occupied by microparticles and/or hydrogel degradation). Compared to hydrogels encapsulated with blank particles, hydrogels encapsulated with collagenase-loaded particles qualitatively showed a decrease in fluorescence over time; however, there was no noticeable increase in void spaces (Figure 4A). This suggests that diffusion of the released enzyme is faster than the kinetics of peptide cleavage, leading to a degradation regime that is more characteristic of bulk degradation. Indeed, the modulus of hydrogels encapsulated with collagenase-loaded microparticles decreased over the course of three days, indicating bulk degradation (Figure 3). The LCSM images were analyzed using MATLAB to quantify the evolution of the void space diameters over time.

For all three conditions, the histograms of the void spaces observed at 90 hrs were significantly different from the histograms observed at 0 hrs; however, this can be attributed to the swelling of the hydrogel rather than any degradation causing growth of void spaces. Therefore, histograms from 46.5 hrs and 90 hrs were compared, as the hydrogels would presumably have reached equilibrium swelling at this point. Only hydrogels loaded with 0.13 mg collagenase/mg PLGA had significantly different ( $p < 0.0001$ ) histograms at 90 hrs compared to 46.5 hrs (Figure 4B). Furthermore, at 90 hrs, histograms from all three conditions were significantly different ( $p < 0.0001$ ).

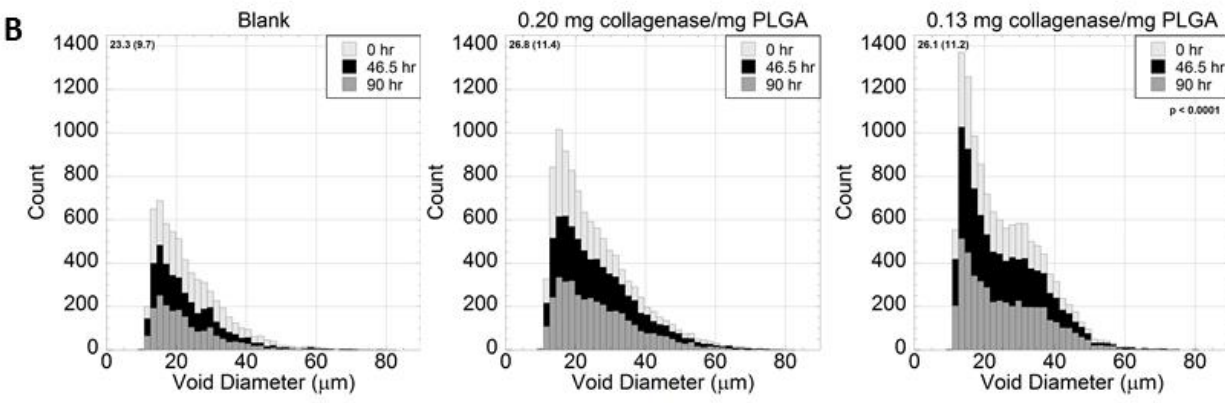
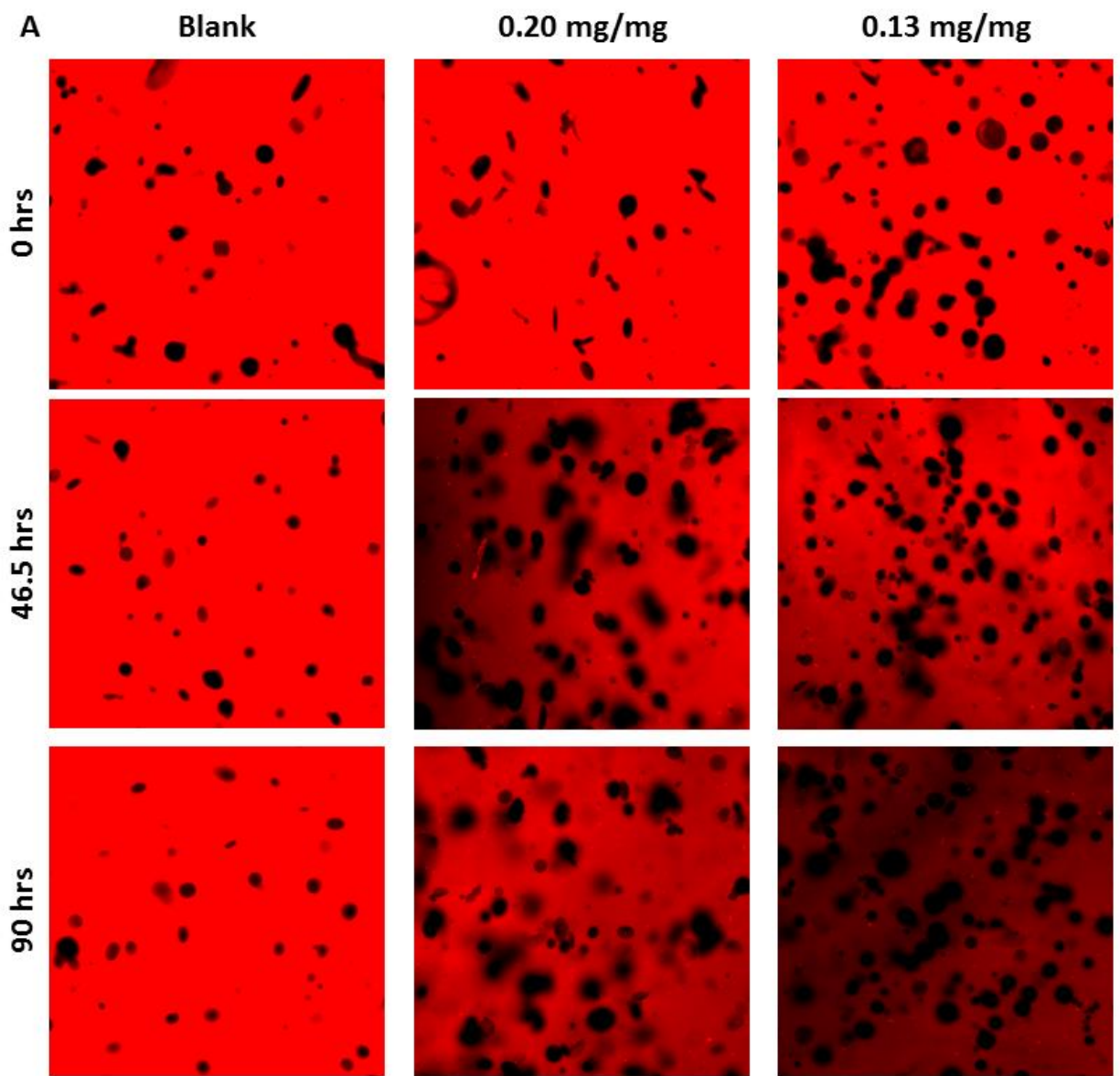


Figure 6. A) Laser scanning confocal microscopy (LSCM) images of fluorescently labeled hydrogels encapsulated with blank particles, 0.20 mg collagenase/mg PLGA, or 0.13 mg collagenase/mg PLGA. The dark regions can be attributed to the space occupied by microparticles and degraded areas of hydrogel. B) Histograms showing the area of void spaces over time. A p-value shows that the histogram from 90 hrs is statistically different from the histogram from 46.5 hrs for the same enzyme concentration. The number of voids counted for hydrogels with blank particles was (n≈2000), with 0.20 mg collagenase/mg PLGA particles was (n≈3000-4000), and 0.13 mg collagenase/mg PLGA particles was (n≈3000-5000). The mean diameter of each distribution is represented in the top left corner of each histogram with the standard deviation represented in parentheses.

#### 4.4 Discussion

Previously, Skaalure *et al.*<sup>2</sup> utilized enzyme-loaded PLGA microparticles encapsulated in MMP-sensitive hydrogels to study the how hydrogel crosslinking density shifted hydrogel degradation towards local or bulk hydrogel degradation regimes. In this chapter, preliminary work is shown analyzing the effects of enzyme concentration on local versus bulk hydrogel degradation regimes. Specifically, PLGA microparticles were fabricated and initially loaded with 0.20 mg collagenase/mg PLGA or 0.13 mg collagenase/mg PLGA. As a negative control, microparticles containing no enzyme were fabricated. As expected, microparticles with 0.20 mg collagenase/mg PLGA released significantly more enzyme compared to microparticles with 0.13 mg collagenase/mg PLGA (Figure 3A).

Complex systems in which both reaction kinetics and diffusion play an important role can be partially characterized utilizing the Thiele Modulus ( $\phi^2$ ) given by

$$\phi^2 = \frac{k_{cat} r_e^2}{D_e} \approx \frac{reaction}{diffusion}$$

where  $k_{cat}$  is the catalytic constant,  $r_e$  is the radius of the enzyme, and  $D_e$  is the diffusivity constant of the enzyme. As inferred from the equation, a high value of Thiele Modulus indicates



a system is reaction dominated whereas a low value of Thiele Modulus indicates a system is diffusion dominated. For the hydrogels and enzymes used in this chapter, the Thiele Modulus is on the order of  $10^{-6}$  suggesting that these systems are heavily diffusion dominated. The radius of the enzyme has previously<sup>2</sup> been estimated to be  $\sim 6.5$  nm and the mesh size of the hydrogels used in this work is on the order of 100 nm meaning that the enzyme can readily diffuse through the hydrogel network. This is reflected in the modulus of the hydrogels encapsulated with enzyme-loaded microparticles. The modulus of these hydrogels decreased drastically over the course of this experiment, characteristic of bulk degradation caused by the enzyme able to readily diffuse throughout the hydrogel. Specifically, hydrogels loaded with 0.20 mg collagenase/mg PLGA particles experienced a  $\sim 40\%$  decrease in modulus and hydrogels loaded with 0.13 mg collagenase/mg PLGA particles experienced an  $\sim 80\%$  reduction in modulus (Figure 3B). Additionally, LSCM of the hydrogels with enzyme-loaded particles qualitatively showed a general decrease in fluorescence (Figure 4A). We estimated that at the maximum rate of diffusion, that it would take  $\sim 100$  seconds for the enzyme to diffuse 100  $\mu\text{m}$  (i.e. 10 times the length of the diameter of a cell). Comparatively, at the maximum reaction rate (proportional to the total enzyme concentration), it would take more than 150 hours for the high enzyme concentration to completely degrade the hydrogel and more than 400 hours for the low enzyme concentration to completely degrade the hydrogel. Thus, this system is primarily diffusion dominated by comparing the timescales of reaction and diffusion.

Given that the Thiele Modulus depends only on the size of the enzyme and the catalytic constant of the enzyme towards its substrate, the Thiele Modulus for both hydrogel conditions loaded with different concentrations of enzyme is the same. However, the hydrogels loaded with

the two different batches of microparticles showed varying degradation behaviors. The particles loaded with a lower concentration of enzyme (0.13 mg collagenase/mg PLGA) degraded the hydrogel more than the particles with a high concentration of enzyme (0.20 mg collagenase/mg PLGA), as evidenced by the significantly lower modulus by ~150 hours. One possible explanation is that a high initial concentration of enzyme increases the reaction rate of peptide cleavage near the cell, whereas a lower concentration of enzyme allows the enzyme to diffuse throughout the hydrogel causing a wider degradation front. Indeed, for a given initial hydrogel crosslinking density, Skaalure *et al.*<sup>2</sup> has suggested that a higher enzyme concentration promotes a sharper degradation front and shifts degradation towards a more reaction-dominated locally degrading regime. Experimentally, the void spaces (corresponding to hydrogel degradation) in hydrogels loaded with 0.13 mg collagenase/mg PLGA particles grew significantly when comparing 46.5 hrs to 90 hrs. This can be attributed to a wide degradation front leading to the fusing of individual void spaces. Comparatively, the void spaces in hydrogels loaded with 0.20 mg collagenase/mg PLGA particles were not significantly different from 46.5 hrs to 90 hrs. This suggests that the degradation front was sharper and did not lead to fusing of void spaces.

Skaalure *et al.*<sup>2</sup> proposed a dimensionless quantity  $\kappa$  further describing a system's reaction-diffusion characteristics given by

$$\kappa = \frac{k_{cat}[e]_0 L^2}{D_e \rho_c} (Q_0 - 1) \exp\left(\frac{1}{Q_0 - 1}\right)$$

where  $[e]_0$  is the initial enzyme concentration,  $\rho_c$  is the critical crosslinking density of the hydrogel (below which the network reaches reverse gelation and becomes soluble polymers again), and  $Q_0$  is the initial volumetric swelling ratio. In general, a higher value of  $\kappa$  suggests that

the degradation front is sharper. The microparticles containing different concentrations of enzyme were encapsulated in hydrogels of identical formulation. In other words, the crosslinking density and initial volumetric swelling ratio are the same and  $\kappa$  for the different microparticle conditions scales with the initial enzyme concentration. The  $\kappa$  for the 0.20 mg collagenase/mg PLGA microparticles was estimated to be about three times the value of  $\kappa$  for the 0.13 mg collagenase/mg PLGA microparticles. These values again show that the particles loaded with a higher concentration of enzyme lead to slightly sharper degradation fronts.

The results reported in this chapter represent preliminary work in investigating critical factors that influence local versus bulk hydrogel degradation. Specifically, enzyme concentration was found to be important with a higher enzyme concentration causing sharper degradation fronts. Further work should be done to validate the model previously developed<sup>2</sup> that describes local versus bulk hydrogel degradation. Other important factors in influencing reaction-diffusion interactions include (but not limited to) enzyme radius and reactivity, and hydrogel crosslinking density. The enzyme radius and reactivity can be altered by changing the enzyme-substrate pair, namely changing the sequence of the peptide crosslinkers to target different matrix-degrading enzymes. If the same enzyme targets are desired, the peptide sequence can potentially be engineered to have different reactivities towards the same enzymes.

The microparticle platform shown in this chapter has several limitations. Namely, the fabrication of the microparticles results in a large size distribution (as can be qualitatively seen in the SEM images) which can lead to variable release profiles. Thus, this can potentially confound data analysis when looking at individual degradation fronts. Tighter control over microparticle size can potentially be achieved by using increasing the stirring rate during emulsification<sup>5</sup> or by

using microfluidics<sup>7</sup>. Additionally, enzyme diffusion gradients in the hydrogel could be affected by the rate at which the enzyme is released from the microparticle. While it is shown in this work that the microparticles have an initial burst release of enzyme, it is unknown the enzyme-release profile of cells. Creating particles that exhibit a release profile resembling that of cells could make these results more translatable to cellular systems.

#### **4.5 Conclusions**

In this work, we expand upon a framework of experimental techniques to decouple the competing effects of hydrogel degradation and tissue production. Specifically, the development of enzyme-loaded microparticles mimic the cell as a point-source of MMPs that degrade the enzyme-sensitive hydrogel. In this chapter, the concentration of enzyme released was found to be an important factor in influencing whether hydrogel degradation follows local or bulk degradation regimes. More work is needed to further elaborate upon the complex interactions between enzyme concentration and crosslinking density to characterize locally and bulk degrading hydrogels.

#### **4.6 Acknowledgments**

Research reported in this publication was supported by the National Institute of Arthritis and Musculoskeletal and Skin Diseases of the National Institutes of Health under Award Number 1R01AR065441. The authors acknowledge the National Institute of Health (NIH) Institutional Pharmaceutical Training fellowship and the Graduate Assistance in Areas of National Need (GAANN) Biomaterials from the Department of Education to SC. The technical assistance of Kristin Nicole Calahan, Mollie Maples, and Pallavi Bhusal is also greatly appreciated.

## 4.7 References

1. Nicodemus, G. D., Skaalure, S. C. & Bryant, S. J. Gel structure impacts pericellular and extracellular matrix deposition which subsequently alters metabolic activities in chondrocyte-laden PEG hydrogels. *Acta Biomater.* **7**, 492–504 (2011).
2. Skaalure, S. C., Akalp, U., Vernerey, F. J. & Bryant, S. J. Tuning Reaction and Diffusion Mediated Degradation of Enzyme-Sensitive Hydrogels. *Adv. Healthc. Mater.* **5**, 432–438 (2016).
3. Dhote, V. & Vernerey, F. J. Mathematical model of the role of degradation on matrix development in hydrogel scaffold. *Biomech. Model. Mechanobiol.* **13**, 167–183 (2013).
4. Akalp, U., Bryant, S. J. & Vernerey, F. J. Tuning tissue growth with scaffold degradation in enzyme-sensitive hydrogels: a mathematical model. *Soft Matter* **12**, 7505–7520 (2016).
5. O'Donnell, P. B. & McGinity, J. W. Preparation of microspheres by the solvent evaporation technique. *Adv. Drug Deliv. Rev.* **28**, 25–42 (1997).
6. Ashton, R. S., Banerjee, A., Punyani, S., Schaffer, D. V. & Kane, R. S. Scaffolds based on degradable alginate hydrogels and poly(lactide-co-glycolide) microspheres for stem cell culture. *Biomaterials* **28**, 5518–5525 (2007).
7. Damiati, S., Kompella, U. B., Damiati, S. A. & Kodzius, R. Microfluidic Devices for Drug Delivery Systems and Drug Screening. *Genes* **9**, (2018).

## **Chapter 5. Understanding the Spatiotemporal Degradation Behavior of Aggrecanase-Sensitive Poly(ethylene glycol) Hydrogels for use in Cartilage Tissue Engineering**

**(As appearing in *Tissue Eng Part A* (15-16):795-810 (2017))**

### **Abstract**

Enzyme-sensitive hydrogels are promising cell delivery vehicles for cartilage tissue engineering. However, a better understanding of their spatiotemporal degradation behavior and its impact on tissue growth is needed. The goal of this study is to combine experimental and computational approaches to provide new insights into spatiotemporal changes in hydrogel crosslink density, spatiotemporal changes in extracellular matrix (ECM) growth, and how these changes influence the evolving macroscopic properties (*i.e.*, mechanical properties) as a function of time. Hydrogels were designed from aggrecanase-sensitive peptide crosslinks using a simple and robust thiol:norbornene photoclick reaction. To study the influence of variations in cellular activity as a result of different donors, chondrocytes were isolated from either juvenile or adult bovine donors. Initially, experimental and computational approaches were combined to a) validate that the model captures the initial mechanical properties of cell-laden aggrecanase-sensitive hydrogels and b) estimate the modulus of cell-secreted ECM using a non-degradable version of the hydrogel. The model was then implemented to characterize the spatial and temporal evolution of hydrogel degradation, ECM growth and overall construct mechanical properties for chondrocytes isolated from two different donors. Overall, this study demonstrates that a) spatial heterogeneities, which form during the encapsulation of chondrocytes, facilitate localized ECM growth and b) the combination of enzyme and ECM synthesis rates, which are characteristics of the donor, can lead to improved ECM growth as shown here for the juvenile

chondrocytes or poor ECM growth as shown for the adult chondrocytes. Overall, this study points to the importance of designing hydrogels specific to each donor.

## 5.1 Introduction

Hydrogels designed with crosslinks that are sensitive to enzymes secreted by encapsulated cells are promising platforms for tissue engineering<sup>1,2</sup>. Enzyme-sensitive hydrogels provide a three-dimensional environment that can be degraded by embedded cells similar to that in the native extracellular matrix (ECM). Several studies have reported on enzyme-sensitive hydrogels for cartilage tissue engineering. For example, chondrocytes embedded in a matrix metalloproteinase (MMP)-2 sensitive hydrogel produced more ECM than in non-degradable hydrogels evident by the formation of a larger pericellular matrix<sup>3</sup> and by a greater amount of overall matrix deposition<sup>4</sup>. Longer-term studies have shown increased ECM deposition and elaboration over the course of twelve weeks in an aggrecanase-sensitive hydrogel containing encapsulated chondrocytes<sup>5</sup>. Hydrogels with crosslinks sensitive to MMP-7<sup>6</sup> or a combination of MMP-7 and aggrecanase<sup>7</sup> supported chondrogenesis of encapsulated mesenchymal stem cells and promoted deposition of cartilage-specific ECM molecules. Overall these studies demonstrate that the inclusion of enzyme-sensitive crosslinks creates an environment that supports ECM deposition and importantly, ECM elaboration, which is critical to creating a macroscopic engineered cartilage tissue.

Tuning hydrogel degradation with ECM synthesis is an important criterion to achieving a successful outcome in tissue engineering. One of the challenges is that the mesh size of the hydrogel network, which encapsulates cells, is several orders of magnitude smaller than the size of many ECM molecules that make up tissues like cartilage<sup>8,9</sup>. For example, cartilage is comprised

predominantly of two main ECM molecules: aggrecan, which can reach molecular weights of  $\sim 1\text{-}3\text{ MDa}$ <sup>10</sup> and collagen type II, which can reach microns in length<sup>11</sup>. As a result, these large ECM molecules are unable to diffuse and deposit within a crosslinked hydrogel<sup>8,9</sup>. Thus, to form a macroscopic tissue without complete loss of mechanical support, hydrogel degradation must closely couple to ECM synthesis rates. This close coupling has been challenging to achieve with some studies reporting improved mechanical properties<sup>12</sup> while others reporting large drops in mechanical properties<sup>13</sup> concomitant with neo-cartilage deposition and growth. This challenge is further exemplified by variations in the activity of the encapsulated cells, which arise from differences in the donor (*e.g.*, age, health, etc.). Enzyme-sensitive hydrogels provide a mechanism whereby hydrogel degradation can occur locally as cell-secreted enzymes diffuse radially outward from the cell and cleave nearby crosslinks, thus providing space where ECM molecules can diffuse and deposit. However, a better understanding of the spatiotemporal degradation behavior of enzyme-sensitive hydrogels and its impact on tissue growth is needed.

Enzyme-sensitive hydrogels lead to degradation behaviors that are highly complex, involving reaction-diffusion phenomena. To understand this complex degradation behavior, we have developed mathematical models to describe the local degradation of enzyme-sensitive hydrogels<sup>13-16</sup>. As cells secrete enzymes, diffusion of these molecules through the hydrogel depend on their relative size compared to the mesh size of the polymer network. The degradation kinetics of the hydrogel are governed by enzyme kinetics that depend on the enzyme and substrate (*e.g.*, enzyme-sensitive crosslinks in a hydrogel) and the local concentration of enzyme. As crosslinks are cleaved locally, the mesh size of the hydrogel increases leading to higher local enzyme diffusion. Thus, the tightly coupled behavior of reaction and diffusion mechanisms leads



to changes in crosslink densities that vary in time and space. This behavior depends on enzyme characteristics (*i.e.*, size, Michaelis-Menten kinetics, concentration) and the initial hydrogel crosslink density. We recently extended the model to include encapsulated cells that synthesize ECM molecules. Through simulations, we demonstrated the importance of closely coupling hydrogel degradation to enzyme and ECM synthesis rates in order to maintain overall mechanical integrity during the transition from predominantly hydrogel to predominantly ECM<sup>17</sup>.

In this study, we combine our mathematical model with an experimental platform of chondrocytes encapsulated in an enzyme-sensitive hydrogel. We chose an aggrecanase-sensitive hydrogel, which we have previously shown is promising for cartilage tissue engineering<sup>5</sup>. Using the same hydrogel formulation, we investigate how changes in the behavior of the encapsulated cells, notably by enzyme and ECM synthesis rates, influence ECM growth and overall construct mechanical properties. By combining computational approaches with experimental platforms, this study aims to describe the spatiotemporal changes in hydrogel crosslink density when coupled with spatiotemporal changes in ECM elaboration and growth, which are difficult to measure experimentally. In addition, computational modeling can help to identify new mechanisms that are key to the experimental system. Moreover, this study investigates two cell sources from bovine donors of different age groups and thus represents one of the major contributing factors (*i.e.*, age) to the observed variations in chondrocyte activity<sup>18</sup>. Ultimately, our long-term goal is to use the knowledge gained from this study to develop a predictive model that identifies optimal designs of degradable hydrogels for a specific donor, which enable matrix deposition and elaboration while maintaining mechanical integrity of the hydrogel during ECM

growth. Thus, the goal of the model is to aid in improving cartilage regeneration for a wide range of donors.

## **5.2 Materials and Methods**

### ***5.2.1 Chondrocyte Isolation***

Bovine chondrocytes were harvested from two different donors: one donor was a ~ three week old juvenile calf (Research 87, Boylston, MA) and the other donor was a ~1.5 year old adult steer (Arapahoe Meats, Lafayette, CO). Due to the nature of the availability of joints, chondrocytes were isolated from the femoral condyles and patellar groove of the stifle joint in the juvenile donor. Chondrocytes were isolated from the metacarpophalangeal joint in the adult donor. The cells are referred herein as juvenile chondrocytes and adult chondrocytes. In brief, cartilage was excised from the joint, cut into small ~1 cubic mm pieces and digested for 15-17 h at 37°C in 600 U/mL collagenase type II (Worthington Biochemical Corp., Lakewood, NJ) in Dulbecco's Modified Eagle Medium (DMEM, Invitrogen, Carlsbad, CA) supplemented with 5% fetal bovine serum (FBS, Atlanta Biologicals, Flowery Branch, GA). Freshly isolated chondrocytes were retrieved after filtering through a sterile 100 µm sieve, followed by several washes in phosphate buffered saline (PBS) with antibiotics (50 U/mL penicillin, 50 µg/mL streptomycin, 20 µg/mL gentamicin, and 0.5 µg/mL fungizone) and 0.02% EDTA (Invitrogen, Carlsbad, CA). Cell viability was determined to be 92% for adult chondrocytes and 87% for juvenile chondrocytes as measured using the trypan blue exclusion assay (Invitrogen).

### ***5.2.2 Enzyme Kinetics Assay***

Enzyme kinetics for aggrecanase were determined using a commercial kit, Sensolyte 520 Aggrecanase-1 Assay Kit (Anaspec, Fremont, CA). Conditioned medium containing aggrecanase

that was secreted by adult chondrocytes was tested. In brief, adult chondrocytes were placed in suspension culture in chondrocyte growth media and stimulated with 1  $\mu\text{g}/\text{mL}$  of lipopolysaccharide (LPS, Sigma-Aldrich) overnight to increase the amount of cell-secreted aggrecanase. The supernatant was collected via centrifugation. The supernatant was incubated for 0-120 minutes over a range of concentrations (10-250  $\mu\text{M}$ ) of a FRET peptide substrate that is specific to cleavage by aggrecanase-1. The total amount of active enzyme was determined using standards of human ADAMTS-4 control (Millipore, Billerica, MA). A Lineweaver-Burk plot was generated to calculate  $k_{cat}$  and  $K_M$ , which were used as a starting point for determining the kinetic constants in the model.

### **5.2.3 Macromer Synthesis**

An 8-arm PEG-norbornene (PEG-NB) macromer was synthesized by reacting 8-arm PEG-NH<sub>2</sub> (20 kDa, Jenkem Technology USA, Plano, TX) with four molar excess 5-norbornene-2-carboxylic acid (Sigma-Aldrich, St. Louis, MO), three molar excess of O-(7-azabenzotriazol-1-yl)-N,N,N',N'-tetramethyluronium hexafluorophosphate (HATU, ChemImpex International, Inc., Woodale, IL) and six molar excess of N,N-Diisopropylethylamine in dimethylformamide (Fisher Scientific, Fairlawn, NJ) overnight at room temperature under argon. The final product, PEG-NB, was recovered and purified by precipitation in diethyl ether (Sigma-Aldrich), filtration, dialysis in de-ionized water over several days, and lyophilization. Norbornene conjugation to each arm of the 8-arm PEG-NH<sub>2</sub> was determined with <sup>1</sup>H nuclear magnetic resonance spectroscopy by comparing the olefinic hydrogen peaks in the norbornene ( $\delta = 5.9\text{-}6.25$  ppm) to the methylene hydrogen peaks in the PEG backbone ( $\delta = 3.4\text{-}3.9$  ppm). The norbornene conjugation was determined to be  $\sim 100\%$ . PEG dithiol (PEGdSH) (Sigma-Aldrich) crosslinker and the aggrecanase-

sensitive peptide crosslinker, CRDTEGEARGSVDR, (GenScript, Piscataway, NJ) were used as received.

#### **5.2.4 Hydrogel Formation and Cell Encapsulation**

A hydrogel precursor solution was prepared to reach a final concentration of 10% (g/g) 8-arm PEG-NB in PBS. This solution was combined with either PEGdSH (0.45 thiol:ene) or CRDTEGEARGSVDR (0.65 thiol:ene) with 0.05% photoinitiator (Irgacure 2959, Ciba Specialty Chemicals, Tarrytown, NY). The solution was sterile-filtered (0.22  $\mu\text{m}$  filter). A schematic of hydrogel formation is shown in Figure 1A. The molar concentration of crosslinker was varied to achieve similar initial mechanical properties for the nondegradable hydrogel and the aggrecanase-sensitive hydrogel, respectively. The difference is attributed to differences in crosslinker molecular weight (*i.e.*, the nondegradable PEGdSH crosslinker is 1000 g/mol and the peptide crosslinker (CRDTEGEARGSVDR) is 1767 g/mol) and thiol reactivity, which depends on the local chemistry of the crosslinker<sup>19</sup>. Freshly isolated chondrocytes were combined with the hydrogel precursor solution at 50 million cells/mL and polymerized with 365 nm light (UVP, Upland, CA) at 6 mW/cm<sup>2</sup> for 7 minutes. Cell-laden hydrogels were cultured in chondrocyte growth medium (DMEM supplemented with 10% FBS, 50 U/mL penicillin, 50  $\mu\text{g}/\text{mL}$  streptomycin, 0.5  $\mu\text{g}/\text{mL}$  fungizone, 10 mM HEPES buffer, 0.1 M MEM-NEAA, 0.4 mM L-proline, 4 mM GlutaGro, 110 mg/L sodium pyruvate, and 50 mg/mL L-ascorbic acid (Sigma-Aldrich)) on a figure eight shaker (70 RPM) at 37°C and 5% CO<sub>2</sub> in a humid environment for up to twelve weeks.

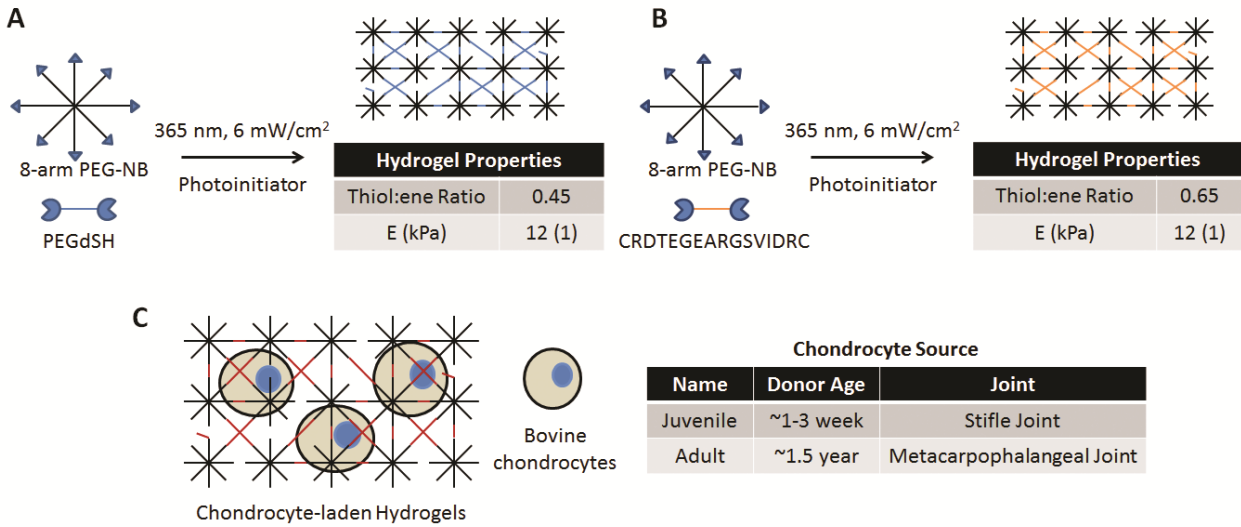


Figure 1. Schematic of hydrogel formation and cell encapsulation by a photoclickable thiol:norbornene reaction. A) Non-degradable hydrogels were formed by reacting monomers of eight-arm PEG-norbornene (PEG-NB) with crosslinkers of PEG-dithiol (PEGdSH) under cytocompatible photoinitiating conditions. The thiol:ene molar ratio used to form the hydrogels and the resulting compressive modulus (E) after cell encapsulation and 24 hours of swelling are provided. B) Enzyme-sensitive hydrogels were formed by reacting monomers of eight-arm PEG-norbornene (PEG-NB) with bis-cysteine peptide crosslinkers sensitive to aggrecanase, CRDTEGEARGSVIDRC, under cytocompatible photoinitiating conditions. The thiol:ene molar ratio used to form the hydrogels and the resulting compressive modulus (E) after cell encapsulation and 24 hours of swelling are provided. C) Two cell sources based on donor age and joint were investigated and are referred to as juvenile chondrocytes and adult chondrocytes.

### 5.2.5 Characterization of Acellular and Cell-Laden Hydrogels

Acellular hydrogels were prepared as described above and allowed to swell to equilibrium for 24 hours in PBS. The equilibrium mass swelling ratio,  $q$ , ( $q = (m_s/m_d)$ ) was determined by measuring the mass of the equilibrium swollen hydrogel ( $m_s$ ) and the dry polymer ( $m_d$ ) after lyophilization. The equilibrium volumetric swelling ratio ( $Q$ ) was determined from the equilibrium mass swelling ratio and assuming densities of the polymer,  $\rho_p$ , ( $1.07 \text{ g/cm}^3$ ) and solvent,  $\rho_s$ , ( $1 \text{ g/cm}^3$ ) by  $Q = 1 + (\rho_p/\rho_s)(q - 1)$ . At day 1, week 3, week 6, week 9, and week 12, cell-laden hydrogel constructs were randomly removed from culture. The compressive modulus of acellular

(n=3) and cell-laden (n=2) hydrogels was measured using a mechanical tester (MTS Synergie 100, 10N, Eden Prairie, MN). Fully hydrated hydrogels were subjected to unconfined compression up to 15% strain at an average rate of 17% strain/min. The compressive modulus was determined in the linear range of the resulting stress-strain curve between 10 and 15% strain. It was assumed that the compressive modulus was a reasonable approximation to the Young's modulus, which is supported by previous work<sup>20</sup>.

### **5.2.6 Viability and Biochemical Analysis**

At day 1, week 3, week 6, week 9, and week 12, cell-laden hydrogel constructs (n=2) were randomly removed from culture and analyzed for viability. Cell viability was assessed using the LIVE/DEAD<sup>®</sup> membrane integrity assay (Calcein AM/ethidium homodimer, Invitrogen) and imaged by confocal microscopy (n=2). At day 1, week 3, week 6, week 9, and week 12, cell-laden hydrogel constructs (n=3) were randomly removed from culture weighed to determine wet weight, snap frozen in liquid nitrogen, lyophilized, and weighed again to obtain dry weights. The medium was collected, snap frozen in liquid nitrogen, and stored at -80°C. In addition, cartilage explants (n=3) were harvested from the femoral condyles of a calf (~3 week old, Research 87), weighed to determine wet weight, snap frozen in liquid nitrogen, lyophilized, and weighed again to obtain dry weights. Hydrogels and cartilage explants were homogenized using a TissueLyser (Qiagen, Hilden, Germany) and enzymatically digested in 4 U/mL papain (Worthington Biochemical Corp.) for 18 h at 60°C. DNA content was determined in the hydrogels using Hoechst 33258 (Polysciences, Inc. Warrington, PA)<sup>20</sup>. DNA content was converted to number of cells using 3.9 pg DNA/juvenile chondrocyte and 2.9 pg DNA/adult chondrocyte, which was determined by generating a standard curve of known cell number to DNA content. Total cell number was scaled

by estimating the percent viability through semi-quantitative analysis of LIVE/DEAD® images. A colorimetric assay based on 1,9-dimethylmethylene blue (Sigma–Aldrich St. Louis, MO) was used to quantify the amount of sulfated glycosaminoglycans (sGAGs)<sup>22</sup> converted to moles assuming a molecular weight of 10<sup>6</sup> g/mol<sup>10</sup>. Total collagen content was assessed using the hydroxyproline assay assuming a 10% hydroxyproline content in collagen<sup>23</sup> and converted to moles assuming a molecular weight of 123 kDA, which is based on a commercially available bovine collagen II product (ab134539, Abcam, Cambridge, MA). The total amounts of sGAGs and collagen were quantified in the hydrogels, media, and cartilage explants. The ECM production rate on a per cell basis reported herein is defined as the ECM (sGAG plus collagen) that is retained in the hydrogel and then normalized total cell number.

### ***5.2.7 Histology and Immunohistochemistry***

At day 1, week 6 and week 12, cell-laden hydrogel constructs (n=2) were randomly removed from culture and analyzed by histology and immunohistochemistry methods. Hydrogel constructs were fixed in 4% paraformaldehyde at 4°C, paraffin embedded, dehydrated, and sectioned at 10 µm. Prior to primary antibody treatment for collagen II, sections were treated with 2000 U/mL hyaluronidase for 1 h at 37°C (Sigma-Aldrich). Sections were treated with anti-collagen II antibody (1:50, USBiological, Salem, MA). Prior to primary antibody treatment for aggrecan, sections were treated with Retrieagen A (BD Biosciences), 100 mU/mL chondroitinase-ABC (Sigma-Aldrich), and 34 mU/mL keratinase (MP Biomedical, Solon, OH) for 1 h at 37°C. Sections were treated with anti-aggrecan antibody (1:5, USBiological). After primary antibody treatment, sections were treated with either AlexaFluor 488 (collagen II) or 546 (aggrecan) conjugated secondary antibodies (1:200, Invitrogen). Cell nuclei were counterstained

with DAPI (Invitrogen). Stained sections were mounted with Fluoromount-G (Southern Biotech, Birmingham, AL). Sections receiving no primary antibody treatment served as negative controls. Sections were imaged on a laser scanning confocal microscope (CLSM, Zeiss LSM 510, Thornwood, NY) at 100x and 400x. At day 1, week 6, and week 12, sections were stained with Safranin-O/Fast Green to visualize sGAGs. Cell nuclei were counterstained with haematoxylin. Sections were imaged at 100x and 400x on a laser scanning confocal microscope as well as at 200x using a brightfield microscope (Axiovert 40 C, Zeiss, Thornwood, NY).

The thickness of the extracellular matrix (ECM) was estimated in non-degradable hydrogels to provide an estimate the modulus of the ECM. Microscopy images of Safranin-O/FastGreen stained sections were chosen for this analysis because it was possible to distinguish between the matrix within the cell and the matrix surrounding the cell. Only the dense matrix immediately surround the cell was measured, which correlated with the immunohistochemical staining for aggrecan and collagen type II. In brief, the distance between the cellular boundary and the matrix boundary was estimated using ImageJ (National Institutes of Health) for a total of 49 cells per time point.

### ***5.2.8 Aggrecanase Activity***

At day 1, week 3, week 6, week 9, and week 12, aggrecanase activity was measured in the constructs (n=3) using a commercial kit, Sensolyte 520 Aggrecanase-1 Assay Kit (Anaspec, Fremont, CA). Cell-laden hydrogel constructs were homogenized in assay buffer with 0.1% Triton X-100. Samples were incubated with a FRET peptide substrate that is specific to cleavage by aggrecanase-1 1 h at 37°C and fluorescence was measured. A control (n=2) of 0.5 ng and 1 ng of ADAMTS-4 (Millipore) was used to quantify the mol of substrate cleaved per mol of aggrecanase.



### **5.2.9 Statistical Analysis**

Experimental data are reported as a mean with standard deviation shown as error bars in plots or shown parenthetically in the text. For comparisons between initial modulus of acellular and cellular gels, a student's T-test assuming unpaired data with equal variance was performed ( $t(4)=2.821$ ,  $p=0.048$ ). For the modulus of cell-laden degradable hydrogels, a two-way analysis of variance ( $\alpha=0.05$ ) was performed with time and donor as factors. A one-way analysis of variance ( $\alpha=0.05$ ) with Tukey's post-hoc was performed with time as a factor for the modulus of cell-laden hydrogels for non-degradable hydrogels and degradable hydrogels. Normal probability plots of the residuals were generated and were found to support the normal distribution assumption (plots not shown).

### **5.2.10 Mathematical and Numerical Modeling**

To predict the combined cell mediated hydrogel degradation and ECM growth, we used a multiscale computational approach<sup>16,17,24</sup> that spans three characteristic length scales (Figure 2). These include: a) the sub-micro scale that describes hydrogel degradation and the associated change in mechanical properties as well as enzyme and ECM diffusion, which are based on well-established relationships derived from thermodynamics, physics and statistical methods, b) the micro scale that captures the interaction within small populations of cells (*e.g.*, one to six cells) and the surrounding gel, and c) the macroscale that considers a large population of cells and the evolution of a millimeter-size construct sample.

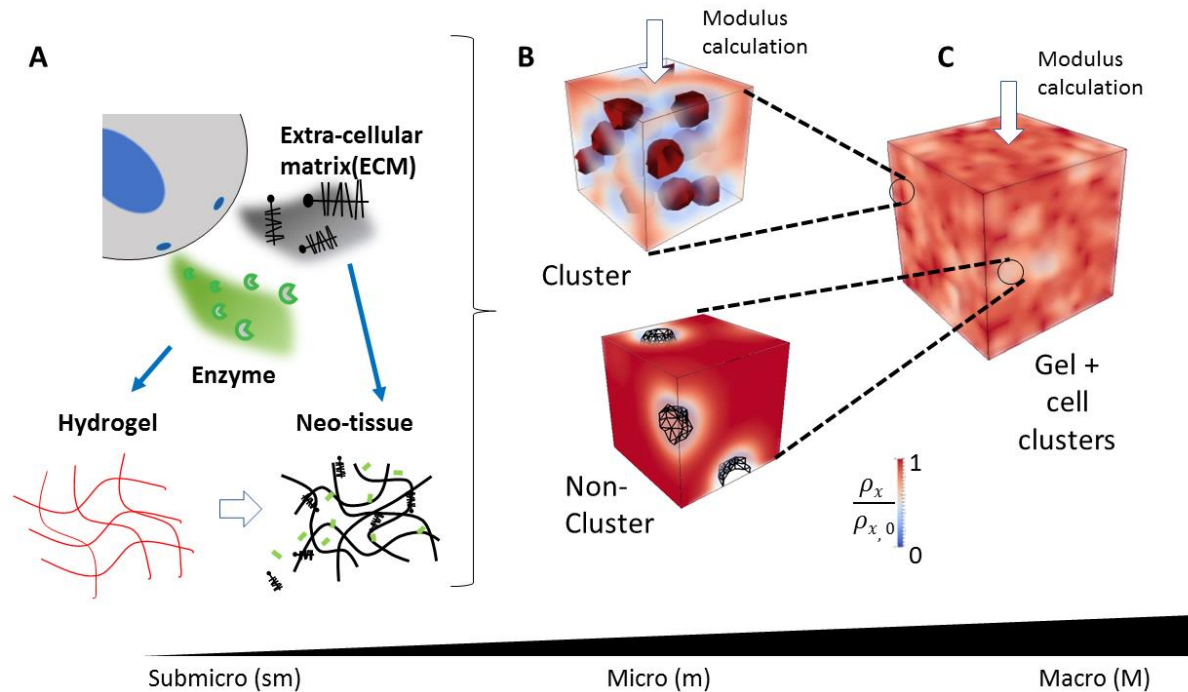


Figure 2. A multiscale computational model is used to describe spatiotemporal behavior of cell-secreted enzymes, hydrogel degradation, ECM growth, and macroscopic properties. A) At the sub-microscale, the model describes the spatiotemporal evolution of the hydrogel crosslink density where cell-secreted enzymes cleave hydrogel crosslinks in the polymer network (red) allowing for the spatial elaboration of neo-tissue. A chondrocyte is depicted secreting enzymes (green) and ECM molecules (black). Complete degradation near the cell surface is required for ECM molecule diffusion. B) At the microscale, the model considers regions of high cell densities (i.e., clusters of cells) and regions of low cell densities (single cells, i.e., non-clusters) to describe the evolution of mechanical properties. Particularly, the spatial crosslinking density around cells is characterized. C) The macroscale considers clustered cell distributions over large regions and its effect in the temporal evolution of mechanical properties.

At the sub-micro scale (Figure 2A), the model was used to describe the spatiotemporal evolution of hydrogel crosslink density as a function of enzyme synthesized by cells. The equations used in the model are well-established for polymer networks<sup>25,26</sup> and are given below. The reader is also referred to our previously published work for additional details<sup>16,17</sup>. A key feature of hydrogel degradation is the point at which the hydrogel reaches reverse gelation, *i.e.*, the point at which a sufficient number of crosslinks have been cleaved and the hydrogel

transitions from a solid polymer network to a soluble highly branched polymer. This point can be related to the concept of network connectivity as described by standard statistical models of network formation<sup>27</sup>. We thus define the minimum fraction of hydrogel crosslinks,  $\beta$ , that is needed to maintain a polymer network by:

$$\beta = \frac{1}{\sqrt{r(f_{ene} - 1)(f_{thiol} - 1)}} \quad (\text{Eq. 1})$$

where  $r$  is the molar ratio of thiols to norbornenes,  $f_{ene}$  is the number of PEG arms functionalized with norbornene, and  $f_{thiol}$  is the number of PEG arms functionalized with thiols. For the aggrecanase-sensitive hydrogel used in this study,  $r = 0.45$ ,  $f_{ene} = 8$ , and  $f_{thiol} = 2$ . Due to the lower reactivity of the thiols in the cysteine<sup>19</sup>, the value of  $r$  was chosen based on the non-degradable hydrogel formulation to better reflect the actual crosslinking efficiency in the degradable hydrogel formulation. The critical crosslink density,  $\rho_c$  is defined as the crosslink density when the hydrogel undergoes reverse gelation and is given by  $\rho_c = \beta\rho_x^0$ , where  $\rho_x^0$  is the initial crosslink density. This relationship has been used to describe the point of reverse gelation in other types of degrading hydrogels<sup>28,29</sup>. The value of  $\rho_x^0$  was determined from Flory-Rehner and rubber elasticity theories<sup>26</sup> following methods previously described<sup>30</sup>. Specifically, these theories relate crosslink density to the equilibrium volumetric swelling ratio and the compressive modulus of the hydrogel, which are determined from experiments described above. We, thus define hydrogel crosslink density as a function of location (coordinate  $x$ ) and time ( $t$ ):

$$\rho_x = \rho_x(x, t) \text{ when } \rho_x > \rho_c \quad (\text{Eq. 2})$$

$$\rho_x(x, t) = 0 \text{ when } \rho_x \leq \rho_c \quad (\text{Eq. 3})$$

Diffusion of enzyme through the hydrogel is assumed to follow Fickian diffusion<sup>31</sup>

wherein the enzyme concentration ( $c_e$ ) is described a function of location and time by:

$$\frac{Dc_e}{Dt} = \nabla \cdot [D_e(\rho_x) \nabla c_e] \quad (\text{Eq. 4})$$

where  $D_e$  is the diffusivity of the enzyme in the hydrogel.  $D_e$  is a function of the hydrogel crosslink density and enzyme size as described by Lustig and Peppas<sup>32</sup>:

$$\frac{D_e}{D_e^\infty} = \left(1 - \frac{r_e}{\xi(\rho_x)}\right) \exp\left(-Y \left(\frac{v_{2,s}}{1 - v_{2,s}}\right)\right) \quad (\text{Eq. 5})$$

where  $D_e^\infty$  is the diffusivity of the enzyme in the swelling solvent at 37°C and is estimated by the Stokes-Einstein relationship,  $r_e$  is the enzyme radius,  $\xi$  is the hydrogel mesh size, which is a function of  $\rho_x$ ,  $Y$  is the ratio of the critical volume required for translational movement of the diffusing species relative to the average free volume occupied by the solvent molecules, which is assumed to be unity<sup>32</sup>, and  $v_{2,s}$  is the polymer volume fraction, which is equivalent to  $1/Q$ . The hydrogel mesh size,  $\xi$ , is further described by

$$\xi(\rho_x) = l \sqrt{\frac{3\rho_p C_n}{M_r \rho_x} v_{2,s}^{-1/3}} \quad (\text{Eq. 6})$$

where  $l$  is the average bond length, which for PEG is 0.150 nm,  $C_n$  is the characteristic ratio of the polymer, which for PEG is assumed to be 4.0<sup>33</sup>, and  $M_r$  is the molecular weight of the polymer repeat unit, which for PEG is 44 g/mol. Once the hydrogel reaches  $\rho_c$ , mesh size becomes infinite and diffusivity of the enzyme reduces to  $D_e^\infty$ .

Hydrogel degradation is modeled by changes in hydrogel crosslink density in the swollen state ( $\rho_x^s$ ), which is assumed to be analogous to crosslink (*i.e.*, enzyme substrate) concentration,

following Michaelis-Menten kinetics, as described by<sup>16,29</sup>

$$\frac{D\rho_x^s}{Dt} = -k_{cat}c_e \left( \frac{\rho_x^s}{K_M + \rho_x^s} \right) \quad (\text{Eq. 7})$$

where  $k_{cat}$  is the catalyst rate constant and  $K_M$  is the Michaelis constant. The initial condition was defined such that when  $t = 0$ , then  $\rho_x^s = \rho_0^s$ . The relationship between the crosslink density in the swollen state ( $\rho_x^s$ ) and the dry state ( $\rho_x$ ) is given by  $\rho_x^s = \rho_x(1/(Q - 1))$ . Since the majority of the degradation regime is within the region surrounding the cell<sup>16</sup>, it is assumed that changes in swelling of the bulk hydrogel are negligible. The rate of deactivation of enzyme is determined by:

$$\frac{Dc_e}{Dt} = -k_d c_e \quad (\text{Eq.8})$$

where  $k_d$  is the deactivation rate constant.

To model diffusion of newly synthesized ECM molecules, several assumptions were made. We only consider the primary cartilage-ECM molecules of aggrecan and collagen type II. Because these two ECM macromolecules are large relative to the mesh size of the hydrogel, their diffusion will be restricted to the space immediately surrounding the cell<sup>9</sup>. Following Eq. 4, the diffusivity of the ECM molecules,  $D_{ECM}$ , reduces to zero, when the hydrogel is intact. Once the hydrogel crosslink density reaches  $\rho_c$ , diffusion of ECM molecules occurs and is assumed to follow diffusion in the swelling solvent (*i.e.*, culture medium, which is assumed to have similar properties to water) at 37°C. The diffusivity of ECM,  $D_{ECM}^\infty$ , was estimated by the Stokes-Einstein relationship. The ECM concentration ( $c_{ECM}$ ) is assumed to follow Fickian diffusion and is described as a function of location and time by

$$\frac{Dc_{ECM}}{Dt} = D_{ECM}^{\infty} \nabla^2 c_{ECM}. \quad (\text{Eq. 9})$$

It was assumed that ECM diffusion occurs rapidly (*i.e.*, hours) relative to the time scale of the experiment (*i.e.*, weeks) and thus estimating the ECM diffusivity in culture medium serves as a reasonable approximation. For example, the average distance between cells is  $\sim 50 \mu\text{m}$ , a distance that takes 40 h for the ECM molecules to diffuse in the solvent.

The modulus ( $E$ ) of the hydrogel construct represents the contribution from the hydrogel, the ECM, and encapsulated cells. At small strains, the stress-strain relationship for the hydrogel network can be linearized from rubber elasticity as

$$\boldsymbol{\sigma}_g = \frac{E_{gel}}{(1 + \nu)} \left( \boldsymbol{\epsilon}_g + \frac{\nu}{(1 - 2\nu)} \text{tr}(\boldsymbol{\epsilon}_g) \mathbf{1} \right) \quad (\text{Eq. 10})$$

where  $\boldsymbol{\sigma}_g$  is the stress tensor in the gel,  $\boldsymbol{\epsilon}_g$  is the strain tensor,  $\mathbf{1}$  is the identity tensor,  $E_{gel}$  is the Young's modulus of the gel,  $\nu$  is the Poisson's ratio,  $R$  is the gas constant, and  $T$  is temperature. The Poisson's ratio was assumed to be close to 0.5, which is a reasonable approximation for elastic materials<sup>34</sup>. The modulus of the hydrogel was estimated from rubber elasticity theory<sup>35</sup> assuming a linear elastic model described by

$$E_{gel} = 2(1 + \nu)\rho_x RTQ^{-1/3} \quad (\text{Eq. 11})$$

This relationship has been used to relate the mechanical properties to crosslink density for similar PEG hydrogels<sup>36</sup>.

The mechanical properties of the deposited ECM under small strains can be assumed to be represented by a linear elastic isotropic material such that the stiffness increases with

continuous ECM deposition. Consistent with previous work<sup>37</sup>, the stress-strain equation is given by

$$\boldsymbol{\sigma}_m = \frac{E_{ECM}}{(1 + \nu)} \left( \boldsymbol{\epsilon}_m + \frac{\nu}{(1 - 2\nu)} \text{tr}(\boldsymbol{\epsilon}_m) \mathbf{1} \right) \quad (\text{Eq. 12})$$

where  $\boldsymbol{\sigma}_m$  is the stress tensor in the ECM,  $\boldsymbol{\epsilon}_m$  is the strain tensor,  $\mathbf{1}$  is the identity tensor, and  $\nu$ , the Poisson's ratio, is taken as 0.22<sup>38,39</sup>. The modulus of the ECM was assumed to be proportional to the concentration of ECM,  $E_{ECM} \propto C_{ECM}$ . Thus, the evolving  $E_{ECM}$  could be estimated from the experimentally determined concentration of ECM at each time point.

The chondrocytes are assumed to be incompressible with an elastic modulus of  $\sim 0.6$  kPa kPa<sup>40</sup>. For simplicity we assume that the ECM and chondrocytes follow linear elastic behaviour at small strains under quasi-static loading. At small strains, the stress-strain relationship for cells can be linearized from rubber elasticity as

$$\boldsymbol{\sigma}_{cell} = \frac{E_{cell}}{(1 + \nu)} \left( \boldsymbol{\epsilon}_{cell} + \frac{\nu}{(1 - 2\nu)} \text{tr}(\boldsymbol{\epsilon}_{cell}) \mathbf{1} \right) \quad (\text{Eq. 13})$$

where  $\boldsymbol{\sigma}_{cell}$  is the stress tensor in the cell,  $\boldsymbol{\epsilon}_{cell}$  is the strain tensor, and  $\mathbf{1}$  is the identity tensor.

At the microscale (Figure 2B), a representative volume element (RVE) was employed to model the localized hydrogel degradation as well as the production, transport and deposition of ECM molecules within the degraded regions around a group of cells. The model, based on a multiphasic mixture formulation<sup>41</sup>, is able to characterize hydrogel degradation as described above, ECM growth, and the evolution of associated mechanical properties. In particular, the construct's modulus depends on: a) the degradation of the hydrogel governed by the enzyme concentration, diffusion and kinetics as defined from the multi-phasic model at sub-micron scale

and b) the diffusion and deposition of ECM as defined by a flux of ECM synthesis from the cell surface determined by experiments. The RVEs are treated as multiphase elements where the three components are assumed to be non-interpenetrating. In other words, the RVEs are comprised of discrete regions of either the hydrogel network, ECM, or cells. Here, only the ECM that is deposited and retained within the hydrogel is considered in the ECM synthesis rates (*i.e.*, all of the ECM that is synthesized by the cell is deposited). The average stress of the RVE derived from homogenization methods<sup>42,43</sup> is given by

$$\overline{\sigma}_{ij} = \frac{1}{\overline{V}} \int_{\overline{S}} \sigma_{ij} dV = \frac{1}{\overline{V}} \int_{\overline{S}} \frac{1}{2} (\tau_i x_j + \tau_j x_i) dS \quad (\text{Eq. 14})$$

where  $\overline{V}$  and  $\overline{S}$  are the volume and boundary surface of the RVE, and indices  $i$  and  $j$  can take values 1,2,3 representing the directions. The vector  $\mathbf{x}$  represents the position vector and  $\boldsymbol{\tau}$  represents the traction vector at the boundary surface of the RVE. The modulus of the RVE is given by

$$E = \frac{\overline{\sigma}_{11}}{\overline{\epsilon}_{11}} \quad (\text{Eq. 15})$$

where  $\overline{\sigma}_{11}$  and  $\overline{\epsilon}_{11}$  are the average uniaxial compressive stress and strain on the RVE in the direction of loading estimated using homogenization methods. Boundary conditions are applied on the RVE to produce an overall compressive strain of  $\overline{\epsilon}_{11}$  in the direction of loading, 1, while it is unrestrained in the other two normal directions, 2 and 3.

Finally, the macroscale (Figure 2C) considered the effect of inhomogeneous (clustered) cell distributions over large regions. This feature has indeed been identified to be significant in our



estimation of mechanical properties. For this, we constructed a macro-scale RVE (millimeter size) in which the cell population was represented by a binary density distribution that varied spatially. In short, the cell density in clusters ( $f_c$ ) and in the background ( $f_b$ , where  $f_b < f_c$ ) as well as the average cluster size were determined by a cluster analysis from experimental histological or viability images by confocal microscopy. These distributions were reproduced by assigning a random cluster distribution in the macroscopic RVE. The evolution of local mechanical properties in each region was then determined by the micro-analysis performed for the two characteristic cell densities  $f_c$  and  $f_b$ . The evolution of averaged macroscopic properties was assessed using computational homogenization and a three-dimensional finite-element analysis as described at the micro level. At the macroscale, hydrogels are considered to comprise of RVEs of either clustered cells or non-clustered cells. RVEs with their corresponding moduli are then computed with finite element analysis to compute the overall modulus of the construct.

### 5.3 Results and Discussion

Hydrogels were designed from aggrecanase-sensitive peptide crosslinks using a simple and robust thiol-norbornene photoclick reaction (Figure 1A and B)<sup>44,45</sup>. To study the influence of variations in cellular activity as a result of different donors, chondrocytes isolated from either juvenile or adult bovine donors were investigated (Figure 1C). Initially, experimental and computational approaches were combined to a) validate that the model captures the initial mechanical properties of cell-laden aggrecanase-sensitive hydrogels and b) estimate the modulus of cell-secreted ECM using a non-degradable version of the hydrogel. The model was then implemented to characterize the spatial and temporal evolution of hydrogel degradation, ECM growth and overall construct mechanical properties for chondrocytes isolated from two different

donors. Overall, this study demonstrates that a) spatial heterogeneities, which form during the encapsulation of chondrocytes, facilitate localized ECM growth and b) the combination of enzyme and ECM synthesis rates, which are characteristics of the donor, can lead to improved ECM growth as shown here for the juvenile chondrocytes or poor ECM growth as shown for the adult chondrocytes. Overall, this study points to the importance of designing hydrogels specific to each donor.

### **5.3.1 Model Inputs**

Inputs to the model were determined from experimental data obtained in this study or from literature and are summarized in Table 1. The values in Table 1 were used for both donors, regardless of donor age. The initial properties for acellular aggrecanase-sensitive hydrogels are summarized for compressive modulus ( $E_0$ ),  $\beta$ , which is related to the reverse gelation point, and the initial crosslink density in the swollen state, which is analogous to substrate concentration. The diameter of a chondrocyte was previously determined to be  $11.5 \mu\text{m}^8$ . The radius of aggrecanase was assumed to be 10 nm, which was approximated from previous studies that found MMPs to be  $\sim 8.5 \text{ nm}^{16}$  and considering that aggrecanase has a higher molecular weight than many MMPs. The diffusivity of the enzyme ( $D_e^\infty$ ) in an aqueous solvent was estimated based on Stokes-Einstein diffusivity assuming properties of water and the radius of the enzyme. In this study, we have lumped aggrecan and collagen into one input of ECM. Since both aggrecan and collagen molecules are large, we have for simplicity assumed a size (*i.e.*, ECM radius) based on collagen type II of  $20,000 \text{ nm}^{46}$ . The diffusivity of the ECM ( $D_{ECM}^\infty$ ) in an aqueous solvent was estimated based on Stokes-Einstein diffusivity assuming properties of water and the radius of the ECM. Although the size of collagen and aggrecan molecules are likely to vary within cartilage and

also vary with the age of the donor<sup>47,48</sup>, this large radius will enable the model to capture the experimentally observed phenomena. Notably in experiments, aggrecan and collagen ECM molecules are restricted to the pericellular space until the hydrogel reaches reverse gelation. The ECM homeostatic concentration was measured experimentally from native cartilage explants and assumed to be similar regardless of the age of the donor. The ECM homeostatic concentration is provided as a reference for the target ECM concentration.

Table 2. Input parameters used in the model.

Parameter	Definition	Value	Unit
$E_0$	Initial hydrogel modulus	12.7	<i>kPa</i>
$\beta$	Network connectivity	0.563	--
$\rho_x^{s,0}$	Initial peptide concentration	140-160	$\mu M$
$r_{cell}$	Cell radius	5.75 <sup>[8]</sup>	$\mu m$
$r_e$	Hydrodynamic radius of aggrecanase	10	<i>nm</i>
$D_e^\infty$	Diffusivity of aggrecanase in pure solvent	$3.4 \times 10^{-5}$	$mm^2/s$
$c_m^o$	ECM homeostatic concentration*	$1.3 \times 10^{-3}$	<i>M</i>
$r_m$	Hydrodynamic radius of ECM molecules	20,000 <sup>[31]</sup>	<i>nm</i>
$D_{ECM}^\infty$	Diffusion of ECM molecules in pure solvent	$1.7 \times 10^{-8}$	$mm^2/s$

### **5.3.2 Assessing Spatial Heterogeneities in Crosslink Density: Combined Modeling and Experimental Results**

When cells were encapsulated in the aggrecanase-sensitive hydrogel, the experimentally measured compressive modulus dropped ( $p=0.048$ ) by 10% from 10 to 9 kPa (Figure 3A). Note that a different set of hydrogels were prepared for this experiment; this explains the difference in the initial modulus from the long-term cellular studies. Chondrocytes have been shown to have a modulus of  $\sim 0.6$  kPa<sup>40</sup>; however, the volume fraction of cells that are encapsulated is relatively low (at  $f \sim 0.02$ ) and on its own cannot explain this drop in modulus. One potential explanation is that cells inhibit the polymerization resulting in a decrease in the hydrogel crosslink density in the immediate vicinity of the cell. Since the hydrogels are formed via a photoinitiated radical-mediated click reaction and in the presence of oxygen, several types of radicals are generated. These radicals include photoinitiator radicals, propagating radicals, and reactive oxygen species. Each of these radical species has the potential to react with cells through several mechanisms such as lipid peroxidation<sup>49</sup>, modification of transmembrane proteins<sup>50</sup>, and cell-surface thiols<sup>51</sup>. Indeed, we have previously shown that radical-induced polymerizations can lead to lipid peroxidation of the cell membrane on chondrocytes during the encapsulation process<sup>52</sup>. These observations point to the ability of cells to inhibit the polymerization reaction and induce spatial heterogeneities in hydrogel crosslink density.

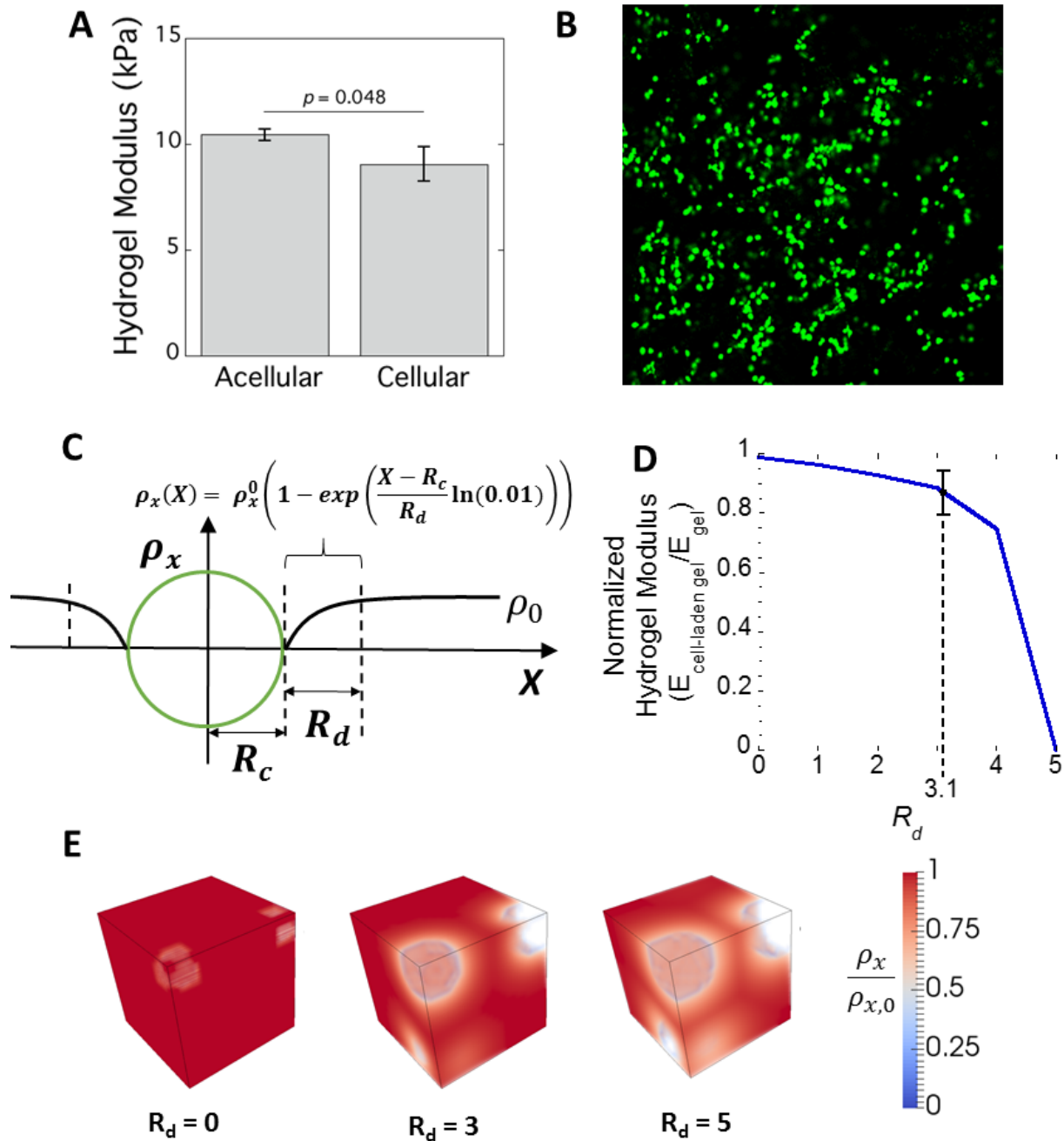


Figure 3. Characterization of the initial properties of cell-laden aggrecanase-sensitive hydrogels. A) The compressive modulus of aggrecanase-sensitive hydrogels with and without encapsulated chondrocytes. B) Representative confocal microscopy image of living (green) juvenile chondrocytes encapsulated in an aggrecanase-sensitive hydrogel at day 1. There is evidence of spatial heterogeneities in cell distribution, showing regions with clustering of cells and regions of single cells. Magnification is 100x. C) The term  $R_d$  is introduced, which describes the extent of a hydrogel crosslink density gradient around cells immediately after encapsulation.  $R_d$  is defined as

the distance between the cell boundary (shown in orange) to the point at which the crosslinking density reaches 99% of the bulk hydrogel crosslinking ( $\rho_{x,o}$ ). D) Modeling results describing the compressive modulus of a cell-laden hydrogel (solid blue line) as a function of increasing  $R_d$ . The cells are assumed to have a modulus of 1 kPa. The ordinate axis is normalized to the modulus of the gel with no cells corresponding to a  $R_d$  value of zero. The crossover point of the experimentally determined compressive modulus of a cell-laden aggrecanase-sensitive hydrogel (solid black dot) and the simulated compressive modulus yields an average value of  $R_d$  (dotted black line). E) Representative volume elements (RVEs) of cells with increasing  $R_d$ . As  $R_d$  increases, the crosslinking density between cells decreases which causing a reduction in the overall compressive modulus and leading to failure of the hydrogel. Note that reverse gelation occurs at  $\rho_x/\rho_{x,o} = 0.563$ . The experimental data shown here are for juvenile chondrocytes.

To account for spatial variations in the initial hydrogel crosslink density, we introduce the term  $R_d$ , which describes the distance from which the crosslink density ranges from zero at the surface of the cell to that of the bulk hydrogel (Figure 3C).  $R_d$  is expressed in terms of cell radius, *i.e.*, a  $R_d = 2$  means a distance that is two times the cell radius. Using the model, the compressive modulus was predicted for different values of  $R_d$  (Figure 3D) assuming the cell volume fraction given in Table 2. An  $R_d$  of zero indicates no inhibition of the polymerization leading to a ~3% drop in modulus due to the presence of the soft chondrocytes. With increasing  $R_d$ , the modulus continues to drop. The model matches the experimental data when  $R_d$  is 3.1, corresponding to a mean compressive modulus of 9 kPa (Figure 3D). A sharp decline in modulus with increasing  $R_d$  is attributed to the fact that spherical regions of low crosslink densities around cells start to overlap. As  $R_d$  increases, the crosslinking density between cells also decreases (Figure 3E) which manifests itself in a larger drop in the bulk compressive modulus. Once the hydrogel crosslink density is below its critical crosslink density ( $\rho_c$ ), a crosslink network no longer exists. For the cell volume fraction in Table 2, this phenomenon occurs when  $R_d$  is equal to or greater than five. The results from the model strongly point to a region surrounding the cells as having a lower crosslink density.

Table 2. Volume fraction of cells used in the modeling experiments.

Simulation	Description	Volume fraction of cells ( $f$ )
$R_d$	Uniform Cell Distribution	0.019
ECM stiffness at 6 weeks in non-degradable gels	Cluster	0.124
	Background	0.018
ECM stiffness at 12 weeks in non-degradable gels	Cluster	0.088
	Background	0.008
Multicellular RVEs, Modulus vs Time in Aggrecanase-Sensitive Hydrogels	Adult chondrocyte clusters	0.065
	Adult chondrocyte background	0.030
	Juvenile chondrocyte clusters	0.045
	Juvenile chondrocyte background	0.018

### 5.3.3 Estimating ECM modulus: Combined Modeling and Experimental Results

To predict ECM growth in the aggrecanase-sensitive hydrogels, we first needed to estimate the modulus of the growing ECM. To do this, non-degradable hydrogels were employed, where the hydrogel properties were known and the crosslink density did not vary in time. This approach was necessary because not all of the parameters were known in the aggrecanase-sensitive hydrogel and thus we could not use these hydrogels to estimate the ECM modulus. Hence any increase in modulus is attributed to the ECM. For the juvenile chondrocytes, the

compressive modulus of the hydrogel constructs increased with culture time (Figure 4A). ECM production rate on a per cell basis was estimated from the total ECM concentration measured at discrete time points. We assumed that the production rate measured at a particular time point (*e.g.*, week 3) was representative from the previously measured time point (*e.g.*, day 1 to week 3) (Figure 4B). No change in modulus was observed when adult chondrocytes were encapsulated (data not shown). We therefore used juvenile chondrocytes to estimate ECM modulus.



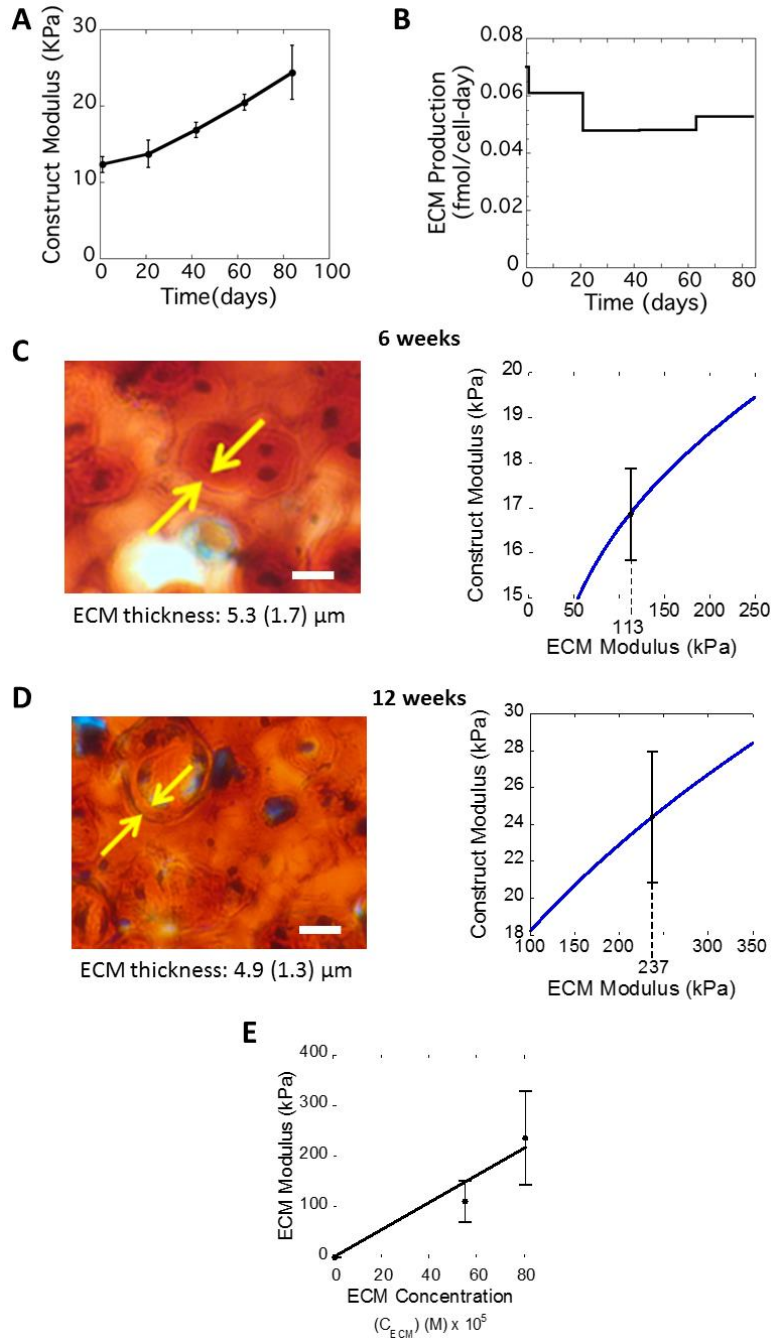


Figure 4. Characterization of the ECM modulus in non-degradable hydrogels seeded with juvenile chondrocytes. A) The compressive modulus of non-degradable hydrogel constructs encapsulated with chondrocytes with culture time. B) Production rate of ECM molecules (sGAGs and total collagen) by encapsulated chondrocytes in non-degradable hydrogels with culture time. C) Representative microscopy image of a section stained for sGAGs (red) of chondrocytes encapsulated in non-degradable hydrogels at 6 weeks. Scale bar is 25  $\mu\text{m}$ . The yellow arrows indicate the thickness of the ECM with average and (standard deviation). Modeling results for construct modulus as a function of different ECM moduli. The crossover point of the simulated construct modulus (solid blue line) and the experimental construct modulus (solid black dot)

gives the estimated ECM modulus (dotted black line). D) Representative microscopy image of a section stained for sGAGs (red) of chondrocytes encapsulated in non-degradable hydrogels at 12 weeks. Scale bar is 25  $\mu\text{m}$ . The yellow arrows indicate the thickness of the ECM with average and (standard deviation). Modeling results for construct modulus as a function of different ECM moduli. The crossover point of the simulated construct modulus (solid blue line) and the experimental construct modulus (solid black dot) gives the estimated ECM modulus (dotted black line). E) The ECM modulus as a function of ECM concentration ( $C_{\text{ECM}}$ ) within the hydrogel construct as determined by the model (circle). A linear fit gives a relationship between the ECM concentration and the ECM modulus.

To model the experimental system, we considered a group of chondrocytes embedded within a nondegradable hydrogel of known modulus. Because the large ECM molecules are restricted to the pericellular space in non-degradable hydrogels, the thickness of this matrix was semi-quantified from histological images that were stained for sGAGs at six and twelve weeks. The ECM deposition surrounding the cells was measured as indicated by the arrows in Figure 4C and D. It is important to note that although positive staining for sGAGs is found throughout the extracellular space of the hydrogel, these molecules did not stain positive for aggrecan. Thus, these small sGAG-rich molecules are assumed to be from processed aggrecan molecules<sup>53,54</sup> that are able to diffuse through the hydrogel. Since these molecules are not associated with full-length aggrecan or collagen, we treat these as unlinked molecules, which do not contribute to the overall modulus of the construct and thus are not included in the production rates. However, positive staining for sGAGs in the region immediately surrounding the cells matches the staining for aggrecan and collagen type II and therefore this region is considered the deposited (*i.e.*, linked) ECM. The thickness of this ECM was determined to be 5 (2)  $\mu\text{m}$  at six weeks and 5 (1)  $\mu\text{m}$  at twelve weeks, which is similar to that previously reported<sup>55</sup>.

The distribution of chondrocytes in the histological images indicated clustering of cells (*e.g.*, ~2 to 4) which is attributed to cell proliferation. Although the model does not currently

include cell proliferation, cell clustering was captured by randomly distributing spherical clusters of cells with three cells in each cluster while maintaining the same overall concentration. Simulations were run with clusters of cells (see Table 2 for corresponding  $f$  values), each of which having a matrix surrounding each cell with a thickness of 5  $\mu\text{m}$ , an  $R_d$  of 3.1 and bulk hydrogel modulus of 12.6 kPa. Matching the experimental data to the simulations resulted in an ECM modulus that ranged between 76-170 kPa at week six (Figure 4C) and between 150-340 kPa at week twelve (Figure 4D). The values of ECM modulus were compared to the total concentration of ECM measured experimentally in the hydrogels. Total ECM was determined by quantifying sGAG and collagen contents as a function of culture time and normalizing to wet weights. ECM mass was converted to molarity assuming molecular weights for aggrecan<sup>10</sup> and collagen and normalizing to the volume of solvent, which is assumed to have properties of water. The relationship between  $c_{ECM}$  (*i.e.*, concentration of ECM molecules) and  $E_{ECM}$  (*i.e.*, modulus of ECM) followed a linear trend showing an increase in ECM modulus with an increase in total ECM concentration (Figure 4E). The  $c_{ECM}$  of adult cells was about 15% of the  $c_{ECM}$  of juvenile cells at 12 weeks, so the modulus contribution by the ECM synthesized by adult chondrocytes was determined to be negligible. We therefore assumed this relationship where ECM modulus is predicted from experimentally measured ECM concentration. This relationship was then used in the modeling experiments with the aggrecanase-sensitive hydrogel.

#### **5.3.4 1-Dimensional Single Cell Simulations: Enzyme and Hydrogel Fronts**

The submicro-level of the model (Figure 2A) was used to describe changes in hydrogel crosslink density and enzyme concentration as a function of distance from the cell membrane and over time. The experimentally measured values of initial hydrogel properties (Table 1) and

aggrecanase concentration served as inputs to the model. Aggrecanase concentration was measured in the constructs and assumed to represent a snapshot of enzyme concentration over the course of 24 h. As such, an enzyme rate of production on a per cell basis for juvenile chondrocytes (Figure 5A) and adult chondrocytes (Figure 5D) was estimated from experiments. We assumed that the production rate measured at a particular time point (*e.g.*, week 3) was representative from the previously measured time point (*e.g.*, day 1 to week 3). The enzyme-substrate kinetics was initially estimated using a commercially available kit for aggrecanase and determined to be  $k_{cat} = 0.41 \text{ s}^{-1}$  and  $K_M = 391 \text{ }\mu\text{M}$ . However, the kit uses a different peptide substrate and the peptide is in solution. Studies have reported higher catalytic activity of enzymes to its peptide substrate when the peptide substrate is immobilized into a hydrogel<sup>29</sup> and this observation is further supported by our previous work<sup>16</sup>. Thus, the true value of  $k_{cat}$  in our hydrogel system is expected to be higher. Additionally, we have assumed Michaelis-Menten kinetics as described by equation (7); however this equation does not take into account enzyme inhibition. Studies have reported that aggrecanase is inhibited by TIMP3,<sup>56,57</sup> which has been shown to be secreted by chondrocytes<sup>58</sup> and  $\alpha$ 2-macroglobulin<sup>59</sup>, a global inhibitor of matrix degrading enzymes, which is present in serum<sup>60</sup>. For molecules present in serum, such as  $\alpha$ 2-macroglobulin, the concentration of the inhibitor may be assumed to be constant during the culture period. Thus, the inclusion of an inhibitor in essence can be captured through changes in the value of  $K_M$ . We therefore varied  $k_{cat}$ ,  $K_M$  and  $k_d$  to match the experimentally determined modulus of the construct as a function of time to that determined by the model for each donor.

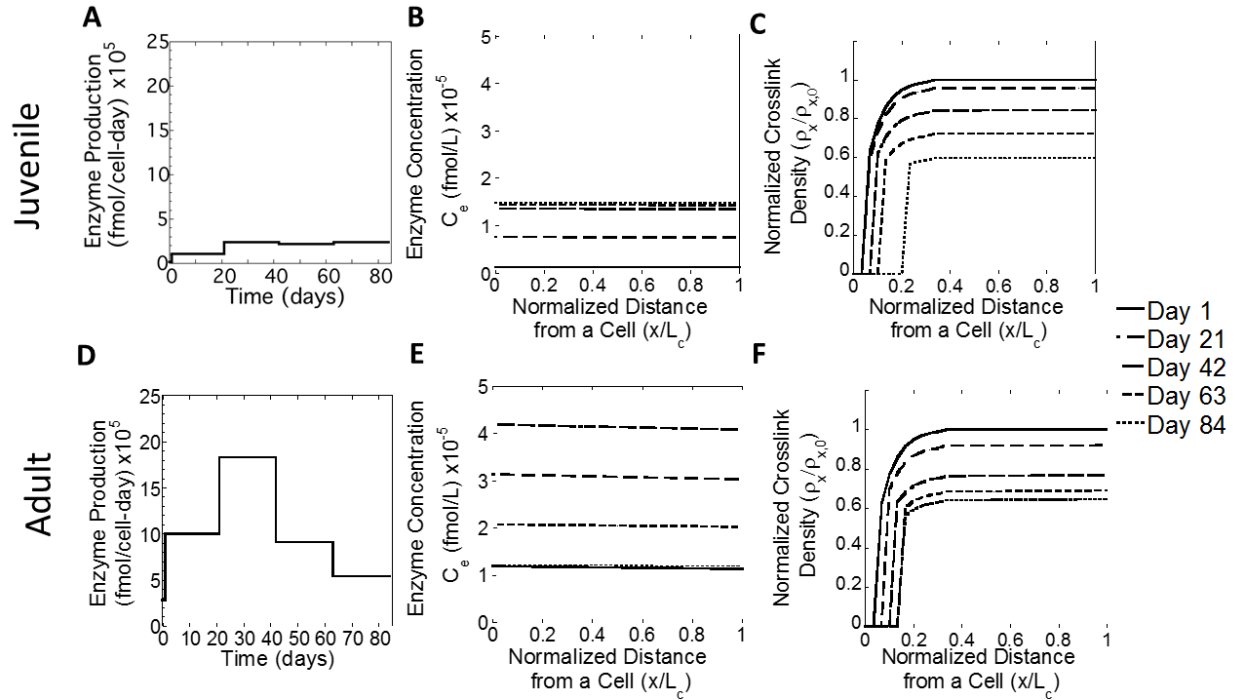


Figure 5. Characterization of the spatiotemporal degradation of aggrecanase-sensitive hydrogels. A and D) Rate of enzyme (aggrecanase) production per cell per day for juvenile and adult chondrocytes encapsulated in the aggrecanase-sensitive hydrogel is shown. B and E) Enzyme (aggrecanase) concentration as a function of distance from the cell ( $x$ ) normalized to a critical length,  $L_c$  (defined as the average distance between two individual cells assuming a homogenous distribution of cells, which is  $50 \mu\text{m}$ ), where  $x=0$  is the boundary of a single cell is shown. Enzyme concentration is shown for day 1, week 3, week 6, week 9 and week 12 for juvenile and adult chondrocytes. C and F) Hydrogel crosslink density (normalized to the initial crosslinking density  $\rho_{x,0}$ ) is shown as a function of distance from the cell ( $x$ ) normalized to a critical length,  $L_c$  is shown. Hydrogel crosslink density is shown for day 1, week 3, week 6, week 9 and week 12 for juvenile and adult chondrocytes. The critical length,  $L_c$ , is  $50 \mu\text{m}$ .

Modeling results for aggrecanase concentration and hydrogel crosslink density as a function of distance from the cell surface and over the course of 12 weeks are shown for juvenile (Figure 5B and 5C) and adult (Figure 5E and 5F) chondrocytes. The distance is normalized to the average distance between cells, referred to as the characteristic length  $L_c$ , which was estimated as  $\sim 50 \mu\text{m}$  based on a homogeneous cell distribution ( $f=0.02$ ) However, it is important to recognize that the cells will be closer together than  $L_c$  in the cell clusters and farther apart than

$L_c$  in the background. To match the experimental construct modulus to the simulated construct modulus at each time point, the kinetic constants for the juvenile chondrocytes were assumed to be  $k_{cat} = 1.9 \text{ s}^{-1}$ ,  $K_M = 391 \text{ } \mu\text{M}$ , and  $k_d = 0.097 \text{ day}^{-1}$  and for adult chondrocytes were assumed to be  $k_{cat} = 0.95 \text{ s}^{-1}$ ,  $K_M = 1173 \text{ } \mu\text{M}$ , and  $k_d = 0.72 \text{ day}^{-1}$ . A higher  $k_{cat}$  coupled with a lower  $K_M$  and lower  $k_d$  points to overall faster hydrogel degradation times by the juvenile chondrocytes. On the contrary, a lower  $k_{cat}$  coupled with a higher  $K_M$  and higher  $k_d$  points to slower hydrogel degradation times by the adult chondrocytes. This suggests that the juvenile chondrocytes in general may be more active than the adult chondrocytes, which has been observed previously<sup>18</sup>.

Results from the model provide information regarding enzyme concentration and hydrogel crosslink density as a function of location and time, which is not possible through experiments alone. The modeling results show enzyme concentration gradients at each snapshot in time (Figure 5B and 5E). The gradients are relatively constant with distance, which indicates that the size of the enzyme to the mesh size of the hydrogel is small such that diffusion is not inhibited. The differences in enzyme concentration over time, thus, arises due to changes in the temporal secretion rates by the chondrocytes themselves. In general, aggrecanase concentration was higher for the adult chondrocytes and appeared to peak between weeks three and six. On the contrary, the juvenile chondrocytes secreted much lower levels of aggrecanase. Despite these differences in enzyme concentration, the hydrogels with juvenile chondrocytes degraded more rapidly (described next) when compared to the adult chondrocyte which may in part be attributed to a lower level of inhibitor concentration; although the presence of inhibitors was not investigated in this work.

The crosslink density, on the other hand, varied significantly with distance from the cell surface. Initially, the spatial variation in crosslink density is due to the  $R_d$  effect. With time, cells secrete enzymes that diffuse and cleave the hydrogel crosslinks. Since the hydrogel in the immediate vicinity of the cell is at a lower crosslink density, this region reaches reverse gelation resulting in complete dissolution of the hydrogel in this region. With time, this region grows and a degradation front propagates away from the cell surface. These characteristic features are similar for both donors, but the magnitude differs due to the different values for the kinetic constants that were chosen for each donor.

### ***5.3.5 3-Dimensional Multi-Cell Simulations: Macroscopic Hydrogel and ECM Evolution***

The micro-scale (Figure 2B) to macro-scale (Figure 2C) levels of the model were used to simulate the temporal evolution of the bulk compressive modulus of hydrogels embedded with juvenile or adult chondrocytes. ECM production rate on a per cell basis was estimated from the total ECM concentration measured at discrete time points. We assumed, as before, that the production rate measured at a particular time point (*e.g.*, week 3) was representative from the previously measured time point (*e.g.*, day 1 to week 3) (Figure 6A). In the degradable hydrogels, rate of ECM production decreased with time, but was higher for the juvenile chondrocytes compared to the adult chondrocytes (Figure 6A). For the adult cells, a negative ECM production rate was observed from 9 to 12 weeks, which corresponds to an overall reduction in ECM content and is attributed to degradation of the ECM. This observation by adult chondrocytes may be indicative of increased proteolytic activity<sup>61</sup>. It is worth noting that the ECM production rates were lower in the degradable hydrogels (Figure 6A) when compared to the non-degradable hydrogels (Figure 4B).

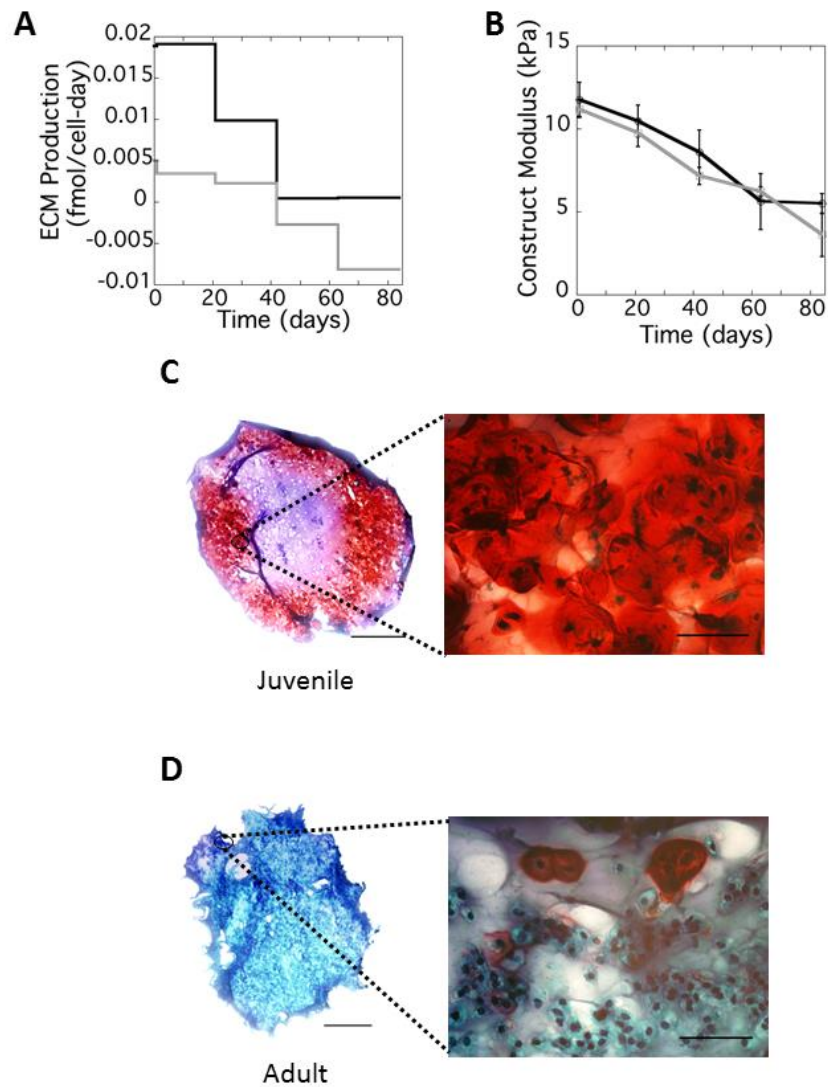


Figure 6. Characterization of ECM production and construct modulus for aggrecanase-sensitive hydrogels encapsulated with juvenile or adult chondrocytes over 12 weeks. A) Production rate of ECM molecules (sGAGs and total collagen) by chondrocytes in aggrecanase-sensitive hydrogels. B) The experimentally measured compressive modulus of aggrecanase-sensitive hydrogels for juvenile (black) and adult (gray) chondrocytes as a function of culture time. The overall compressive modulus of the cell-laden constructs steadily decreased with culture time ( $p < 0.001$ ) and was affected ( $p = 0.049$ ) by cell source. C and D) Representative microscopy images of a section stained for sGAGs (red) of juvenile or adult chondrocytes encapsulated in aggrecanase-sensitive hydrogels at 12 weeks. Scale bar is 1 mm. Scale bars for zoomed in sections of hydrogel are 50  $\mu\text{m}$ .



Chondrocytes synthesize and secrete ECM precursors that assemble extracellularly to form the large macromolecules of aggrecan and collagen. The ECM production rates reported here are for the ECM molecules that are retained within the hydrogel and thus correspond to the deposited ECM. However, it is possible for the ECM precursors (*i.e.*, unlinked ECM molecules) to diffuse out of the hydrogel. The total amount of ECM, which includes the ECM retained in the gel and the ECM released from the hydrogel, was determined and found to be similar between degradable and non-degradable hydrogels (Figure 7). Thus, it is reasonable to postulate that as the hydrogel degrades and the mesh size increases, diffusivity of the unlinked ECM molecules increases leading to their loss from the hydrogel. It is also plausible that differences in matrix degrading enzymes exist, which leads to degradation and loss of ECM, but these were not specifically investigated. Since soluble unlinked ECM molecules do not contribute significantly to the modulus of the hydrogel construct, they were not considered in the model.

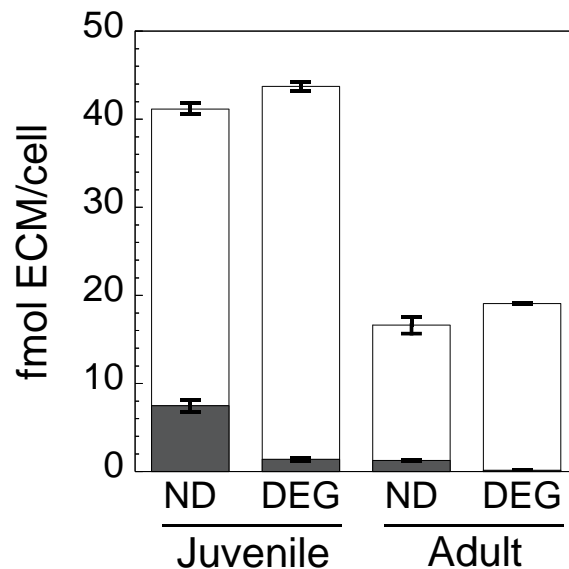


Figure 7. Cumulative amount of ECM produced for juvenile and adult chondrocytes encapsulated in nondegradable (ND) and degradable (DEG) hydrogels after 12 weeks of culture. The amount

found in media (white bar) and the amount found in the constructs (grey bar) are shown. Total amount of ECM was similar in nondegradable and degradable hydrogels for the same cell source.

The overall compressive modulus of the cell-laden constructs steadily decreased with culture time ( $p < 0.001$ ) and was affected ( $p = 0.049$ ) by cell source, *i.e.*, juvenile and adult chondrocytes (Figure 6B). A representative section of a cell-laden hydrogel stained for sGAGs illustrates the greater amount of ECM that is deposited by the juvenile (Figure 6C) compared to the adult (Figure 6D) chondrocytes. Furthermore juvenile and adult chondrocyte-laden hydrogels revealed heterogeneities in cell density with regions in the construct that have relatively high cell density and other regions that have a scarce cell density.

To capture these spatial heterogeneities in cell density in the model, we simulated regions of cell clusters and regions of single cells (*i.e.*, background) at the micro-scale level. Representative 3D volume elements (RVEs) are shown for juvenile and adult chondrocytes in regions of cell clusters (Figure 8A and C) and regions of low cell density (Figure 8B and D). For each RVE, spatial distributions for normalized crosslink density and separately for enzyme concentration are shown. Each RVE is compared to experiments where we observe in both simulations and experiments: a) regions with cell clusters evident by positive staining for aggrecan and collagen type II and an interconnected matrix between cells and b) regions where cells were farther apart with no evidence of matrix interconnectivity between cells (*i.e.*, the matrix appeared pericellular). When cells are close together in clusters, ECM elaboration around each cell has a greater chance to percolate with the ECM of neighboring cells as a result of faster hydrogel degradation within these regions. On the contrary, when cells are farther apart the deposited ECM is restricted to the pericellular space where cells are separated by the presence of hydrogel that prevents any interaction with neighboring cells. Without introducing spatial

heterogeneities in cell density, the model was not able to capture the differences observed experimentally in the elaboration of ECM within the clusters and that in the background.

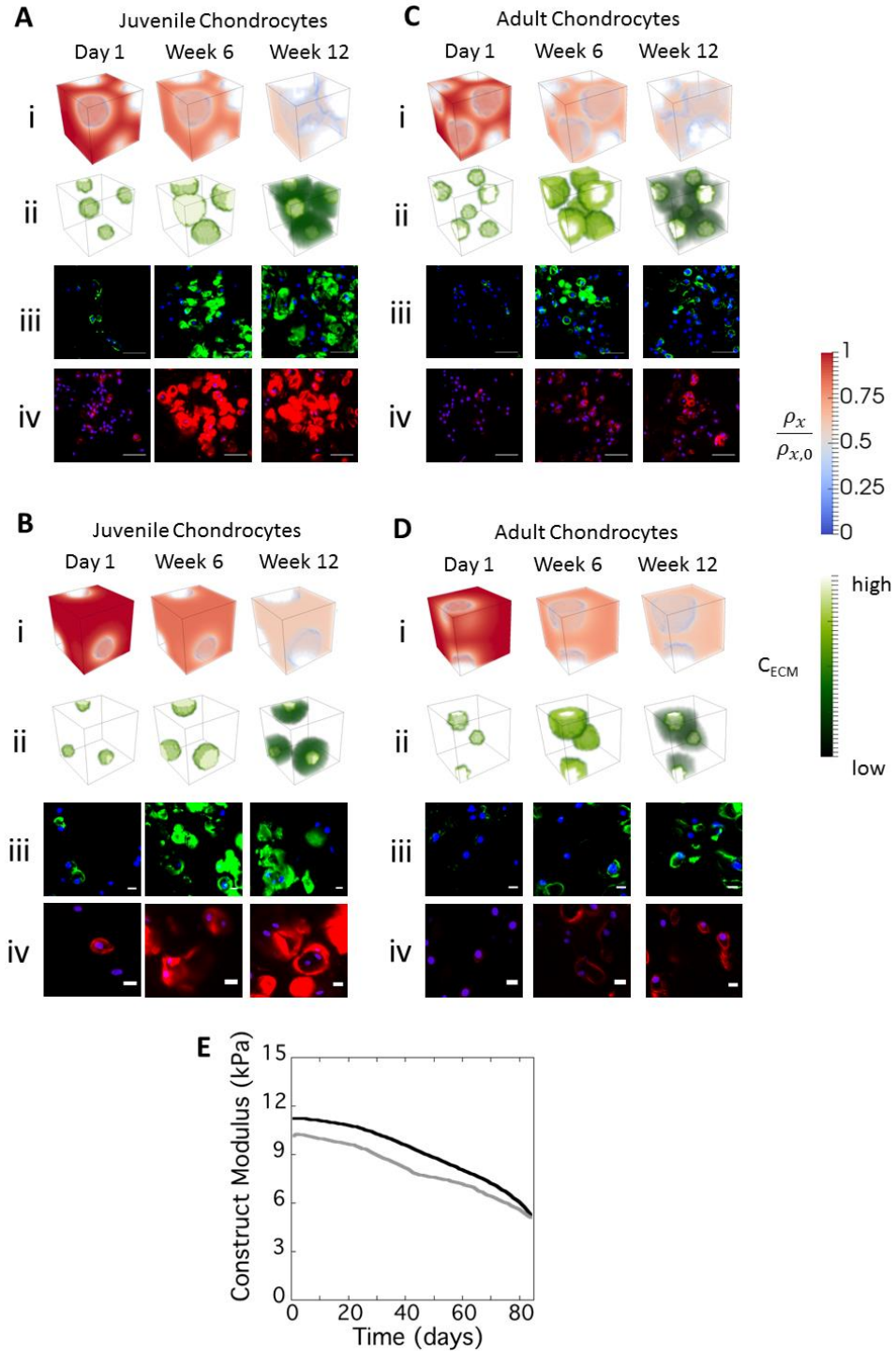


Figure 8. A) The degradation of the polymer network through time in the environment of multiple juvenile cells (i). The tissue evolution through time in the environment of multiple juvenile cells (ii). Collagen II immunohistological stains of juvenile cells (iii). Aggrecan immunohistological stains of juvenile cells (iv). B) The degradation of the polymer network through time in the environment of multiple juvenile cells (i). The tissue evolution through time in the environment

of multiple juvenile cells (ii). Collagen II immunohistological stains of juvenile cells (iii). Aggrecan immunohistological stains of juvenile cells (iv). C) The degradation of the polymer network through time in the environment of multiple adult cells (i). The tissue evolution through time in the environment of multiple adult cells (ii). Collagen II immunohistological stains of adult cells (iii). Aggrecan immunohistological stains of adult cells (iv). D) The degradation of the polymer network through time in the environment of multiple adult cells (i). The tissue evolution through time in the environment of multiple adult cells (ii). Collagen II immunohistological stains of adult cells (iii). Aggrecan immunohistological stains of adult cells (iv). Panels A and C represent modeling results and experimental observations in clustered regions, while panels B and D represent nonclustered regions. Scale bar is 50  $\mu\text{m}$ .

To determine the overall mechanical properties at the macro-scale level, RVEs of cell clusters and RVE single cells ( $f$  values in Table 2) were combined (Figure 2C). The overall compressive modulus, which represents the combined modulus of the hydrogel, ECM, and encapsulated cells, was estimated by the model (Figure 8E) to capture the same trends observed experimentally (Figure 6A). Collectively, the modeling results point to the juvenile cells as having both a higher capacity for ECM deposition, but also a higher enzyme activity, despite lower levels of enzyme, which together explain the temporal changes in the overall modulus of the construct. On the contrary, these data point to adult cells as having a low capacity for ECM deposition, but also a lower enzyme activity, where the overall modulus of the construct is largely attributed to the remaining hydrogel. Thus, the model points to the regulation of enzymes as playing an important role in the cell-mediated degradation of the hydrogel. Although the model was fit to the experimentally determined construct modulus to estimate values for the kinetic constants, the model captures the local variations of ECM deposition and growth for each donor that were observed experimentally. Importantly, the model is able to provide information that is not accessible by experimental measurements and specifically describes how hydrogel crosslink density, enzyme concentration, and ECM growth vary with location and time for each donor. It is important to note that in both the juvenile and adult chondrocyte-laden hydrogels, the overall

modulus decreased with culture time by ~50% in twelve weeks. With the knowledge gained from the model, our future efforts aim to identify hydrogel formulations that will further minimize any loss in modulus as the construct transitions from hydrogel to ECM.

There are several limitations of the experimental and modeling approach that are important to note. It was not possible to measure aggrecanase and ECM synthesis rates in real time and therefore our estimates of their production rates may under or over estimate and may vary between juvenile and adult chondrocytes. These potential discrepancies may manifest in the different values for the kinetic constants that were chosen for the juvenile and adult chondrocytes to match the experimental data. We assumed an average value for  $R_d$  and average synthesis rates for each cell. However, chondrocytes isolated from full depth cartilage are a heterogeneous population of cells that have been shown to exhibit different cellular responses. Thus these variations may also contribute to the formation of clusters and a connected matrix in some cells, but not in other cells. It was also not possible to accurately identify the distribution of cell clusters within the experimental system and therefore the computational model used random placements of the different representative volume elements to build the 3D macroscopic model of the cell-laden construct. Temporal changes in cell proliferation and cell death add further complexity to cell distributions, which were not explicitly captured in the model. We assumed a simple relationship between the concentration of ECM (sGAG and collagen) and the modulus of the ECM. This relationship, however, does not account for potential differences in other key molecules that contribute to the mechanical properties of cartilage (e.g., collagen crosslinking), which could lead to differences in the modulus of the ECM between the non-degradable and degradable hydrogels. Finally, this study is limited to one donor from each age

group. We have previously reported similar cellular behaviors in chondrocytes isolated from juvenile and adult donors of similar age, where the former showed a more anabolic response with increased ECM synthesis and the latter showed decreased ECM synthesis<sup>18,62</sup>, which is consistent with the observations in this study.

## 5.4 Conclusions

Overall, our model was able to capture the experimental findings and observations of ECM growth by chondrocytes encapsulated in an aggrecanase-sensitive hydrogel for two different donors. The model provided new insights into how hydrogel crosslink density, enzyme concentration and ECM growth vary in space and time. By combining experimental and computational approaches, we identified two key features of the cell-laden hydrogels, which were not previously known and which are critical to facilitating ECM growth. The first is the presence of an  $R_d$ , where encapsulated cells inhibit the crosslinking efficiency in the immediate vicinity of the cell. This  $R_d$  is critical for creating regions where the hydrogel reaches its reverse gelation point and degrades completely while the bulk hydrogel remains intact. Since enzyme molecules diffuse rapidly through the hydrogel, this initial spatial variation in crosslink density is critical to achieving spatiotemporal variations in crosslink density over time that is necessary to achieve ECM growth and ECM connectivity within the cell clusters. The second key feature is the spatial heterogeneities in the location of cells, where regions of high cell densities are found that with the presence of  $R_d$  facilitated macroscopic evolution of ECM. Collectively, the introduction of an  $R_d$  and spatial heterogeneities in cell density into the model was necessary to capture the experimentally observed ECM growth. We further demonstrate that the model can describe the behavior of cells from two very different donors, one donor leading to improved ECM growth

with the other donor leading to poor ECM growth. Since our model is derived from a system of equations based on thermodynamics, physics, and statistical methods, it can readily be extended to other cell-laden hydrogels of different chemistry and cell type. Furthermore, our long-term goal is to use this model to predict optimal hydrogel designs for a particular donor, especially for poor performers, and thus improve tissue engineering for a wide range of donors. The hydrogel platform used herein is highly flexible with respect to controlling the initial hydrogel properties and selecting different enzyme-substrate pairs to control the catalytic and Michaelis-Menten constants. Thus, the model may help to overcome the challenges associated with donor-to-donor variability.

## 5.5 Acknowledgments

Research reported in this publication was supported by the National Institute of Arthritis and Musculoskeletal and Skin Diseases of the National Institutes of Health under Award Number 1R01AR065441. The authors acknowledge the National Institute of Health (NIH) Institutional Pharmaceutical Training fellowship and the Graduate Assistance in Areas of National Need (GAANN) Biomaterials from the Department of Education to SC. The technical assistance of Shankar Lalitha Sridhar and Stacey Skaalure is greatly appreciated.

## 5.6 References

1. Tibbitt, M. W. & Anseth, K. S. Hydrogels as extracellular matrix mimics for 3D cell culture. *Biotechnol. Bioeng.* **103**, 655–663 (2009).
2. Tibbitt, M. W., Rodell, C. B., Burdick, J. A. & Anseth, K. S. Progress in material design for biomedical applications. *Proc Natl Acad Sci U S A.* **112**, 14444–14451 (2015).
3. Park, Y., Lutolf, M. P., Hubbell, J. A., Hunziker, E. B. & Wong, M. Bovine primary chondrocyte culture in synthetic matrix metalloproteinase-sensitive poly(ethylene glycol)-based hydrogels as a scaffold for cartilage repair. *Tissue Eng.* **10**, 515–522 (2004).



4. Sridhar, B. V., Brock J.L., Silver, J.S., Leight, J.L., Randolph, M.A., Anseth, K.S. Development of a cellularly degradable PEG hydrogel to promote articular cartilage extracellular matrix deposition. *Adv. Healthc. Mater.* **4**, 702–713 (2015).
5. Skaalure, S. C., Chu, S. & Bryant, S. J. An enzyme-sensitive PEG hydrogel based on aggrecan catabolism for cartilage tissue engineering. *Adv. Healthc. Mater.* **4**, 420–431 (2015).
6. Bahney, C. S., Hsu, C.-W., Yoo, J. U., West, J. L. & Johnstone, B. A bioresponsive hydrogel tuned to chondrogenesis of human mesenchymal stem cells. *FASEB J.* **25**, 1486–1496 (2011).
7. Parmar, P. A., Skaalure, S.C., Chow, L.W., St-Pierre, J.P., Stoichevska, V., Peng, Y.Y., Werkmeister, J.A., Ramshaw, J.A., Stevens, M.M., Temporally degradable collagen-mimetic hydrogels tuned to chondrogenesis of human mesenchymal stem cells. *Biomaterials* **99**, 56–71 (2016).
8. Bryant, S. J. & Anseth, K. S. Hydrogel properties influence ECM production by chondrocytes photoencapsulated in poly (ethylene glycol) hydrogels. *J. Biomed. Mater. Res.* **59**, 63–72 (2002).
9. Nicodemus, G. D., Skaalure, S. C. & Bryant, S. J. Gel structure has an impact on pericellular and extracellular matrix deposition, which subsequently alters metabolic activities in chondrocyte-laden PEG hydrogels. *Acta Biomater.* **7**, 492–504 (2011).
10. Hascall, V. C. & Sajdera, S. W. Physical properties and polydispersity of proteoglycan from bovine nasal cartilage. *J. Biol. Chem.* **245**, 4920–4930 (1970).
11. Lodish, H. & Baltimore, D.I. Collagen: The Fibrous Proteins of the Matrix. In: *Molecular Cell Biology*. NY: W. H. Freeman, 2000. Chapter 22.3.
12. Neumann, A. J., Quinn, T. & Bryant, S. J. Nondestructive evaluation of a new hydrolytically degradable and photo-clickable PEG hydrogel for cartilage tissue engineering. *Acta Biomater.* **39**, 1–11 (2016).
13. Roberts, J. J., Nicodemus, G. D., Greenwald, E. C. & Bryant, S. J. Degradation improves tissue formation in (un)loaded chondrocyte-laden hydrogels. *Clin. Orthop.* **469**, 2725–2734 (2011).
14. Vernerey, F. J., Greenwald, E. C. & Bryant, S. J. Triphasic mixture model of cell-mediated enzymatic degradation of hydrogels. *Comput. Methods Biomech. Biomed. Engin.* **15**, 1197–1210 (2012).
15. Dhote, V. *et al.* On the role of hydrogel structure and degradation in controlling the transport of cell-secreted matrix molecules for engineered cartilage. *J. Mech. Behav. Biomed. Mater.* **19**, 61–74 (2013).
16. Skaalure, S. C., Akalp, U., Vernerey, F. J. & Bryant, S. J. Tuning reaction and diffusion mediated degradation of enzyme-sensitive hydrogels. *Adv. Healthc. Mater.* **5**, 432–438 (2016).

17. Akalp, U., Bryant, S. J. & Vernerey, F. J. Tuning tissue growth with scaffold degradation in enzyme-sensitive hydrogels: a mathematical model. *Soft Matter* **12**, 7505–7520 (2016).
18. Farnsworth, N. L., Antunez, L. R. & Bryant, S. J. Dynamic compressive loading differentially regulates chondrocyte anabolic and catabolic activity with age. *Biotechnol. Bioeng.* **110**, 2046–2057 (2013).
19. Lutolf, M. P., Tirelli, N., Cerritelli, S., Cavalli, L. & Hubbell, J. A. Systematic modulation of Michael-type reactivity of thiols through the use of charged amino acids. *Bioconjug. Chem.* **12**, 1051–1056 (2001).
20. Roberts, J. J., Earnshaw, A., Ferguson, V. L. & Bryant, S. J. Comparative study of the viscoelastic mechanical behavior of agarose and poly(ethylene glycol) hydrogels. *J. Biomed. Mater. Res. B Appl. Biomater.* **99B**, 158–169 (2011).
21. Kim, Y.-J., Sah, R. L. Y., Doong, J.-Y. H. & Grodzinsky, A. J. Fluorometric assay of DNA in cartilage explants using Hoechst 33258. *Anal. Biochem.* **174**, 168–176 (1988).
22. Templeton, D. M. The basis and applicability of the dimethylmethylene blue binding assay for sulfated glycosaminoglycans. *Connect. Tissue Res.* **17**, 23–32 (1988).
23. Woessner, J. F. The determination of hydroxyproline in tissue and protein samples containing small proportions of this imino acid. *Arch. Biochem. Biophys.* **93**, 440–447 (1961).
24. Dhote, V. & Vernerey, F. J. Mathematical model of the role of degradation on matrix development in hydrogel scaffold. *Biomech. Model. Mechanobiol.* **13**, 167–183 (2014).
25. Peppas, N. A. *Structure and Properties of Polymeric Materials*. (1984).
26. Peppas, N. A. *Hydrogels in Medicine and Pharmacy, Vol.2. Polymers*. (CRC Press, 1987).
27. Macosko, C. & Miller, D. R. A new derivation of average molecular weights of nonlinear polymers. *Macromolecules* **9**, 199–206 (1976).
28. Tibbitt, M. W., Kloxin, A. M., Sawicki, L. A. & Anseth, K. S. Mechanical properties and degradation of chain and step-polymerized photodegradable hydrogels. *Macromolecules* **46**, 2785–2792 (2013).
29. Lutolf, M. P. *et al.* Synthetic matrix metalloproteinase-sensitive hydrogels for the conduction of tissue regeneration: Engineering cell-invasion characteristics. *Proc Natl Acad Sci U S A.* **100**, 5413–5418 (2003).
30. Akalp, U. *et al.* Determination of the polymer-solvent interaction parameter for PEG hydrogels in water: application of a self learning algorithm. *Polymer* **66**, 135–147 (2015).
31. Brannon-Peppas, L. & Peppas, N. A. Solute and penetrant diffusion in swellable polymers. IX. The mechanisms of drug release from pH-sensitive swelling-controlled systems. *J. Controlled Release* **8**, 267–274 (1989).

32. Lustig, S. R. & Peppas, N. A. Solute diffusion in swollen membranes. IX. Scaling laws for solute diffusion in gels. *J. Appl. Polym. Sci.* **36**, 735–747 (1988).
33. Merrill, E. W., Dennison, K. A. & Sung, C. Partitioning and diffusion of solutes in hydrogels of poly(ethylene oxide). *Biomaterials* **14**, 1117–1126 (1993).
34. Anderson, M. L., Mott, P. H. & Roland, C. M. The compression of bonded rubber disks. *Rubber Chem. Technol.* **77**, 293–302 (2004).
35. Anseth, K. S., Bowman, C. N. & Brannon-Peppas, L. Mechanical properties of hydrogels and their experimental determination. *Biomaterials* **17**, 1647–1657 (1996).
36. Gould, S. T., Darling, N. J. & Anseth, K. S. Small peptide functionalized thiol–ene hydrogels as culture substrates for understanding valvular interstitial cell activation and de novo tissue deposition. *Acta Biomater.* **8**, 3201–3209 (2012).
37. Akalp, U., Bryant, S. J. & Vernerey, F. J. Tuning tissue growth with scaffold degradation in enzyme-sensitive hydrogels: a mathematical model. *Soft Matter* **12**, 7505–7520 (2016).
38. Wong, M., Ponticciello, M., Kovanen, V. & Jurvelin, J. S. Volumetric changes of articular cartilage during stress relaxation in unconfined compression. *J. Biomech.* **33**, 1049–1054 (2000).
39. Mow, V. C., Gibbs, M. C., Lai, W. M., Zhu, W. B. & Athanasiou, K. A. Biphasic indentation of articular cartilage-II. A numerical algorithm and an experimental study. *J. Biomech.* **22**, 853–861 (1989).
40. Guilak, F., Jones, W. R., Ting-Beall, H. P. & Lee, G. M. The deformation behavior and mechanical properties of chondrocytes in articular cartilage. *Osteoarthritis Cartilage* **7**, 59–70 (1999).
41. Vernerey, F. J. A mixture approach to investigate interstitial growth in engineering scaffolds. *Biomech. Model. Mechanobiol.* **15**, 259–278 (2016).
42. Aboudi, J., Arnold, S. M. & Bednarczyk, B. A. *Micromechanics of Composite Materials: A Generalized Multiscale Analysis Approach*. (Butterworth-Heinemann, 2012).
43. Nemat-Nasser, S. & Hori, M. *Micromechanics: overall properties of heterogeneous materials*. (Elsevier, 2013).
44. Hoyle, C. E. & Bowman, C. N. Thiol–ene click chemistry. *Angew. Chem. Int. Ed.* **49**, 1540–1573 (2010).
45. Fairbanks, B. D. *et al.* A versatile synthetic extracellular matrix mimic via thiol–norbornene photopolymerization. *Adv. Mater.* **21**, 5005–5010 (2009).
46. Kääh, M. J., Ap Gwynn, I. & Nötzli, H. P. Collagen fibre arrangement in the tibial plateau articular cartilage of man and other mammalian species. *J. Anat.* **193**, 23–34 (1998).
47. Firestein, G. S., Budd, R., Gabriel, S. E., McInnes, I. B. & O’Dell, J. R. *Kelley and Firestein’s Textbook of Rheumatology*. (Elsevier Health Sciences, 2016).

48. Li, Y., Wei, X., Zhou, J. & Wei, L. The age-related changes in cartilage and osteoarthritis. *BioMed Res. Int.* **2013**, e916530 (2013).
49. Lobo, V., Patil, A., Phatak, A. & Chandra, N. Free radicals, antioxidants and functional foods: Impact on human health. *Pharmacogn. Rev.* **4**, 118–126 (2010).
50. Richards, D. M. C., Dean, R. T. & Jessup, W. Membrane proteins are critical targets in free radical mediated cytolysis. *Biochim. Biophys. Acta BBA - Biomembr.* **946**, 281–288 (1988).
51. Donoghue, N., Yam, P. T., Jiang, X. M. & Hogg, P. J. Presence of closely spaced protein thiols on the surface of mammalian cells. *Protein Sci. Publ. Protein Soc.* **9**, 2436–2445 (2000).
52. Farnsworth, N., Bensard, C. & Bryant, S. J. The role of the PCM in reducing oxidative stress induced by radical initiated photoencapsulation of chondrocytes in poly(ethylene glycol) hydrogels. *Osteoarthritis Cartilage* **20**, 1326–1335 (2012).
53. Flannery, C. *et al.* Variability in the G3 domain content of bovine aggrecan from cartilage extracts and chondrocyte cultures. *Arch. Biochem. Biophys.* **297**, 52–60 (1992).
54. Ilic, M. Z., Robinson, H. C. & Handley, C. J. Characterization of aggrecan retained and lost from the extracellular matrix of articular cartilage: involvement of carboxy-terminal processing in the catabolism of aggrecan. *J. Biol. Chem.* **273**, 17451–17458 (1998).
55. Nicodemus, G. D. & Bryant, S. J. The role of hydrogel structure and dynamic loading on chondrocyte gene expression and matrix formation. *J. Biomech.* **41**, 1528–1536 (2008).
56. Kashiwagi, M., Tortorella, M., Nagase, H. & Brew, K. TIMP-3 Is a potent inhibitor of Aggrecanase 1 (ADAM-TS4) and Aggrecanase 2 (ADAM-TS5). *J. Biol. Chem.* **276**, 12501–12504 (2001).
57. Hashimoto, G., Aoki, T., Nakamura, H., Tanzawa, K. & Okada, Y. Inhibition of ADAMTS4 (aggrecanase-1) by tissue inhibitors of metalloproteinases (TIMP-1, 2, 3 and 4). *FEBS Lett.* **494**, 192–195 (2001).
58. Gavrilovic, J., Hembry, R. M., Reynolds, J. J. & Murphy, G. Tissue inhibitor of metalloproteinases (TIMP) regulates extracellular type I collagen degradation by chondrocytes and endothelial cells. *J. Cell Sci.* **87 ( Pt 2)**, 357–362 (1987).
59. Tortorella, M. D. *et al.*  $\alpha$ 2-macroglobulin is a novel substrate for ADAMTS-4 and ADAMTS-5 and represents an endogenous inhibitor of these enzymes. *J. Biol. Chem.* **279**, 17554–17561 (2004).
60. Dangott, L. J. & Cunningham, L. W. Residual  $\alpha$ 2-macroglobulin in fetal calf serum and properties of its complex with thrombin. *Biochem. Biophys. Res. Commun.* **107**, 1243–1251 (1982).
61. Loeser, R. F. Aging and osteoarthritis: the role of chondrocyte senescence and aging changes in the cartilage Matrix. *Osteoarthr. Cartil. OARS Osteoarthr. Res. Soc.* **17**, 971–979 (2009).

62. Skaalure, S. C., Milligan, I. L. & Bryant, S. J. Age impacts extracellular matrix metabolism in chondrocytes encapsulated in degradable hydrogels. *Biomed. Mater.* **7**, 024111 (2012).

**Chapter 6: Local heterogeneities improve matrix connectivity in degradable and photoclickable PEG hydrogels for applications in tissue engineering**

**(As appearing in *ACS Biomater. Sci. Eng.*, 2017, 3 (10), pp 2480–2492 (2017))**

**Abstract**

Hydrolytically degradable poly(ethylene glycol) (PEG) hydrogels are promising platforms for cell encapsulation and tissue engineering. One of the challenges, however, is that hydrolysis leads to bulk degradation and correspondingly, a decrease in the mechanical integrity of the hydrogel. Since extracellular matrix (ECM) molecules that make up tissues are typically large, their transport is limited until substantial hydrogel degradation occurs at which time structural integrity is nearly lost. Despite these challenges, prior studies have reported macroscopic neotissue growth in hydrolytically degradable hydrogels. The exact mechanisms that lead to the observed improved tissue growth are not well understood. The goal of this study was to combine experimental methods with a multiscale mathematical model to analyze hydrogel degradation concomitant with neotissue growth in PEG hydrogels with a focus on cartilage tissue engineering. Primary bovine chondrocytes were encapsulated at increasing cell densities (50, 100, and 150 million cells/mL of precursor solution) in a radical-mediated photoclickable hydrogel formed from 8-arm poly(ethylene glycol)-co-caprolactone endcapped with norbornene and PEG dithiol crosslinkers. Neotissue growth was assessed by compressive modulus, biochemical content, and immunohistochemistry. Two observations were made in the experimental system. First, the distribution of cells was not uniform and regions of cell clustering were identified and were more pronounced with increasing cell density. The second was that a significant decrease in the compressive modulus of cell-laden hydrogels was observed with increasing cell concentration

post-encapsulation. The latter could be explained by the mathematical model by introducing spatial heterogeneities in crosslinking density around cells, which can arise due to cells interacting with the radical-mediated polymerization during encapsulation. When the two heterogeneities, cell clustering and variation in hydrogel crosslinking, were introduced into the mathematical model, the model captured the experimentally observed spatial evolution of ECM and the construct modulus as a function of cell density and culture time. Overall, increasing cell density, which caused more pronounced heterogeneities, led to improved ECM formation, ECM connectivity and overall modulus. Findings from this study strongly point to the importance of heterogeneities in retaining mechanical integrity as the constructs transfers from hydrogel to neotissue.

## 6.1 Introduction

Synthetic hydrogels designed with crosslinks that are susceptible to hydrolysis are promising for tissue engineering<sup>1</sup>. The use of synthetic precursors enables hydrogels to be formed with highly reproducible and controllable macroscopic properties. Furthermore, the choice of chemistry for the hydrolytically labile linker provides control over the degradation kinetics<sup>2,3</sup>. Thus, a wide range of mechanical properties (*e.g.*, moduli of 1's to 1000's kPa) and degradation profiles (*e.g.*, spanning days to months) can be achieved. As such, hydrolytically labile hydrogels have been investigated for a range of tissue engineering applications including cartilage<sup>4-7</sup>, bone<sup>8-10</sup>, tendon and ligament<sup>11,12</sup>, neural<sup>13</sup>, and smooth muscle and vascular<sup>14,15</sup>.

One of the challenges with using synthetic hydrogels for cell encapsulation and tissue engineering is that the mesh size (ca. 1-10's of nm) of the polymer network is much smaller than the size of many extracellular matrix (ECM) molecules that make up tissues. For example, mature

collagen fibers can reach ca. 1-10's of thousands of nanometers in length<sup>16,17</sup>. Thus, degradation is necessary to achieve macroscopic tissue growth. The highly water swollen nature of the hydrogel leads to bulk degradation and consequently an exponential decrease in crosslink density with time<sup>18,19</sup>. However, a point is reached where a sufficient number of crosslinks has been cleaved and the hydrogel transitions from a crosslinked polymer to a water soluble branched polymer, a phenomenon referred to as reverse gelation<sup>19,20</sup>. Although the mesh size increases as crosslinks are broken during degradation, it is still too small even at reverse gelation to enable the large ECM molecules, like collagen fibers, to diffuse through the network and deposit<sup>21</sup>. As a result, reverse gelation must occur simultaneously with ECM macroscopic growth in order to achieve a seamless transition from hydrogel to neotissue and prevent loss of mechanical integrity. This requirement is particularly challenging given the inherent variability in tissue synthesis capabilities by cells as a function of donor (e.g., donor age, cell type, etc.).

Despite these challenges, hydrolytically degradable hydrogels with encapsulated cells have yielded a macroscopic engineered tissue<sup>4,10</sup>, suggesting an important underlying phenomenon that is important to their success. A previous study reported heterogeneities at the micron-scale when cartilage cells (i.e., chondrocytes) were encapsulated in poly(ethylene glycol) hydrogels formed by radical mediated chain polymerization<sup>22</sup>. This finding was evident by the observation of large spatial variations in cell deformation despite a uniform macroscopic deformation applied to the hydrogel. Although the exact mechanism that contributed to the macroscopic heterogeneities was not identified, another study reported that cells during encapsulation are capable of reacting with propagating radicals<sup>23</sup> and may act as chain transfer agents to locally inhibit polymerization. Collectively, these findings point to the existence of



heterogeneities within cell-laden crosslinked hydrogels. Such heterogeneities in crosslinking may help explain why hydrolytically degradable hydrogels have, in some cases, promoted neotissue growth. A better understanding of the role of heterogeneities on macroscopic tissue growth is, however, needed.

The goal of this study was to combine experimental approaches with computational models to investigate the impact of spatial heterogeneities in crosslink density on macroscopic tissue evolution. Because it is difficult to probe experimentally the local heterogeneities in network structure, we employed a recently developed mathematical model that describes the coupled phenomena of hydrogel degradation and ECM elaboration by encapsulated cells<sup>24,25</sup>. For the experimental approach, we chose a hydrolytically degradable and photo-clickable poly(ethylene glycol) (PEG) hydrogel that we recently described and demonstrated its promise in cartilage tissue engineering leading to macroscopic cartilage-like tissue growth<sup>4</sup>. In the work herein, cell density was varied as a means to investigate how cell proximity combined with local heterogeneities impact ECM growth during hydrogel degradation. Computational modelling was employed to provide mechanistic insight into how spatial heterogeneities in crosslink density and cell distribution affect ECM connectivity during hydrogel degradation. Using chondrocytes and their associated cartilaginous ECM, which is rich in collagen, as a model system, we provide evidence for the importance of local heterogeneities to achieving macroscopic ECM elaboration while minimizing loss of mechanical integrity of the evolving construct. This new insight may offer novel approaches to introduce heterogeneities into hydrogels which lead to spatial variations in hydrogel degradation and thus may overcome some of the challenges with using hydrolytically degradable hydrogels for cell encapsulation and tissue engineering.

## 6.2 Materials and Methods

### 6.2.1 Macromer Synthesis

Macromers of 8-arm PEG-caprolactone functionalized with norbornene (PEG<sub>8arm</sub>-CAP-NB) were synthesized in a two-step process using protocols adapted from Bryant, et al.<sup>26</sup> Briefly, 8-arm PEG-hexaglycerol (20 kDa, JenKem Technology, Allen, TX) was reacted with 1.5 molar excess  $\epsilon$ -caprolactone using tin(II) ethylhexanoate as the ring opening catalyst. The reaction was carried out at 140°C for 6 h under vacuum. The intermediate product PEG-CAP was recovered by precipitation in ice-cold diethyl ether. PEG-CAP was reacted overnight at room temperature under argon with *N,N'*-diisopropylcarbodiimide (10 molar excess), 4-dimethylaminopyridine (1 molar excess), pyridine (10 molar excess) and 5-norbornene-2-carboxylic acid (10 molar excess) in dichloromethane. The final product, PEG-CAP-NB, was purified through filtration over activated carbon and precipitated in diethyl ether. The precipitate was dried and dissolved in a minimal amount of chloroform. The solution was washed twice in a glycine buffer and once in a brine solution. The purified product was recovered via precipitation in diethyl ether, lyophilized, and confirmed by <sup>1</sup>H nuclear magnetic resonance spectroscopy. The number of caprolactones per PEG arm was determined to be on average 1.26 by comparing the peak area for the methylene protons in the caprolactone ( $\delta = 2.25$ -2.4 ppm) to the peak area of the methylene protons in PEG ( $\delta = 3.25$ -3.9 ppm). Norbornene conjugation was determined to be 65% by comparing the peak area of the vinyl protons ( $\delta = 5.9$ -6.25 ppm) to the methylene protons in PEG.

### **6.2.2 Chondrocyte Isolation**

Chondrocytes were harvested from bovine articular cartilage from the femoral patellar groove and femoral condyles of a 1-3 week old calf (Research 87, Marlborough, MA). Cartilage slices were rinsed in phosphate-buffered saline (PBS) supplemented with 50 U/mL penicillin and 50 µg/mL streptomycin (P/S), 0.5 µg/mL fungizone, and 20 µg/mL gentamicin (Invitrogen, Carlsbad, CA). Cartilage slices were digested for 15-17 hours at 37°C in 600 U/mL collagenase type II (Worthington Biochemical, Lakewood, NJ) in Dulbecco's Modified Eagle Medium (DMEM) (Invitrogen, Carlsbad, CA) with 5% fetal bovine serum (FBS) (Atlanta Biologicals, Lawrenceville, GA). The cartilage digest was filtered through a 100 µm cell strainer (Falcon, Corning, NY) and collagenase was inactivated with 0.02% ethylenediaminetetraacetic acid in PBS (Invitrogen, Carlsbad, CA). Chondrocytes were recovered and washed in PBS by several centrifugation steps and resuspended in PBS with antibiotics. Cell viability was >70% post-digestion as determined using the Trypan Blue exclusion assay (Invitrogen, Carlsbad, CA).

### **6.2.3 Chondrocyte Encapsulation and Culture**

PEG-CAP-NB was solubilized in PBS one day before cell encapsulation and stored at 4°C to minimize hydrolysis. A precursor solution was prepared with 10% (g/g) PEG-CAP-NB, PEG dithiol (PEGdSH 1 kDa, 1:1 thiol:norbornene, Sigma-Aldrich, St. Louis, MO), and 0.05% (g/g) photoinitiator (Irgacure 2959, Ciba Specialty Chemicals, Tarrytown, NY) in PBS. Freshly isolated chondrocytes were combined with the precursor solution at 50, 100, or 150 million cells/mL precursor solution. Cell-laden PEG-CAP hydrogels were formed by photopolymerization with UV light (352 nm, 5 mW/cm<sup>2</sup>) for 7 minutes. Hydrogels were rinsed in PBS with antibiotics and then cultured in 4.5 mL chondrocyte growth medium (DMEM supplemented with 10% FBS, 50 U/mL

P/50 µg/mL S, 0.5 µg/mL fungizone, 20 µg/mL gentamicin, 10 mM HEPES buffer, 0.1 M MEM-NEAA, 0.4 mM L-proline, 4 mM GlutaGro, 110 mg/L sodium pyruvate, and 50 mg/mL L-ascorbic acid) at 37°C and 5% CO<sub>2</sub> in a humid environment. Medium was changed every 2-3 d.

#### **6.2.4 Hydrogel Construct Characterization**

Cell viability was assessed with the LIVE/DEAD<sup>®</sup> assay (Invitrogen, Carlsbad, CA) at 0, 4, and 12 weeks on constructs (n=2) per experimental condition. Constructs were cut in half and images were acquired from different regions of a cross section within the constructs at 100x using a confocal laser scanning microscopy (Zeiss LSM 5 Pascal). The other half of each construct was used for immunohistochemistry as described below. At week 0 (i.e., 24 hours post encapsulation), 4, and 12, hydrogels were assessed for compressive modulus (n=3). The diameter and height of hydrogels were recorded. Hydrogels were compressed to 15% strain at a rate of 0.5 mm/min (MTS Synergie 100, 10N). The compressive modulus was measured by estimating the slope of the linear region of stress-strain curves from 10-15% strain.

#### **6.2.5 Biochemical Analysis**

The same constructs processed for compression tests were subsequently analyzed for biochemical content (n=3). The lyophilized hydrogels were homogenized using a TissueLyser and enzymatically digested in 0.125 mg/mL papain for 18 h at 60°C. The DNA content was determined using Hoechst 33258 (Polysciences, Inc. Warrington, PA)<sup>27</sup>. Cell number was determined based on DNA content, assuming 7.7 pg DNA per chondocyte<sup>27</sup>. The dimethyl methylene blue (DMMB, Sigma–Aldrich St. Louis, MO) colorimetric assay was used to measure the amount of sulfated glycosaminoglycans (sGAGs)<sup>28</sup>. Total collagen content was assessed using the hydroxyproline

assay and assuming a 10% hydroxyproline content in collagen<sup>29</sup>. Bovine cartilage explants were also analyzed for biochemical and DNA content.

### **6.2.6 Immunohistochemistry**

At weeks 0 (24 hours post encapsulation), 4, and 12 half constructs were harvested for immunohistochemical analysis (IHC) (n=2). Constructs were fixed overnight in 4% paraformaldehyde at 4°C and transferred to 30% sucrose in PBS for 2-3 d. Samples were embedded in TissueTek OCT compound (Sakura Finetek USA, Torrance, CA) and frozen in isopentane and liquid nitrogen. Sections (10 µm) were obtained from the center of the construct (the cut side) with a Leica CM1850 cryostat (Leica Microsystems Inc., Buffalo Grove, IL). Sections were stained with primary antibodies for collagen II (1:50, C7510-21C, US Biologicals, Swampscott, MA) and aggrecan (1:100, ab3778, Abcam). Prior to antibody treatment, sections underwent antigen retrieval (Retrievagen A, BD Biosciences, San Jose, CA) and were treated with 200 U hyaluronidase (Sigma-Aldrich, St. Louis, MO) (for anti-collagen II and anti-aggrecan), or 3.4 mU keratanase I (MP Biomedical, Solon, OH) and 10 mU chondroitinase-ABC (Sigma-Aldrich) (for anti-aggrecan) for 1 h at 37°C. After primary antibody treatment, sections were treated with either AlexaFluor 488 or 546 conjugated secondary antibodies (Invitrogen, Carlsbad, CA) for collagen II and aggrecan, respectively. Cell nuclei were counterstained with DAPI (Invitrogen). Stained sections were mounted with Fluoromount-G (Southern Biotech, Birmingham, AL) and imaged via laser scanning confocal microscopy at 100x and 400x. Sections receiving no primary antibody treatment served as negative controls.

### **6.2.7 Modeling**

Since the global growth process and local degradation around cells occur at different length-scales (millimeter and micrometer, respectively), we adopted a hierarchical multiscale approach<sup>30</sup> that follows three steps (Figure 1). At the submicro level, the model describes the hydrogel properties (i.e., crosslinking density and mechanical properties) that evolve over time as the hydrogel degrades. At the micro level, the construct is described by representative volume elements (RVEs) containing a finite number of cells embedded in a hydrogel whose crosslink density ( $\rho_x$ ) can vary with distance ( $x$ ) and time ( $t$ ) such that  $\rho_x(x, t)$ . Diffusion of ECM molecules depends on hydrogel crosslinking. At the macro level, large populations of cells are considered as well as their effect on the evolution of mechanical properties that result from hydrogel degradation and ECM growth.

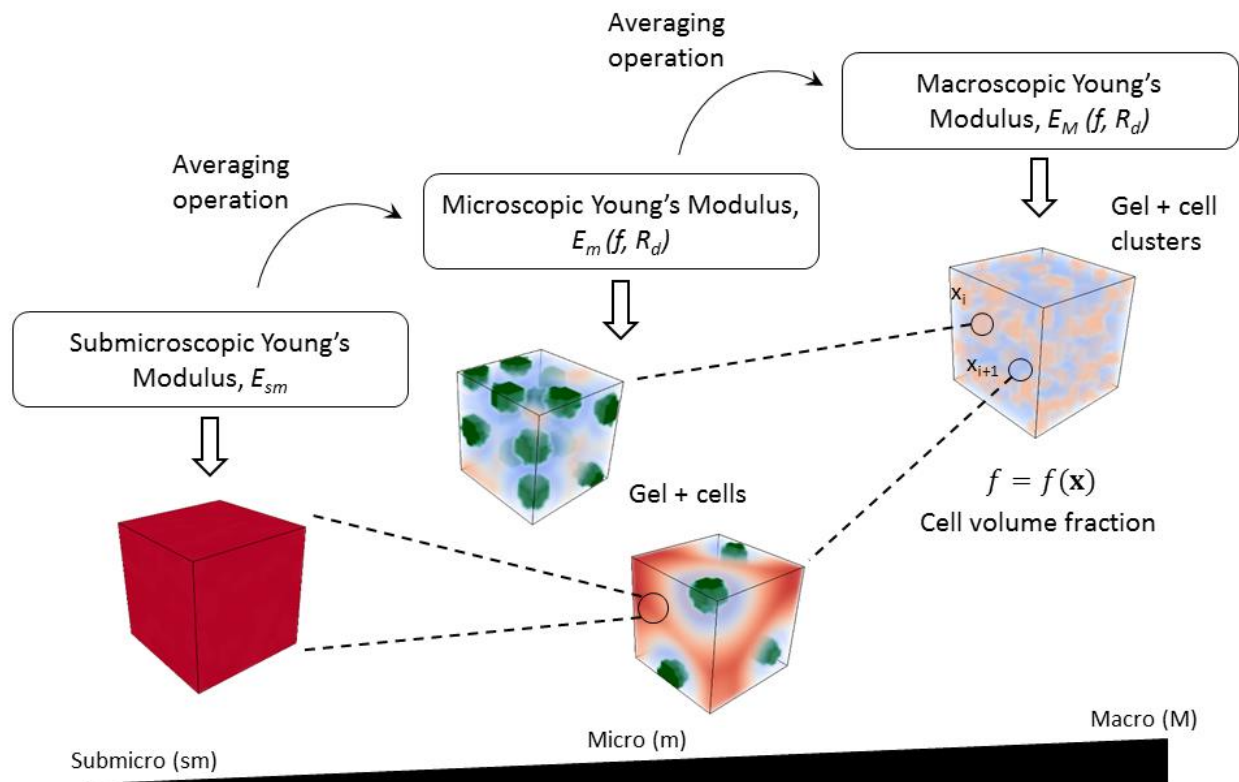


Figure 1. A hierarchical multiscale computational approach of a cell-laden hydrogel. The submicro-scale is represented by the hydrogel. The micro-scale is represented by a finite number of cells embedded in a hydrogel whose crosslink density varies according to its distance from the cell. The macro-scale is represented by a macroscopic hydrogel construct for which cell density is located at a macroscopic point  $\mathbf{x}_i$  and is represented by a heterogeneous function  $f(\mathbf{x})$ .

The model at the submicro-scale was used to describe hydrogel properties as a function of space and time resulting from hydrogel degradation. The polymer network undergoes hydrolytic degradation of ester bonds that flank the ends of each crosslink. Hydrogel degradation continues until it reaches reverse gelation, the point at which a sufficient number of crosslinks has been cleaved such that the hydrogel transitions from a solid polymer network to highly branched soluble polymer chains. The critical crosslink density,  $\rho_c$ , is defined as the crosslink density when the hydrogel reaches reverse gelation. The value of  $\rho_c$  was determined experimentally by degrading PEG-CAP hydrogels in chondrocyte growth medium, but in the

absence of cells. The crosslink density immediately prior to reverse gelation was determined from the experimental measurements of mass swelling ratio, density of the polymer and solvent, and the compressive modulus, which relate to crosslink density through Flory-Rehner and rubber elasticity theories<sup>31</sup> following methods described by Akalp *et al.*<sup>32</sup>

The mechanics of the hydrogel construct, which is comprised of the hydrogel and deposited ECM are dictated by two mechanisms. First, the degradation of the gel which is assumed to follow a pseudo first order kinetics such that

$$\begin{aligned}\rho_x(t) &= \rho_x^0 e^{-kt} \text{ when } \rho_x > \rho_c \\ \rho_x &= 0 \text{ when } \rho_x \leq \rho_c\end{aligned}\tag{Eq. 1}$$

where  $k$  is a pseudo-first order reaction rate constant for hydrolysis. When the hydrogel reaches reverse gelation ( $\rho_c$ ), the hydrogel is no longer crosslinked. The kinetic constant was determined experimentally by fitting degradation of PEG-CAP gels (as described above for determining  $\rho_c$ ) to an exponential decay function. Second, the diffusion of cell-secreted ECM molecules occurs at the cell membrane and is modeled with the classical reaction-diffusion equation

$$\partial c_m / \partial t = D_m \nabla^2 c_m - S_m\tag{Eq. 2}$$

where  $c_m$  is the unlinked fluid-like ECM concentration,  $D_m$  is the diffusion constant and  $S_m = k_m c_m$  is the rate of linkage of ECM molecules depending linearly on  $c_m$ . The constant  $k_m$  is calculated to fit the model prediction and experimental observations. The rate of production of ECM at the cell surface is described in terms of the flux,  $J_m$ , which is assumed to behave homeostatically as  $J_m = J_m^0 (1 - c_m / c_{m,0})$ , and applied as boundary condition for solving Eq. 2.



The deposition of solid-like linked ECM is given by  $\partial \bar{c} / \partial t = S_m$ , where  $\bar{c}$  is the concentration of linked ECM.

To model diffusion of newly synthesized and secreted ECM molecules, several assumptions were made. We only consider the main two cartilage ECM molecules, aggrecan and collagen type II, which make up the majority of the ECM of cartilage. Because these two ECM macromolecules are quite large (collagen type II has been reported to be 20,000 nm<sup>33</sup> and full length aggrecan has been reported to be up to 400 nm<sup>34</sup>) relative to the mesh size of the hydrogel (ca., 10-100 nm), their diffusion will be restricted to the space immediately surrounding the cell.<sup>17</sup> The diffusivity of the ECM molecules,  $D_m$ , vanishes to zero when the hydrogel is intact. Once the hydrogel crosslink density reaches the critical crosslinking density at reverse gelation (i.e.,  $\rho_x \leq \rho_c$ ), diffusion of ECM molecules occurs and is assumed to follow diffusion in the swelling solvent (i.e., culture medium, which is assumed to have similar properties to water) at 37°C estimated by the Stokes-Einstein relationship.

Solving the above linear equations with standard finite element techniques in the RVE, it is possible to evaluate the mechanical properties, represented by the Young's modulus,  $E$ , of any point in the micro-scale domain. The modulus is determined through the knowledge of the crosslink density and ECM concentration. At any point in the micro-scale domain, the modulus of the construct is comprised of one of the following: the polymer network, the ECM, or the encapsulated cells. The three components are assumed to be non-interpenetrating; that is, each point is made up of only one component. At small strains, the stress-strain relationship for each component can be generalized from rubber elasticity as

$$\sigma_i = \frac{E_i}{(1 + \nu)} \left( \epsilon_i + \frac{\nu}{(1 - 2\nu)} \text{tr}(\epsilon_i) \mathbf{1} \right) \quad (\text{Eq. 3})$$

$i = \text{Hydrogel (i.e., the polymer network); ECM (i.e., synthesized neotissue); or cells.}$

where  $\sigma_i$  is the stress tensor,  $\epsilon_i$  is the strain tensor,  $\mathbf{1}$  is the identity tensor,  $E_i$  is the Young's modulus,  $\nu$  is the Poisson's ratio,  $R$  is the gas constant, and  $T$  is the temperature. The Poisson's ratio for the polymer network was assumed to be close to 0.5 for elastic materials<sup>35</sup>. The Poisson's ratio for cartilage ECM is taken as 0.22<sup>36,37</sup>. The modulus of polymer network was estimated from rubber elasticity theory<sup>38</sup> assuming a linear elastic model described by

$$E_{gel} = 2(1 + \nu)\rho_x RTQ^{-1/3} \quad (\text{Eq. 4})$$

This relationship has been used to relate the mechanical properties to crosslink density for similar PEG hydrogels<sup>39</sup>. The chondrocytes are also treated as incompressible components with an elastic modulus of  $\sim 0.6$  kPa<sup>40</sup>. The modulus of ECM is assumed to be linearly proportional to the concentration of linked ECM molecules that form a solid 3D network,  $E_{ECM} \propto \bar{c}$ . We assume that the ECM and chondrocytes follow linear elastic behavior when under small strains and quasi-static loading.

At the microscale, RVEs are used to model local hydrogel degradation as well as synthesis, transport, and deposition of ECM molecules. The model is based on a multiphasic mixture formulation<sup>41</sup> that predicts the evolution of hydrogel mechanical properties as a function of hydrogel degradation and the diffusion and deposition of ECM. Using computational homogenization techniques<sup>42</sup> that consists of computing the overall compressive stress on the RVE resulting from a compressive strain of 10%, it is possible to calculate the effective Young's

modulus of the construct at different times during the hydrogel degradation - tissue growth process. The overall stress of the RVE derived from homogenization methods<sup>43,44</sup> is given as

$$\overline{\sigma_{ij}} = \frac{1}{\overline{V}} \int_{\overline{S}} \sigma_{ij} dV = \frac{1}{\overline{V}} \int_{\overline{S}} \frac{1}{2} (\tau_i x_j + \tau_j x_i) dS \quad (\text{Eq. 5})$$

where  $\overline{V}$  and  $\overline{S}$  are the volume and boundary surface of the RVE, and  $i$  and  $j$  can take values 1, 2, and 3 to represent different directions. The vector  $\mathbf{x}$  is the position vector and  $\boldsymbol{\tau}$  is the traction vector at the boundary surface of the RVE. The modulus of the RVE is given by

$$E = \frac{\overline{\sigma_{11}}}{\overline{\epsilon_{11}}} \quad (\text{Eq. 6})$$

where  $\overline{\sigma_{11}}$  and  $\overline{\epsilon_{11}}$  are the average uniaxial compressive stress and strain on the RVE in the direction of loading (direction 1). Boundary conditions are applied on the RVE to produce an overall compressive strain of  $\overline{\epsilon_{11}}$  in the direction of loading while it is unrestrained in the other two normal directions (directions 2 and 3).

To further examine the evolution of the construct at the macro-scale, we build a macroscopic RVE for which the cell density located at a macroscopic point  $\mathbf{x}$  is represented by a heterogeneous function  $f(\mathbf{x})$  *a priori* determined by a cluster analysis on microscopy images stained for live cells (see Hydrogel Construct Characterization section). This was done by counting the number of cells in a rectangular window, small enough to capture local variations in cell distribution, that is traversed over the entire image to obtain the spatial distribution of cell density  $f(\mathbf{x})$  in the construct. Based on this analysis from multiple images that are from different regions in a construct, the average cluster area and inter-cluster distance were estimated. Using

a simple model, the cell clusters and their distribution were characterized using the cluster fraction defined based on the average cluster area and number of clusters per unit area of the image, and the cell area fraction within the cluster ( $f_c$ ) and the background regions ( $f_b$ ). A cluster map was generated from each representative microscopy image of live cells. The 2D cluster maps were translated to 3D by adjusting the number of cell clusters, cluster cell population proportionally based on the size and shape of the cluster and thickness of the section in the microscopy image. Clusters were randomly placed within the matrix for each cell density, and the cluster shapes were randomly generated corresponding to the average cluster volume using a self-avoiding random walk algorithm<sup>45</sup>. Thus, the function  $f(\mathbf{x})$ , together with the mapping determined at the micro-scale, enables us to follow the time evolution of each point in the construct through the function  $E(\mathbf{x}, t) = E(f(\mathbf{x}), t)$ . As shown in Figure 1 (macro-level), a finite-element analysis is then performed to compute the macroscopic secant modulus of the construct using a computational homogenization procedure similar to that introduced at the micro-scale.

### **6.2.8 Statistics**

Mechanical and biochemical data are presented as the mean with standard deviation ( $n=3$ ) or in a dot plot. One-way ANOVA with cell density as the factor was performed for the initial construct characterization at Week 0. Two-way ANOVA was performed in Minitab 17 for modulus and biochemical data with cell density and culture time as the factors. Modeling data are presented as the mean with standard deviation from three simulations.

### **6.3 Results and Discussion**

The experimental system consisted of primary bovine chondrocytes that were encapsulated in a photoclickable and hydrolytically susceptible hydrogel based on PEG-CAP

chemistry. Three cell densities were investigated at 50 million (M), 100M, and 150M cells per mL of precursor solution prior to encapsulation, which are referred to herein as low, medium, and high cell density, respectively. The cell-laden hydrogels were characterized one-day post-encapsulation. Viable cells were evident, although some dead cells were also present (Figure 2A). All cell densities exhibited heterogeneous cell distribution with the higher cell densities presenting denser regions of cells. Cell number was determined based on DNA content and the number of cells that were encapsulated with each cell seeding density increased proportionally as expected (Figure 2B). The compressive modulus of the hydrogel in the absence of cells was determined to be 46 kPa, but was lower for the cell-laden hydrogels and decreased ( $p < 0.0001$ ) with increasing cell density (Figure 2C).

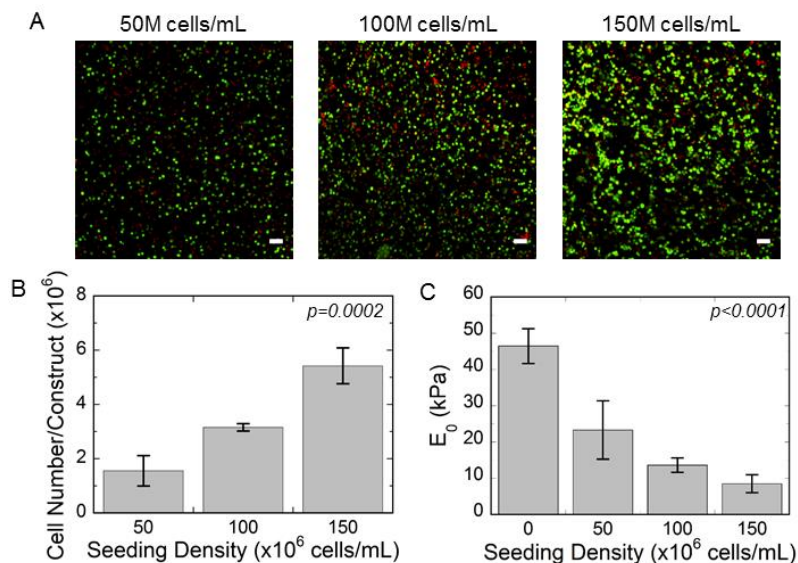


Figure 2. A) Representative confocal microscopy images of cell viability one-day after encapsulation in PEG-CAP hydrogels for seeding densities of 50, 100, and 150 million chondrocytes per volume (mL) of precursor solution. Live cells fluoresce green; dead cells fluoresce red; scale bar = 50  $\mu$ m. B) Cell number measured through DNA content one-day after encapsulation for seeding densities of 50, 100, and 150 million chondrocytes per volume (mL) of precursor solution. C) The initial compressive modulus of cell-laden PEG-CAP hydrogel one-day

after encapsulation for seeding densities of 0, 50, 100, and 150 million chondrocytes/mL of precursor solution.

The computational model was initially used to describe the hydrogel with encapsulated cells, but prior to hydrogel degradation and ECM deposition. The model parameters (Table 1) included the modulus of the hydrogel, which was assumed to be 46 kPa, as measured experimentally, and the modulus of a chondrocyte, which was assumed to be  $\sim 0.6$  kPa<sup>40</sup>. To capture the experimentally observed spatial heterogeneities in cell distribution, cell clusters were introduced into the computational model (parameters listed in Table 2). At the micro-scale, the volume fraction of cells ( $f$ ) can vary where regions have high cell concentration, which are referred to as clusters, and other regions have low cell concentration, which are referred to as background. Herein, cell clusters are defined by local regions of increased cell density  $f$  identified by a local cell density map from live cell microscopy images (Figure 3A). Once characterized, 3D simulations were carried out where the clusters were randomly placed in 3D. Representative simulations show cluster size and distribution for each cell density case (Figure 3B). In addition, representative simulations showing the cellular distribution in the background and in the cluster regions are also shown. At the macroscopic scale, regions of high cell density (i.e., a cell cluster) and similarly regions of low cell density (i.e., background) are captured in the model. With increasing cell concentration, the clusters were denser (i.e., high local cell density) though the proximity of clusters was not affected by cell seeding density. Accounting for spatial heterogeneities in cell distribution and the presence of cells, the computational model predicted the macroscopic compressive modulus of the cell-laden hydrogels with increasing cell density (Figure 3C). A decrease ( $p < 0.0001$ ) in the modulus with increasing cell concentration was observed, but not to the same extent that was observed experimentally. For example, in the high

cell density condition, the model predicted a ~5% drop compared to ~80% drop that was observed experimentally.

Table 1. Model Parameters

Parameter	Definition	Value	Units	Source
$E_0$	Initial hydrogel modulus	46.5	kPa	Experiment
$E_{cell}$	Cell modulus	0.6	kPa	Literature <sup>40</sup>
$\beta$	Network connectivity	0.096	--	Experiment
$k$	Degradation rate constant	0.066	day <sup>-1</sup>	Experiment
$r_{cell}$	Cell radius	5	$\mu\text{m}$	Literature <sup>16</sup>
$c_{m,0}$	ECM homeostatic concentration*	$1.5 \times 10^{-3}$	M	Experiment
$r_m$	Hydrodynamic radius of ECM molecules	400-20,000	nm	Literature <sup>34,46</sup>
$D_m^\infty$	Diffusion of ECM molecules in pure solvent	$1.7 \times 10^{-8}$	mm <sup>2</sup> /s	Stokes-Einstein
$J_m^0$	ECM production rate	$5.2 \times 10^{-17}$	moles/cell/day	Experiment

Table 2. Cluster and Background Parameters

Simulation	Total volume fraction of cells ( $f$ )	Cluster ( $f_c$ )	Background ( $f_b$ )
<b>50M</b>	0.014	0.02	0.012
<b>100M</b>	0.025	0.05	0.022
<b>150M</b>	0.038	0.077	0.034



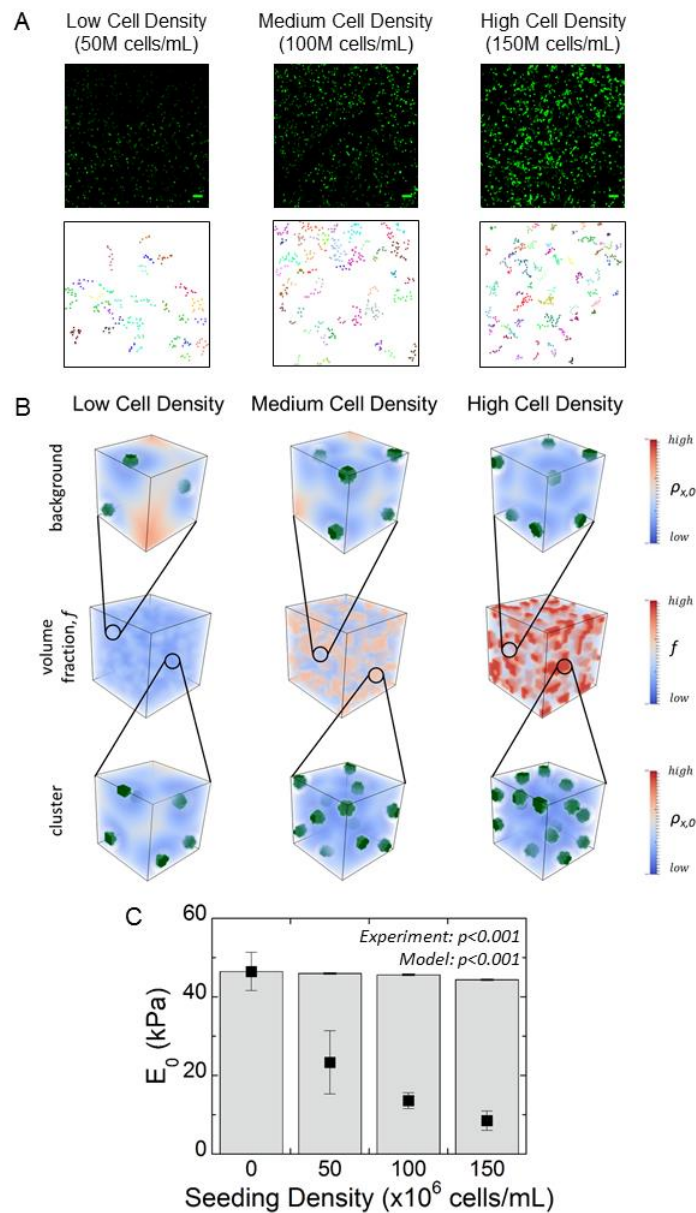


Figure 3. A) Top Row: Representative confocal microscopy images of only live cells (green) in hydrogels with encapsulated chondrocytes at low (50M cells/mL), medium (100M cells/mL) and high (150M cells/mL) cell seeding densities, which were used in the cluster analysis. The microscopy images are the same images in Figure 2A, but with only live cells depicted. Scale bar = 50  $\mu\text{m}$ . Bottom Row: 2D simulation results showing cluster mapping for each of the three different cell densities. B) Top/bottom rows: Representative volume elements for microscale background and clustered cell densities, respectively, for low, medium, and high cell seeding densities showing the crosslink density gradient. Cells are shown in green. Middle row: Macroscale constructs with a heterogeneous distribution of cell volume fraction. C) Modeling

results (gray bars) of the initial macroscopic compressive modulus ( $E_0$ ) assuming the hydrogel constructs act as a composite material with the presence of cell clusters and the experimentally determined initial compressive modulus (black squares). Errors bars represent standard deviation for the model (n=5) and experiments (n=3).

To investigate heterogeneities that result from a spatial variation in crosslink density surrounding the encapsulated cells, we introduce into the model the parameter,  $R_d$  (Figure 4A).  $R_d$  is defined as the distance between the outer surface of the cell membrane, where crosslink density is zero, and the location at which the crosslink density equals 99% of the initial crosslink density (i.e., that of the initial hydrogel in the absence of cells). For simplicity, we report  $R_d/R_c$  where  $R_c$  is the radius of a cell. In other words, a value of  $R_d/R_c = 5$  indicates a distance that is 5x the cell radius or 25  $\mu\text{m}$ . We adopted a simple empirical relationship to describe crosslink density as a function of distance ( $x$ ) from the cell surface:

$$\rho_x(x) = \rho_x^0 \left( 1 - \exp\left(-k \frac{x}{R_d}\right) \right) \text{ with } k = \ln(0.01) \quad (\text{Eq. 7})$$

To illustrate the effect of  $R_d$  on the spatial variation of hydrogel crosslink density using our model, two macroscopic volume fraction of cells were investigated,  $f = 0.05$  and  $f = 0.20$ , and over a range of  $R_d/R_c$  values from 0 to 27. The normalized crosslink density (i.e.,  $\rho_x/\rho_{x,0}$ ) was determined as a function of distance from one cell to another (denoted by  $d_{cell}$ ) (Figure 4B). With increasing cell volume fraction,  $d_{cell}$  decreases. Several key observations can be made. For an  $R_d$  of zero, the normalized crosslink density is uniform and at a value of one across the entire distance between two cells, regardless of the volume fraction of cells. With increasing  $R_d$ , the crosslink density varies across the distance between two cells. When  $R_d$  of two cells overlaps, the maximum crosslink density is lower than the initial crosslink density of bulk hydrogel. With a higher volume fraction of cells where cells are closer together, the maximum crosslink density

between two cells is even lower for the same  $R_d$  due a more pronounced overlap in  $R_d$ . Accounting for spatial heterogeneities in cell distribution and the presence of cells (as described above), the macroscopic compressive modulus of the hydrogel was determined for varying values of  $R_d$  (Figure 4C). The compressive modulus decreased with increasing  $R_d$  and decreased even to a greater extent for higher values of  $f$ . Using the model with both cell clusters and the presence of an  $R_d$ , we sought to estimate a value of  $R_d$  for the experimental PEG-CAP hydrogel system. Since the same hydrogel formulation, encapsulation conditions, and cell source were similar in all three cell density conditions, the value of  $R_d$  is expected to be similar regardless of cell concentration. The cell cluster size and distribution determined above for each cell density was used. Simulations were run with varying values of  $R_d$ . A plot of modulus versus  $R_d$  was overlaid with the experimental modulus (Figure 4D). Each simulation was run with a randomly generated cluster distribution resulting in variations between each simulation. A value of 27 was estimated for  $R_d/R_c$  or an  $R_d$  of 135  $\mu\text{m}$  for the constructs. The experimental modulus and the computationally determined modulus with an  $R_d/R_c$  of 27 are also shown in Figure 4E.

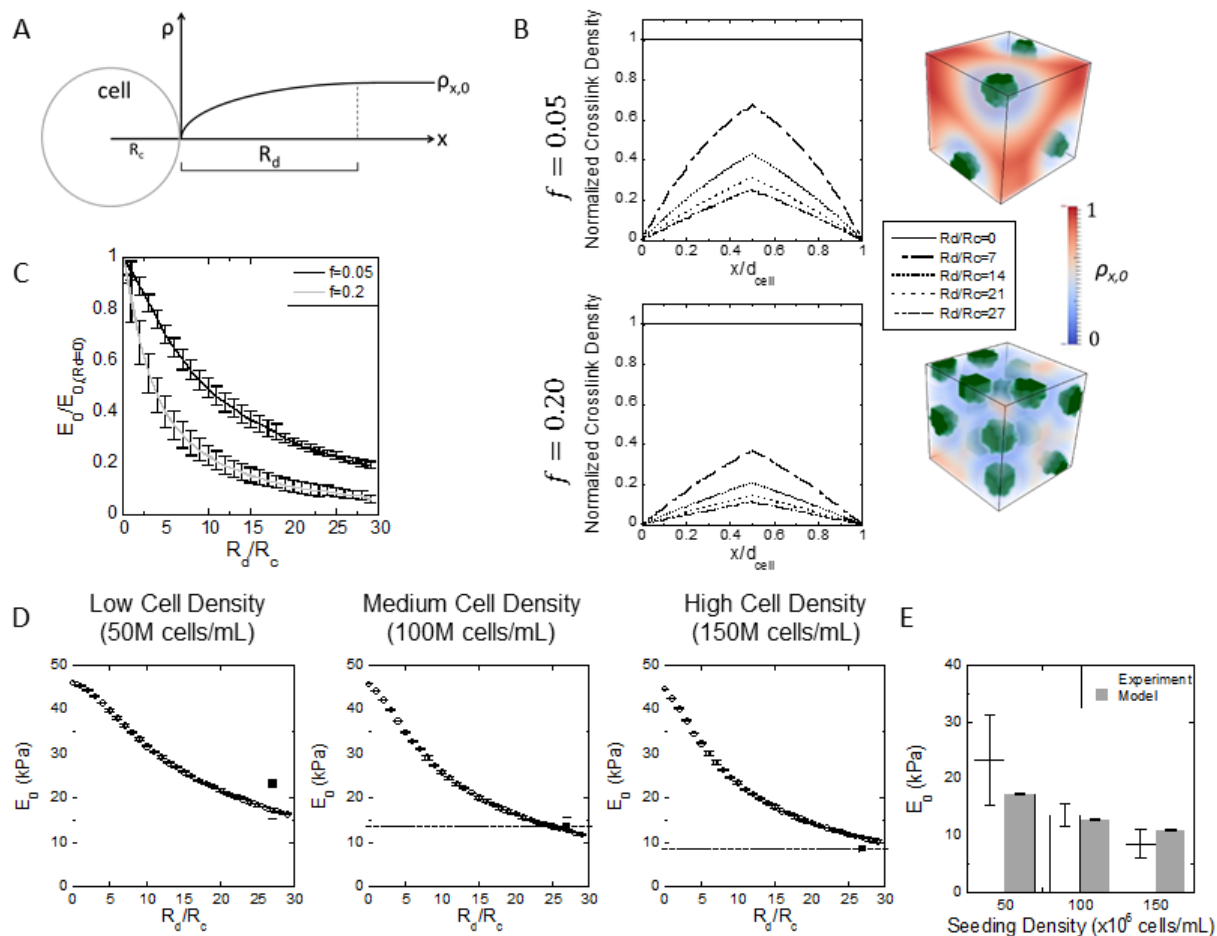


Figure 4. A) A schematic of  $R_d$ . The radius  $R_d$  is defined as the zone where the hydrogel crosslink density is reduced due to the cell's interaction with radicals. As such,  $R_d$  controls the crosslink density at a distance  $x$  from the cell surface. B) The effect of  $R_d$  on the spatial variation in hydrogel crosslink density between two cells. Two cases are shown for a low local cell volume fraction ( $f=0.05$ ) and a high local cell volume fraction ( $f=0.20$ ) for varying values of  $R_d$ . Results from 3D simulations for  $f=0.05$  (top) and  $f=0.20$  (bottom) are shown for the two cases for  $R_d/R_c = 7$  where cells (green) are embedded within a hydrogel. The spatial variation in crosslink density ( $\rho_x$ ) is shown decreasing from red (equivalent to the bulk crosslink density) to blue (equivalent to the reverse gelation point). The distance between cells ( $d_{\text{cell}}$ ) varies based on the volume fraction and was  $3.43 \mu\text{m}$  and  $1.42 \mu\text{m}$  for  $f=0.05$  and  $f=0.20$ , respectively. C) Simulation results are shown for the macroscopic compressive modulus for the two cases of cell volume fraction as a function of  $R_d/R_c$ . The modulus is normalized to the modulus at  $R_d=0$ . The black line represents  $f=0.05$  and the gray line represents  $f=0.20$ . Simulation data are presented as mean with standard deviation for  $n=3$ . D) Simulations for the initial compressive modulus of low, medium, and high cell seeding density are shown as a function of  $R_d/R_c$ . An  $R_d/R_c$  of 27 was selected based on minimizing the error between simulations and experiments (black squares). Data are presented as mean with standard deviation ( $n=3$ ). E) The initial compressive modulus for each seeding density for both

the experiments (white bars) and simulations with  $R_d/R_c=27$  (gray bars). Experimental and modeling data are presented as mean with standard deviation ( $n=3$ ).

Cell-laden hydrogels for each cell density were cultured up to 12 weeks and assessed for compressive modulus, cellular content, and biochemical (Figure 5). The compressive modulus varied ( $p=0.001$ ) with time and was moderately affected ( $p=0.1$ ) by cell density. There was interaction ( $p=0.01$ ) between time and cell density. For example, the modulus for the low cell density condition dropped ( $p=0.14$ ) slightly at week 4, but then increased ( $p=0.007$ ) by week 12. On the contrary for the high cell density case, the modulus increased ( $p=0.01$ ) with time. DNA content did not vary ( $p=0.86$ ) with time, but was affected ( $p<0.001$ ) by cell density, as expected. The sulfated glycosaminoglycan (sGAG) content increased ( $p<0.001$ ) with time and was moderately affected ( $p=0.08$ ) by cell density. By week 12, the high cell density condition had the highest sGAG content. When normalized to DNA, sGAG was affected ( $p=0.053$ ) by cell density and affected ( $p<0.001$ ) by time with the highest sGAG content in the high cell density condition at week 12. Total collagen content increased ( $p<0.001$ ) with time and was moderately affected ( $p=0.08$ ) by cell density. By week 12, the high cell density condition had the highest total content. When normalized to DNA, cell density was no longer a factor in total collagen content. In general, there was minimal interaction between cell density and time for sGAG and collagen and when normalized to DNA.

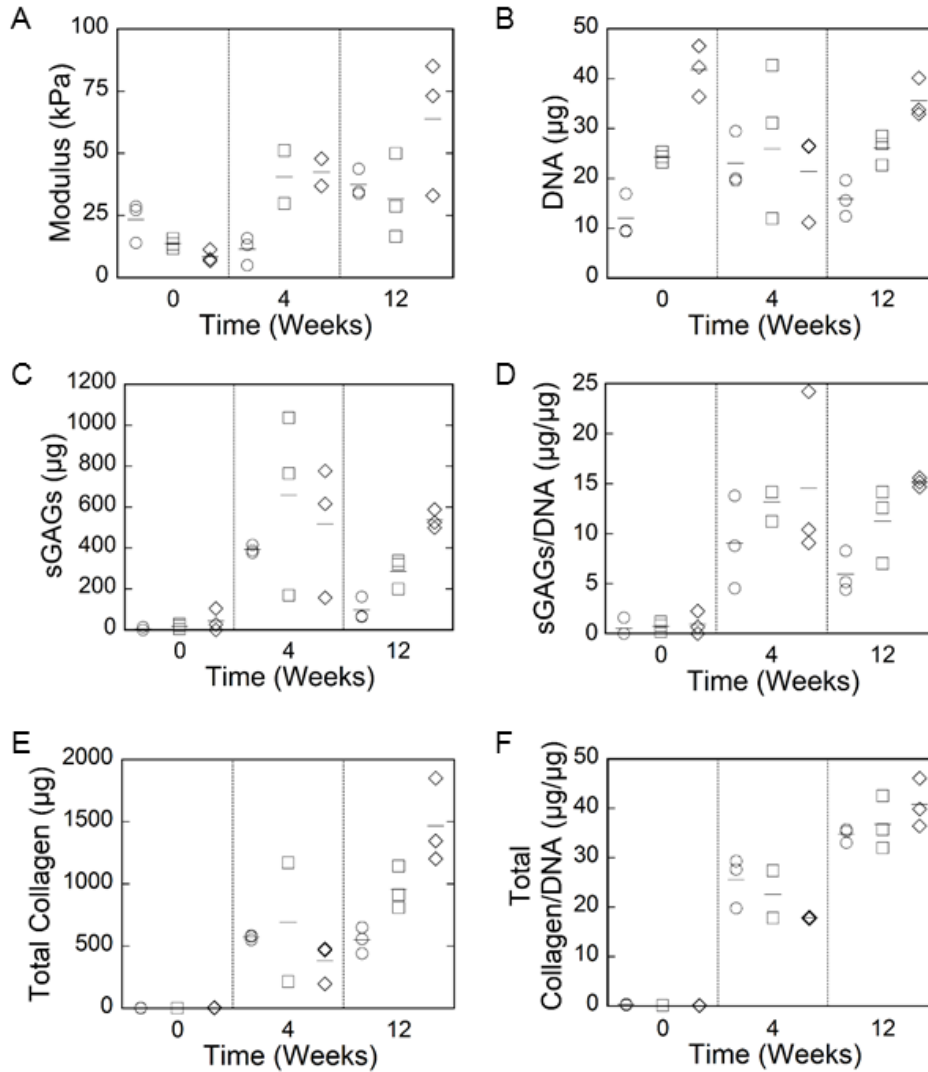


Figure 5. Characterization of the cell-laden hydrogel constructs as a function of culture time for A) compressive modulus, B) DNA content, C) sulfated glycosaminoglycan (sGAG) content per construct, D) sGAG per DNA, E) total collagen content per construct, and F) total collagen content per DNA for low (50M cells/mL) (o), medium (100M cells/mL) (□), and high (150M cells/mL) (◇) density. Dot plots are shown for individual repeats and the horizontal line represents the mean.

The quality and spatial organization of the newly deposited ECM was assessed by immunohistochemistry for aggrecan and collagen II (Figure 6), the two major ECM molecules that make-up cartilage. Aggrecan and collagen II were detected as early as one-day post-encapsulation (referred to as week 0) and both ECM molecules were present throughout the 12-

week culture period for all hydrogel conditions regardless of cell density. In all cell density conditions, the ECM was localized to the pericellular space at day 1 (week 0). In the low cell density hydrogel (Figure 6A) at week 4, the spatial distribution of ECM differed between constructs showing either ECM restricted to the pericellular space or showing interconnected ECM between adjacent cells. By week 12, an ECM had formed across the entire construct. In the medium cell density (Figure 6B) and high cell density (Figure 6C) conditions, the ECM by week 4 was interconnected and present throughout all constructs. Similar results were observed at week 12.

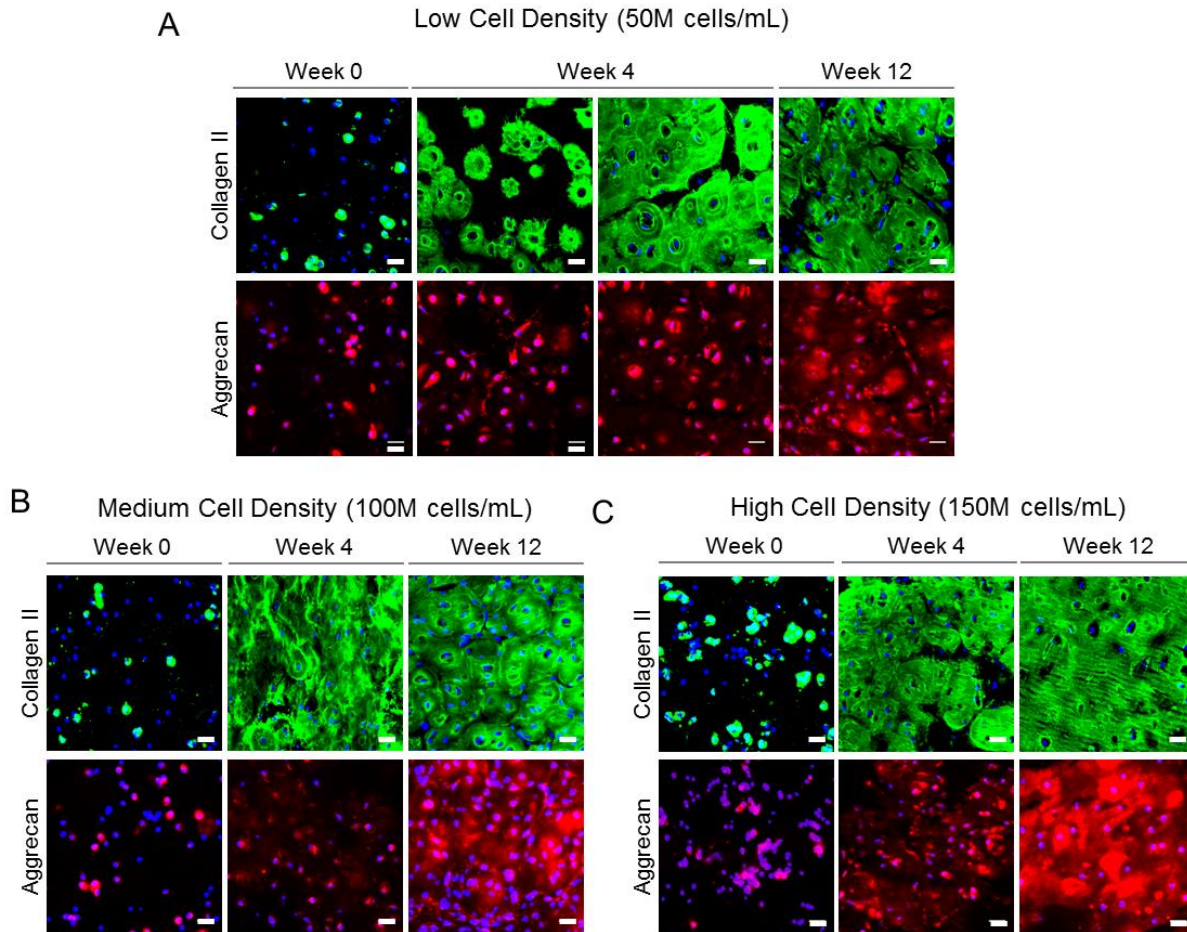


Figure 6. Representative confocal microscopy images of immunohistological sections stained for collagen II and aggrecan after 1 day (i.e., week 0), week 4 or week 12 of culture for hydrogel with low (A), medium (B) and high (C) cell densities. Nuclei are stained with DAPI (blue). Scale bar = 20  $\mu\text{m}$ .

The computational model was then used to describe the crosslink density, ECM accumulation, in the hydrogel and compressive modulus as a function of culture time up to 30 days (Figure 7), at which point the hydrogel had degraded. The model used the cluster analysis described above for each of the three cell densities and a value of 27 for  $R_d/R_c$ . The remaining model parameters are given in Table 1. The ECM homeostatic concentration ( $c_{m,0}$ ) was determined from the ECM (collagen and GAG) concentration of fresh juvenile bovine cartilage explants. The ECM production rate per cell ( $J_m^0$ ) was calculated from the total ECM synthesis



produced over the first four weeks divided by 28 days and the total number of cells at four weeks.  $J_m^0$  was assumed to be constant. The simulation results are shown in Figure 7. The average crosslink density decreased with time concomitant with an increase in average ECM accumulation in the hydrogel for all cell densities (Figure 7A). The high cell density condition, which started with the lowest initial average crosslink density, led to the greatest amount of ECM accumulation within the hydrogel by day 30. Snap shots of crosslink density and ECM accumulation from 3D simulations are shown at day 0, 15, and 30 (Figure 7B). The low cell density condition had more diffuse and less dense regions of accumulated ECM. On the contrary, regions of dense ECM are observed in the medium cell density condition and was even more pronounced in the high cell density condition. The compressive modulus of the construct, which combines the modulus of the hydrogel and the modulus of the ECM, as a function of time was also determined in the simulations (Figure 7C). The modulus decreased for all conditions, which corresponded to a decrease in the crosslinking density with minimal deposited ECM. However, the modulus begins to increase as the ECM forms its own interconnected matrix. This transition occurred the earliest in the high cell density condition and took the longest to occur in the low cell density condition. The experimentally measured modulus corresponded to the simulation results at day 28.

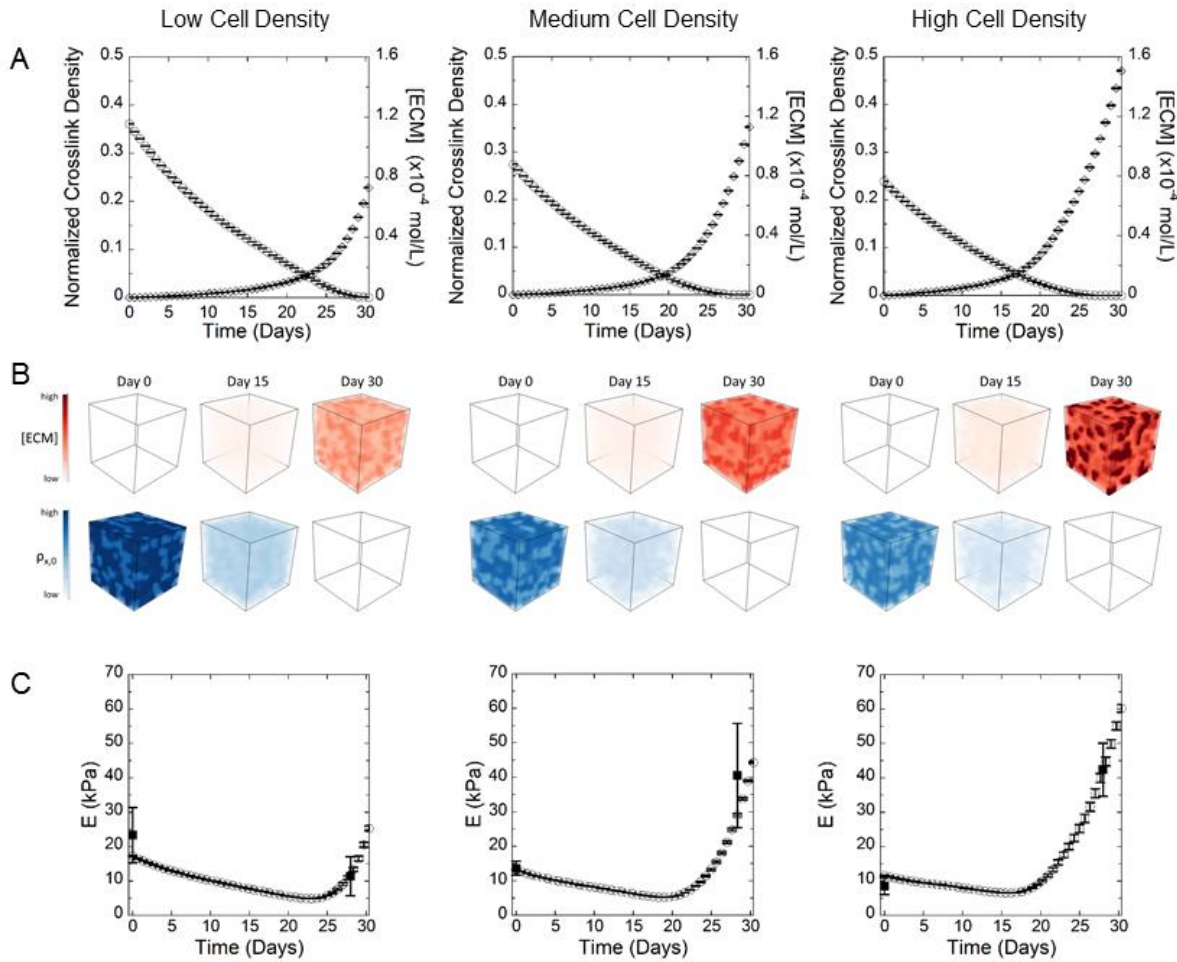


Figure 7. Simulation results for low, medium, and high cell densities showing A) normalized crosslink density (o) and ECM concentration ( $\diamond$ ), where crosslink density is normalized to the crosslink density of the acellular construct, and B) representative volume elements depicting the spatial distribution of ECM and crosslink density at 0, 15, and 30 days for low, medium, and high cell densities. C) Evolution of  $E$ , the compressive modulus, (o) over time (experimental data from week 0 and 4 shown as solid squares,  $\blacksquare$ ). Error bars represent standard deviation from 3 different simulations or experimental replicates ( $n=3$ ).

This study describes local heterogeneities within a cell-laden hydrogel that arise from two phenomena: (a) clustering of cells and (b) spatial variations in the hydrogel crosslink density. Using a combined experimental and theoretical approach, the local heterogeneities were defined along with spatiotemporal mapping of both crosslink density and ECM evolution. With increasing cell density within the hydrogel, the local heterogeneities were further magnified. Results from

this work demonstrate that with increasing local heterogeneities, the amount of deposited ECM is higher concomitant with improved ECM evolution and an overall higher modulus. Taken together, our findings point towards heterogeneities as being important to achieve macroscopic ECM evolution in hydrolytically degradable PEG hydrogels.

When cells were encapsulated in the PEG-CAP hydrogels, a stark decrease in the compressive modulus was observed, which was more pronounced with higher cell concentrations at the time of encapsulation. The volume fraction of cells, which are softer than the hydrogel, ranged from 0.014-0.038 in the hydrogel and was not sufficient to explain the large drop in modulus. This observation, thus, led to the introduction of heterogeneities into our previously developed computational model in an effort to explain the results. The presence of cell clusters was evident in the hydrogels through confocal microscopy images. Clustering of cells is attributed to cell aggregation that occurred during the processing of the cells prior to encapsulation. Chondrocytes are known to aggregate<sup>47</sup>, and, although methods were employed to minimize aggregates, the cells were not perfectly dispersed within the hydrogel immediately after encapsulation. Accounting for cell clusters within the model confirmed a decrease in modulus with increasing cell concentration, but not to the same degree that was observed experimentally. Given the prior evidence that chondrocytes interact with propagating radicals during encapsulation<sup>23</sup>, chondrocytes may act as chain transfer agents and inhibit polymerization. Since radicals are short lived, this termination would be restricted to regions nearby cells. With the introduction of  $R_d$  combined with the presence of cell clusters, the model was able to explain the experimentally observed drop in modulus. In regions with cell clusters where cells are in close proximity to one another, their  $R_d$ 's overlap such that the overall

crosslinking density in these regions is lower. With increasing cell concentration, the distance between cells within the background (i.e., not in clusters) and the distance between clusters becomes smaller and can begin to approach  $R_d$ , such that even in the bulk the overall crosslink density may be lower. Thus, the increasing number and size of cell clusters coupled with a high value of  $R_d$  is able to explain the reduction in the overall compressive modulus with increasing cell density.

The value for  $R_d/R_c$  was estimated to be  $\sim 27$  or equivalent to and  $R_d$  of  $\sim 135 \mu\text{m}$ . There are several factors that may impact the magnitude of the  $R_d$  region, including diffusion and termination of radicals and the hydrophilic nature of the monomers. Propagating radicals can be stabilized by the surrounding chemistry, which increases their lifetime<sup>48</sup> and thus will increase the probability of interacting with cells. The addition of hydrophobic caprolactone units to the multi-arm PEG creates an amphiphilic molecule where block copolymers of PEG and caprolactone groups have been shown to form micelles in aqueous solvents<sup>49,50</sup>. Thus, it is reasonable to postulate that as cells terminate radicals, the effects on propagation may extend farther into the polymerizing solution due to the amphiphilic nature of the PEG-CAP chemistry. In support of this postulation, several studies have reported a drop in modulus after encapsulating chondrocytes at a cell seeding density of 50 M in hydrogels formed by radical mediated polymerization. For example, the compressive modulus dropped by 10% in a PEG hydrogel formed from 8-arm PEG-NB with peptide sensitive crosslinks<sup>51</sup>, by 18% in PEG hydrogels formed from PEG dimethacrylate monomers<sup>16</sup>, and by 42% in a hydrogel formed by co-polymerizing poly(lactic acid)-*b*-PEG-*b*-poly(lactic acid) dimethacrylate with acrylated poly(vinyl alcohol)<sup>52</sup>. The latter chemistry, which experienced the greatest drop in modulus, is the least hydrophilic. Moreover, in the study with

the PEG hydrogel containing peptide crosslinkers, the  $R_d/R_c$  was estimated to be three or an  $R_d$  of  $\sim 15 \mu\text{m}^{54}$ . Thus, the hydrophilic nature of the monomers appear to have a significant effect on the value of  $R_d$ .

The presence of an  $R_d$  and clusters is able to explain the observed ECM growth within the different hydrolytically degradable hydrogels. In regions of lower crosslink density (i.e., in the clusters), the hydrogel will reach reverse gelation much faster within the cell clusters when compared to regions where the cells are more dispersed and farther apart (i.e., in the background). This phenomenon enables ECM elaboration and ECM connectivity between adjacent cells in the clusters while the background regions maintain a crosslinked hydrogel. Thus, the transition from hydrogel to ECM depends on the number of cells, clusters, and cluster size. Indeed, our results show that in the low cell density condition, which has smaller cell clusters, the overall modulus drops by  $\sim 50\%$  at four weeks. This observation is consistent with the idea that as the hydrogel degrades, but with limited ECM interconnectivity, the overall modulus must decrease. On the other hand, in the medium and high cell density conditions, the overall modulus increased by  $\sim 3$ -fold at four weeks. This observation is consistent with the idea that although the hydrogel is degrading, there is substantial macroscopic ECM that forms within the large cluster regions, which contributes to the overall modulus.

The model was able to capture the overall evolution of ECM growth and construct modulus as a function of time for the PEG-CAP hydrogels with varying initial cell concentrations. Since the model describes hydrogel degradation that is coupled to ECM molecule transport and deposition, but does not describe maturation of the ECM alone, the model was limited to the timescale of hydrogel degradation ( $\sim 30$  days). Results from the model provide insights into the

spatiotemporal behavior of the construct as it transitions from hydrogel to ECM. Experimental limitations prevent the real time continuous analysis of the modulus evolution. The model provides insights into the drop in modulus that occurs as the constructs degrade initially prior to significant ECM deposition and elaboration. This effect was most pronounced in the low cell density condition, which reported a ~70% modulus drop in the first ~24 days prior to recovery of the modulus by 30 days. The medium and high cell density cases reached a minimum modulus at earlier times and exhibited a greater recovery in the first 30 days. The simulation results support the idea that higher cell seeding densities lead to increased ECM connectivity through the following mechanisms. Encapsulation at high cell densities lead to an overall lower *bulk* crosslink density as single cells in the background and cells within the clusters are closer together and this leads to overlapping  $R_d$ 's. This effect causes the hydrogel to reach reverse gelation faster especially in the clusters, which creates space for ECM transport and deposition within the clusters. As clusters are closer together, interconnectivity of the ECM between clusters occurs leading to an overall ECM interconnectivity within the hydrogel.

Long-term by twelve weeks, the engineered neo-cartilage tissue was largely similar across all three conditions. The low cell density condition by week 12 reached a modulus that was similar to the medium and high cell density conditions at week 4, where the latter two conditions appeared to maintain their mechanical properties after week 4. The high cell density condition resulted in the greatest total amount of deposited ECM per construct and on a per cell basis. These findings suggest that differences in the spatiotemporal degradation of the hydrogel due the local heterogeneities have profound effects on neotissue growth. Herein, our findings indicate that starting with a lower cell seeding density, which corresponds to a higher initial

modulus, results in less ECM deposition, a considerable drop in mechanical properties, and a slow transition to an interconnected neotissue. Alternatively, starting with a high cell seeding density, which corresponds to a lower initial compressive modulus, results in a more rapid transition to intact neo-cartilage. Although the modulus in the high cell density condition was relatively low at 8 kPa, hydrogels can be readily designed with hydrolytically susceptible bonds that have a higher hydrolysis kinetic constant than the ester bonds used in this study. Thus, a hydrogel with a higher initial crosslinking density and hence modulus can be designed to achieve similar degradation rates to those investigated in this work.

Overall, this study highlights the importance of heterogeneities within a cell-laden hydrolytically labile hydrogel. On the contrary, homogeneous networks, such as those formed from orthogonal click reactions<sup>53</sup> have been promoted for their consistent properties throughout the polymer network<sup>20</sup>. This aspect is important when studying the effects of local cues, such as matrix stiffness, on cells encapsulated in 3D hydrogels. However, in the context of tissue engineering, our results strongly point to the need to introduce local heterogeneities into the network structure to improve matrix connectivity and promote a seamless transition from hydrogel to neotissue.

There are several limitations in this study that are important to note. We assumed an average value of  $R_d$  based on the experimentally determined decrease in bulk compressive modulus when increasing the cell seeding density. However, chondrocytes were isolated from full thickness cartilage and are a heterogeneous population of cells that may have different cellular responses<sup>54</sup>, leading to heterogeneous evolutions in  $R_d$ . The model did not account for any changes in the cell population that arise due to cell proliferation and cell death. However,

the cell number as measured experimentally through DNA content did not change with culture time and thus may not have been a significant factor for the model. This study is limited to one biological donor and thus variations in  $R_d$  and cell clustering may vary from donor to donor and requires additional studies.

## **6.4 Conclusions**

Using a combined experimental and computational approach, this study introduces the importance of local heterogeneities in achieving a seamless transition from hydrogel to neotissue in cell-laden hydrolytically labile hydrogels formed from radical mediated polymerizations. Two local heterogeneities were identified. The first is the presence of cell clusters. The second is the local inhibition of the polymerization in the vicinity of the cell creating a region with reduced crosslinking. When combined, the two local heterogeneities create regions within the cell clusters that have a low crosslink density and thus degrade the fastest and create space for ECM transport and deposition. With increasing cell concentration within the hydrogel the local heterogeneities are magnified and this improves the overall outcome with enhanced mechanical properties and overall higher amounts of ECM.

## **6.5 Acknowledgments**

Research reported in this publication was supported by the National Institute of Arthritis and Musculoskeletal and Skin Diseases of the National Institutes of Health under Award Number 1R01AR065441. The authors acknowledge the National Institute of Health (NIH) Institutional Pharmaceutical Training fellowship and the Graduate Assistance in Areas of National Need (GAANN) Biomaterials from the Department of Education to SC. The technical assistance of Margaret Schneider, Shankar Lalitha Sridhar, and Gaspard de Roucy is greatly appreciated.



## 6.6 References

1. Nicodemus, G. D. & Bryant, S. J. Cell Encapsulation in Biodegradable Hydrogels for Tissue Engineering Applications. *Tissue Eng. Part B Rev.* **14**, 149–165 (2008).
2. Metters, A. T., Bowman, C. N. & Anseth, K. S. A Statistical Kinetic Model for the Bulk Degradation of PLA-b-PEG-b-PLA Hydrogel Networks. *J. Phys. Chem. B* **104**, 7043–7049 (2000).
3. Martens, P., Metters, A. T., Anseth, K. S. & Bowman, C. N. A Generalized Bulk-Degradation Model for Hydrogel Networks Formed from Multivinyl Cross-linking Molecules. *J. Phys. Chem. B* **105**, 5131–5138 (2001).
4. Neumann, A. J., Quinn, T. & Bryant, S. J. Nondestructive evaluation of a new hydrolytically degradable and photo-clickable PEG hydrogel for cartilage tissue engineering. *Acta Biomater.* **39**, 1–11 (2016).
5. Dadsetan, M., Szatkowski, J. P., Yaszemski, M. J. & Lu, L. Characterization of Photo-Cross-Linked Oligo[poly(ethylene glycol) fumarate] Hydrogels for Cartilage Tissue Engineering. *Biomacromolecules* **8**, 1702–1709 (2007).
6. Bryant, S. J. & Anseth, K. S. Controlling the spatial distribution of ECM components in degradable PEG hydrogels for tissue engineering cartilage. *J. Biomed. Mater. Res. A* **64A**, 70–79 (2003).
7. Park, H., Temenoff, J. S., Holland, T. A., Tabata, Y. & Mikos, A. G. Delivery of TGF- $\beta$ 1 and chondrocytes via injectable, biodegradable hydrogels for cartilage tissue engineering applications. *Biomaterials* **26**, 7095–7103 (2005).
8. Wang, Y. *et al.* In vitro study on the degradation of lithium-doped hydroxyapatite for bone tissue engineering scaffold. *Mater. Sci. Eng. C* **66**, 185–192 (2016).
9. Andriano, K. P., Tabata, Y., Ikada, Y. & Heller, J. In vitro and in vivo comparison of bulk and surface hydrolysis in absorbable polymer scaffolds for tissue engineering. *J. Biomed. Mater. Res.* **48**, 602–612 (1999).
10. Lam, C. X. F., Hutmacher, D. W., Schantz, J.-T., Woodruff, M. A. & Teoh, S. H. Evaluation of polycaprolactone scaffold degradation for 6 months in vitro and in vivo. *J. Biomed. Mater. Res. A* **90A**, 906–919 (2009).
11. Lu, H. H. *et al.* Anterior cruciate ligament regeneration using braided biodegradable scaffolds: in vitro optimization studies. *Biomaterials* **26**, 4805–4816 (2005).
12. Cooper, J. A., Lu, H. H., Ko, F. K., Freeman, J. W. & Laurencin, C. T. Fiber-based tissue-engineered scaffold for ligament replacement: design considerations and in vitro evaluation. *Biomaterials* **26**, 1523–1532 (2005).
13. Mahoney, M. J. & Anseth, K. S. Three-dimensional growth and function of neural tissue in degradable polyethylene glycol hydrogels. *Biomaterials* **27**, 2265–2274 (2006).

14. Kim, B.-S. & Mooney, D. J. Engineering smooth muscle tissue with a predefined structure. *J. Biomed. Mater. Res.* **41**, 322–332 (1998).
15. Fidkowski, C. *et al.* Endothelialized Microvasculature Based on a Biodegradable Elastomer. *Tissue Eng.* **11**, 302–309 (2005).
16. Bryant, S. J. & Anseth, K. S. Hydrogel properties influence ECM production by chondrocytes photoencapsulated in poly(ethylene glycol) hydrogels. *J. Biomed. Mater. Res.* **59**, 63–72 (2002).
17. Nicodemus, G. D., Skaalure, S. C. & Bryant, S. J. Gel structure has an impact on pericellular and extracellular matrix deposition, which subsequently alters metabolic activities in chondrocyte-laden PEG hydrogels. *Acta Biomater.* **7**, 492–504 (2011).
18. Metters, A. T., Bowman, C. N. & Anseth, K. S. Verification of scaling laws for degrading PLA-b-PEG-b-PLA hydrogels. *AIChE J.* **47**, 1432–1437 (2001).
19. Metters, A. T., Anseth, K. S. & Bowman, C. N. A Statistical Kinetic Model for the Bulk Degradation of PLA-b-PEG-b-PLA Hydrogel Networks: Incorporating Network Non-Idealities. *J. Phys. Chem. B* **105**, 8069–8076 (2001).
20. Tibbitt, M. W., Kloxin, A. M., Sawicki, L. A. & Anseth, K. S. Mechanical Properties and Degradation of Chain and Step-Polymerized Photodegradable Hydrogels. *Macromolecules* **46**, 2785–2792 (2013).
21. Bryant, S. J., Bender, R. J., Durand, K. L. & Anseth, K. S. Encapsulating chondrocytes in degrading PEG hydrogels with high modulus: Engineering gel structural changes to facilitate cartilaginous tissue production. *Biotechnol. Bioeng.* **86**, 747–755 (2004).
22. Bryant, S. J., Anseth, K. S., Lee, D. A. & Bader, D. L. Crosslinking density influences the morphology of chondrocytes photoencapsulated in PEG hydrogels during the application of compressive strain. *J. Orthop. Res.* **22**, 1143–1149 (2004).
23. Farnsworth, N., Bensard, C. & Bryant, S. J. The role of the PCM in reducing oxidative stress induced by radical initiated photoencapsulation of chondrocytes in poly(ethylene glycol) hydrogels. *Osteoarthritis Cartilage* **20**, 1326–1335 (2012).
24. Dhote, V. & Vernerey, F. J. Mathematical model of the role of degradation on matrix development in hydrogel scaffold. *Biomech. Model. Mechanobiol.* **13**, 167–183 (2013).
25. Dhote, V. *et al.* On the role of hydrogel structure and degradation in controlling the transport of cell-secreted matrix molecules for engineered cartilage. *J. Mech. Behav. Biomed. Mater.* **19**, 61–74 (2013).
26. Bryant, S. J., Cuy, J. L., Hauch, K. D. & Ratner, B. D. Photo-patterning of porous hydrogels for tissue engineering. *Biomaterials* **28**, 2978–2986 (2007).
27. Kim, Y.-J., Sah, R. L. Y., Doong, J.-Y. H. & Grodzinsky, A. J. Fluorometric assay of DNA in cartilage explants using Hoechst 33258. *Anal. Biochem.* **174**, 168–176 (1988).

28. Templeton, D. M. The basis and applicability of the dimethylmethylene blue binding assay for sulfated glycosaminoglycans. *Connect. Tissue Res.* **17**, 23–32 (1988).
29. Woessner, J. F. The determination of hydroxyproline in tissue and protein samples containing small proportions of this imino acid. *Arch. Biochem. Biophys.* **93**, 440–447 (1961).
30. Vernerey, F., Liu, W. K. & Moran, B. Multi-scale micromorphic theory for hierarchical materials. *J. Mech. Phys. Solids* **55**, 2603–2651 (2007).
31. Flory, P. J. *Principles of Polymer Chemistry*. (Cornell University Press, 1953).
32. Akalp, U. *et al.* Determination of the polymer-solvent interaction parameter for PEG hydrogels in water: Application of a self learning algorithm. *Polymer* **66**, 135–147 (2015).
33. Kääh, M. J., Ap Gwynn, I. & Nötzli, H. P. Collagen fibre arrangement in the tibial plateau articular cartilage of man and other mammalian species. *J. Anat.* **193**, 23–34 (1998).
34. Ng, L. *et al.* Individual cartilage aggrecan macromolecules and their constituent glycosaminoglycans visualized via atomic force microscopy. *J. Struct. Biol.* **143**, 242–257 (2003).
35. Anderson, M. L., Mott, P. H. & Roland, C. M. The Compression of Bonded Rubber Disks. *Rubber Chem. Technol.* **77**, 293–302 (2004).
36. Wong, M., Ponticiello, M., Kovanen, V. & Jurvelin, J. S. Volumetric changes of articular cartilage during stress relaxation in unconfined compression. *J. Biomech.* **33**, 1049–1054 (2000).
37. Mow, V. C., Gibbs, M. C., Lai, W. M., Zhu, W. B. & Athanasiou, K. A. Biphasic indentation of articular cartilage—II. A numerical algorithm and an experimental study. *J. Biomech.* **22**, 853–861 (1989).
38. Anseth, K. S., Bowman, C. N. & Brannon-Peppas, L. Mechanical properties of hydrogels and their experimental determination. *Biomaterials* **17**, 1647–1657 (1996).
39. Gould, S. T., Darling, N. J. & Anseth, K. S. Small peptide functionalized thiol–ene hydrogels as culture substrates for understanding valvular interstitial cell activation and de novo tissue deposition. *Acta Biomater.* **8**, 3201–3209 (2012).
40. Guilak, F., Jones, W. R., Ting-Beall, H. P. & Lee, G. M. The deformation behavior and mechanical properties of chondrocytes in articular cartilage. *Osteoarthritis Cartilage* **7**, 59–70 (1999).
41. Vernerey, F. J. A mixture approach to investigate interstitial growth in engineering scaffolds. *Biomech. Model. Mechanobiol.* **15**, 259–278 (2016).
42. Vernerey, F. J., Liu, W. K., Moran, B. & Olson, G. A micromorphic model for the multiple scale failure of heterogeneous materials. *J. Mech. Phys. Solids* **56**, 1320–1347 (2008).

43. Aboudi, J., Arnold, S. M. & Bednarczyk, B. A. *Micromechanics of Composite Materials*. (Butterworth-Heinemann, 2013).
44. Nemat-Nasser, S. & Hori, M. *Micromechanics: Overall Properties of Heterogeneous Materials*. (Elsevier, 2013).
45. Madras, N. & Sokal, A. D. The pivot algorithm: A highly efficient Monte Carlo method for the self-avoiding walk. *J. Stat. Phys.* **50**, 109–186 (1988).
46. Brannon-Peppas, L. & Peppas, N. A. Solute and penetrant diffusion in swellable polymers. IX. The mechanisms of drug release from pH-sensitive swelling-controlled systems. *J. Controlled Release* **8**, 267–274 (1989).
47. Gigout, A., Buschmann, M. D. & Jolicoeur, M. Chondrocytes Cultured in Stirred Suspension with Serum-Free Medium Containing Pluronic-68 Aggregate and Proliferate While Maintaining Their Differentiated Phenotype. *Tissue Eng. Part A* **15**, 2237–2248 (2009).
48. Tanaka, H., Sato, T. & Otsu, T. Long-lived polymer radicals, 2. An ESR study on the reactions of the propagating polymer radicals of N-methylacrylamide and N-methylmethacrylamide with vinyl monomers at room temperature. *Makromol. Chem.* **181**, 2421–2431 (1980).
49. Cho, H., Lai, T. C. & Kwon, G. S. Poly(ethylene glycol)-block-poly( $\epsilon$ -caprolactone) micelles for combination drug delivery: Evaluation of paclitaxel, cyclophosphamide and gossypol in intraperitoneal xenograft models of ovarian cancer. *J. Controlled Release* **166**, 1–9 (2013).
50. Tian, Y. *et al.* Utilization of micelles formed from poly(ethylene glycol)-block-poly( $\epsilon$ -caprolactone) block copolymers as nanocarriers to enable hydrophobic red two-photon absorbing (2PA) emitters for cells imaging. *J. Biomed. Mater. Res. A* **93**, 1068 (2010).
51. Chu, S., Sridhar, S. L., Skaalure, S. C., Vernerey, F. J. & Bryant, S. J. Understanding the Spatiotemporal Degradation Behavior of Aggrecanase-Sensitive Poly(ethylene glycol) Hydrogels for use in Cartilage Tissue Engineering. *Tissue Eng. Part A* (2017). doi:10.1089/ten.TEA.2016.0490
52. Martens, P. J., Bryant, S. J. & Anseth, K. S. Tailoring the Degradation of Hydrogels Formed from Multivinyl Poly(ethylene glycol) and Poly(vinyl alcohol) Macromers for Cartilage Tissue Engineering. *Biomacromolecules* **4**, 283–292 (2003).
53. Hoyle, C. E. & Bowman, C. N. Thiol–Ene Click Chemistry. *Angew. Chem. Int. Ed.* **49**, 1540–1573 (2010).
54. Coates, E. E. & Fisher, J. P. Phenotypic Variations in Chondrocyte Subpopulations and Their Response to In Vitro Culture and External Stimuli. *Ann. Biomed. Eng.* **38**, 3371–3388 (2010).

## **Chapter 7. Improving the Tissue Engineering Potential of Adult Chondrocytes via Growth Factors**

### **Abstract**

The success of tissue engineering strategies utilizing autologous chondrocytes is highly dependent on the regenerative capabilities of the donor cells. Donor age has been identified as a crucial factor in the cells metabolic activity with older cells showing less potent regenerative potential and more osteoarthritic risk. In this chapter, we demonstrate that the application of growth factors can increase the anabolic capacity of older cells. Specifically, application of soluble IGF-1 at 50 ng/mL increased hydroxyproline production of adult chondrocytes encapsulated in poly (ethylene glycol) hydrogels compared to chondrocytes of the same donor that did not receive IGF-1. IGF-1 also reduced the enzyme activity of adult chondrocytes to similar levels of young chondrocytes. Finally, we describe a strategy for personalizing hydrogel design to further close the gap in tissue engineering outcomes of donors of varying regenerative ability.

### **7.1 Introduction**

In recent years, there has been growing recognition that the next era of medicine will be defined by what is known as personalized (or precision) medicine. In 2015, the Obama administration announced that it will invest \$215 million to the Precision Medicine Initiative, whose long-term goal was to study one million Americans to better understand specific genetic predispositions and risk factors for disease<sup>1,2</sup>. Currently, the practice of personalized medicine primarily includes the sequencing of individual genomes to select and optimize appropriate therapies, which can be a costly approach. While the effort to move towards personalized

medicine is expensive, it will reduce healthcare costs in the long run by improving the efficiency of therapies and reducing the number of failed treatments.

Personalized medicine is defined as the medical treatment tailored to individuals or subpopulations of individuals that share similar characteristics such as their susceptibility to certain diseases or responses to drug treatments. Some forms of current medical practices and research techniques may be considered personalized therapies. Pharmaceutical compounding involves the transformation of a drug from one form to another. For example, a pill may be turned into a liquid which may be more amenable to administer to children. In recent years, researchers have been decellularizing extracellular matrices (e.g. liver, heart, etc.) and repopulating it with patient cells<sup>3-6</sup>. The decellularized matrix then provides cues to direct the cells towards a phenotype appropriate of their tissue. In regard to tissue engineering and scaffolds, 3D printing has allowed researchers precision spatial control over constructs. 3D printing has been used to print auricular cartilage constructs<sup>7</sup> as well as cranial bone implants<sup>8</sup> with matching morphology specific to the patient. In the context of cartilage tissue engineering, autologous chondrocyte implantation (ACI) is a current clinical treatment which may be considered as a personalized treatment due to the use of the patient's own chondrocytes.

The use of autologous chondrocytes in tissue engineering reduces the risk of immune rejection of the biomaterial implant by the body; however, the success of ACI is currently limited by the regenerative capabilities of the chondrocytes. It has been reported that certain individual factors correlate to the cartilage production of cells including sex, general level of fitness, weight, and age<sup>9-11</sup>. The production of hyaline-like cartilage proteins, collagen II and aggrecan, have been shown to be significantly reduced with age. Thus, the objective of this study is two-fold: 1) to

identify a dosage of growth factors (one of many possible external stimuli to alter cellular bioactivity) that reduces the gap in anabolic capabilities between younger and older chondrocytes; and 2) to propose a platform to tailor a synthetic hydrogel formulation specific to the needs of a subpopulation of chondrocytes.

Our approach first included 2D culture of young and adult bovine chondrocytes over a week (to minimize dedifferentiation) in chemically defined media. We administered basic fibroblast growth factor (FGF-2) and insulin-like growth factor 1 (IGF-1) to older chondrocytes at three different concentrations. After identifying the best performing growth factor (measured by collagen and glycosaminoglycan production), this study was then translated into 3D culture over four weeks. Young and adult chondrocytes were encapsulated in PEG-based hydrogels sensitive to matrix metalloproteinases (MMPs). Additionally, a discussion on the future directions of this work is included to elaborate further on growth factor administration as well as rationally designing hydrogels tailored to subpopulations of chondrocytes.

## **7.2 Materials and Methods**

### ***7.2.1 Chondrocyte Isolation***

Bovine chondrocytes were harvested from two different donors: one donor was a ~ three-week-old juvenile calf (Research 87, Boylston, MA) and the other donor was a ~1.5 year old adult steer (Arapahoe Meats, Lafayette, CO). Due to the nature of the availability of joints, chondrocytes were isolated from the femoral condyles and patellar groove of the stifle joint in the juvenile donor. Chondrocytes were isolated from the metacarpophalangeal joint in the adult donor. The cells are referred herein as young chondrocytes and adult chondrocytes. In brief, cartilage was excised from the joint, cut into small ~1 cubic mm pieces and digested for 15-17 h

at 37°C in 600 U/mL collagenase type II (Worthington Biochemical Corp., Lakewood, NJ) in Dulbecco's Modified Eagle Medium (DMEM; Invitrogen, Carlsbad, CA). Freshly isolated chondrocytes were retrieved after filtering through a sterile 100 µm sieve, followed by several washes in phosphate buffered saline (PBS) with antibiotics (50 U/mL penicillin, 50 µg/mL streptomycin, 20 µg/mL gentamicin, and 0.5 µg/mL fungizone) and 0.02% EDTA (Invitrogen, Carlsbad, CA). Cell viability was determined to be >98% for young chondrocytes and >97% for adult chondrocytes as measured using the trypan blue exclusion assay (Sigma-Aldrich, St. Louis, MO).

### **7.2.2 2D Growth Factor Screen**

Freshly harvested young and adult chondrocytes were plated in 6 well plates (2x10<sup>6</sup> chondrocytes/well, n=3 wells per time point for three time points) with chondrocyte growth media (DMEM with antibiotics (50 U/mL penicillin, 50 µg/mL streptomycin, 20 µg/mL gentamicin, and 0.5 µg/mL fungizone)) containing 10% FBS (Atlanta Biologicals, Flowery Branch, GA) to promote cell attachment. Chondrocytes were allowed to attach to the well plate for 24 h in media containing serum. After one day, the media was aspirated and the wells were washed with warm PBS with antibiotics. The media was replaced with a chemically defined media containing TGF-β3 (hereafter referred to as base media) to maintain the chondrocyte phenotype. The chemically defined media was made of DMEM-F12 (ThermoFisher, Fair Lawn, NJ) supplemented with antibiotics (50 U/mL penicillin, 50 µg/mL streptomycin, 20 µg/mL gentamicin, and 0.5 µg/mL fungizone), 1% ITS+ Premix (BD Biosciences, Franklin Lakes, NJ), 10 mM HEPES (Invitrogen), 1.5 mM GlutaGro (VWR International, Radnor, PA), 0.25 mM L-Proline (Sigma-Aldrich), 20 mg/mL L-ascorbic acid (Sigma-Aldrich), and sodium pyruvate (Sigma-Aldrich) to a final concentration of



100 µg/mL. Media was replaced with fresh base media on day 4. Young chondrocytes were treated with base media. Adult chondrocytes were treated with base media as well as base media with added soluble FGF-2 (at 5, 50, or 100 ng/mL) or IGF-1 (at 5, 50, or 100 ng/mL). TGF-β3 was purchased from R&D Systems (Minneapolis, MN). FGF-2 and IGF-1 was purchased from PeproTech (Rocky Hill, NJ).

On day 1 (24 h incubation with chemically defined media), day 4, and day 7, media was collected from all wells and flash-frozen in liquid nitrogen and stored at -80C. At each time point, three wells were trypsinized to collect the cells. Wells were rinsed with PBS + antibiotics and treated with 0.25% trypsin-EDTA (ThermoFisher, Fair Lawn, NJ) for 5 mins at 37°C. The trypsin-cell suspension was collected and the well was rinsed with PBS and collected. The trypsin-cell suspension was centrifuged at 1200 rpm for 10 min. The trypsin was aspirated and the cells were resuspended in chondrocyte growth media to deactivate the trypsin. The media-cell suspension was centrifuged at 1200 rpm for 10 min. The media was aspirated and the cells were washed in PBS once and centrifuged again. The PBS was aspirated and the cell pellets were flash frozen and stored in -20C until analysis.

### **7.2.3 Macromer Synthesis**

An 8-arm PEG-norbornene (PEG-NB) macromer was synthesized by reacting 8-arm PEG-NH<sub>2</sub> (20 kDa, Jenkem Technology USA, Plano, TX) with four molar excess 5-norbornene-2-carboxylic acid (Sigma-Aldrich, St. Louis, MO), three molar excess of O-(7-azabenzotriazol-1-yl)-N,N,N',N'-tetramethyluronium hexafluorophosphate (HATU, ChemImpex International, Inc., Woodale, IL) and six molar excess of N,N-Diisopropylethylamine in dimethylformamide (Fisher Scientific, Fairlawn, NJ) overnight at room temperature under argon. The final product, PEG-NB,

was recovered and purified by precipitation in diethyl ether (Sigma-Aldrich), filtration, dialysis in de-ionized water over several days, and lyophilization. Norbornene conjugation to each arm of the 8-arm PEG-NH<sub>2</sub> was determined with <sup>1</sup>H nuclear magnetic resonance spectroscopy by comparing the olefinic hydrogen peaks in the norbornene ( $\delta = 5.9\text{-}6.25$  ppm) to the methylene hydrogen peaks in the PEG backbone ( $\delta = 3.4\text{-}3.9$  ppm). The norbornene conjugation was determined to be ~100%. PEG dithiol (PEGdSH) (Sigma-Aldrich) crosslinker and the MMP-sensitive peptide crosslinker, GCVPLS-LYSGCG, (GenScript, Piscataway, NJ) were used as received.

#### **7.2.4 Chondrocyte Expansion**

Freshly harvested chondrocytes from young and adult donors were expanded in 2D to achieve desirable cell encapsulation concentrations. Chondrocyte expansion was limited to under one week to minimize dedifferentiation. 10<sup>6</sup> chondrocytes were seeded per T-225 flask and allowed to attach to the surface for 24 h in chondrocyte growth media containing FBS. Fresh media was supplied to each flask after one day and replaced every 2-3 days afterwards. After 6 days of expansion, cells were lifted from the plate with 0.25% trypsin-EDTA and washed with chondrocyte media with serum three times. Cell sheets were digested for two hours in an enzyme solution containing dispase (ThermoFisher, Fair Lawn, NJ) and liberase (ThermoFisher) in Hank's Balanced Salt Solution (HBSS; Quality Biological, Gaithersburg, MD) on a figure-eight shaker plate at 70 rpm 37°C. The final concentration of the digest solution was 4.4 U/mL dispase and 0.008 mg/mL liberase. The digest was filtered through 70  $\mu$ m cell strainers to remove any large undigested sheets. The filtrate containing cells was quenched in PBS supplemented with 0.16 mg/mL EDTA and washed in chondrocyte growth media twice. The cells were counted using the

trypan blue exclusion assay (Sigma-Aldrich). Cell numbers increased by 2-3x while maintaining >90% viability.

### **7.2.5 Hydrogel Formation and 3D Cell Culture**

A hydrogel precursor solution was prepared to reach a final concentration of 10% (g/g) 8-arm PEG-NB in PBS. This solution was combined with the peptide crosslinker GCVPLS-LYSGCG (0.8 thiol:ene) with 0.05% photoinitiator (Irgacure 2959, Ciba Specialty Chemicals, Tarrytown, NY). The solution was sterile-filtered (0.22  $\mu\text{m}$  filter). Expanded young and adult chondrocytes were combined with the hydrogel precursor solution at 150 million cells/mL and polymerized with 352 nm light (UVP, Upland, CA) at 6 mW/cm<sup>2</sup> for 5 minutes. Cell-laden hydrogels were cultured in chondrocyte growth medium (DMEM supplemented with 10% FBS, 50 U/mL penicillin, 50  $\mu\text{g}/\text{mL}$  streptomycin, 0.5  $\mu\text{g}/\text{mL}$  fungizone, 10 mM HEPES buffer, 0.1 M MEM-NEAA, 0.4 mM L-proline, 4 mM GlutaGro, 110 mg/L sodium pyruvate, and 50 mg/mL L-ascorbic acid (Sigma-Aldrich)) at 37°C and 5% CO<sub>2</sub> in a humid environment for up to four weeks.

### **7.2.6 Hydrogel Characterization**

At day 1, week 2, and week 4, cell-laden hydrogel constructs were randomly removed from culture. The compressive modulus of cell-laden hydrogels (n=3) was measured using a mechanical tester (MTS Synergie 100, 10N, Eden Prairie, MN). Fully hydrated hydrogels were subjected to unconfined compression up to 15% strain at an average rate of 10% strain/min. The compressive modulus was determined in the linear range of the resulting stress-strain curve between 10 and 15% strain.

### **7.2.7 Biochemical Assays**

At day 1, week 2, and week 4, cell-laden hydrogel constructs (n=2-3) were randomly removed from culture and analyzed for viability. Cell viability was assessed using the LIVE/DEAD<sup>®</sup> membrane integrity assay (Calcein AM/ethidium homodimer, Invitrogen) and imaged by confocal microscopy. At day 1, week 2, and week 4, cell-laden hydrogel constructs (n=3) were randomly removed from culture weighed to determine wet weight, snap frozen in liquid nitrogen, lyophilized, and weighed again to obtain dry weights. The medium was collected, snap frozen in liquid nitrogen, and stored at -80°C until analysis. Hydrogels and cell pellets were homogenized using a TissueLyser (Qiagen, Hilden, Germany) and enzymatically digested in 4 U/mL papain (Worthington Biochemical Corp.) for 18 h at 60°C. DNA content was determined in the hydrogels and in the cell pellets using Hoechst 33258 (Polysciences, Inc. Warrington, PA)<sup>20</sup>. A colorimetric assay based on 1,9-dimethylmethylene blue (Sigma-Aldrich St. Louis, MO) was used to quantify the amount of sulfated glycosaminoglycans (sGAGs)<sup>13</sup>. Total collagen content was assessed using the hydroxyproline assay. The total amounts of sGAGs and collagen were quantified in the hydrogels.

### **7.2.8 Enzyme Activity Assays**

At day 1, week 2, and week 4, enzyme activity was measured in the constructs (n=2-3) using a commercial kit, Sensolyte 520 Generic MMP Assay Kit (Anaspec, Fremont, CA). Cell-laden hydrogel constructs were homogenized using a TissueLyser (Qiagen) in PBS with 0.1% Triton X-100. Samples were incubated with a FRET peptide substrate that is susceptible to cleavage by a variety of MMPs for 1 h at 37°C and fluorescence was measured.

### **7.2.9 Immunohistochemistry and Microscopy**

At day 1, week 2, and week 4, cell-laden hydrogel constructs (n=2-3) were randomly removed from culture and analyzed by histology and immunohistochemistry methods. Hydrogel constructs were fixed in 4% paraformaldehyde at 4°C, paraffin embedded, dehydrated, and sectioned into 10 µm thick slices. Prior to primary antibody treatment for collagen II and C1, 2C epitopes, sections were treated with 2000 U/mL hyaluronidase (Sigma-Aldrich) for 1 h at 37°C. Sections were treated with anti-collagen II antibody (1:50, USBiological, Salem, MA) or with anti-C1, 2C antibody (IBEX Pharma, Montreal, Canada). Prior to primary antibody treatment for collagen I epitopes, sections were treated with 1 mg/mL pepsin (Sigma-Aldrich) for 1 h at 37°C. After primary antibody treatment, sections were treated with AlexaFluor 488 conjugated secondary antibodies (1:200, Invitrogen). Cell nuclei were counterstained with DAPI (Invitrogen). Stained sections were mounted with Fluoromount-G (Southern Biotech, Birmingham, AL). Sections receiving no primary antibody treatment served as negative controls. At day 1, week 2, and week 4, sections were stained with Safranin-O/Fast Green to visualize sGAGs. Cell nuclei were counterstained with haematoxylin. Sections were imaged at 400x on a laser scanning confocal microscope (Axiovert 40 C, Zeiss, Thornwood, NY).

### **7.2.10 Statistics**

Data are presented as mean with error bars representing standard deviation. Measures of modulus, DNA, hydroxyproline, sGAG, and enzyme activity were analyzed with an ANOVA with a Tukey's post-hoc test ( $\alpha = 0.05$ ) to determine significant differences between conditions at specific time points.

## 7.3 Results and Discussion

### 7.3.1 Effect of FGF-2 and IGF-1 on Matrix Production on Chondrocytes Cultured in 2D

In regards to cartilage repair therapies involving autologous chondrocyte implantation, younger patients typically have higher successful outcomes compared to older patients due to their greater ability to regenerate extracellular matrix<sup>15</sup> made up of collagen and aggrecan proteins and sulfated glycosaminoglycans. In order to improve ACI outcomes for older patients, one such strategy is to improve the anabolic capabilities of older chondrocytes by providing growth factors to stimulate matrix production. The goal of this study was to demonstrate that, with the use of growth factors, it is possible to increase the anabolic potential of adult chondrocytes to closer emulate the regenerative capabilities of young chondrocytes.

We performed a short-term study applying two different growth factors at different dosages (5, 50, and 100 ng/mL) to adult chondrocytes in 2D and analyzed their effect on sulfated glycosaminoglycan (sGAG) and hydroxyproline production. Fibroblast growth factor 2 (FGF-2) has been shown to induce chondrocyte proliferation<sup>16</sup> and insulin-like growth factor 1 (IGF-1) has been shown to reduce cartilage degradation and increase proteoglycan production<sup>17</sup>. In native cartilage, sGAGs can be found in the aggrecan protein complex and hydroxyproline is a common amino acid residue found in collagen proteins. Thus, sGAGs and hydroxyproline are important markers of cartilage tissue. To minimize the potential for dedifferentiation of chondrocytes cultured in 2D, we kept the study to under one week and supplemented the media with TGF- $\beta$ <sup>3</sup><sup>18</sup>.

After six days of cell culture, adult chondrocytes left untreated with growth factors produced significantly less hydroxyproline ( $p < 0.05$ ) (Figure 1A) and less sGAGs ( $p < 0.05$ ) (Figure

1B) compared to untreated young chondrocytes, consistent with previous reports in the literature<sup>9–11</sup>. Furthermore, many dosages of either growth factor FGF-2 or IGF-1 did not significantly increase matrix production by adult chondrocytes over six days. However, adult chondrocytes treated with IGF-1 at 50 ng/mL showed no statistical difference in hydroxyproline (Figure 1A) and sGAG (Figure 1B) production compared to young chondrocytes and had a significant increase compared to day 1. This suggests that soluble IGF-1 at 50 ng/mL can improve the anabolic capabilities of adult chondrocytes to rival that of young chondrocytes.

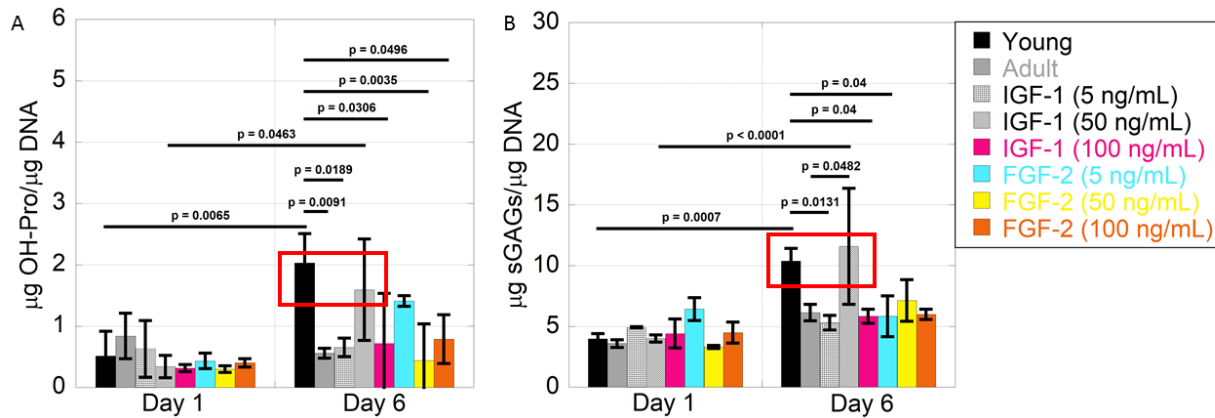


Figure 1. A) Hydroxyproline production normalized to DNA content of young and adult chondrocytes cultured over a period of six days. B) sGAG production normalized to DNA content of young and adult chondrocytes cultured over a period of six days. By day 6, application of soluble IGF-1 at 50 ng/mL enhanced hydroxyproline and sGAG production of adult chondrocytes similar to that of young chondrocytes (highlighted by a red rectangle).

### 7.3.2 Effect of IGF-1 on Matrix Production on Chondrocytes Cultured in 3D

Cartilage tissue engineering strategies utilizing chondrocytes encapsulated in a 3D biomaterial is a promising platform because the 3D environment maintains the rounded morphology of chondrocytes and supports the chondrogenic phenotype. Additionally, PEG based hydrogels create a hydrophilic environment for encapsulated cells<sup>19</sup> and offer the potential for a reduced host response when implanted in the body.

In this study, young and adult chondrocytes were encapsulated in PEG hydrogels sensitive to MMP degradation and cultured for up to four weeks. Adult chondrocytes were further treated with IGF-1 and 50 ng/mL as this concentration proved to be effective in the short 2D study previously described. In previous works, we have shown that encapsulating chondrocytes at a cell concentration of  $150 \times 10^6$  cells/mL of precursor solution provided macroscopic collagen II connectivity by 12 weeks<sup>20</sup>. To reach these cell numbers, freshly harvested chondrocytes were expanded in culture over a period of one week. During culture, chondrocytes deposited an extracellular matrix that physically entrapped the cells in matrix sheets. These sheets were enzymatically digested although the cells tended to form clusters afterwards. Upon encapsulation into hydrogels, these clusters were apparent when hydrogels were stained with calcein to assess viability (Figure 2). Throughout the four-week study, a high viability was observed for all cell donor and media conditions.



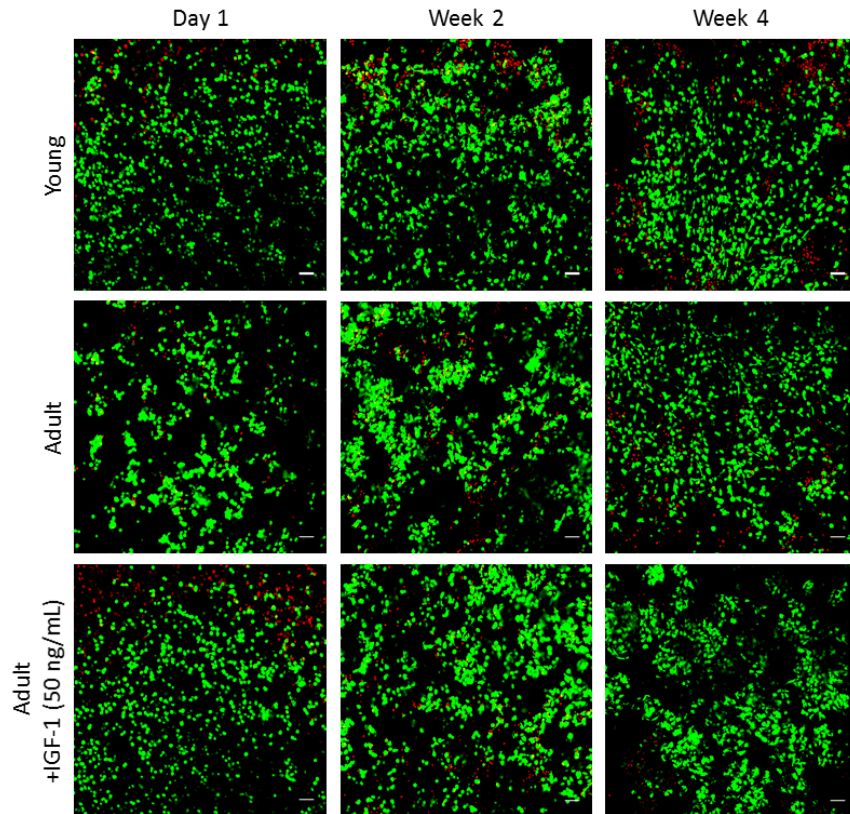


Figure 2. Representative confocal microscopy image of living (green) juvenile chondrocytes encapsulated in MMP-sensitive hydrogels. There is evidence of spatial heterogeneities in cell distribution, showing regions with clustering of cells and regions of single cells. Magnification is 100x. Viability remained high throughout the four-week culture. Scale bars are 50  $\mu$ m.

Chondrocyte proliferation was observed in both young and adult populations. Comparatively, adult chondrocyte populations never reached similar levels to young chondrocytes ( $p < 0.05$ ) although treatment with IGF-1 slightly stimulated adult chondrocyte proliferation (Figure 3A). Calcein staining showing viable chondrocytes and chondrocyte proliferation show that these hydrogel platforms support chondrocyte encapsulation. Over the four weeks of culture, all hydrogel conditions show a decrease in hydrogel mechanics at week 2 with some recovery by week 4 (Figure 3B).

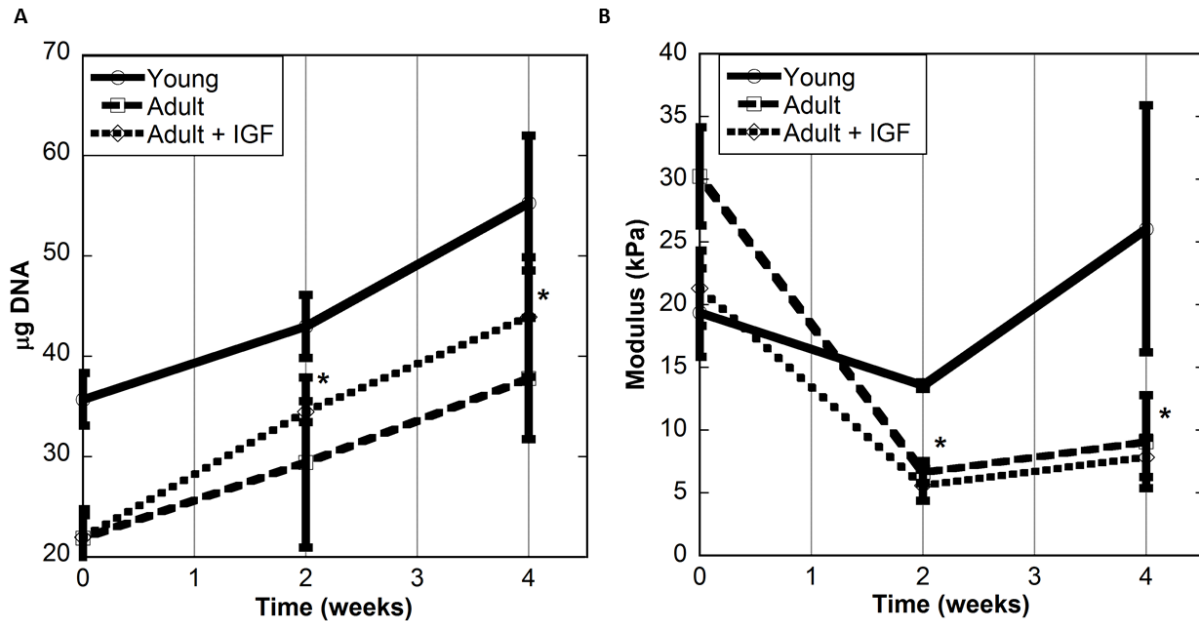


Figure 3. Average DNA content (A) and bulk compressive modulus (B) of cell-laden hydrogels through four weeks. In (A), an (\*) denotes that the DNA content in both hydrogel conditions with adult chondrocytes were significantly different than hydrogels encapsulated with young chondrocytes at each time point. In (B), an (\*) denote that the average modulus of both hydrogel conditions with adult chondrocytes were significantly different than hydrogels encapsulated with young chondrocytes at each time point.

Hydrogel constructs were assayed for collagen (via measuring hydroxyproline) and sGAG content over 12 weeks (Figure 4). Young chondrocytes produced significantly more hydroxyproline compared to adult chondrocytes regardless of growth factor treatment ( $p < 0.05$ ). This is consistent with the recovery in hydrogel modulus seen in construct encapsulated with young chondrocytes as more tissue was produced. There were no significant differences in sGAG production across the conditions (Figure 4B).

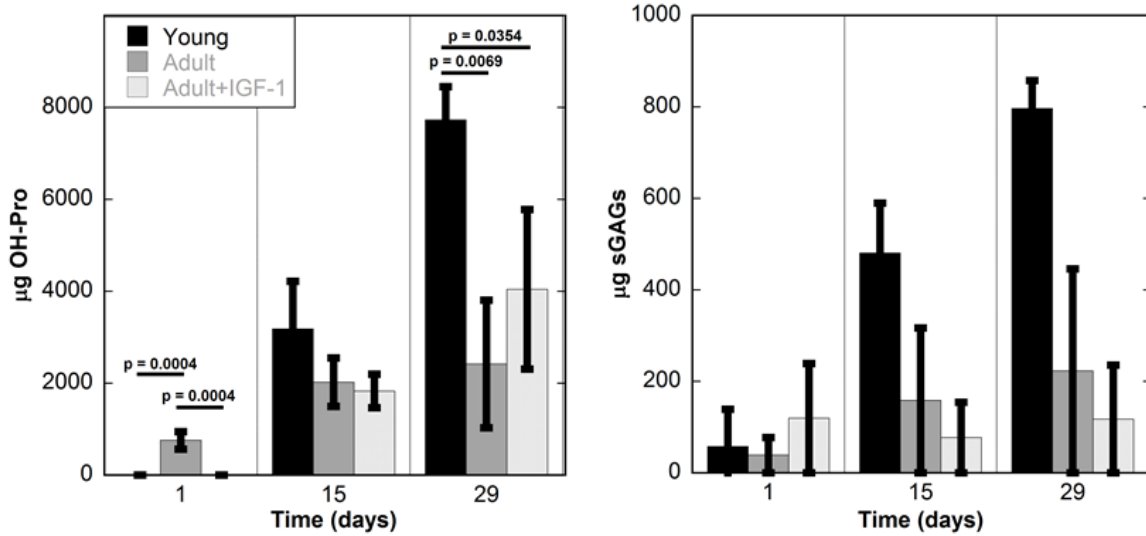


Figure 4. A) Cumulative hydroxyproline production in hydrogel constructs encapsulated with young and adult chondrocytes cultured over a period of four weeks. B) Cumulative sGAG production in hydrogel constructs encapsulated young and adult chondrocytes cultured over a period of four weeks.

Interestingly, application of IGF-1 reduced enzyme activity in adult chondrocytes to similar levels seen in young chondrocytes (Figure 5). Application of IGF-1 significantly reduced enzyme activity in adult chondrocytes ( $p=0.0182$ ) compared to adult chondrocytes receiving no treatment. Literature has shown that adult chondrocytes have higher matrix catabolic processes compared to young chondrocytes<sup>21</sup>. In other words, adult chondrocytes produce enzymes that break down the matrix faster than they can produce neotissue. In this study, these results suggest that using growth factors is a potential way to shift the metabolic processes of adult chondrocytes to a more anabolic state.

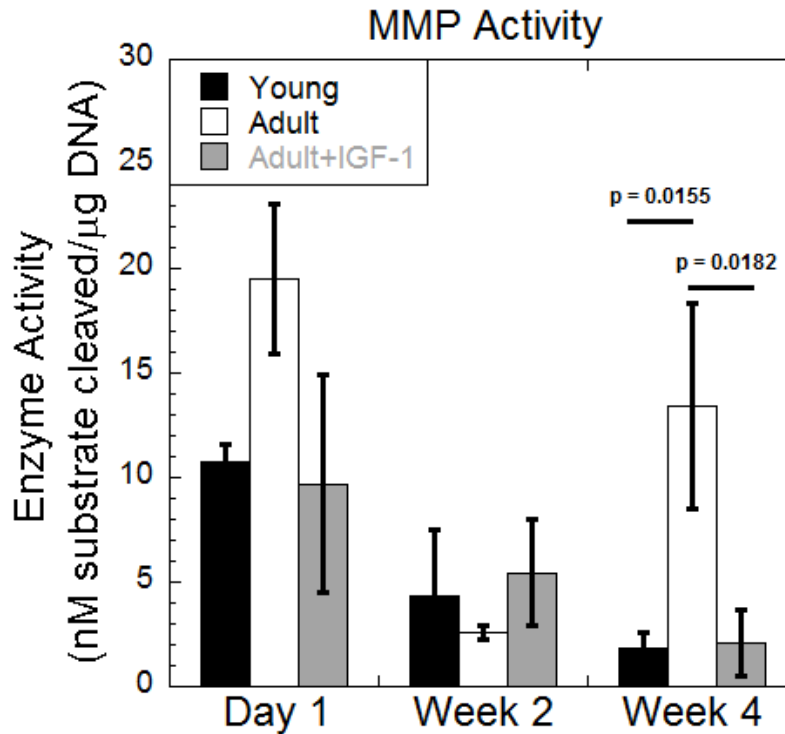


Figure 5. Enzyme activity of young and adult chondrocytes cultured over a period of four weeks. Application of soluble IGF-1 at 50 ng/mL reduced enzyme activity of adult chondrocytes by week 4.

To visualize the spatial distribution of cartilage specific tissues, hydrogel sections were stained with Safranin-O to visualize sGAG distribution (Figure 6) and immunostained with collagen II-specific fluorophore-conjugated secondary antibodies (Figure 7), collagen I-specific fluorophore-conjugated secondary antibodies (Figure 8), and C1, 2C (a marker of collagen degradation)-specific fluorophore-conjugated secondary antibodies (Figure 9). On day 1, both young and adult chondrocytes showed minimal sGAG deposition. By week four, young and adult chondrocytes showed similar spatial deposition of sGAG with slightly more intense staining in hydrogels encapsulated with young chondrocytes (Figure 6). This is consistent with the quantitative assessment of sGAG accumulation in hydrogels showing no significant differences in sGAG production between young and adult chondrocytes (Figure 4B).

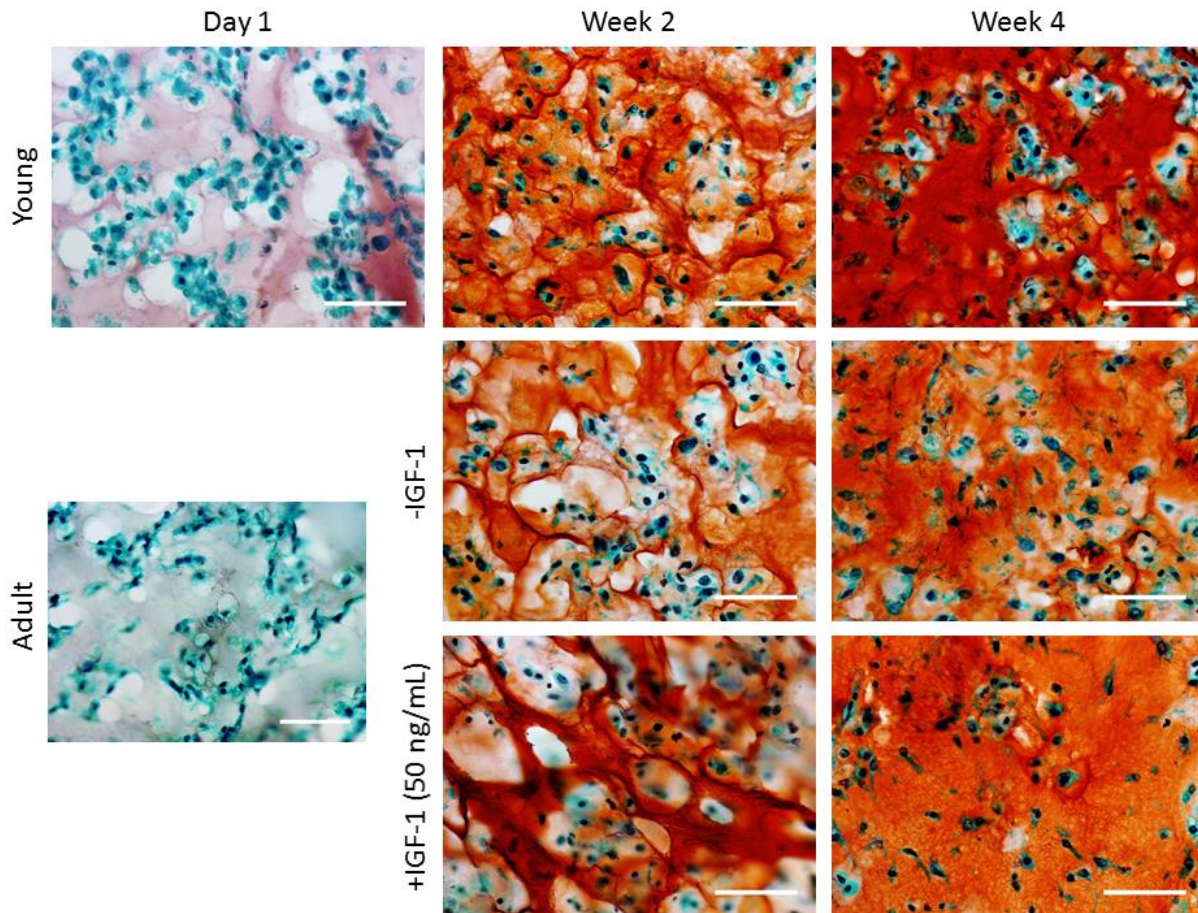


Figure 6. Representative microscopy images of hydrogel sections stained for sGAGs (red) of young or adult chondrocytes encapsulated in MMP-sensitive hydrogels. Scale bars are 50  $\mu\text{m}$ .

Chondrocytes cultured in 2D have been shown to dedifferentiate and produce a mechanically inferior, collagen I-rich fibrocartilage. Comparatively, healthy native cartilage is composed of collagen II. Collagen II immunostaining shows that both young and adult chondrocytes deposited hyaline-like cartilage (Figure 7). By week two, collagen II matrices primarily existed in the pericellular space with some matrix connectivity. By week four, collagen II produced by young chondrocytes began to form large collagen II sheets. Collagen II matrix connectivity was also observed in adult chondrocytes, although not to the extent seen in matrices deposited by young chondrocytes. Comparatively, adult chondrocytes seemed to express a

similar amount of collagen I compared to young chondrocytes regardless of IGF-1 stimulation (Figure 8).

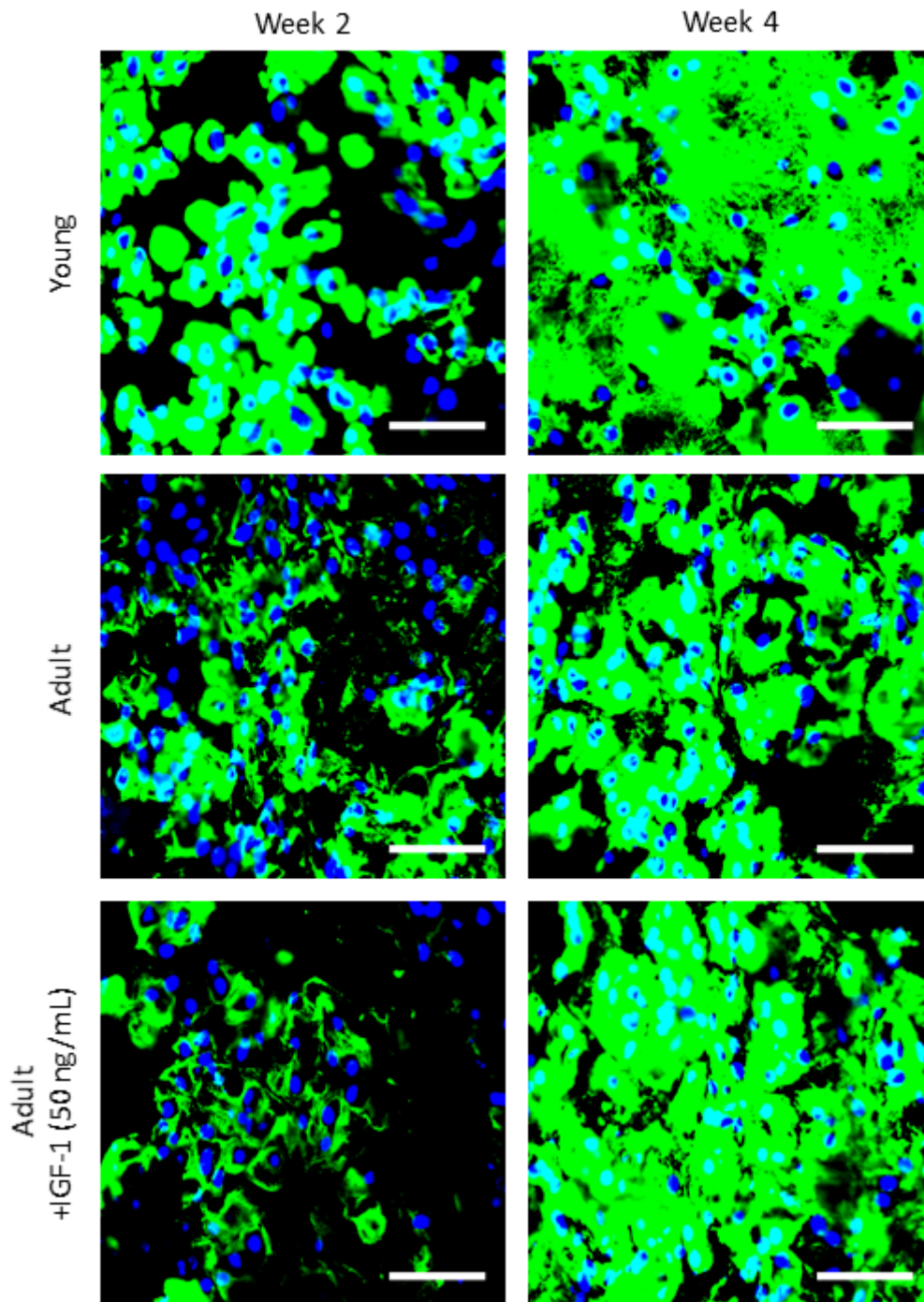


Figure 7. Representative microscopy images of hydrogel sections stained for collagen II (green) of young or adult chondrocytes encapsulated in MMP-sensitive hydrogels. Cell nuclei were counterstained with DAPI (blue). Scale bars are 50  $\mu$ m.

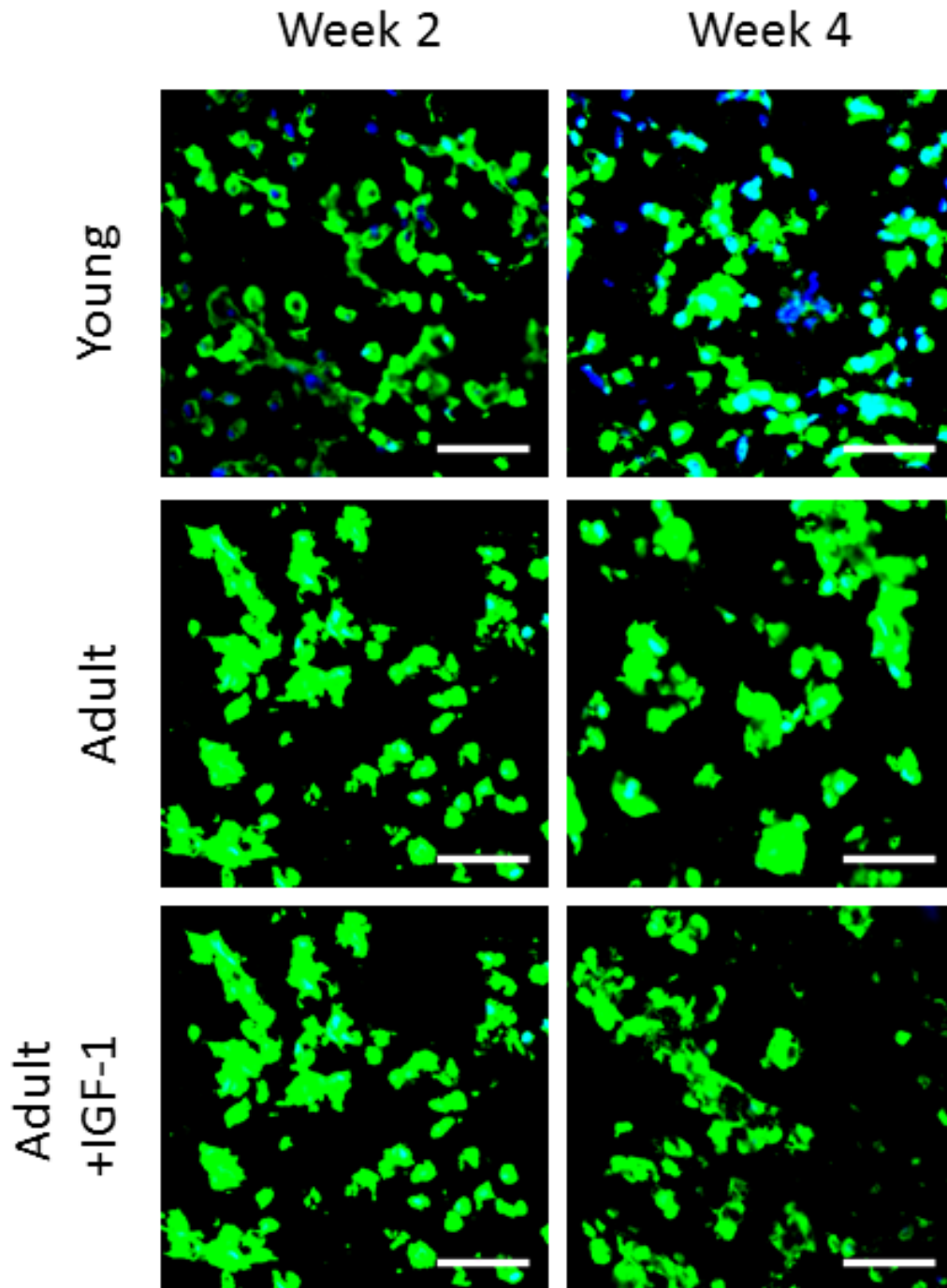


Figure 8. Representative microscopy images of hydrogel sections stained for collagen I (green) of young or adult chondrocytes encapsulated in MMP-sensitive hydrogels. Cell nuclei were counterstained with DAPI (blue). Scale bars are 50  $\mu$ m.



Quantitative assessment of hydroxyproline content showed that young chondrocytes produced significantly more total collagen compared to adult chondrocytes (Figure 4A). Immunostaining of collagen II revealed similar levels of collagen II production across all hydrogel conditions; however, immunostaining C1, 2C staining showed similar levels of collagen degradation across all hydrogel conditions (Figure 9). Although collagen II is the primary collagen found in healthy cartilage, collagen types III, VI, IX, X, XI, XII and XIV are all found in mature cartilage<sup>22</sup>. It is possible the constructs with young chondrocytes produced other types of collagen that was quantified but was not captured in histological images.

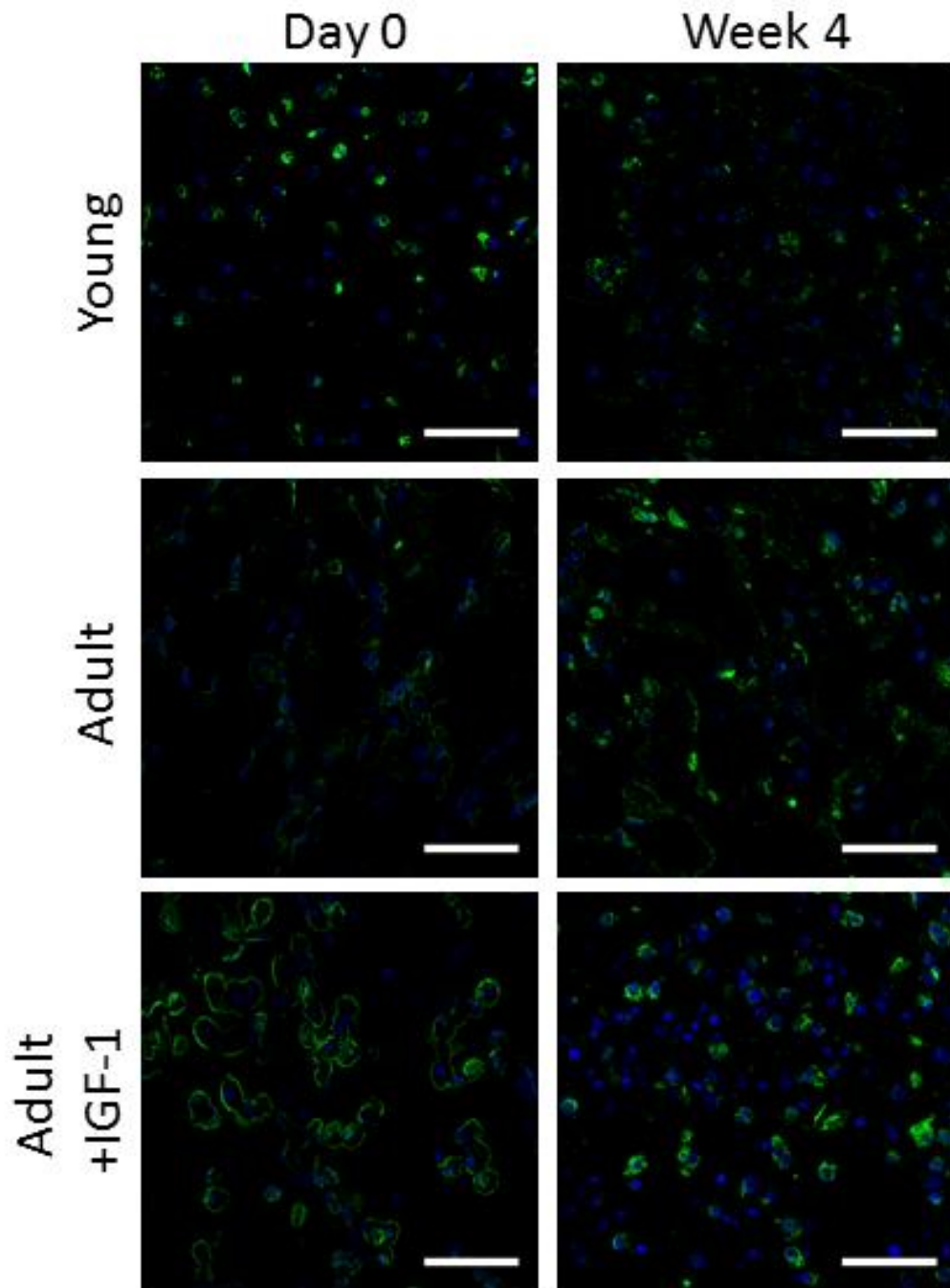


Figure 9. Representative microscopy images of hydrogel sections stained for the C1, 2C epitope (green), a marker of collagen degradation, of young or adult chondrocytes encapsulated in MMP-sensitive hydrogels. Cell nuclei were counterstained with DAPI (blue). Scale bars are 50  $\mu\text{m}$ .

Hydrogels sensitive to MMP degradation with encapsulated young and adult chondrocytes showed a slight decrease in mechanics followed by recovery by week four,

suggesting that this enzyme-degradable hydrogel platform could be promising for even catabolically active adult chondrocytes. Collagen II production was similar for both young and adult chondrocytes; however, young chondrocytes may be producing other types of collagen that are found in mature cartilage. IGF-1 stimulation of adult chondrocytes had negligible effect on the matrix production capabilities of adult chondrocytes; however, it did reduce MMP activity while stimulating chondrocyte proliferation. This suggests that other growth factor candidates could have a significant effect on increasing the regenerative capabilities of adult chondrocytes.

### ***7.3.3 Personalizing Matrix Assisted Autologous Chondrocyte Implantation (MACI)***

Recently, there has been growing effort in the medical field to tailor medical therapies to an individual or subpopulations of demographics with similar characteristics. While the initial cost to develop the framework and strategies to personalize medicine is expensive, healthcare costs in the long run will be reduced by increasing patient success outcomes and minimizing inefficient treatments. In the context of tissue engineering, personalizing hydrogel-based therapies holds the potential of increasing successful MACI outcomes for a wide variety of patients. A proposed personalized hydrogel framework is detailed in Figure 10.

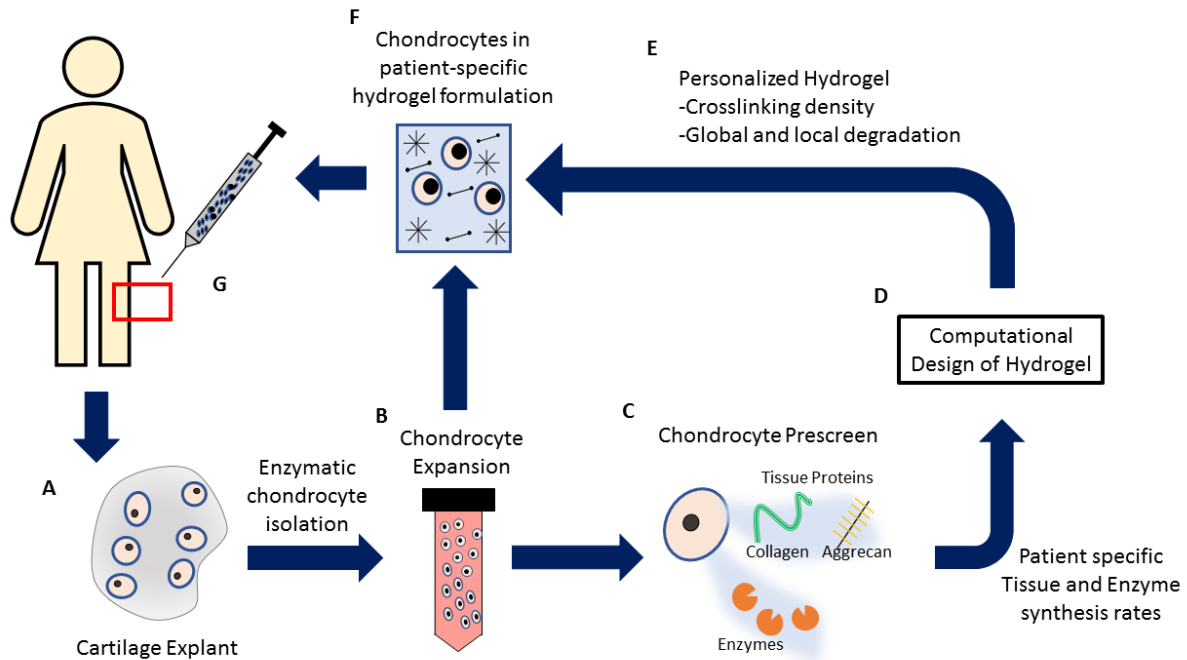


Figure 10. Schematic representation of a personalized hydrogel platform. A) A cartilage explant is obtained from the patient from a non-load bearing section of cartilage. B) After liberation from the cartilage matrix, harvested chondrocytes are expanded in culture. C) During chondrocyte expansion, the chondrocytes are screened for their tissue and enzyme production capacities. In the case of cartilage tissue engineering, collagen and aggrecan (or sGAGs) are of importance. D) The patient's specific tissue and enzyme synthesis rates are input parameters to a computational model that simulates tissue deposition and enzyme-mediated hydrogel degradation based on patient specific rates. E) The computational model formulates a patient-specific hydrogel design in order to match hydrogel degradation and tissue production to avoid construct failure. F) The expanded chondrocytes from step (B) are combined with a precursor solution matching the hydrogel formulation designed in step (E). G) The chondrocyte-precursor solution is injected into the cartilage defect and polymerized *in situ*.

In MACI, autologous chondrocytes are harvested from the patient (Figure 10A). Autologous chondrocytes as a cell source have the benefits of a minimized immune response upon reimplantation into the body as well as avoiding the hurdles associated with differentiation into the chondrogenic phenotype. In order to reach ample numbers for hydrogel encapsulation, chondrocytes are expanded in culture (Figure 10B). During expansion, the cells are screened for their tissue and enzyme production rates (Figure 10C). In the context of cartilage tissue

engineering, tissue proteins of interest include collagen and aggrecan, although other tissue molecules can be quantified for other tissue engineering applications. Enzyme production is also quantified which is important in designing enzyme-sensitive hydrogels. Here, the enzyme-cleavable sequence in the hydrogel can be altered to target specific enzymes. In this step, chemical cues can also be applied to augment synthesis rates. The patient specific tissue and enzyme production rates are used as an input parameter to a computational model that formulates a hydrogel to promote the spatial elaboration of tissue while minimizing the loss of construct mechanics (Figure 10D). Previously, this model has been used to demonstrate that hydrogel degradation is a critical feature of hydrogels that allows for tissue deposition<sup>23,24</sup>. This model has also been used to describe tissue diffusion in the context of hydrogel degradation<sup>25</sup>. Recently, we have also utilized this model to predict the spatial and temporal changes of hydrogel degradation and tissue diffusion of young and adult chondrocytes<sup>15</sup>. The model formulates a patient-tailored hydrogel design that describes a crosslinking density (Figure 10E). The expanded chondrocytes are combined with a precursor solution (Figure 10F) that forms a hydrogel that matches the crosslinking density described by the model. This chondrocyte-precursor solution is then injected back into the cartilage defect of the patient and polymerized *in situ* (Figure 10G).

#### **7.4 Conclusions and Future Work**

In hydrogel-based tissue engineering strategies utilizing autologous chondrocytes, patient success outcomes are highly dependent on the regenerative capabilities of the donor cells. As such, there is a big gap in successful outcomes based on a variety of donor characteristics with age being a major factor. By designing hydrogels tailored to patients, the gap in successful outcomes can potentially be minimized. To close this gap, the regenerative capabilities of older

cells must be augmented. In this work, we have demonstrated that growth factors may be a potential solution to increasing the tissue regenerative capabilities of adult chondrocytes.

## 7.5 Acknowledgments

Research reported in this publication was supported by the National Institute of Arthritis and Musculoskeletal and Skin Diseases of the National Institutes of Health under Award Number 1R01AR065441. The authors acknowledge the National Institute of Health (NIH) Institutional Pharmaceutical Training fellowship and the Graduate Assistance in Areas of National Need (GAANN) Biomaterials from the Department of Education to SC. The technical assistance of Mollie Maples is greatly appreciated.

## 7.6 References

1. White House Precision Medicine Initiative. *The White House* Available at: <https://obamawhitehouse.archives.gov/node/333101>. (Accessed: 19th May 2018)
2. Aguado, B. A., Grim, J. C., Rosales, A. M., Watson-Capps, J. J. & Anseth, K. S. Engineering precision biomaterials for personalized medicine. *Sci. Transl. Med.* **10**, eaam8645 (2018).
3. Ott, H. C. *et al.* Perfusion-decellularized matrix: using nature's platform to engineer a bioartificial heart. *Nat. Med.* **14**, 213–221 (2008).
4. Song, J. J. & Ott, H. C. Organ engineering based on decellularized matrix scaffolds. *Trends Mol. Med.* **17**, 424–432 (2011).
5. Saldin, L. T., Cramer, M. C., Velankar, S. S., White, L. J. & Badyal, S. F. Extracellular matrix hydrogels from decellularized tissues: Structure and function. *Acta Biomater.* **49**, 1–15 (2017).
6. Gilpin, A. & Yang, Y. Decellularization Strategies for Regenerative Medicine: From Processing Techniques to Applications. *BioMed Res. Int.* **2017**, (2017).
7. Zhou, G. *et al.* In Vitro Regeneration of Patient-specific Ear-shaped Cartilage and Its First Clinical Application for Auricular Reconstruction. *EBioMedicine* **28**, 287–302 (2018).
8. Honigmann, P. *et al.* Patient-Specific Surgical Implants Made of 3D Printed PEEK: Material, Technology, and Scope of Surgical Application. *BioMed Research International* (2018). doi:10.1155/2018/4520636

9. Payne, K. A., Didiano, D. M. & Chu, C. R. Donor sex and age influence the chondrogenic potential of human femoral bone marrow stem cells. *Osteoarthritis Cartilage* **18**, 705–713 (2010).
10. Tetlow, L. C., Adlam, D. J. & Woolley, D. E. Matrix metalloproteinase and proinflammatory cytokine production by chondrocytes of human osteoarthritic cartilage: associations with degenerative changes. *Arthritis Rheum.* **44**, 585–594 (2001).
11. Skaalure, S. C., Milligan, I. L. & Bryant, S. J. Age impacts extracellular matrix metabolism in chondrocytes encapsulated in degradable hydrogels. *Biomed. Mater.* **7**, 024111 (2012).
12. Kim, Y.-J., Sah, R. L. Y., Doong, J.-Y. H. & Grodzinsky, A. J. Fluorometric assay of DNA in cartilage explants using Hoechst 33258. *Anal. Biochem.* **174**, 168–176 (1988).
13. Templeton, D. M. The basis and applicability of the dimethylmethylene blue binding assay for sulfated glycosaminoglycans. *Connect. Tissue Res.* **17**, 23–32 (1988).
14. Hascall, V. C. & Sajdera, S. W. Physical properties and polydispersity of proteoglycan from bovine nasal cartilage. *J. Biol. Chem.* **245**, 4920–4930 (1970).
15. Chu, S. *et al.* Understanding the Spatiotemporal Degradation Behavior of Aggrecanase-Sensitive Poly(ethylene glycol) Hydrogels for Use in Cartilage Tissue Engineering. *Tissue Eng. Part A* **23**, 795–810 (2017).
16. Khan, I. M., Palmer, E. A. & Archer, C. W. Fibroblast growth factor-2 induced chondrocyte cluster formation in experimentally wounded articular cartilage is blocked by soluble Jagged-1. *Osteoarthritis Cartilage* **18**, 208–219 (2010).
17. Tyler, J. A. Insulin-like growth factor 1 can decrease degradation and promote synthesis of proteoglycan in cartilage exposed to cytokines. *Biochem. J.* **260**, 543–548 (1989).
18. Byers, B. A., Mauck, R. L., Chiang, I. E. & Tuan, R. S. Transient exposure to transforming growth factor beta 3 under serum-free conditions enhances the biomechanical and biochemical maturation of tissue-engineered cartilage. *Tissue Eng. Part A* **14**, 1821–1834 (2008).
19. Nicodemus, G. D. & Bryant, S. J. Cell Encapsulation in Biodegradable Hydrogels for Tissue Engineering Applications. *Tissue Eng. Part B Rev.* **14**, 149–165 (2008).
20. Schneider, M. C. *et al.* Local Heterogeneities Improve Matrix Connectivity in Degradable and Photoclickable Poly(ethylene glycol) Hydrogels for Applications in Tissue Engineering. *ACS Biomater. Sci. Eng.* **3**, 2480–2492 (2017).
21. Skaalure, S. C., Chu, S. & Bryant, S. J. An Enzyme-sensitive PEG Hydrogel Based on Aggrecan Catabolism for Cartilage Tissue Engineering. *Adv. Healthc. Mater.* **4**, 420–431 (2015).
22. Eyre, D. Articular cartilage and changes in Arthritis: Collagen of articular cartilage. *Arthritis Res.* **4**, 30–35 (2002).

23. Dhote, V. & Vernerey, F. J. Mathematical model of the role of degradation on matrix development in hydrogel scaffold. *Biomech. Model. Mechanobiol.* **13**, 167–183 (2013).
24. Dhote, V. *et al.* On the role of hydrogel structure and degradation in controlling the transport of cell-secreted matrix molecules for engineered cartilage. *J. Mech. Behav. Biomed. Mater.* **19**, 61–74 (2013).
25. Sridhar, S. L. *et al.* Heterogeneity is key to hydrogel-based cartilage tissue regeneration. *Soft Matter* **13**, 4841–4855 (2017).



## Chapter 8. Conclusions and Recommendations

### 8.1 Conclusions

Matrix Autologous Chondrocyte Implantation (MACI) has potential in cartilage tissue engineering for healing cartilage defects before the onset of osteoarthritis. The use of autologous chondrocytes is a double-edged sword in that it can potentially reduce the risk of implant rejection however the variability of cells from donor to donor precludes the possibility of a 'one-size-fits-all' hydrogel. As the field increasingly moves towards designing cell-mediated hydrogel degradation, donor variability further adds another layer of complexity. A critical challenge in designing degradable hydrogels is finely balancing the rate of tissue deposition by encapsulated cells and the rate of hydrogel degradation to prevent construct failure. The findings from this dissertation overall support the importance of examining the effects of polymer network heterogeneities on hydrogel degradation and tissue deposition. This work established 1) that cells cause spatial heterogeneities in polymer network formation and this effect can vary with donor age, 2) that these spatial heterogeneities are important for macroscopic tissue formation, and 3) that growth factors can be a possible strategy to improve MACI outcomes in older donors.

Hydrogels made from synthetic polymers offer the user a high degree of control over material mechanics and degradation<sup>1</sup>. Thus, hydrogels can be highly reproducible and predictable. However, there are some studies that report discrepancies in hydrogel properties once cells are encapsulated<sup>2-5</sup>. Initial work (Chapter 3) sought to characterize the initial state of crosslinking density in newly formed hydrogels and to explore some of the underlying cell-polymer interactions that result in a decrease in hydrogel modulus. In this work, primary bovine chondrocytes were encapsulated in a variety of radical-mediated photopolymerized systems.

Across all radical-mediated systems investigated, cell encapsulation concentration was found to be significant in affecting the over bulk compressive modulus, with higher concentrations reducing the modulus more. Furthermore, the degree to which the modulus was reduced was affected by the donor from which the cells were harvested. The nondegradable crosslinker PEGdSH was found to interact with the cells while in the precursor solution leading to an overall reduction in the monomer concentration in solution, thus forming hydrogels that were mechanically softer had there been no cells in solution. Furthermore, a gradient in crosslinking density was observed centered around encapsulated cells caused by radical quenching around the cell<sup>6</sup>. Together, this work shows that cells cause spatial heterogeneities in polymer network formation and encapsulated cells can reduce the crosslinking density on a local and bulk scale.

In Chapter 4, a previous framework of experimental techniques were expanded upon to explore the critical factors of different degradation regimes of enzyme-sensitive hydrogels. Specifically, microparticles fabricated from poly (lactic-co-glycolic acid) (PLGA) were loaded with collagenase. Thus, these microparticles can be used to study analogous enzyme-secreting cells that degrade the hydrogel network without the confounding phenomenon of tissue formation. The microparticles were loaded with different concentrations of enzyme and showed that a higher enzyme concentration actually led to a slower reduction in the bulk compressive modulus compared to a lower enzyme concentration. The higher concentration of enzyme caused a slightly sharper degradation front leading to a more localized degradation.

Chapter 5 and 6 aimed to investigate how these cell-mediated heterogeneities in crosslinking density (Chapter 3) worked to affect tissue formation of encapsulated cells in an enzymatically degradable system and a hydrolytically degradable system. Juvenile and adult chondrocytes were encapsulated in an aggrecanase degradable system (Chapter 5). Enzymes secreted by the encapsulated chondrocytes were found to be able to readily diffuse throughout the hydrogel causing the gel to degrade on a bulk scale. However, spatial heterogeneities in crosslinking caused by the encapsulated cells allowed for some regions of the gel to reach reverse gelation permitting the spatial elaboration of tissue while the bulk of the gel remained intact. Additionally, regions of high cell densities were found that, with the presence of these spatial heterogeneities in crosslinking density, facilitated the macroscopic evolution of extracellular matrix. These effects were also found to be critical for tissue development in hydrolytically degradable systems (Chapter 6). Due to the ubiquitous presence of water in hydrogels, hydrolytically degradable systems should theoretically reach reverse gelation on a global scale. However, the spatial heterogeneities in crosslinking results in heterogeneous degradation. Together, these spatial heterogeneities were found to be critical in achieving a seamless transition from hydrogel to neotissue.

Chapter 7 focused on increasing the anabolic capabilities of older chondrocytes in an attempt to close the gap in regenerative capabilities between donors of different age. Bovine chondrocytes harvested from a young calf and a mature steer were encapsulated into an MMP-degradable hydrogel. One set of hydrogels encapsulated with adult chondrocytes were further given a constant dose of soluble IGF-1 in the media. Application of soluble IGF-1 increased hydroxyproline production of adult chondrocytes encapsulated in MMP sensitive hydrogels

compared to chondrocytes of the same donor that did not receive IGF-1. IGF-1 also reduced the enzyme activity of adult chondrocytes to similar levels of young chondrocytes. These findings show that using growth factors is a promising way to develop a MACI hydrogel platform for a wide range of donors.

The findings of this dissertation reveal the importance of examining the interactions between encapsulated chondrocytes and their surrounding hydrogel environment in order to develop a hydrogel platform that can be tailored towards individual patients. Characterization of the hydrogel environment immediately after polymerization is critical in order to understand the resulting degradation behavior. Furthermore, examining the spatiotemporal behavior of hydrogel degradation is critical in understanding the resulting tissue development of encapsulated cells. Finally, these findings together with the use of growth factors can contribute towards developing a hydrogel platform tailored to patients thereby reducing the gap in successful outcomes of tissue engineering strategies due to age.

## **8.2 Recommendations**

The findings in this dissertation represent efforts towards developing a personalized MACI platform with the ultimate goal of improving the success of tissue engineering outcomes for a wide range of patients. Cell-mediated hydrogel degradation is a promising strategy to promote tissue development while minimizing hydrogel failure; however, it needs to be tailored towards individual donor needs due to variable cellular enzyme synthesis rates. It is agreed upon that personalized medicine will require some *in silico* component to optimize therapies towards patients<sup>7</sup>. In this work, a developing model is used to help analyze and characterize experimental

observations. Most notably, this model allows us to characterize the concentration of enzyme and tissue around cells as a function of space and time.

Since the model is derived from a system of equations based on thermodynamics, physics, and statistical methods, it can readily be extended to other cell-laden hydrogels of different chemistry and cell type. Furthermore, our long-term goal is to use this model to predict optimal hydrogel designs for a particular donor, especially for poor performers, and thus improve tissue engineering for a wide range of donors. The hydrogel platform used herein is highly flexible with respect to controlling the initial hydrogel properties and selecting different enzyme-substrate pairs to control the catalytic and Michaelis-Menten constants. Thus, the model may help to overcome the challenges associated with donor-to-donor variability. Ultimately, this model may prove a powerful tool in the predictive and rational design of hydrogels while also serving as a means to study the complex relationship between hydrogel degradation and tissue formation.

### ***8.2.1 Hydrogel Characterization and Control over Cell-Polymer Interactions***

One of the key findings in this dissertation was that encapsulated cells cause local and bulk reductions in hydrogel crosslinking through sequestering monomers and quenching propagating radicals. As these interactions were ultimately found to be beneficial in tissue formation, a more thorough understanding of these interactions would be prudent.

In this work, a small subset of poly (ethylene glycol) (PEG) based polymers were investigated and the findings suggest that thiols<sup>8</sup> play a role in cell-polymer interactions that cause bulk reductions in hydrogel modulus. Other functional groups (such as acrylates) and polymer properties (such as polymer size, architecture, and hydrophobic character) were also

implicated in affecting cell-polymer interactions and should be investigated further. Cells also created local reductions in crosslinking density forming a gradient of polymer network around them. We hypothesized that propagating radicals were quenched by the cells resulting in the early termination of propagating radicals. The identification of these radicals may be critical in exerting control over the size of this polymer network gradient. Control over cell-polymer interactions and heterogeneities in polymer network formation will allow researchers another degree of control over hydrogel design.

As stated previously, characterization of the initial state of the hydrogel network is critical in understanding the resulting degradation behavior. A more sensitive technique capable of measuring the material modulus on a microscale around encapsulated cells would more definitively show local reductions in modulus. Such techniques might include atomic force microscopy or microrheology. This may also prove useful in studying the mechanical properties of newly formed tissue.

### ***8.2.2 Characterizing Hydrogel Degradation***

Hydrogel degradation has been identified as a critical feature in promoting cartilage tissue development of encapsulated cells. Cell-mediated degradation is attractive due to its potential to localize hydrogel degradation around cells while still maintaining hydrogel mechanics. In this dissertation, the effect of enzyme concentration on degradation was analyzed. Other parameters in hydrogel design should also be investigated. For instance, Michaelis-Menten catalytic constants  $k_{cat}$  and  $K_M$  can be investigated by changing enzyme-substrate pairs or tailoring the sequence of peptide crosslinkers to affect conversion.

### **8.2.3 Stimulation of Chondrocytes to Augment Anabolic Activity**

Chondrocytes can be stimulated to increase their matrix producing potential. In Chapter 7, adult chondrocytes are stimulated with IGF-1 to increase hydroxyproline production and decrease enzyme activity. Adult chondrocytes were stimulated with soluble IGF-1; however, tethering IGF-1 into the polymer network can potentially improve tissue production even more. Tethering growth factors into the polymer network presents the growth factor in a localized, concentrated manner and have been used with moderate success<sup>9,10</sup>. Other growth factors also warrant investigation such as the family of TGF- $\beta$ s and BMPs<sup>11,12</sup> which have been shown to have beneficial to the chondrogenic phenotype (either chondrogenic differentiation or increased matrix production).

### **8.3 Long Term Goals**

The long-term goal of this project is to robustly characterize local and bulk hydrogel degradation in enzyme-degradable and hydrolytically degradable systems and its effect on tissue formation of encapsulated chondrocytes. By developing methods to achieve multiple degradation behaviors (such as slow or fast degrading hydrolytically-labile crosslinks, wide or sharp degradation fronts in enzymatically sensitive hydrogels, or even perhaps a mixed mode of degradation), it is possible to design hydrogels that are tailored towards patient specific needs. In order to do this, *in silico* methods will be critical in considering all the important factors in hydrogel design while simulating outcomes that span the experimental space. The findings in this dissertation are a part of a larger effort to develop a computational model that can describe spatiotemporal enzymatic and hydrolytic hydrogel degradation and tissue elaboration. Additionally, the work detailed in this dissertation identified several critical factors that are

important in hydrogel design for cartilage tissue engineering, such as cell-polymer interactions and cell spacing. The ultimate goal of this project is to develop a computational model capable of rationally designing hydrogels to fit the needs of a wide range of patients accounting for donor variability due to age, sex, and lifestyle factors amongst other considerations.

#### 8.4 References

1. Nicodemus, G. D. & Bryant, S. J. Cell Encapsulation in Biodegradable Hydrogels for Tissue Engineering Applications. *Tissue Eng. Part B Rev.* **14**, 149–165 (2008).
2. Appelman, T. P., Mizrahi, J., Elisseeff, J. H. & Seliktar, D. The differential effect of scaffold composition and architecture on chondrocyte response to mechanical stimulation. *Biomaterials* **30**, 518–525 (2009).
3. Bryant, S. J. & Anseth, K. S. Hydrogel properties influence ECM production by chondrocytes photoencapsulated in poly (ethylene glycol) hydrogels. *J. Biomed. Mater. Res.* **59**, 63–72 (2002).
4. Neumann, A. J., Quinn, T. & Bryant, S. J. Nondestructive evaluation of a new hydrolytically degradable and photo-clickable PEG hydrogel for cartilage tissue engineering. *Acta Biomater.* **39**, 1–11 (2016).
5. Rice, M. A., Waters, K. R. & Anseth, K. S. Ultrasound monitoring of cartilaginous matrix evolution in degradable PEG hydrogels. *Acta Biomater.* **5**, 152–161 (2009).
6. Farnsworth, N., Bensard, C. & Bryant, S. J. The role of the PCM in reducing oxidative stress induced by radical initiated photoencapsulation of chondrocytes in poly(ethylene glycol) hydrogels. *Osteoarthritis Cartilage* **20**, 1326–1335 (2012).
7. Aguado, B. A., Grim, J. C., Rosales, A. M., Watson-Capps, J. J. & Anseth, K. S. Engineering precision biomaterials for personalized medicine. *Sci. Transl. Med.* **10**, eaam8645 (2018).
8. Aubry, S. *et al.* Cell-surface thiols affect cell entry of disulfide-conjugated peptides. *FASEB J.* **23**, 2956–2967 (2009).
9. Sridhar, B. V., Doyle, N. R., Randolph, M. A. & Anseth, K. S. Covalently tethered TGF- $\beta$ 1 with encapsulated chondrocytes in a PEG hydrogel system enhances extracellular matrix production. *J. Biomed. Mater. Res. A* **102**, 4464–4472 (2014).
10. Schneider, M. C., Chu, S., Randolph, M. A. & Bryant, S. J. An in vitro and in vivo comparison of cartilage growth in chondrocyte-laden matrix metalloproteinase-sensitive poly(ethylene glycol) hydrogels with localized transforming growth factor  $\beta$ 3. *Acta Biomater.* (2019). doi:10.1016/j.actbio.2019.03.046



11. Vinatier, C., Mrugala, D., Jorgensen, C., Guicheux, J. & Noël, D. Cartilage engineering: a crucial combination of cells, biomaterials and biofactors. *Trends Biotechnol.* **27**, 307–314 (2009).
12. Nestic, D. *et al.* Cartilage tissue engineering for degenerative joint disease. *Adv. Drug Deliv. Rev.* **58**, 300–322 (2006).

## BIBLIOGRAPHY

### Chapter 1

1. Nicodemus, G. D. & Bryant, S. J. Cell Encapsulation in Biodegradable Hydrogels for Tissue Engineering Applications. *Tissue Eng. Part B Rev.* **14**, 149–165 (2008).
2. Glowacki, J. & Mizuno, S. Collagen scaffolds for tissue engineering. *Biopolymers* **89**, 338–344 (2008).
3. A library of tunable agarose carbomer-based hydrogels for tissue engineering applications: The role of cross-linkers - Rossi - 2012 - Journal of Applied Polymer Science - Wiley Online Library. Available at: <https://onlinelibrary.wiley.com/doi/epdf/10.1002/app.34731>. (Accessed: 29th September 2018)
4. Jin, R. *et al.* Synthesis and characterization of hyaluronic acid–poly(ethylene glycol) hydrogels via Michael addition: An injectable biomaterial for cartilage repair. *Acta Biomater.* **6**, 1968–1977 (2010).
5. Chung, C. & Burdick, J. A. Engineering cartilage tissue. *Adv. Drug Deliv. Rev.* **60**, 243–262 (2008).
6. Lutolf, M. P. & Hubbell, J. A. Synthetic biomaterials as instructive extracellular microenvironments for morphogenesis in tissue engineering. *Nat. Biotechnol.* **23**, 47–55 (2005).
7. AO Research Institute Davos, Clavadelerstrasse 8, 7270 Davos Platz, Switzerland *et al.* Tissue engineering for articular cartilage repair – the state of the art. *Eur. Cell. Mater.* **25**, 248–267 (2013).
8. Bryant, S. J., Durand, K. L. & Anseth, K. S. Manipulations in hydrogel chemistry control photoencapsulated chondrocyte behavior and their extracellular matrix production. *J. Biomed. Mater. Res. A* **67A**, 1430–1436 (2003).
9. Lutolf, M. P. *et al.* Synthetic matrix metalloproteinase-sensitive hydrogels for the conduction of tissue regeneration: Engineering cell-invasion characteristics. *Proc. Natl. Acad. Sci.* **100**, 5413–5418 (2003).
10. Sridhar, B. V., Doyle, N. R., Randolph, M. A. & Anseth, K. S. Covalently tethered TGF- $\beta$ 1 with encapsulated chondrocytes in a PEG hydrogel system enhances extracellular matrix production. *J. Biomed. Mater. Res. A* **102**, 4464–4472 (2014).

11. Sridhar, B. V. *et al.* Development of a Cellularly Degradable PEG Hydrogel to Promote Articular Cartilage Extracellular Matrix Deposition. *Adv. Healthc. Mater.* **4**, 702–713 (2015).
12. Skaalure, S. C., Chu, S. & Bryant, S. J. An Enzyme-sensitive PEG Hydrogel Based on Aggrecan Catabolism for Cartilage Tissue Engineering. *Adv. Healthc. Mater.* **4**, 420–431 (2015).
13. Aisenbrey, E. A. & Bryant, S. J. A MMP7-sensitive photoclickable biomimetic hydrogel for MSC encapsulation towards engineering human cartilage. *J. Biomed. Mater. Res. A* **0**,
14. Bryant, S. J. & Anseth, K. S. Hydrogel properties influence ECM production by chondrocytes photoencapsulated in poly (ethylene glycol) hydrogels. *J. Biomed. Mater. Res.* **59**, 63–72 (2002).
15. Anseth, K. S., Bowman, C. N. & Brannon-Peppas, L. Mechanical properties of hydrogels and their experimental determination. *Biomaterials* **17**, 1647–1657 (1996).
16. Engler, A. J., Sen, S., Sweeney, H. L. & Discher, D. E. Matrix Elasticity Directs Stem Cell Lineage Specification. *Cell* **126**, 677–689 (2006).
17. Chaudhuri, O. *et al.* Substrate stress relaxation regulates cell spreading. *Nat. Commun.* **6**, 6365 (2015).
18. Hydrogels with tunable stress relaxation regulate stem cell fate and activity | Nature Materials. Available at: <https://www.nature.com/articles/nmat4489>. (Accessed: 14th November 2018)
19. Richardson, B. M., Wilcox, D. G., Randolph, M. A. & Anseth, K. S. Hydrazone covalent adaptable networks modulate extracellular matrix deposition for cartilage tissue engineering. *Acta Biomater.* (2018). doi:10.1016/j.actbio.2018.11.014
20. Xia, L.-W. *et al.* Nano-structured smart hydrogels with rapid response and high elasticity. *Nat. Commun.* **4**, 2226 (2013).
21. Secondary Photocrosslinking of Click Hydrogels To Probe Myoblast Mechanotransduction in Three Dimensions - Journal of the American Chemical Society (ACS Publications). Available at: <https://pubs.acs.org/doi/10.1021/jacs.8b07551>. (Accessed: 15th November 2018)
22. Brown, T. E. *et al.* Photopolymerized dynamic hydrogels with tunable viscoelastic properties through thioester exchange. *Biomaterials* **178**, 496–503 (2018).

23. Kääh, M. J., Ap Gwynn, I. & Nötzli, H. P. Collagen fibre arrangement in the tibial plateau articular cartilage of man and other mammalian species. *J. Anat.* **193**, 23–34 (1998).
24. Nap, R. J. & Szleifer, I. Structure and Interactions of Aggrecans: Statistical Thermodynamic Approach. *Biophys. J.* **95**, 4570–4583 (2008).
25. Horkay, F., Basser, P. J., Hecht, A.-M. & Geissler, E. Gel-like behavior in aggrecan assemblies. *J. Chem. Phys.* **128**, 135103 (2008).
26. Ng, L. *et al.* Individual cartilage aggrecan macromolecules and their constituent glycosaminoglycans visualized via atomic force microscopy. *J. Struct. Biol.* **143**, 242–257 (2003).
27. Kiani, C., Chen, L., Wu, Y. J., Yee, A. J. & Yang, B. B. Structure and function of aggrecan. *Cell Res.* **12**, 19–32 (2002).
28. Bryant, S. J. & Anseth, K. S. Controlling the spatial distribution of ECM components in degradable PEG hydrogels for tissue engineering cartilage. *J. Biomed. Mater. Res. A* **64A**, 70–79 (2003).
29. Dhote, V. *et al.* On the role of hydrogel structure and degradation in controlling the transport of cell-secreted matrix molecules for engineered cartilage. *J. Mech. Behav. Biomed. Mater.* **19**, 61–74 (2013).
30. Neumann, A. J., Quinn, T. & Bryant, S. J. Nondestructive evaluation of a new hydrolytically degradable and photo-clickable PEG hydrogel for cartilage tissue engineering. *Acta Biomater.* **39**, 1–11 (2016).
31. Metters, A. T., Bowman, C. N. & Anseth, K. S. A Statistical Kinetic Model for the Bulk Degradation of PLA-b-PEG-b-PLA Hydrogel Networks. *J. Phys. Chem. B* **104**, 7043–7049 (2000).
32. Martens, P., Metters, A. T., Anseth, K. S. & Bowman, C. N. A Generalized Bulk-Degradation Model for Hydrogel Networks Formed from Multivinyl Cross-linking Molecules. *J. Phys. Chem. B* **105**, 5131–5138 (2001).
33. Skaalure, S. C., Akalp, U., Vernerey, F. J. & Bryant, S. J. Tuning Reaction and Diffusion Mediated Degradation of Enzyme-Sensitive Hydrogels. *Adv. Healthc. Mater.* **5**, 432–438 (2016).
34. Flory, P. J. *Principles of Polymer Chemistry*. (Cornell University Press, 1953).
35. Lustig, S. R. & Peppas, N. A. Solute diffusion in swollen membranes. IX. Scaling laws for solute diffusion in gels. *J. Appl. Polym. Sci.* **36**, 735–747 (1988).

36. Metters, A. T., Anseth, K. S. & Bowman, C. N. Fundamental studies of a novel, biodegradable PEG-b-PLA hydrogel. *Polymer* **41**, 3993–4004 (2000).
37. Lalitha Sridhar, S. & Vernerey, F. Localized Enzymatic Degradation of Polymers: Physics and Scaling Laws. *Phys. Rev. Appl.* **9**, 031001 (2018).
38. Sridhar, S. L. *et al.* Heterogeneity is key to hydrogel-based cartilage tissue regeneration. *Soft Matter* **13**, 4841–4855 (2017).
39. Akalp, U., Bryant, S. J. & Vernerey, F. J. Tuning tissue growth with scaffold degradation in enzyme-sensitive hydrogels: a mathematical model. *Soft Matter* **12**, 7505–7520 (2016).
40. Dhote, V. & Vernerey, F. J. Mathematical model of the role of degradation on matrix development in hydrogel scaffold. *Biomech. Model. Mechanobiol.* **13**, 167–183 (2013).
41. Aguado, B. A., Grim, J. C., Rosales, A. M., Watson-Capps, J. J. & Anseth, K. S. Engineering precision biomaterials for personalized medicine. *Sci. Transl. Med.* **10**, eaam8645 (2018).
42. Behery, O., Siston, R. A., Harris, J. D. & Flanigan, D. C. Treatment of Cartilage Defects of the Knee: Expanding on the Existing Algorithm. *Clin. J. Sport Med.* **24**, 21–30 (2014).
43. Bryant, S. J. & Vernerey, F. J. Programmable Hydrogels for Cell Encapsulation and Neo-Tissue Growth to Enable Personalized Tissue Engineering. *Adv. Healthc. Mater.* **7**, (2018).

### Chapter 3

1. Skaalure, S. C., Chu, S. & Bryant, S. J. An Enzyme-sensitive PEG Hydrogel Based on Aggrecan Catabolism for Cartilage Tissue Engineering. *Adv. Healthc. Mater.* **4**, 420–431 (2015).
2. Aisenbrey, E. A. & Bryant, S. J. A MMP7-sensitive photoclickable biomimetic hydrogel for MSC encapsulation towards engineering human cartilage. *J. Biomed. Mater. Res. A* **0**,
3. Liu, M. *et al.* Injectable hydrogels for cartilage and bone tissue engineering. *Bone Res.* **5**, 17014 (2017).
4. Patel, D., Sharma, S., Screen, H. R. C. & Bryant, S. J. Effects of cell adhesion motif, fiber stiffness, and cyclic strain on tenocyte gene expression in a tendon mimetic fiber composite hydrogel. *Biochem. Biophys. Res. Commun.* **499**, 642–647 (2018).
5. Aurand, E. R., Lampe, K. J. & Bjugstad, K. B. Defining and designing polymers and hydrogels for neural tissue engineering. *Neurosci. Res.* **72**, 199–213 (2012).
6. Fairbanks, B. D. *et al.* A Versatile Synthetic Extracellular Matrix Mimic via Thiol-Norbornene Photopolymerization. *Adv. Mater.* **21**, 5005–5010 (2009).

7. Nicodemus, G. D. & Bryant, S. J. Cell Encapsulation in Biodegradable Hydrogels for Tissue Engineering Applications. *Tissue Eng. Part B Rev.* **14**, 149–165 (2008).
8. Engler, A. J., Sen, S., Sweeney, H. L. & Discher, D. E. Matrix Elasticity Directs Stem Cell Lineage Specification. *Cell* **126**, 677–689 (2006).
9. Bryant, S. J. & Anseth, K. S. Hydrogel properties influence ECM production by chondrocytes photoencapsulated in poly(ethylene glycol) hydrogels. *J. Biomed. Mater. Res.* **59**, 63–72 (2002).
10. Bryant, S. J. & Anseth, K. S. Controlling the spatial distribution of ECM components in degradable PEG hydrogels for tissue engineering cartilage. *J. Biomed. Mater. Res. A* **64A**, 70–79 (2003).
11. Appelman, T. P., Mizrahi, J., Elisseeff, J. H. & Seliktar, D. The differential effect of scaffold composition and architecture on chondrocyte response to mechanical stimulation. *Biomaterials* **30**, 518–525 (2009).
12. Neumann, A. J., Quinn, T. & Bryant, S. J. Nondestructive evaluation of a new hydrolytically degradable and photo-clickable PEG hydrogel for cartilage tissue engineering. *Acta Biomater.* **39**, 1–11 (2016).
13. Rice, M. A., Waters, K. R. & Anseth, K. S. Ultrasound monitoring of cartilaginous matrix evolution in degradable PEG hydrogels. *Acta Biomater.* **5**, 152–161 (2009).
14. Nguyen, K. T. & West, J. L. Photopolymerizable hydrogels for tissue engineering applications. *Biomaterials* **23**, 4307–4314 (2002).
15. Roberts, J. J. & Bryant, S. J. Comparison of Photopolymerizable Thiol-ene PEG and Acrylate-Based PEG Hydrogels for Cartilage Development. *Biomaterials* **34**, 9969–9979 (2013).
16. Kuhl, T. *et al.* Direct Measurement of Polyethylene Glycol Induced Depletion Attraction between Lipid Bilayers. *Langmuir* **12**, 3003–3014 (1996).
17. Kim, M. *et al.* Surface Plasmon Resonance Study of the Binding of PEO–PPO–PEO Triblock Copolymer and PEO Homopolymer to Supported Lipid Bilayers. *Langmuir* **34**, 6703–6712 (2018).
18. Yasuda, S. *et al.* Dystrophic heart failure blocked by membrane sealant poloxamer. *Nature* **436**, 1025–1029 (2005).
19. Liu-Snyder, P., Logan, M. P., Shi, R., Smith, D. T. & Borgens, R. B. Neuroprotection from secondary injury by polyethylene glycol requires its internalization. *J. Exp. Biol.* **210**, 1455–1462 (2007).
20. Mina, E. W., Lasagna-Reeves, C., Glabe, C. G. & Kaye, R. Poloxamer 188 Copolymer Membrane Sealant Rescues Toxicity of Amyloid Oligomers In Vitro. *J. Mol. Biol.* **391**, 577–585 (2009).

21. Chapter 18 Induction of Mammalian Somatic Cell Hybridization by Polyethylene Glycol. *Methods Cell Biol.* **15**, 325–338 (1977).
22. Ross, P. C. & Hui, S. W. Polyethylene glycol enhances lipoplex-cell association and lipofection. *Biochim. Biophys. Acta BBA - Biomembr.* **1421**, 273–283 (1999).
23. Bryant, S. J., Cuy, J. L., Hauch, K. D. & Ratner, B. D. Photo-patterning of porous hydrogels for tissue engineering. *Biomaterials* **28**, 2978–2986 (2007).
24. Skaalure, S. C., Akalp, U., Vernerey, F. J. & Bryant, S. J. Tuning Reaction and Diffusion Mediated Degradation of Enzyme-Sensitive Hydrogels. *Adv. Healthc. Mater.* **5**, 432–438 (2016).
25. Sanchez-Adams, J. & Athanasiou, K. A. Biomechanical Characterization of Single Chondrocytes. in *Cellular and Biomolecular Mechanics and Mechanobiology* (ed. Gefen, A.) **4**, 247–266 (Springer Berlin Heidelberg, 2010).
26. Sasazaki, Y., Seedhom, B. B. & Shore, R. Morphology of the bovine chondrocyte and of its cytoskeleton in isolation and in situ: are chondrocytes ubiquitously paired through the entire layer of articular cartilage? *Rheumatology* **47**, 1641–1646 (2008).
27. Aubry, S. *et al.* Cell-surface thiols affect cell entry of disulfide-conjugated peptides. *FASEB J.* **23**, 2956–2967 (2009).
28. Woodward, C. E. & Forsman, J. Density Functional Study of Surface Forces in Solutions Containing Star-Shaped Polymers. *Macromolecules* **37**, 7034–7041 (2004).
29. Li, Y., Wei, X., Zhou, J. & Wei, L. The Age-Related Changes in Cartilage and Osteoarthritis. *BioMed Res. Int.* **2013**, e916530 (2013).
30. Loeser, R. F. Aging and Osteoarthritis: The Role of Chondrocyte Senescence and Aging Changes in the Cartilage Matrix. *Osteoarthr. Cartil. OARS Osteoarthr. Res. Soc.* **17**, 971–979 (2009).
31. Yang, L., Carlson, S. G., McBurney, D. & Horton, W. E. Multiple Signals Induce Endoplasmic Reticulum Stress in Both Primary and Immortalized Chondrocytes Resulting in Loss of Differentiation, Impaired Cell Growth, and Apoptosis. *J. Biol. Chem.* **280**, 31156–31165 (2005).
32. Yang, L., McBurney, D., Tang, S.-C., Carlson, S. G. & Horton, W. E. A novel role for Bcl-2 associated-athanogene-1 (Bag-1) in regulation of the endoplasmic reticulum stress response in mammalian chondrocytes. *J. Cell. Biochem.* **102**, 786–800 (2007).
33. Loeser, R. F. *et al.* Articular Chondrocytes Express the Receptor for Advanced Glycation End Products. *Arthritis Rheum.* **52**, 2376–2385 (2005).
34. O’Brien, A. K. & Bowman, C. N. Impact of Oxygen on Photopolymerization Kinetics and Polymer Structure. *Macromolecules* **39**, 2501–2506 (2006).

35. Bentivoglio Ruiz, C., Machado, L., Volponi, J. & Segura Pino, E. Oxygen Inhibition and Coating Thickness Effects on Uv Radiation Curing of Weatherfast Clearcoats Studied by Photo-DSC. *J. Therm. Anal. Calorim.* **75**, 507–512 (2004).
36. Farnsworth, N., Bensard, C. & Bryant, S. J. The role of the PCM in reducing oxidative stress induced by radical initiated photoencapsulation of chondrocytes in poly(ethylene glycol) hydrogels. *Osteoarthritis Cartilage* **20**, 1326–1335 (2012).
37. Lobo, V., Patil, A., Phatak, A. & Chandra, N. Free radicals, antioxidants and functional foods: Impact on human health. *Pharmacogn. Rev.* **4**, 118–126 (2010).
38. Farnsworth, N., Bensard, C. & Bryant, S. J. The role of the PCM in reducing oxidative stress induced by radical initiated photoencapsulation of chondrocytes in poly(ethylene glycol) hydrogels. *Osteoarthritis Cartilage* **20**, 1326–1335 (2012).
39. Richards, D. M. C., Dean, R. T. & Jessup, W. Membrane proteins are critical targets in free radical mediated cytolysis. *Biochim. Biophys. Acta BBA - Biomembr.* **946**, 281–288 (1988).
40. Donoghue, N., Yam, P. T., Jiang, X. M. & Hogg, P. J. Presence of closely spaced protein thiols on the surface of mammalian cells. *Protein Sci. Publ. Protein Soc.* **9**, 2436–2445 (2000).

#### Chapter 4

1. Nicodemus, G. D., Skaalure, S. C. & Bryant, S. J. Gel structure impacts pericellular and extracellular matrix deposition which subsequently alters metabolic activities in chondrocyte-laden PEG hydrogels. *Acta Biomater.* **7**, 492–504 (2011).
2. Skaalure, S. C., Akalp, U., Vernerey, F. J. & Bryant, S. J. Tuning Reaction and Diffusion Mediated Degradation of Enzyme-Sensitive Hydrogels. *Adv. Healthc. Mater.* **5**, 432–438 (2016).
3. Dhote, V. & Vernerey, F. J. Mathematical model of the role of degradation on matrix development in hydrogel scaffold. *Biomech. Model. Mechanobiol.* **13**, 167–183 (2013).
4. Akalp, U., Bryant, S. J. & Vernerey, F. J. Tuning tissue growth with scaffold degradation in enzyme-sensitive hydrogels: a mathematical model. *Soft Matter* **12**, 7505–7520 (2016).
5. O'Donnell, P. B. & McGinity, J. W. Preparation of microspheres by the solvent evaporation technique. *Adv. Drug Deliv. Rev.* **28**, 25–42 (1997).
6. Ashton, R. S., Banerjee, A., Punyani, S., Schaffer, D. V. & Kane, R. S. Scaffolds based on degradable alginate hydrogels and poly(lactide-co-glycolide) microspheres for stem cell culture. *Biomaterials* **28**, 5518–5525 (2007).
7. Damiaty, S., Kompella, U. B., Damiaty, S. A. & Kodzius, R. Microfluidic Devices for Drug Delivery Systems and Drug Screening. *Genes* **9**, (2018).



## Chapter 5

1. Tibbitt, M. W. & Anseth, K. S. Hydrogels as extracellular matrix mimics for 3D cell culture. *Biotechnol. Bioeng.* **103**, 655–663 (2009).
2. Tibbitt, M. W., Rodell, C. B., Burdick, J. A. & Anseth, K. S. Progress in material design for biomedical applications. *Proc Natl Acad Sci U S A.* **112**, 14444–14451 (2015).
3. Park, Y., Lutolf, M. P., Hubbell, J. A., Hunziker, E. B. & Wong, M. Bovine primary chondrocyte culture in synthetic matrix metalloproteinase-sensitive poly(ethylene glycol)-based hydrogels as a scaffold for cartilage repair. *Tissue Eng.* **10**, 515–522 (2004).
4. Sridhar, B. V., Brock J.L., Silver, J.S., Leight, J.L., Randolph, M.A., Anseth, K.S. Development of a cellularly degradable PEG hydrogel to promote articular cartilage extracellular matrix deposition. *Adv. Healthc. Mater.* **4**, 702–713 (2015).
5. Skaalure, S. C., Chu, S. & Bryant, S. J. An enzyme-sensitive PEG hydrogel based on aggrecan catabolism for cartilage tissue engineering. *Adv. Healthc. Mater.* **4**, 420–431 (2015).
6. Bahney, C. S., Hsu, C.-W., Yoo, J. U., West, J. L. & Johnstone, B. A bioresponsive hydrogel tuned to chondrogenesis of human mesenchymal stem cells. *FASEB J.* **25**, 1486–1496 (2011).
7. Parmar, P. A., Skaalure, S.C., Chow, L.W., St-Pierre, J.P., Stoichevska, V., Peng, Y.Y., Werkmeister, J.A., Ramshaw, J.A., Stevens, M.M., Temporally degradable collagen-mimetic hydrogels tuned to chondrogenesis of human mesenchymal stem cells. *Biomaterials* **99**, 56–71 (2016).
8. Bryant, S. J. & Anseth, K. S. Hydrogel properties influence ECM production by chondrocytes photoencapsulated in poly (ethylene glycol) hydrogels. *J. Biomed. Mater. Res.* **59**, 63–72 (2002).
9. Nicodemus, G. D., Skaalure, S. C. & Bryant, S. J. Gel structure has an impact on pericellular and extracellular matrix deposition, which subsequently alters metabolic activities in chondrocyte-laden PEG hydrogels. *Acta Biomater.* **7**, 492–504 (2011).
10. Hascall, V. C. & Sajdera, S. W. Physical properties and polydispersity of proteoglycan from bovine nasal cartilage. *J. Biol. Chem.* **245**, 4920–4930 (1970).
11. Lodish, H. & Baltimore, D.I. Collagen: The Fibrous Proteins of the Matrix. In: *Molecular Cell Biology*. NY: W. H. Freeman, 2000. Chapter 22.3.
12. Neumann, A. J., Quinn, T. & Bryant, S. J. Nondestructive evaluation of a new hydrolytically degradable and photo-clickable PEG hydrogel for cartilage tissue engineering. *Acta Biomater.* **39**, 1–11 (2016).
13. Roberts, J. J., Nicodemus, G. D., Greenwald, E. C. & Bryant, S. J. Degradation improves tissue formation in (un)loaded chondrocyte-laden hydrogels. *Clin. Orthop.* **469**, 2725–2734 (2011).

14. Vernerey, F. J., Greenwald, E. C. & Bryant, S. J. Triphasic mixture model of cell-mediated enzymatic degradation of hydrogels. *Comput. Methods Biomech. Biomed. Engin.* **15**, 1197–1210 (2012).
15. Dhote, V. *et al.* On the role of hydrogel structure and degradation in controlling the transport of cell-secreted matrix molecules for engineered cartilage. *J. Mech. Behav. Biomed. Mater.* **19**, 61–74 (2013).
16. Skaalure, S. C., Akalp, U., Vernerey, F. J. & Bryant, S. J. Tuning reaction and diffusion mediated degradation of enzyme-sensitive hydrogels. *Adv. Healthc. Mater.* **5**, 432–438 (2016).
17. Akalp, U., Bryant, S. J. & Vernerey, F. J. Tuning tissue growth with scaffold degradation in enzyme-sensitive hydrogels: a mathematical model. *Soft Matter* **12**, 7505–7520 (2016).
18. Farnsworth, N. L., Antunez, L. R. & Bryant, S. J. Dynamic compressive loading differentially regulates chondrocyte anabolic and catabolic activity with age. *Biotechnol. Bioeng.* **110**, 2046–2057 (2013).
19. Lutolf, M. P., Tirelli, N., Cerritelli, S., Cavalli, L. & Hubbell, J. A. Systematic modulation of Michael-type reactivity of thiols through the use of charged amino acids. *Bioconjug. Chem.* **12**, 1051–1056 (2001).
20. Roberts, J. J., Earnshaw, A., Ferguson, V. L. & Bryant, S. J. Comparative study of the viscoelastic mechanical behavior of agarose and poly(ethylene glycol) hydrogels. *J. Biomed. Mater. Res. B Appl. Biomater.* **99B**, 158–169 (2011).
21. Kim, Y.-J., Sah, R. L. Y., Doong, J.-Y. H. & Grodzinsky, A. J. Fluorometric assay of DNA in cartilage explants using Hoechst 33258. *Anal. Biochem.* **174**, 168–176 (1988).
22. Templeton, D. M. The basis and applicability of the dimethylmethylene blue binding assay for sulfated glycosaminoglycans. *Connect. Tissue Res.* **17**, 23–32 (1988).
23. Woessner, J. F. The determination of hydroxyproline in tissue and protein samples containing small proportions of this imino acid. *Arch. Biochem. Biophys.* **93**, 440–447 (1961).
24. Dhote, V. & Vernerey, F. J. Mathematical model of the role of degradation on matrix development in hydrogel scaffold. *Biomech. Model. Mechanobiol.* **13**, 167–183 (2014).
25. Peppas, N. A. *Structure and Properties of Polymeric Materials.* (1984).
26. Peppas, N. A. *Hydrogels in Medicine and Pharmacy, Vol.2. Polymers.* (CRC Press, 1987).
27. Macosko, C. & Miller, D. R. A new derivation of average molecular weights of nonlinear polymers. *Macromolecules* **9**, 199–206 (1976).
28. Tibbitt, M. W., Kloxin, A. M., Sawicki, L. A. & Anseth, K. S. Mechanical properties and degradation of chain and step-polymerized photodegradable hydrogels. *Macromolecules* **46**, 2785–2792 (2013).

29. Lutolf, M. P. *et al.* Synthetic matrix metalloproteinase-sensitive hydrogels for the conduction of tissue regeneration: Engineering cell-invasion characteristics. *Proc Natl Acad Sci U S A.* **100**, 5413–5418 (2003).
30. Akalp, U. *et al.* Determination of the polymer-solvent interaction parameter for PEG hydrogels in water: application of a self learning algorithm. *Polymer* **66**, 135–147 (2015).
31. Brannon-Peppas, L. & Peppas, N. A. Solute and penetrant diffusion in swellable polymers. IX. The mechanisms of drug release from ph-sensitive swelling-controlled systems. *J. Controlled Release* **8**, 267–274 (1989).
32. Lustig, S. R. & Peppas, N. A. Solute diffusion in swollen membranes. IX. Scaling laws for solute diffusion in gels. *J. Appl. Polym. Sci.* **36**, 735–747 (1988).
33. Merrill, E. W., Dennison, K. A. & Sung, C. Partitioning and diffusion of solutes in hydrogels of poly(ethylene oxide). *Biomaterials* **14**, 1117–1126 (1993).
34. Anderson, M. L., Mott, P. H. & Roland, C. M. The compression of bonded rubber disks. *Rubber Chem. Technol.* **77**, 293–302 (2004).
35. Anseth, K. S., Bowman, C. N. & Brannon-Peppas, L. Mechanical properties of hydrogels and their experimental determination. *Biomaterials* **17**, 1647–1657 (1996).
36. Gould, S. T., Darling, N. J. & Anseth, K. S. Small peptide functionalized thiol–ene hydrogels as culture substrates for understanding valvular interstitial cell activation and de novo tissue deposition. *Acta Biomater.* **8**, 3201–3209 (2012).
37. Akalp, U., Bryant, S. J. & Vernerey, F. J. Tuning tissue growth with scaffold degradation in enzyme-sensitive hydrogels: a mathematical model. *Soft Matter* **12**, 7505–7520 (2016).
38. Wong, M., Ponticiello, M., Kovanen, V. & Jurvelin, J. S. Volumetric changes of articular cartilage during stress relaxation in unconfined compression. *J. Biomech.* **33**, 1049–1054 (2000).
39. Mow, V. C., Gibbs, M. C., Lai, W. M., Zhu, W. B. & Athanasiou, K. A. Biphasic indentation of articular cartilage-II. A numerical algorithm and an experimental study. *J. Biomech.* **22**, 853–861 (1989).
40. Guilak, F., Jones, W. R., Ting-Beall, H. P. & Lee, G. M. The deformation behavior and mechanical properties of chondrocytes in articular cartilage. *Osteoarthritis Cartilage* **7**, 59–70 (1999).
41. Vernerey, F. J. A mixture approach to investigate interstitial growth in engineering scaffolds. *Biomech. Model. Mechanobiol.* **15**, 259–278 (2016).
42. Aboudi, J., Arnold, S. M. & Bednarczyk, B. A. *Micromechanics of Composite Materials: A Generalized Multiscale Analysis Approach.* (Butterworth-Heinemann, 2012).
43. Nemat-Nasser, S. & Hori, M. *Micromechanics: overall properties of heterogeneous materials.* (Elsevier, 2013).

44. Hoyle, C. E. & Bowman, C. N. Thiol–ene click chemistry. *Angew. Chem. Int. Ed.* **49**, 1540–1573 (2010).
45. Fairbanks, B. D. *et al.* A versatile synthetic extracellular matrix mimic via thiol-norbornene photopolymerization. *Adv. Mater.* **21**, 5005–5010 (2009).
46. Kääh, M. J., Ap Gwynn, I. & Nötzli, H. P. Collagen fibre arrangement in the tibial plateau articular cartilage of man and other mammalian species. *J. Anat.* **193**, 23–34 (1998).
47. Firestein, G. S., Budd, R., Gabriel, S. E., McInnes, I. B. & O’Dell, J. R. *Kelley and Firestein’s Textbook of Rheumatology*. (Elsevier Health Sciences, 2016).
48. Li, Y., Wei, X., Zhou, J. & Wei, L. The age-related changes in cartilage and osteoarthritis. *BioMed Res. Int.* **2013**, e916530 (2013).
49. Lobo, V., Patil, A., Phatak, A. & Chandra, N. Free radicals, antioxidants and functional foods: Impact on human health. *Pharmacogn. Rev.* **4**, 118–126 (2010).
50. Richards, D. M. C., Dean, R. T. & Jessup, W. Membrane proteins are critical targets in free radical mediated cytolysis. *Biochim. Biophys. Acta BBA - Biomembr.* **946**, 281–288 (1988).
51. Donoghue, N., Yam, P. T., Jiang, X. M. & Hogg, P. J. Presence of closely spaced protein thiols on the surface of mammalian cells. *Protein Sci. Publ. Protein Soc.* **9**, 2436–2445 (2000).
52. Farnsworth, N., Bensard, C. & Bryant, S. J. The role of the PCM in reducing oxidative stress induced by radical initiated photoencapsulation of chondrocytes in poly(ethylene glycol) hydrogels. *Osteoarthritis Cartilage* **20**, 1326–1335 (2012).
53. Flannery, C. *et al.* Variability in the G3 domain content of bovine aggrecan from cartilage extracts and chondrocyte cultures. *Arch. Biochem. Biophys.* **297**, 52–60 (1992).
54. Ilic, M. Z., Robinson, H. C. & Handley, C. J. Characterization of aggrecan retained and lost from the extracellular matrix of articular cartilage: involvement of carboxy-terminal processing in the catabolism of aggrecan. *J. Biol. Chem.* **273**, 17451–17458 (1998).
55. Nicodemus, G. D. & Bryant, S. J. The role of hydrogel structure and dynamic loading on chondrocyte gene expression and matrix formation. *J. Biomech.* **41**, 1528–1536 (2008).
56. Kashiwagi, M., Tortorella, M., Nagase, H. & Brew, K. TIMP-3 Is a potent inhibitor of Aggrecanase 1 (ADAM-TS4) and Aggrecanase 2 (ADAM-TS5). *J. Biol. Chem.* **276**, 12501–12504 (2001).
57. Hashimoto, G., Aoki, T., Nakamura, H., Tanzawa, K. & Okada, Y. Inhibition of ADAMTS4 (aggrecanase-1) by tissue inhibitors of metalloproteinases (TIMP-1, 2, 3 and 4). *FEBS Lett.* **494**, 192–195 (2001).
58. Gavrilovic, J., Hembry, R. M., Reynolds, J. J. & Murphy, G. Tissue inhibitor of metalloproteinases (TIMP) regulates extracellular type I collagen degradation by chondrocytes and endothelial cells. *J. Cell Sci.* **87 ( Pt 2)**, 357–362 (1987).

59. Tortorella, M. D. *et al.*  $\alpha$ 2-macroglobulin is a novel substrate for ADAMTS-4 and ADAMTS-5 and represents an endogenous inhibitor of these enzymes. *J. Biol. Chem.* **279**, 17554–17561 (2004).
60. Dangott, L. J. & Cunningham, L. W. Residual  $\alpha$ 2-macroglobulin in fetal calf serum and properties of its complex with thrombin. *Biochem. Biophys. Res. Commun.* **107**, 1243–1251 (1982).
61. Loeser, R. F. Aging and osteoarthritis: the role of chondrocyte senescence and aging changes in the cartilage Matrix. *Osteoarthr. Cartil. OARS Osteoarthr. Res. Soc.* **17**, 971–979 (2009).
62. Skaalure, S. C., Milligan, I. L. & Bryant, S. J. Age impacts extracellular matrix metabolism in chondrocytes encapsulated in degradable hydrogels. *Biomed. Mater.* **7**, 024111 (2012).

## Chapter 6

1. Nicodemus, G. D. & Bryant, S. J. Cell Encapsulation in Biodegradable Hydrogels for Tissue Engineering Applications. *Tissue Eng. Part B Rev.* **14**, 149–165 (2008).
2. Metters, A. T., Bowman, C. N. & Anseth, K. S. A Statistical Kinetic Model for the Bulk Degradation of PLA-b-PEG-b-PLA Hydrogel Networks. *J. Phys. Chem. B* **104**, 7043–7049 (2000).
3. Martens, P., Metters, A. T., Anseth, K. S. & Bowman, C. N. A Generalized Bulk-Degradation Model for Hydrogel Networks Formed from Multivinyl Cross-linking Molecules. *J. Phys. Chem. B* **105**, 5131–5138 (2001).
4. Neumann, A. J., Quinn, T. & Bryant, S. J. Nondestructive evaluation of a new hydrolytically degradable and photo-clickable PEG hydrogel for cartilage tissue engineering. *Acta Biomater.* **39**, 1–11 (2016).
5. Dadsetan, M., Szatkowski, J. P., Yaszemski, M. J. & Lu, L. Characterization of Photo-Cross-Linked Oligo[poly(ethylene glycol) fumarate] Hydrogels for Cartilage Tissue Engineering. *Biomacromolecules* **8**, 1702–1709 (2007).
6. Bryant, S. J. & Anseth, K. S. Controlling the spatial distribution of ECM components in degradable PEG hydrogels for tissue engineering cartilage. *J. Biomed. Mater. Res. A* **64A**, 70–79 (2003).
7. Park, H., Temenoff, J. S., Holland, T. A., Tabata, Y. & Mikos, A. G. Delivery of TGF- $\beta$ 1 and chondrocytes via injectable, biodegradable hydrogels for cartilage tissue engineering applications. *Biomaterials* **26**, 7095–7103 (2005).
8. Wang, Y. *et al.* In vitro study on the degradation of lithium-doped hydroxyapatite for bone tissue engineering scaffold. *Mater. Sci. Eng. C* **66**, 185–192 (2016).

9. Andriano, K. P., Tabata, Y., Ikada, Y. & Heller, J. In vitro and in vivo comparison of bulk and surface hydrolysis in absorbable polymer scaffolds for tissue engineering. *J. Biomed. Mater. Res.* **48**, 602–612 (1999).
10. Lam, C. X. F., Hutmacher, D. W., Schantz, J.-T., Woodruff, M. A. & Teoh, S. H. Evaluation of polycaprolactone scaffold degradation for 6 months in vitro and in vivo. *J. Biomed. Mater. Res. A* **90A**, 906–919 (2009).
11. Lu, H. H. *et al.* Anterior cruciate ligament regeneration using braided biodegradable scaffolds: in vitro optimization studies. *Biomaterials* **26**, 4805–4816 (2005).
12. Cooper, J. A., Lu, H. H., Ko, F. K., Freeman, J. W. & Laurencin, C. T. Fiber-based tissue-engineered scaffold for ligament replacement: design considerations and in vitro evaluation. *Biomaterials* **26**, 1523–1532 (2005).
13. Mahoney, M. J. & Anseth, K. S. Three-dimensional growth and function of neural tissue in degradable polyethylene glycol hydrogels. *Biomaterials* **27**, 2265–2274 (2006).
14. Kim, B.-S. & Mooney, D. J. Engineering smooth muscle tissue with a predefined structure. *J. Biomed. Mater. Res.* **41**, 322–332 (1998).
15. Fidkowski, C. *et al.* Endothelialized Microvasculature Based on a Biodegradable Elastomer. *Tissue Eng.* **11**, 302–309 (2005).
16. Bryant, S. J. & Anseth, K. S. Hydrogel properties influence ECM production by chondrocytes photoencapsulated in poly(ethylene glycol) hydrogels. *J. Biomed. Mater. Res.* **59**, 63–72 (2002).
17. Nicodemus, G. D., Skaalure, S. C. & Bryant, S. J. Gel structure has an impact on pericellular and extracellular matrix deposition, which subsequently alters metabolic activities in chondrocyte-laden PEG hydrogels. *Acta Biomater.* **7**, 492–504 (2011).
18. Metters, A. T., Bowman, C. N. & Anseth, K. S. Verification of scaling laws for degrading PLA-b-PEG-b-PLA hydrogels. *AIChE J.* **47**, 1432–1437 (2001).
19. Metters, A. T., Anseth, K. S. & Bowman, C. N. A Statistical Kinetic Model for the Bulk Degradation of PLA-b-PEG-b-PLA Hydrogel Networks: Incorporating Network Non-Idealities. *J. Phys. Chem. B* **105**, 8069–8076 (2001).
20. Tibbitt, M. W., Kloxin, A. M., Sawicki, L. A. & Anseth, K. S. Mechanical Properties and Degradation of Chain and Step-Polymerized Photodegradable Hydrogels. *Macromolecules* **46**, 2785–2792 (2013).
21. Bryant, S. J., Bender, R. J., Durand, K. L. & Anseth, K. S. Encapsulating chondrocytes in degrading PEG hydrogels with high modulus: Engineering gel structural changes to facilitate cartilaginous tissue production. *Biotechnol. Bioeng.* **86**, 747–755 (2004).
22. Bryant, S. J., Anseth, K. S., Lee, D. A. & Bader, D. L. Crosslinking density influences the morphology of chondrocytes photoencapsulated in PEG hydrogels during the application of compressive strain. *J. Orthop. Res.* **22**, 1143–1149 (2004).

23. Farnsworth, N., Bensard, C. & Bryant, S. J. The role of the PCM in reducing oxidative stress induced by radical initiated photoencapsulation of chondrocytes in poly(ethylene glycol) hydrogels. *Osteoarthritis Cartilage* **20**, 1326–1335 (2012).
24. Dhote, V. & Vernerey, F. J. Mathematical model of the role of degradation on matrix development in hydrogel scaffold. *Biomech. Model. Mechanobiol.* **13**, 167–183 (2013).
25. Dhote, V. *et al.* On the role of hydrogel structure and degradation in controlling the transport of cell-secreted matrix molecules for engineered cartilage. *J. Mech. Behav. Biomed. Mater.* **19**, 61–74 (2013).
26. Bryant, S. J., Cuy, J. L., Hauch, K. D. & Ratner, B. D. Photo-patterning of porous hydrogels for tissue engineering. *Biomaterials* **28**, 2978–2986 (2007).
27. Kim, Y.-J., Sah, R. L. Y., Doong, J.-Y. H. & Grodzinsky, A. J. Fluorometric assay of DNA in cartilage explants using Hoechst 33258. *Anal. Biochem.* **174**, 168–176 (1988).
28. Templeton, D. M. The basis and applicability of the dimethylmethylene blue binding assay for sulfated glycosaminoglycans. *Connect. Tissue Res.* **17**, 23–32 (1988).
29. Woessner, J. F. The determination of hydroxyproline in tissue and protein samples containing small proportions of this imino acid. *Arch. Biochem. Biophys.* **93**, 440–447 (1961).
30. Vernerey, F., Liu, W. K. & Moran, B. Multi-scale micromorphic theory for hierarchical materials. *J. Mech. Phys. Solids* **55**, 2603–2651 (2007).
31. Flory, P. J. *Principles of Polymer Chemistry*. (Cornell University Press, 1953).
32. Akalp, U. *et al.* Determination of the polymer-solvent interaction parameter for PEG hydrogels in water: Application of a self learning algorithm. *Polymer* **66**, 135–147 (2015).
33. Kääh, M. J., Ap Gwynn, I. & Nötzli, H. P. Collagen fibre arrangement in the tibial plateau articular cartilage of man and other mammalian species. *J. Anat.* **193**, 23–34 (1998).
34. Ng, L. *et al.* Individual cartilage aggrecan macromolecules and their constituent glycosaminoglycans visualized via atomic force microscopy. *J. Struct. Biol.* **143**, 242–257 (2003).
35. Anderson, M. L., Mott, P. H. & Roland, C. M. The Compression of Bonded Rubber Disks. *Rubber Chem. Technol.* **77**, 293–302 (2004).
36. Wong, M., Ponticiello, M., Kovanen, V. & Jurvelin, J. S. Volumetric changes of articular cartilage during stress relaxation in unconfined compression. *J. Biomech.* **33**, 1049–1054 (2000).
37. Mow, V. C., Gibbs, M. C., Lai, W. M., Zhu, W. B. & Athanasiou, K. A. Biphasic indentation of articular cartilage—II. A numerical algorithm and an experimental study. *J. Biomech.* **22**, 853–861 (1989).

38. Anseth, K. S., Bowman, C. N. & Brannon-Peppas, L. Mechanical properties of hydrogels and their experimental determination. *Biomaterials* **17**, 1647–1657 (1996).
39. Gould, S. T., Darling, N. J. & Anseth, K. S. Small peptide functionalized thiol–ene hydrogels as culture substrates for understanding valvular interstitial cell activation and de novo tissue deposition. *Acta Biomater.* **8**, 3201–3209 (2012).
40. Guilak, F., Jones, W. R., Ting-Beall, H. P. & Lee, G. M. The deformation behavior and mechanical properties of chondrocytes in articular cartilage. *Osteoarthritis Cartilage* **7**, 59–70 (1999).
41. Vernerey, F. J. A mixture approach to investigate interstitial growth in engineering scaffolds. *Biomech. Model. Mechanobiol.* **15**, 259–278 (2016).
42. Vernerey, F. J., Liu, W. K., Moran, B. & Olson, G. A micromorphic model for the multiple scale failure of heterogeneous materials. *J. Mech. Phys. Solids* **56**, 1320–1347 (2008).
43. Aboudi, J., Arnold, S. M. & Bednarczyk, B. A. *Micromechanics of Composite Materials*. (Butterworth-Heinemann, 2013).
44. Nemat-Nasser, S. & Hori, M. *Micromechanics: Overall Properties of Heterogeneous Materials*. (Elsevier, 2013).
45. Madras, N. & Sokal, A. D. The pivot algorithm: A highly efficient Monte Carlo method for the self-avoiding walk. *J. Stat. Phys.* **50**, 109–186 (1988).
46. Brannon-Peppas, L. & Peppas, N. A. Solute and penetrant diffusion in swellable polymers. IX. The mechanisms of drug release from pH-sensitive swelling-controlled systems. *J. Controlled Release* **8**, 267–274 (1989).
47. Gigout, A., Buschmann, M. D. & Jolicoeur, M. Chondrocytes Cultured in Stirred Suspension with Serum-Free Medium Containing Pluronic-68 Aggregate and Proliferate While Maintaining Their Differentiated Phenotype. *Tissue Eng. Part A* **15**, 2237–2248 (2009).
48. Tanaka, H., Sato, T. & Otsu, T. Long-lived polymer radicals, 2. An ESR study on the reactions of the propagating polymer radicals of N-methylacrylamide and N-methylmethacrylamide with vinyl monomers at room temperature. *Makromol. Chem.* **181**, 2421–2431 (1980).
49. Cho, H., Lai, T. C. & Kwon, G. S. Poly(ethylene glycol)-block-poly( $\epsilon$ -caprolactone) micelles for combination drug delivery: Evaluation of paclitaxel, cyclophosphamide and gossypol in intraperitoneal xenograft models of ovarian cancer. *J. Controlled Release* **166**, 1–9 (2013).
50. Tian, Y. *et al.* Utilization of micelles formed from poly(ethylene glycol)-block-poly( $\epsilon$ -caprolactone) block copolymers as nanocarriers to enable hydrophobic red two-photon absorbing (2PA) emitters for cells imaging. *J. Biomed. Mater. Res. A* **93**, 1068 (2010).
51. Chu, S., Sridhar, S. L., Skaalure, S. C., Vernerey, F. J. & Bryant, S. J. Understanding the Spatiotemporal Degradation Behavior of Aggrecanase-Sensitive Poly(ethylene glycol)



Hydrogels for use in Cartilage Tissue Engineering. *Tissue Eng. Part A* (2017). doi:10.1089/ten.TEA.2016.0490

52. Martens, P. J., Bryant, S. J. & Anseth, K. S. Tailoring the Degradation of Hydrogels Formed from Multivinyl Poly(ethylene glycol) and Poly(vinyl alcohol) Macromers for Cartilage Tissue Engineering. *Biomacromolecules* **4**, 283–292 (2003).
53. Hoyle, C. E. & Bowman, C. N. Thiol–Ene Click Chemistry. *Angew. Chem. Int. Ed.* **49**, 1540–1573 (2010).
54. Coates, E. E. & Fisher, J. P. Phenotypic Variations in Chondrocyte Subpopulations and Their Response to In Vitro Culture and External Stimuli. *Ann. Biomed. Eng.* **38**, 3371–3388 (2010).

## Chapter 7

1. White House Precision Medicine Initiative. *The White House* Available at: <https://obamawhitehouse.archives.gov/node/333101>. (Accessed: 19th May 2018)
2. Aguado, B. A., Grim, J. C., Rosales, A. M., Watson-Capps, J. J. & Anseth, K. S. Engineering precision biomaterials for personalized medicine. *Sci. Transl. Med.* **10**, eaam8645 (2018).
3. Ott, H. C. *et al.* Perfusion-decellularized matrix: using nature’s platform to engineer a bioartificial heart. *Nat. Med.* **14**, 213–221 (2008).
4. Song, J. J. & Ott, H. C. Organ engineering based on decellularized matrix scaffolds. *Trends Mol. Med.* **17**, 424–432 (2011).
5. Saldin, L. T., Cramer, M. C., Velankar, S. S., White, L. J. & Badylak, S. F. Extracellular matrix hydrogels from decellularized tissues: Structure and function. *Acta Biomater.* **49**, 1–15 (2017).
6. Gilpin, A. & Yang, Y. Decellularization Strategies for Regenerative Medicine: From Processing Techniques to Applications. *BioMed Res. Int.* **2017**, (2017).
7. Zhou, G. *et al.* In Vitro Regeneration of Patient-specific Ear-shaped Cartilage and Its First Clinical Application for Auricular Reconstruction. *EBioMedicine* **28**, 287–302 (2018).
8. Honigmann, P. *et al.* Patient-Specific Surgical Implants Made of 3D Printed PEEK: Material, Technology, and Scope of Surgical Application. *BioMed Research International* (2018). doi:10.1155/2018/4520636
9. Payne, K. A., Didiano, D. M. & Chu, C. R. Donor sex and age influence the chondrogenic potential of human femoral bone marrow stem cells. *Osteoarthritis Cartilage* **18**, 705–713 (2010).
10. Tetlow, L. C., Adlam, D. J. & Woolley, D. E. Matrix metalloproteinase and proinflammatory cytokine production by chondrocytes of human osteoarthritic cartilage: associations with degenerative changes. *Arthritis Rheum.* **44**, 585–594 (2001).

11. Skaalure, S. C., Milligan, I. L. & Bryant, S. J. Age impacts extracellular matrix metabolism in chondrocytes encapsulated in degradable hydrogels. *Biomed. Mater.* **7**, 024111 (2012).
12. Kim, Y.-J., Sah, R. L. Y., Doong, J.-Y. H. & Grodzinsky, A. J. Fluorometric assay of DNA in cartilage explants using Hoechst 33258. *Anal. Biochem.* **174**, 168–176 (1988).
13. Templeton, D. M. The basis and applicability of the dimethylmethylene blue binding assay for sulfated glycosaminoglycans. *Connect. Tissue Res.* **17**, 23–32 (1988).
14. Hascall, V. C. & Sajdera, S. W. Physical properties and polydispersity of proteoglycan from bovine nasal cartilage. *J. Biol. Chem.* **245**, 4920–4930 (1970).
15. Chu, S. *et al.* Understanding the Spatiotemporal Degradation Behavior of Aggrecanase-Sensitive Poly(ethylene glycol) Hydrogels for Use in Cartilage Tissue Engineering. *Tissue Eng. Part A* **23**, 795–810 (2017).
16. Khan, I. M., Palmer, E. A. & Archer, C. W. Fibroblast growth factor-2 induced chondrocyte cluster formation in experimentally wounded articular cartilage is blocked by soluble Jagged-1. *Osteoarthritis Cartilage* **18**, 208–219 (2010).
17. Tyler, J. A. Insulin-like growth factor 1 can decrease degradation and promote synthesis of proteoglycan in cartilage exposed to cytokines. *Biochem. J.* **260**, 543–548 (1989).
18. Byers, B. A., Mauck, R. L., Chiang, I. E. & Tuan, R. S. Transient exposure to transforming growth factor beta 3 under serum-free conditions enhances the biomechanical and biochemical maturation of tissue-engineered cartilage. *Tissue Eng. Part A* **14**, 1821–1834 (2008).
19. Nicodemus, G. D. & Bryant, S. J. Cell Encapsulation in Biodegradable Hydrogels for Tissue Engineering Applications. *Tissue Eng. Part B Rev.* **14**, 149–165 (2008).
20. Schneider, M. C. *et al.* Local Heterogeneities Improve Matrix Connectivity in Degradable and Photoclickable Poly(ethylene glycol) Hydrogels for Applications in Tissue Engineering. *ACS Biomater. Sci. Eng.* **3**, 2480–2492 (2017).
21. Skaalure, S. C., Chu, S. & Bryant, S. J. An Enzyme-sensitive PEG Hydrogel Based on Aggrecan Catabolism for Cartilage Tissue Engineering. *Adv. Healthc. Mater.* **4**, 420–431 (2015).
22. Eyre, D. Articular cartilage and changes in Arthritis: Collagen of articular cartilage. *Arthritis Res.* **4**, 30–35 (2002).
23. Dhote, V. & Vernerey, F. J. Mathematical model of the role of degradation on matrix development in hydrogel scaffold. *Biomech. Model. Mechanobiol.* **13**, 167–183 (2013).
24. Dhote, V. *et al.* On the role of hydrogel structure and degradation in controlling the transport of cell-secreted matrix molecules for engineered cartilage. *J. Mech. Behav. Biomed. Mater.* **19**, 61–74 (2013).

25. Sridhar, S. L. *et al.* Heterogeneity is key to hydrogel-based cartilage tissue regeneration. *Soft Matter* **13**, 4841–4855 (2017).

## Chapter 8

1. Nicodemus, G. D. & Bryant, S. J. Cell Encapsulation in Biodegradable Hydrogels for Tissue Engineering Applications. *Tissue Eng. Part B Rev.* **14**, 149–165 (2008).
2. Appelman, T. P., Mizrahi, J., Elisseff, J. H. & Seliktar, D. The differential effect of scaffold composition and architecture on chondrocyte response to mechanical stimulation. *Biomaterials* **30**, 518–525 (2009).
3. Bryant, S. J. & Anseth, K. S. Hydrogel properties influence ECM production by chondrocytes photoencapsulated in poly (ethylene glycol) hydrogels. *J. Biomed. Mater. Res.* **59**, 63–72 (2002).
4. Neumann, A. J., Quinn, T. & Bryant, S. J. Nondestructive evaluation of a new hydrolytically degradable and photo-clickable PEG hydrogel for cartilage tissue engineering. *Acta Biomater.* **39**, 1–11 (2016).
5. Rice, M. A., Waters, K. R. & Anseth, K. S. Ultrasound monitoring of cartilaginous matrix evolution in degradable PEG hydrogels. *Acta Biomater.* **5**, 152–161 (2009).
6. Farnsworth, N., Bensard, C. & Bryant, S. J. The role of the PCM in reducing oxidative stress induced by radical initiated photoencapsulation of chondrocytes in poly(ethylene glycol) hydrogels. *Osteoarthritis Cartilage* **20**, 1326–1335 (2012).
7. Aguado, B. A., Grim, J. C., Rosales, A. M., Watson-Capps, J. J. & Anseth, K. S. Engineering precision biomaterials for personalized medicine. *Sci. Transl. Med.* **10**, eaam8645 (2018).
8. Aubry, S. *et al.* Cell-surface thiols affect cell entry of disulfide-conjugated peptides. *FASEB J.* **23**, 2956–2967 (2009).
9. Sridhar, B. V., Doyle, N. R., Randolph, M. A. & Anseth, K. S. Covalently tethered TGF- $\beta$ 1 with encapsulated chondrocytes in a PEG hydrogel system enhances extracellular matrix production. *J. Biomed. Mater. Res. A* **102**, 4464–4472 (2014).
10. Schneider, M. C., Chu, S., Randolph, M. A. & Bryant, S. J. An in vitro and in vivo comparison of cartilage growth in chondrocyte-laden matrix metalloproteinase-sensitive poly(ethylene glycol) hydrogels with localized transforming growth factor  $\beta$ 3. *Acta Biomater.* (2019). doi:10.1016/j.actbio.2019.03.046
11. Vinatier, C., Mrugala, D., Jorgensen, C., Guicheux, J. & Noël, D. Cartilage engineering: a crucial combination of cells, biomaterials and biofactors. *Trends Biotechnol.* **27**, 307–314 (2009).
12. Nestic, D. *et al.* Cartilage tissue engineering for degenerative joint disease. *Adv. Drug Deliv. Rev.* **58**, 300–322 (2006).